VOLUME 77 SEPTEMBER 13, 1973 NUMBER 19

JPCHAx

THE JOURNAL OF PHYSICAL CHEMISTRY

PUBLISHED BIWEEKLY BY THE AMERICAN CHEMICAL SOCIETY

THE JOURNAL OF

PHYSICAL CHEMISTRY

AMERICAN CHEMICAL SOCIETY, *1155 Sixteenth St., N.W., Washington, D. C. 20036*

Books and Journals Division

JOHN K CRUM *Director*
RUTH REYNARD *Assistant to the Director*

CHARLES R. BERTSCH *Head, Editorial Processing Department*
D. H. MICHAEL BOWEN *Head, Journals Department*
BACIL GUILEY *Head, Graphics and Production Department*
SELDON W. TERRANT *Head, Research and Development Department*

 Published biweekly by the American Chemical Society at 20th and Northampton Sts., Easton, Pa. 18042. Second-class postage paid at Washington, D. C., and at additional mailing offices.

All manuscripts should be sent to *The Journal of Physical Chemistry*, Department of Chemistry, University of Minnesota, Minneapolis, Minn. 55455.

Additions and Corrections are published once yearly in the final issue. See Volume 76, Number 26 for the proper form.

Extensive or unusual alterations in an article after it has been set in type are made at the author's expense, and it is understood that by requesting such alterations the author agrees to defray the cost thereof.

The American Chemical Society and the Editor of *The Journal of Physical Chemistry* assume no responsibility for the statements and opinions advanced by contributors.

Correspondence regarding accepted copy, proofs, and reprints should be directed to Editorial Processing Department, American Chemical Society, 20th and Northampton Sts., Easton, Pa. 18042. Head: CHARLES R. BERTSCH. Assistant Editor: EDWARD A. BORGER. Editorial Assistant: JOSEPH E. YURVATI.

Advertising Office: Centcom, Ltd., 142 East Avenue, Norwalk, Conn. 06851.

Business and Subscription Information

Send all new and renewal subscriptions *with payment* to: Office of the Controller, 1155 16th Street, N.W., Washington, D. C. 20036. Subscriptions should be renewed promptly to avoid a break in your series. All correspondence and telephone calls regarding changes of address, claims for missing issues, subscription service, the status of records, and accounts should be directed to Manager, Membership and Subscription Services, American Chemical Society, P.O. Box 3337, Columbus, Ohio 43210. Telephone (614) 421-7230.

On changes of address, include both old and new addresses with ZIP code numbers, accompanied by mailing label from a recent issue. Allow four weeks for change to become effective.

Claims for missing numbers will not be allowed (1) if loss was due to failure of notice of change in address to be received before the date specified, (2) if received more than sixty days from date of issue plus time normally required for postal delivery of journal and claim, or (3) if the reason for the claim is "issue missing from files."

Subscription rates (1973): members of the American Chemical Society, $20.00 for 1 year; to nonmembers, $60.00 for 1 year. Those interested in becoming members should write to the Admissions Department, American Chemical Society, 1155 Sixteenth St., N.W., Washington, D. C. 20036. Postage to Canada and countries in the Pan-American Union, $5.00; all other countries, $6.00. Single copies for current year: $3.00. Rates for back issues from Volume 56 to date are available from the Special Issues Sales Department, 1155 Sixteenth St., N.W., Washington, D. C. 20036.

Subscriptions to this and the other ACS periodical publications are available on microfilm. Supplementary material not printed in this journal is now available in microfiche form on a current subscription basis. For information on microfilm or microfiche subscriptions, write Special Issues Sales Department at the address above.

Notice to Authors last printed in the issue of June 21, 1973

THE JOURNAL OF
PHYSICAL CHEMISTRY

Volume 77, Number 19 September 13, 1973

JPCHAx 77(19) 2257–2366 (1973)
ISSN 0022-3654

Kinetic Isotope Effects in Reactions of Hot Methyl Radicals with Hydrogen
Cheng-Teh Ting and Ralph E. Weston, Jr.* 2257

Intramolecular Photolytic Interactions of Aromatic Carboxylic Acids in Solution
Lalitha J. Mittal, J. P. Mittal, and E. Hayon* 2267

Ionization Constants and Spectral Characteristics of Some Semiquinone Radicals in Aqueous Solution **P. S. Rao and E. Hayon*** 2274

Electronic Absorption and Emission of Aromatic Hydroxycarbonium Ions
Nicolae Filipescu,* Saroj K. Chakrabarti, and Peter G. Tarassoff 2276

Binding of Methylmercury Chloride to the Model Peptide, *N*-Acetyl-L-cysteine. A Proton Magnetic Resonance Study **Paul G. Simpson, Ted E. Hopkins, and Rizwanul Haque*** 2282

Configuration Coordinate Model for the Hydrated Electron. II. Jahn–Teller Splitting of the Excited State **M. Tachiya,* Y. Tabata, and K. Oshima** 2286

Application of a New Equation Based on Enthalpies of Formation and Ionization Potentials to the Problem of the Nature of Bonding in Weak Molecular Complexes **Manjit S. Sambhi** 2290

Hydrogen-Bonded Species of Acetic Acid in Inert Solvents
Mark A. Goldman and Merle T. Emerson* 2295

Thermodynamics of Electrolytes. II. Activity and Osmotic Coefficients for Strong Electrolytes with One or Both Ions Univalent **Kenneth S. Pitzer* and Guillermo Mayorga** 2300 ■

Ionization and Electron Transfer Reactions in Linde Type Y Zeolites
Paul H. Kasai* and Roland J. Bishop, Jr. 2308

Conversion of Amorphous Calcium Phosphate to Microcrystalline Hydroxyapatite. A pH-Dependent, Solution-Mediated, Solid–Solid Conversion
Adele Ludin Boskey* and Aaron S. Posner 2313 ■

Kinetics of Binding of Pyrophosphate to Magnesium Ions **R. C. Patel* and R. S. Taylor** 2318

Surface-Chemical Properties of Highly Fluorinated Compounds Containing Oxygen in the Aliphatic Chain **Marianne K. Bernett and W. A. Zisman*** 2324

Ultrasonic Absorption in Aqueous Solutions of Nucleotides and Nucleosides. I. Effect of pH and Concentration **Jacques Lang, Jean Sturm, and Raoul Zana*** 2329 ■

Thermodynamics and the Effect of Guanidine Hydrochloride and Potassium Chloride on the Hydrophobic Hydration of Tetra-*n*-butylammonium Bromide and Tetra-*n*-pentylammonium Bromide in Water **B. Chawla, S. Sunder, and J. C. Ahluwalia*** 2335 ■

Equilibrium Studies by Electron Spin Resonance. IV. Enthalpies of Ion Pairing for Substituted Nitrobenzene Anion Radicals **Gerald R. Stevenson* and Luis Echegoyen** 2339

Transitions in Mesophase Forming Systems. V. Kinetics of Transformation and Properties of Cholesteryl Stearate **Fraser P. Price* and Joachim H. Wendorff** 2342

The Chromium–Iodine System **Chyi-Feng Shieh and N. W. Gregory*** 2346

Equilibrium Distribution of Lithium and Bismuth between Liquid Lithium–Bismuth Alloys and Molten Lithium Chloride at 650–800° **L. M. Ferris,* M. A. Bredig, and F. J. Smith** 2351 ■

Electronic Interaction between the Vinyl Group and Its Substituents
A. Katrib and J. W. Rabalais* 2358

COMMUNICATIONS TO THE EDITOR

Hydrocarbon Adsorption Effects on the Unit Cell Constant of NaY Zeolites
. . . **P. Gallezot and B. Imelik*** 2364

Selective Hydrogen Atom Abstraction by Hydrogen Atoms in Neopentane–Alkane Mixtures at 77°K
. . . **Terunobu Wakayama, Tetsuo Miyazaki,* Kenji Fueki, and Zen-ichiro Kuri** 2365

■ Supplementary material for this paper is available separately, in photocopy or microfiche form. Ordering information is given in the paper.

* In papers with more than one author, the asterisk indicates the name of the author to whom inquiries about the paper should be addressed.

AUTHOR INDEX

Ahluwalia, J. C., 2335

Bernett, M. K., 2324
Bishop, R. J., Jr., 2308
Boskey, A. L., 2313
Bredig, M. A., 2351

Chakrabarti, S. K., 2276
Chawla, B., 2335

Echegoyen, L., 2339
Emerson, M. T., 2295

Ferris, L. M., 2351
Filipescu, N., 2276
Fueki, K., 2365

Gallezot, P., 2364
Goldman, M. A., 2295
Gregory, N. W., 2346

Haque, R., 2282
Hayon, E., 2267, 2274
Hopkins, T. E., 2282

Imelik, B., 2364

Kasai, P. H., 2308
Katrib, A., 2358
Kuri, Z., 2365

Lang, J., 2329

Mayorga, G., 2300
Mittal, J. P., 2267
Mittal, L. J., 2267
Miyazaki, T., 2365

Oshima, K., 2286

Patel, R. C., 2318
Pitzer, K. S., 2300
Posner, A. S., 2313
Price, F. P., 2342

Rabalais, J. W., 2358
Rao, P. S., 2274

Sambhi, M. S., 2290
Shieh, C.-F., 2346
Simpson, P. G., 2282
Smith, F. J., 2351
Stevenson, G. R., 2339
Sturm, J., 2329
Sunder, S., 2335

Tabata, Y., 2286
Tachiya, M., 2286
Tarassoff, P. G., 2276
Taylor, R. S., 2318
Ting, C.-T., 2257

Wakayama, T., 2365
Wendorff, J. H., 2342
Weston, R. E., Jr., 2257

Zana, R., 2329
Zisman, W. A., 2324

THE JOURNAL OF
PHYSICAL CHEMISTRY

VOLUME 77, NUMBER 19 SEPTEMBER 13, 1973

Kinetic Isotope Effects in Reactions of Hot Methyl Radicals with Hydrogen[1]

Cheng-Teh Ting and Ralph E. Weston, Jr.*

Department of Chemistry, Brookhaven National Laboratory, Upton, New York 11973 *(Received May 3, 1973)*

Publication costs assisted by Brookhaven National Laboratory

The photolysis at 185 nm of CH_3Br or CD_3Br has been used as a source of "hot" methyl radicals which subsequently abstract a hydrogen atom from methyl bromide or from added hydrogen. Relative rate constants for abstraction from H_2 or D_2 have been determined by isotopic analysis of the methane produced. The results are discussed in terms of various models for the photodissociation dynamics of alkyl halides. The normal isotope effect for the reaction of hot CH_3 with H_2 or D_2 is predicted by cross sections calculated from activated complex theory, but this theory does not predict the inverse effect observed in the corresponding reactions of hot CD_3.

Introduction

The photolysis of diatomic molecules by photons with an energy greater than the bond dissociation energy produces translationally "hot" atoms; *i.e.*, atoms with kinetic energy greater than they would have if they were in thermal equilibrium with their surroundings. Atoms with low-lying excited electronic states (*e.g.*, the halogens) may also become excited electronically. This procedure has been extensively used to produce hot hydrogen atoms from hydrogen halides, and the subsequent reactions of the hot hydrogen atoms have been investigated.

If the molecule undergoing photolysis is polyatomic rather than diatomic, the energy available after bond fission may appear within the molecular fragments as internal energy (vibrational, rotational, or electronic) in addition to relative translational energy. The way in which the available energy is divided among these various degrees of freedom has been investigated in a few cases. For example, the emission spectrum of OH radicals produced by the vacuum uv photolysis of H_2O has been used to determine the vibrational and rotational energy distribution in the radical,[2] the reactivity of hot H atoms has been used to investigate energy partitioning in the photolysis of H_2S,[3] and the photodissociation dynamics of several small polyatomic molecules has been investigated with Wilson's technique of photofragment spectroscopy.[4]

Alkyl halides photodissociate principally to the halogen atom and an alkyl radical. If the wavelength of the incident light is sufficiently short, the alkyl radicals thus formed undergo reactions at room temperature,[5] such as hydrogen abstraction from the alkyl halide or from added hydrocarbons, which are known to have activation energies of several kcal/mole. These are "hot" reactions, analogous to the corresponding reactions of hydrogen atoms with excess kinetic energy, but with the possible added contribution of vibrational and rotational excitation of the radical. Our interest was attracted to the reaction of hot methyl radicals with hydrogen molecules of various isotopic species

$$CH_3^* + H_2, D_2, \text{ or } HD \rightarrow CH_4 \text{ or } CH_3D + H \text{ or } D$$

for several reasons.

(a) The corresponding reaction of methyl radicals at thermal equilibrium has been widely studied,[6] and kinetic isotope effects have been determined.[7]

(b) The reverse reaction, $H + CH_4 \rightarrow H_2 + CH_3$, has been studied both in thermal systems[6] and with hot hydrogen atoms.[8]

(c) The number of atoms is small enough so that quantum chemical calculations of the potential energy surface for the forward reaction, the reverse reaction, and the H-for-H substitution reaction are feasible.[9]

(d) Classical trajectory studies of the dynamics of the H atom abstraction and substitution reactions have been undertaken.[10]

(e) The reduced mass in a CH_3–H_2 collision is about one-half that in a CH_3–D_2 collision, with a proportional change in the available translational energy.

Experimental Section

1. Materials. After bulb-to-bulb distillation, methyl bromide (Matheson) was used without further purification. It was stored in a blackened bulb on the vacuum line, as was methyl-d_3 bromide (Merck Sharp and Dohme, 99.14 atom % D). Deuterium (containing 1% HD) was obtained from Biorad Laboratories. Hydrogen deuteride was prepared by Dr. D. C. Christman of this laboratory; previous analyses show that it contains 1.2% H_2 and 1.0% D_2. Hydrogen, nitrogen, and oxygen used for calibration purposes were obtained from Liquid Carbonic. Methane (Matheson) was used for calibration together with the deuterated methanes (Merck Sharp and Dohme). Hexafluoroethane was obtained from PCR, Inc. The bromine used was Analytical Reagent Grade, obtained from Mallinckrodt.

2. Apparatus. In order to avoid possible complications due to mercury photosensitization, all vacuum manipulations were carried out on a mercury-free vacuum line, pumped by an oil-diffusion pump. Pressures were measured with a calibrated Whittaker Model DM1 digital manometer. Stopcocks and joints that came in contact with bromine were lubricated with Kel-F halocarbon grease.

The photolysis cell was a quartz cylinder, 25 mm in diameter, with a volume of 67 ml. On one end, a Suprasil window allowed transmission of the 185-nm Hg resonance line. A large standard-taper joint on the opposite end could be removed for the insertion of a small capillary tube containing bromine, which served as a scavenger for moderated methyl radicals. Since a mercury-filled Toeppler pump could not be used, the photolysis cell was filled simply by expansion into the cell of reagents from storage bulbs, with appropriate pressure measurements. The bromine-containing capillary was then broken by shaking the cell. After a photolysis run, the reaction mixture was allowed to expand through a trap cooled to −196°, which removed bromine and methyl bromide, into a measured volume. The methane in this sample, a known fraction of the total noncondensable gas in the reaction mixture, was trapped by adsorption on silica gel at −196°, while hydrogen was slowly pumped off. The silica gel trap was then used as an injection loop for the gas chromatographic determination of methane. It was shown that adsorption at −196° and desorption at ~60° could be done quantitatively. In the same way, a second portion of the methane in the reaction mixture was trapped in a small loop with a rubber septum. A hypodermic syringe was used to inject a sample in the gas chromatograph used for isotopic analysis. The part of the vacuum manifold used in the above procedure was made of small-bore and capillary tubing to minimize the volume.

The total yield of methane was determined by gas chromatography, with a 20 ft × ½ in. molecular sieve (13X) column at room temperature, and helium carrier gas. A Varian Aerograph Model 1520 or Model 204 chromatograph with a thermal conductivity detector and a Varian Aerograph Model 475 digital integrator were used. In the case of experiments with CH_3Br, the relative amounts of CH_4 and CH_3D were determined by gas chromatography on an etched glass capillary column of the type described by Bruner, *et al.*[11] Using a column 40–50 m in length, with an inside diameter of 0.25 mm, a column temperature of −196°, and a 30:70 mixture of He and N_2 flowing at a rate of about 0.05 ml/sec as the carrier gas, we were able to obtain almost complete resolution of the elution peaks from a roughly equimolar mixture of CH_4 and CH_3D (Figure 1). Relative peak areas were determined with the flame ionization detector of the Aerograph Model 1520, and the digital integrator; measured amounts of CH_4 and CH_3D were mixed and used for calibration of this analytical method.

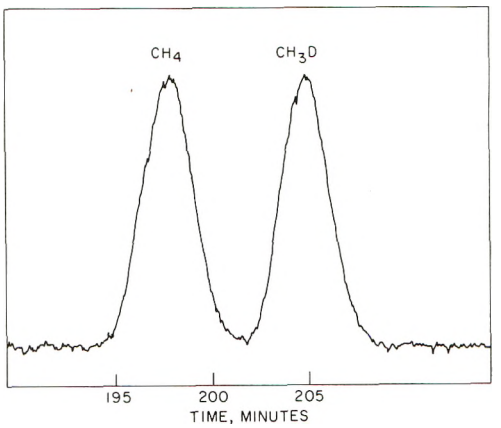

Figure 1. Chromatographic separation of CH_3D and CH_4 on a 50-m etched glass capillary column: column temperature, −196°; carrier gas, 30% He in N_2, flow rate 0.04 ml/sec.

A few mixtures of CH_4 and CH_3D were analyzed by mass spectrometry, using a Hitachi-Perkin-Elmer RMU-7E instrument, and the results were in good agreement with those obtained by gas chromatography.

The glass capillary column did not resolve elution peaks of CD_4 and CD_3H. Instead, these mixtures were analyzed mass spectrometrically, using the parent peaks at m/e 20 and 19.

The light source used in this work was a mercury resonance lamp excited by an rf oscillator.[12] The lamp itself was a spherical quartz bulb about 3 cm in diameter with a 1-cm Suprasil window, containing a drop of mercury. Light emission was optimized by regulating the flow of an air stream through a jacket surrounding the mercury reservoir. The window of the photolysis cell window was placed in contact with the lamp window in order to prevent absorption of 185-nm light by oxygen. The lamp intensity was measured roughly at the beginning and end of a photolysis run by means of an RCA 935 phototube with a Schott UG 11 filter, and a Keithley micro-microammeter. Since the filter transmits in the 300–400-nm region, the intensity of the 185-nm line is not directly measured by this method.

The absolute lamp intensity was measured by photolysis of N_2O, followed by gas chromatographic measurement of the N_2 thus produced. Nitrous oxide is transparent at wavelengths greater than 200 nm, and therefore, the lamp intensity at 185 nm can be calculated from the nitrogen yield and the known quantum efficiency.[13] This result (~5×10^{15} quanta/sec) was then used in calculating quantum yields from the experimental data for methyl bromide photolysis. We also measured the lamp output at 254 nm, using the production of H_2 from HBr as an actinometric method.[14] In this experiment, an interference filter with a 20-nm bandpass and a transmittance of 23% at 254 nm was used to isolate the Hg line. Without the filter, the intensity was about 50% higher at 254 nm than at 185 nm. However, since the quantum yield[15] for methane production by photolysis of CH_3Br at 185 nm is fivefold that at 254 nm, and since the molar extinction coefficients are 70[15] and 1.5,[16] respectively, the effect of 254-nm ra-

diation should be negligible in our experiments. It should be made clear, however, that our work was directed toward measurement of *relative* and not *absolute* quantum yields.

In typical photolysis experiments, the reagent pressures were CH_3Br or CD_3Br, 10 ± 1 Torr; total hydrogen (H_2 + HD + D_2), 15-110 Torr; Br_2, 5-10% of the total pressure. Under these conditions, about 75% of the incident light is absorbed by methyl bromide, and about 5% by bromine. All experiments were performed at room temperature (23 ± 2°). The extent of photolysis was usually such that the total methane produced was ~0.05% of the initial methyl bromide.

Experimental Results

1. Photolysis of CH_3Br Alone. A few measurements of the quantum yield for methane production in the photolysis of methyl bromide were made immediately after actinometry with nitrous oxide. The value obtained was $\Phi_{CH_4} = (1.77 \pm 0.03) \times 10^{-2}$ in good agreement with the value of $(2.0 \pm 0.3) \times 10^{-2}$ obtained previously.[15] The pertinent reactions[17] in this system are

$$CH_3Br + h\nu \rightarrow CH_3^* + Br \quad (1)$$

$$CH_3^* + CH_3Br \rightarrow CH_4 + CH_2Br \quad (2)$$

$$CH_3^* + CH_3Br \rightarrow CH_3 + CH_3Br \quad (3)$$

$$CH_3 + Br_2 \rightarrow CH_3Br + Br \quad (4)$$

$$CH_2Br + Br_2 \rightarrow CH_2Br_2 + Br$$

$$2Br \rightarrow Br_2$$

The asterisk indicates a "hot" radical, with no further specification of its energy content at this point. The quantum yield is

$$\Phi_{CH_4} = \frac{k_2(CH_3Br)}{(k_2 + k_3)(CH_3Br)} \simeq \frac{k_2}{k_3} \quad (A)$$

2. Photolysis of CH_3Br-H_2 Mixtures. This system was investigated in order to estimate the relative effectiveness of H_2 and CH_3Br for thermalizing hot methyl radicals. The additional reactions are

$$CH_3^* + H_2 \rightarrow CH_4 + H \quad (5)$$

$$CH_3^* + H_2 \rightarrow CH_3 + H_2 \quad (6)$$

$$H + Br_2 \rightarrow HBr + Br \quad (7)$$

Application of the steady-state assumption, together with the assumption that $k_2 \ll k_3$ and $k_5 \ll k_6$, leads to the expression

$$\frac{\Phi_{CH_4}^0}{\Phi_{CH_4}}\left[1 + \frac{k_5(H_2)}{k_2(CH_3Br)}\right] \simeq 1 + \frac{k_6(H_2)}{k_3(CH_3Br)} \quad (B)$$

where the superscript ° refers to the case where only CH_3Br is present.

A plot of the left-hand side of this equation against the ratio $(H_2)/(CH_3Br)$ should give a straight line with an intercept of unity, provided the correct value of k_5/k_2 is known. Alternatively, various values of the ratio k_5/k_2 are tried until a reasonable fit of the data to a straight line is obtained (Figure 2). The results are not very precise, and the points at the highest pressures of H_2 deviate from a straight line; however, ranges of 0.05-0.10 for k_5/k_2 and 0.6-0.9 for k_6/k_3 appear acceptable.

While there do not appear to be literature data for relative moderator efficiencies in the CH_3Br photolysis, anal-

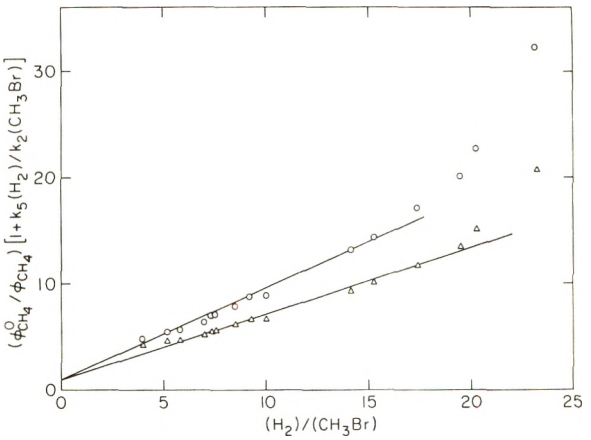

Figure 2. Data from the photolysis of CH_3Br-H_2 mixtures plotted according to eq B: (○) $k_5/k_2 = 0.10$, $k_6/k_3 = 0.86$; (△) $k_5/k_2 = 0.05$, $k_6/k_3 = 0.60$.

ogous data are available[5d,f,j] for the photolysis of CH_3I at 254 nm. From these and eq B, we obtain moderator efficiencies relative to CH_3I of ~0.5 for H_2, D_2, Ne, He, Ar (ref 5f), or ~0.9 for He, Ne, Ar, CO_2 (ref 5d). Doepker and Ausloos[5j] examined the moderator effect of CO_2, which can be related to the moderator efficiency of the polyatomic substrates they used (ethane, propane, 2-methylpropane, butane, cyclohexane, methanol). Efficiencies relative to CO_2 were in the range 1-1.6.

3. Photolysis of CH_3Br-D_2 Mixtures. A few experiments were done with CH_3Br-D_2 mixtures, and relative yields of CH_4 and CH_3D were measured. The additional reactions are

$$CH_3^* + D_2 \rightarrow CH_3D + D \quad (8)$$

$$CH_3^* + D_2 \rightarrow CH_3 + D_2 \quad (9)$$

$$D + Br_2 \rightarrow DBr + Br \quad (10)$$

The relative yields of the two isotopic forms of methane are given by

$$R_{CH_3D}/R_{CH_4} = k_8(D_2)/k_2(CH_3Br) \quad (C)$$

where R_x is the yield of species x. From the data of Table I, we find that the rate constant ratio k_8/k_2 is $(5.0 \pm 0.7) \times 10^{-2}$.

A plot of $\Phi_{CH_4}^0/\Phi_{CH_4}$ against $(D_2)/(CH_3Br)$ provides an estimate of $k_9/k_3 = 0.6$ for the relative moderator efficiencies of D_2 and CH_3Br. Comparison of this with k_6/k_3 shows that H_2 and D_2 are approximately equivalent moderators of hot methyl radicals, with respect to the reaction of these radicals with methyl bromide. However, the kinetic analysis leading to eq C tacitly assumes that added moderator (in this case D_2) will have identical effects on reactions 2 and 8. The small, but apparently real, increase of k_2/k_8 with increasing D_2 pressure is an indication that this assumption is only approximately correct. If the excitation functions for these two reactions differ as shown schematically in Figure 3, then the addition of moderator to the reaction system will decrease the yield of reaction 3 with respect to the yield of reaction 1; of course, the *total* yield of both reactions will also decrease. This "shadowing" effect has been observed in several reactions of hot T atoms produced by nuclear recoil.[18]

To test this assumption, several photolysis runs were carried out with the same amounts of CH_3Br and D_2, but with various amounts of He as a moderator. The additional reaction is

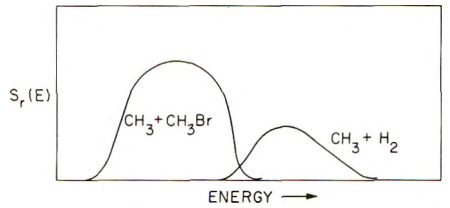

Figure 3. Hypothetical excitation functions which would explain the "shadowing" effect in the reactions of hot methyl radicals with hydrogen and with methyl bromide. $S_r(E)$ is the reactive cross section.

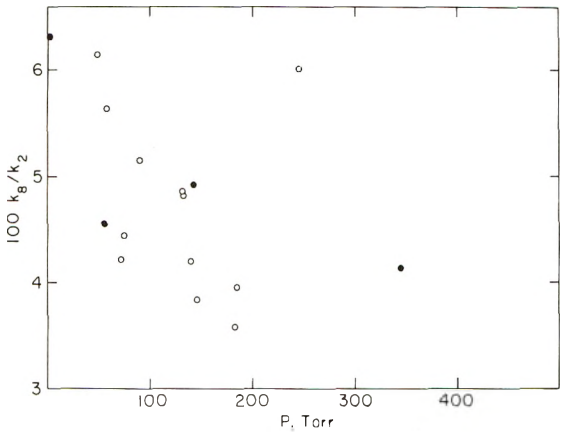

Figure 4. Effect of pressure on the ratio k_8/k_2 calculated from eq C. P is the pressure of gas added to a reaction mixture of D_2 (~50 Torr) and CH_3Br (10 Torr): (○) He; (●) D_2.

$$CH_3^* + He \rightarrow CH_3 + He \qquad (11)$$

The results shown in Figure 4 are again consistent with a "shadowing" effect, since in the absence of such an effect, the addition of inert gas should not change the relative rates of reactions 2 and 8.

The data in Figure 4 also indicate that the moderating efficiencies of D_2 and He are comparable, with respect to lowering the energies of hot methyl radicals below the threshold energy of reaction 8 but not below the threshold energy of reaction 2.

Moderation of hot methyl radicals with respect to abstraction from CH_3Br can also be examined by means of the expression

$$\frac{\Phi_{CH_4}^{\ 0}}{\Phi_{CH_4}} = \frac{k_2(CH_3Br)}{(k_2 + k_3)(CH_3Br)} \times \frac{(k_2 + k_3)(CH_3Br) + (k_8 + k_9)(D_2) + k_{11}(He)}{k_2(CH_3Br)}$$

which can be rearranged to

$$[(\Phi_{CH_4}^{\ 0}/\Phi_{CH_4}) - 1]\frac{(CH_3Br)}{(He)} = \frac{k_{11}}{k_3} + \frac{k_9}{k_2}\frac{(D_2)}{(He)} \qquad (D)$$

A plot of the left-hand side against $(D_2)/(He)$ gives an intercept of 0.24, the moderating efficiency of He relative to CH_3Br, and a slope of 1.2, the efficiency of D_2 relative to CH_3Br.

A few runs were made with hexafluoroethane as the added moderator. Because of difficulties in sample collection, only the CH_3D/CH_4 ratio was measured. This was found to be too small for precise measurement; it is roughly an order of magnitude lower at a given pressure of C_2F_6 than at the same pressure of He. This will be discussed later.

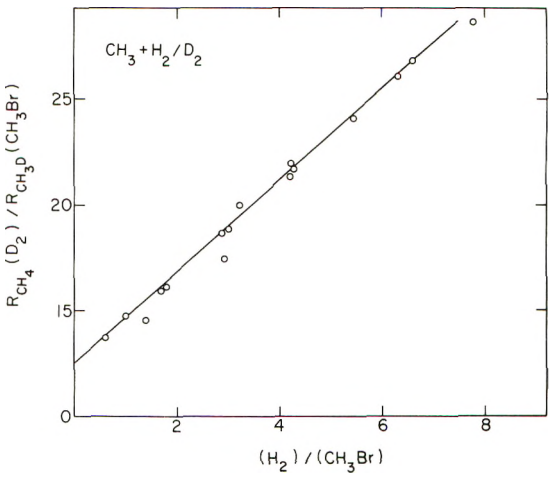

Figure 5. Data from photolysis of CH_3Br–H_2–D_2 mixtures, plotted according to eq E.

4. Photolysis of CH_3Br–H_2–D_2 Mixtures. The emphasis in these experiments was on the relative yields of CH_3D and CH_4, from which the kinetic isotope effect in reactions 5 and 8 can be determined. The expression used for this is

$$\frac{R_{CH_4}}{R_{CH_3D}}\frac{(D_2)}{(CH_3Br)} = \frac{k_2}{k_8} + \frac{k_5}{k_8}\frac{(H_2)}{(CH_3Br)} \qquad (E)$$

The data are plotted according to eq E in Figure 5, and a least-squares analysis gives $k_2/k_8 = 12.5 \pm 0.2$ ($k_8/k_2 = 0.08$) and $k_5/k_8 = 2.12 \pm 0.05$. The latter ratio is in reasonable agreement with the value derived from the ratio k_5/k_2 from the CH_3Br–H_2 system and k_8/k_2 from the CH_3Br–D_2 system.

In all these experiments, the initial pressure of CH_3Br was constant at 10 ± 0.5 Torr, and the *total* initial hydrogen pressure (*i.e.*, $D_2 + H_2$) was also constant (100 Torr) within a few per cent, although the D_2/H_2 ratio was varied. Since other experiments indicate that H_2 and D_2 have comparable moderator efficiencies, we believe that the "shadowing" effect discussed above is not important in these experiments.

5. Photolysis of CD_3Br–H_2–D_2 Mixtures. Analogous experiments were performed with CD_3Br in place of CH_3Br. The new reactions in this system are

$$CD_3Br + h\nu \rightarrow CD_3^* + Br \qquad (12)$$

$$CD_3^* + CD_3Br \rightarrow CD_4 + CD_2Br \qquad (13)$$

$$CD_3^* + H_2 \rightarrow CD_3H + H \qquad (14)$$

$$CD_3^* + D_2 \rightarrow CD_4 + D \qquad (15)$$

and scavenging reactions analogous to those in the CH_3Br photolysis. Rate constant ratios can be obtained from the expression

$$\frac{R_{CD_4}}{R_{CD_3H}}\frac{(H_2)}{(CD_3Br)} = \frac{k_{13}}{k_{14}} + \frac{k_{15}}{k_{14}}\frac{(D_2)}{(CD_3Br)} \qquad (F)$$

The data are plotted according to eq F in Figure 6, and a least-squares analysis gives $k_{13}/k_{14} = 10.8 \pm 0.7$ and $k_{15}/k_{14} = 2.15 \pm 0.20$. Note that the latter ratio corresponds to an *inverse* isotope effect.

Initial reactant pressures were the same as those in the analogous CH_3Br experiments. Again, total hydrogen pressure was constant, and there should not be difficulties due to moderator effects.

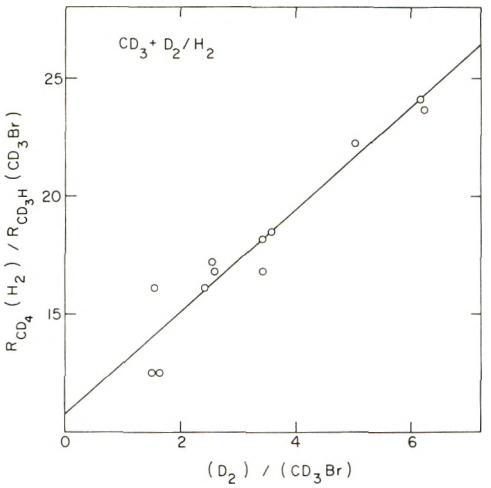

Figure 6. Data from photolysis of CD_3Br–H_2–D_2 mixtures, plotted according to eq F.

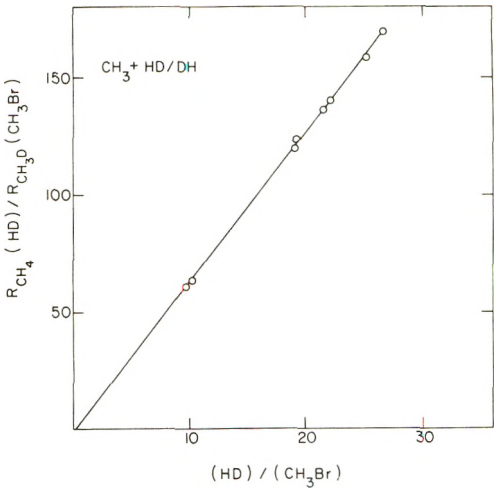

Figure 7. Data from photolysis of CH_3Br–HD mixtures, plotted according to eq G.

6. Photolysis of CH_3Br–HD Mixtures. In principle, this system should permit the study of an *intramolecular* isotope effect from the reactions

$$CH_3 + HD \rightarrow CH_4 + D \quad (16)$$

$$CH_3 + DH \rightarrow CH_3D + H \quad (17)$$

With the added complication of methane production by abstraction from CH_3Br, the product ratio is given by

$$\frac{R_{CH_4}}{R_{CH_3D}}\frac{(HD)}{(CH_3Br)} = \frac{k_2}{k_{17}} + \frac{k_{16}}{k_{17}}\frac{(HD)}{(CH_3Br)} \quad (G)$$

A plot of the data according to this equation is given in Figure 7, and a least-squares analysis leads to the ratios $k_2/k_{17} = -1.95 \pm 1.42$ and $k_{16}/k_{17} = 6.37 \pm 0.07$.

There are important differences between this system and the other two systems used to obtain isotope effects. First, because R_{CH_3D} is small, it was necessary to use relatively high pressures of HD in order to obtain measurable amounts of CH_3D. The large error in k_2/k_{17} (which cannot be negative) results from a long extrapolation along the $(HD)/(CH_3Br)$ axis, about an order of magnitude larger than the extrapolation needed to obtain the corresponding intercepts in the other two systems. Using the rate constant ratios quoted above, we can rearrange eq G to read

$$R_{CH_4}/R_{CH_3D} = 6.37 - 2.0(CH_3Br)/(HD)$$

The experimental conditions are such that $(CH_3Br)/(HD)$ is always ≤ 0.1, so that R_{CH_4}/R_{CH_3D} is insensitive to the ratio, leading to error in k_{16}/k_{17}.

Also, to change the ratio $(HD)/(CH_3Br)$, the initial pressure of HD was varied; when this ratio is large there is increased moderation of the hot methyl radicals. The "shadowing" effect discussed above would lead to an increase in R_{CH_4}/R_{CH_3D} not resulting from a kinetic isotope effect.

This consideration led us to perform a series of experiments in which He was added as an additional moderator, so that the combined pressures of He and HD were about 100 Torr. Relative yields (R_{CH_4}/R_{CH_3D}) were extremely variable (Figure 8) and usually much higher than those predicted from eq G. The added He appears to almost completely prevent abstraction of D from HD, while permitting abstraction of H (chiefly from CH_3Br).

For these reasons, we believe that the rate constant ratios k_2/k_{17} and k_{16}/k_{17} cannot be simply derived from the data in Figure 7, and in particular we believe that the intramolecular isotope effect is not as large as 6.

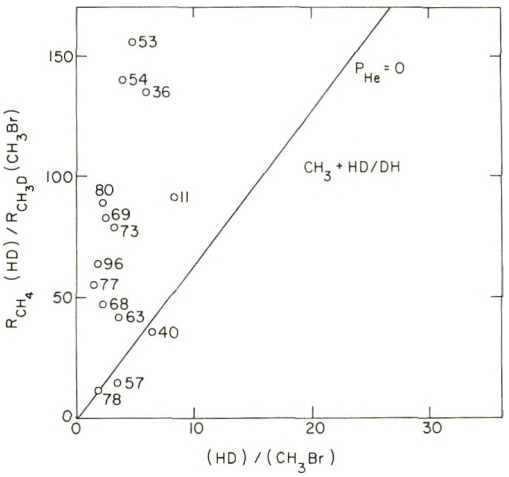

Figure 8. Effect of added He (pressure in Torr indicated by numbers near open circles) on the relative yield of CH_3D and CH_4 in the photolysis of CH_3Br–HD mixtures. The solid line is taken from Figure 7.

Discussion

1. Energy Barrier for the Reaction $CH_3 + H_2 \rightarrow CH_4 + H$. According to activated complex theory, the activation energy, E_a, of a chemical reaction taking place at thermal equilibrium is related to V_a, the height of the potential energy barrier separating reactants and products, by the expression[19]

$$E_a = V_a + RT\Theta$$

where the last term takes into account the temperature dependence of reactant and activated complex partition functions. However, in our experiments the methyl radicals are not in thermal equilibrium with their surroundings, and a quantity of more direct relevance than E_a or V_a is the threshold energy, E_t; *i.e.*, the minimum energy at which reaction can occur, or at which the reactive cross section becomes finite. Except for reactions of atoms, the threshold will depend on both relative translational energy and the vibrational and rotational states of the reactants. Furthermore, if quantum mechanical tunneling through the barrier is significant, E_t is restricted only by

TABLE I: Photolysis of CH_3Br–D_2 Mixtures

P_{D_2}, Torr	P_{CH_3Br}, Torr	R_{CH_3D}/R_{CH_4}	k_8/k_2
395.0	10.8	1.510	0.041
198.2	9.8	0.996	0.049
111.8	9.8	0.520	0.046
55.5	9.9	0.355	0.063
		Mean	$0.050 \pm 0.006_8$

the endothermicity of the reaction. Phenomenologically, the threshold may depend on the sensitivity of the method used to measure the rate of reaction.

The limited data available indicate that differences between V_a, E_a, and E_t are not much larger than the usual experimental errors in these quantities. Gann and Dubrin[20] have determined the threshold energy for the reaction

$$H + C_4D_{10} \rightarrow HD + C_4D_9$$

to be 7–8 kcal/mol, whereas $E_a \simeq$ 8–10 kcal/mol.[21] For the reaction

$$D + H_2 \rightarrow DH + H$$

E_t was found to be 7.5 kcal/mol,[23] whereas the activation energy is 7.6 kcal/mol.[24] For this same reaction, classical trajectory calculations on a surface with a barrier height of 9.13 kcal/mol give an activation energy[25] of 6.9 kcal/mol and a threshold[26] of 6.6 kcal/mol. For the reaction

$$F + H_2 \rightarrow FH + H$$

the experimental[28] activation energy is 1.71 kcal/mol. Classical trajectory calculations[29] on a surface with a barrier height of 0.90 kcal/mol give an activation energy of 1.57 kcal/mol and a threshold of about 0.75 kcal/mol.

The experimental determination of the activation energy for reaction 5 has been discussed elsewhere.[6,7] The best value is $E_{a5} = 10.9$ kcal/mol, with the analogous $E_{a8} = 12.2$ kcal/mol. An estimate of V_a can be made from the experimental value of E_a and a model for the activated complex that will permit the evaluation of Θ. Both a BEBO model and an LEPS model without tunneling[7] indicate that V_a and E_a differ by less than 1 kcal/mol. An LEPS model with tunneling included (and probably overestimated) gives V_a larger that E_a by 2.5 kcal/mol.

We believe, therefore, that the measured activation energies for hydrogen abstraction can be adopted as threshold energies with errors of no more than 1–2 kcal/mol; these values are given in Table V.

2. Photodissociation of Methyl Halides. The absorption spectra of alkyl halides generally exhibit broad bands in the near ultraviolet attributable to n $\rightarrow \sigma^*$ transitions.[30] Methyl iodide vapor has an absorption maximum at 258 nm (ϵ 380), whereas the corresponding peak in methyl bromide is at 203 nm (ϵ 264). The lack of structure in the bands for both molecules indicates that the upper electronic state is a repulsive state, from which dissociation takes place within a time comparable to the period of a molecular vibration.

Because there are low-lying excited states of both Br and I atoms, two dissociation processes are possible

$$CH_3X + h\nu \rightarrow CH_3^* + X(^2P_{3/2}) \quad (1a)$$

or

$$CH_3X + h\nu \rightarrow CH_3^* + X(^2P_{1/2}) \quad (1b)$$

(X = Br or I)

The bond dissociation energy D_0 of the C–I bond in methyl iodide is 54.2–55.0 kcal/mol,[31] and the difference in energies for the two states of the iodine atom is 21.7 kcal/mol (Table II). Photofragment spectroscopy[4f] indicates that photodissociation of CH_3I at 266 nm proceeds predominantly (two-thirds to three-fourths of the total yield) by process 1b, in agreement with spectral analysis.[30a]

Energies of the corresponding photodissociation processes[32,33] of CH_3Br are also given in Table II. The absorption spectrum has been interpreted as indicating that process 1b is unimportant.[34] With the exception of this difference, the photodissociation process for CH_3Br at wavelengths near λ_{max} of the n $\rightarrow \sigma^*$ band should be comparable to that of CH_3I at the corresponding wavelengths.

In addition to processes 1a and 1b, in the case of CH_3I there are minor contributions from

$$CH_3I + h\nu \rightarrow CHI + H_2 \quad (1c)$$

$$CH_3I + h\nu \rightarrow CH_2 + HI \quad (1d)$$

In the photolysis of CH_2TI at $\lambda \leq 315$ nm, Tsao and Root[5o] found evidence for the production of HT by reaction 1c; however, unless the amount of hydrogen produced was large enough to change the isotopic composition of hydrogen used as a reactant, this type of reaction should not affect our measurements of relative methane yields.

Process 1d, which has been reported by Rowland and coworkers[35] in the photolysis of CH_3I at 230 nm, is potentially more troublesome, as the following reactions could then take place

$$^1CH_2 + H_2 \rightarrow CH_4^*(\text{vibrationally excited})$$

$$CH_4^* \rightarrow CH_3 + H$$

$$CH_4^* + M \rightarrow CH_4 + M$$

$$^1CH_2 + M \rightarrow {}^3CH_2 + M$$

$${}^3CH_2 + H_2 \rightarrow CH_4^* \rightarrow CH_3 + H$$

Rowland's results indicate that less than 5% of the photodissociation events produce methylene, and that about 95% of the methylene is produced in the triplet state. Methane produced by reaction with H_2 should be vibrationally excited, with a high probability of decomposition to methyl and hydrogen atom. Braun, Bass, and Pilling[36] found this reaction to be important for singlet methylene, but it was at least two orders of magnitude less rapid for triplet methylene. Furthermore, the thermochemistry of the reaction rules out the possibility that methyl radicals are produced with enough excess energy to react with hydrogen.

To confirm these predictions, we photolyzed CH_3Br–D_2 mixtures, and searched for CH_2D_2 by mass spectrometric analysis of the reaction mixture. It was found to constitute $\leq$3% of the total methane produced, so we conclude that photodissociation process 1a is the only important one in our experiments.

3. Energy Partitioning in the Photolysis of Methyl Bromide. With the assumption that photodissociation by process 1a is the only significant source of methyl radicals in our experiments, we now consider the energetics of this process in some detail.

In the photodissociation of an alkyl halide RX, conservation of energy leads to the expression

$$E_{avl} = h\nu - (D_0 - E_{int}^{RX}) - E_{el}^{X}$$

where E_{avl} is the total energy available after dissociation,

TABLE II: Energetics of Methyl Halide Photodissociation

RX	λ, nm	$h\nu$[a]	D_0	E_{el}^X	E_{int}^{RX}	E_{avl}	Ref
CH_3I	266	107.3	55.0[b]	0.0	1.3	53.6	3f
			54.2[c]	0.0	1.3	54.4	
			55.0	21.7	1.3	31.9	
			54.2	21.7	1.3	32.7	
CH_2TI	276	103.5	56.3[d]	0.0	0.0[d]	47.2	5p
			55.0	0.0	1.3	49.8	
			54.2	0.0	1.3	50.6	
			56.3	21.7	0.0	25.5	
			55.0	21.7	1.3	28.1	
			54.2	21.7	1.3	28.9	
CH_3Br	185	154.6	67.0 ± 2[c]	0.0	1.3	87.6	This work
CD_3Br	185	154.6	68.6 ± 2[e]	0.0	1.3	86.0	This work

[a] All energies in kcal/mole. [b] Value used in ref 3f. [c] Calculated from data in ref 32. [d] Value used in ref 5p. [e] From D_0 for CH_3Br and zero-point vibrational energies of CH_3, CD_3, CH_3Br, and CD_3Br.

$h\nu$ is the energy of the incident photon, D_0 is the energy difference between RX in its ground state and R + X in their ground states, E_{int}^{RX} is the internal energy of RX at the temperature of the experiment, and E_{el}^X is the electronic energy of the halogen atom. The available energy is divided between E_{trans}, the relative translational energy of fragments R and X, and E_{int}^R, the internal energy (rotational and vibrational) of the alkyl radical

$$E_{avl} = E_{trans} + E_{int}^R = E_{trans} + E_{rot}^R + E_{vib}^R$$

Conservation of momentum requires that the translational energy of R (in the laboratory coordinate system) is

$$E_{trans}^R = (M_X/M_{RX})(E_{avl} - E_{int}^R)$$

However, in the center-of-mass coordinate system of the alkyl radical and target molecule AB (A, B = H or D), the relative translation energy is given by

$$E_{CM} = M_{AB}E_{trans}^R/(M_R + M_{AB}) = M_{AB}M_X(E_{avl} - E_{int}^R)/M_{RX}(M_R + M_{AB})$$

The *minimum* energy available for the R + AB reaction is the relative translational energy E_{CM}; if E_{int}^R is not zero, the fraction of it available for reaction will depend on the detailed dynamics of the reaction. Moreover, different models for the photodissociation process lead to significantly different distributions of E_{avl}. We now consider some of these.

A. Pseudodiatomic Model. If the alkyl radical is considered as a structureless mass, E_{int}^R is zero and E_{CM} is given directly in terms of E_{avl} and atomic masses (Table V). There are several arguments against this model. Gordus and Bernstein[16] found an isotopic shift of 280 cm^{-1} between the spectra of CH_3Br and CD_3Br; this is too large to be accounted for by a zero-point energy difference of the C–Br vibrations in the two molecules. Tsao and Root[5p] determined the threshold energy for the reaction of H_2 with CH_2T produced by the photolysis of CH_2TI, and found this to be 103.5 kcal/mol. Even if I atoms are produced in the $^2P_{3/2}$ state, E_{CM} is 4.7 kcal/mol, well below the threshold energy for hydrogen abstraction. In our work, E_{CM} for the $CH_3 + H_2$ system is slightly below the threshold, whereas that for $CH_3 + D_2$ is above the threshold. Nevertheless, the former reaction prevails over the latter.

These arguments are rigorously correct only if the relative kinetic energy distribution of the methyl radicals can be represented by a delta function; the conclusions are somewhat less firm if one takes into account the spread in relative velocities due to the thermal velocity distributions of the parent molecule and the target molecule. Kinematically, this system is particularly unfavorable because the target molecule, due to its light mass, has a mean thermal velocity that is not negligible relative to the methyl radical velocity. The appropriate distribution functions have been derived by Chantry.[37]

The effect of a finite velocity distribution has been estimated from the expression for a bimolecular rate constant in terms of the reduced mass of collision partners μ, the relative kinetic energy E_{rel}, the distribution function $P(E_{rel})$, and the reactive cross section $S_r(E_{rel})$

$$k_{bim} = \int_0^\infty P(E_{rel})S_r(E_{rel})(2E_{rel}/\mu)^{1/2}\, dE_{rel}$$

With a step function for S_r, the rate constant calculated with the step at the assumed threshold value of 10.9 kcal/mol was compared to that calculated with the step at E_{CM}. In the Tsao and Root experiments this ratio is 0.05, so the velocity spread is relatively unimportant. A more realistic form of S_r, such as that described below, will decrease the ratio further.

Similar calculations for our experiments give a ratio of 0.57 for the rate of $CH_3 + H_2$ with the step function at 10.9 kcal/mol compared with that for the step at 8.7 kcal/mol (E_{CM}), so the velocity distribution spills over significantly above the threshold. However, the same ratio for $CH_3 + D_2$ (step function at 12.2 or 15.5 kcal/mol) is greater than unity, since E_{CM} is larger than E_t. Therefore, from the observed kinetic isotope effect, it still appears necessary to assume that internal energy of the methyl radical is available for reaction.

The most direct evidence against the pseudodiatomic model comes from photofragment spectroscopy,[4f] and the results for the photolysis of methyl iodide are given in Table III.

B. Franck-Condon Dissociation Model. In methyl bromide or iodide, the H–C–H interbond angle is 111.8°, whereas in planar methyl it is 120°. If the C–X bond dissociates before relaxation of this angle can take place, the methyl radical will be formed in an excited state of the out-of-plane vibrational mode (ν_2). In terms of ζ, the perpendicular displacement of the C atom from the plane of the three H atoms, the potential energy is given by

$$V = (\tfrac{1}{2})k\zeta^2 + a\zeta^4$$

TABLE III: Energy Partitioning in Photolysis of Methyl Halides

RX	λ, nm	X state	E_{int}^R/E_{avl} Expt[a]	Expt[b]	Statistical	Rigid radical	Soft radical
CH_3I	266	$^2P_{1/2}$	0.12	0.14	0.8–0.9	0.0	0.18
		$^2P_{3/2}$	0.16	0.17	0.8–0.9	0.0	0.18
CH_2TI	276	$^2P_{3/2}$ or $^2P_{1/2}$			0.8–0.9	0.69	0.27
CH_3Br	185	$^2P_{3/2}$			0.8–0.9	0.0	0.18
CD_3Br	185	$^2P_{3/2}$			0.8–0.9	0.0	0.29

[a] With $D_0 = 55.0$ kcal/mol. [b] With $D_0 = 54.2$ kcal/mol.

The force constants in this coordinate system are related to those of Pimentel and coworkers[38] according to

$$k(\text{this work}) = 3k_z(\text{Pimentel}) = 3(0.317 \text{ mdyn Å}^{-1})$$

$$a(\text{this work}) = 9a(\text{Pimentel}) = 9(0.098 \text{ mdyn Å}^{-1})$$

In going from the planar configuration to the methyl configuration of CH_3I, ζ increases from 0 to 0.315 Å, and the resulting potential energy increase is 4.2 kcal/mol. *Ab initio* molecular orbital calculations lead to a similar estimate of the potential energy change (4.5–5.0 kcal/mol).[39] This is very close to the value of E_{int}^R found by Riley and Wilson for dissociation to I ($^2P_{1/2}$), but only about half the value found for dissociation to ground state I.

Recently, kinetic spectroscopy of CH_3 and CD_3, produced by flash photolysis of methyl iodide and dimethylmercury, has been reported by Pimentel and coworkers.[38] Their results seem to disagree with the prediction that ν_2 will be excited, and they propose that excess vibrational energy is localized in the ν_1 (C–H stretching) mode. However, it is not clear just how applicable their results are to Riley and Wilson's experiment or to steady-state photolysis experiments with monochromatic light. Their flash source emits light that probably covers the entire absorption band of methyl iodide, so there is a large spread in E_{avl}. Since the energy required for excitation to the $\nu_1 = 1$ level is about 8.6 kcal/mol, *greater than* E_{int}^R found in the dissociation of CH_3I to form I ($^2P_{1/2}$), it is evident that the excitation of ν_1 cannot be the only form of internal energy in the hot methyl radical.

C. Statistical Vibrational Model. In contrast to the Franck–Condon model is the statistical model proposed by Riley and Wilson, in which E_{avl} is distributed among *all* vibrational modes of the photodissociating molecule. This model gives, as a rough approximation

$$E_{vib}^R = (3N - 7)E_{avl}/(3N - 6)$$

where N is the number of atoms in RX. Thus, for CH_3X, $E_{vib}^R/E_{avl} \simeq 0.9$ (Table III). This is much higher than the experimental ratio, but it would obviously be high enough to account for the reaction with hydrogen (Table V).

D. Rigid Radical Model. The "rigid radical" impulsive model emphasizes the rotational fraction of E_{int}^R. It is assumed that R and X recoil along the C–X bond axis. If R has a center of mass displaced from the line extending the C–X bond, recoil will impart an angular momentum to R. Tsao and Root[5b] have used a similar model in discussing the photolysis of CH_2TI, since isotopic substitution destroys the C_{3v} symmetry of the molecule. However, for CH_3X or CD_3X, this model would predict that $E_{rot}^R = E_{int}^R = 0$; it becomes identical with the pseudodiatomic model, which has already been discussed.

TABLE IV: Internal Energy (kcal/mol) of Methyl Radicals Predicted from Photodissociation Models

RX	E_{avl}	E_{int}^R Expt[c]	Pseudo-diatomic	Statistical	Rigid radical	Soft radical
CH_3I	32.7[a]	4.7	0.0	27.8	0.0	5.9
	54.4[b]	9.4	0.0	46.2	0.0	9.8
CH_2TI	28.9[a]	4.0	0.0	24.6	19.9	7.8
CH_2TI	50.6[b]	8.6	0.0	43.0	34.8	13.6
CH_3Br	87.6	14.9	0.0	74.5	0.0	15.3
CD_3Br	86.0		0.0	73.1	0.0	24.9

[a] I in $^2P_{1/2}$ state. [b] I in $^2P_{3/2}$ state. [c] Calculated with the assumption that E_{int}^R/E_{avl} for CH_3Br and CH_2TI is equal to that measured for CH_3I at 266 nm.

E. Soft Radical Model. A second impulsive model proposes a "soft" radical, with the available energy initially utilized in the recoil of the αC and X atoms. The carbon atom then "collides" with the rest of the alkyl radical, imparting vibrational energy to it. It can be shown that[4e]

$$E_{int}^R/E_{avl} = 1 - [M_C(M_R + M_X)/M_R(M_C + M_X)]$$

Furthermore, this energy is entirely vibrational. The fraction E_{int}^R/E_{avl} calculated from this model is consistently higher than that obtained by photofragment spectroscopy (Tables III and IV). However, calculated values do follow the trend toward a higher ratio observed with larger alkyl groups,[4f] and the ratio calculated for methyl iodide is only 10–20% higher than the mean of the experimental values for dissociation into the two I atom states.

With this model, the total energy available for the reaction of methyl with hydrogen in our experiments is much greater than the threshold energy (Table V). However, the agreement with the photolysis threshold of Tsao and Root is found only if the process they observe produces I ($^2P_{1/2}$) and not I ($^2P_{3/2}$). Our observation that hexafluoroethane is a much better moderator than helium, with respect to the reaction of methyl and deuterium, is also consistent with the prediction that most of the energy of the hot radical is vibrational. Callear and van den Bergh[40] found that polyatomic molecules were 10–20 times as efficient as He for the vibrational relaxation of CH_3*. By contrast, a hard-sphere model for the transfer of translational energy predicts that He is about twice as efficient as C_2F_6.

4. Isotope Effects. The ratios of rate constants for the reactions of hot CH_3 (or CD_3) with H_2 and D_2 found in

TABLE V: Total Energy (kcal/mol) Available for the Reaction R + AB Predicted from Photodissociation Models

		$E_{int}^{R} + E_{CM}$					
RX	AB	Expt	Pseudo-diatomic	Statistical	Rigid radical	Soft radical	Threshold
CH_2TI^a	H_2	10.0	2.7	25.0	20.7	9.8	10.9
CH_2TI^b	H_2	12.5	4.7	43.8	36.3	17.5	10.9
CH_3Br	H_2	22.1	8.7	75.9	8.7	22.5	10.9
CH_3Br	HD	25.1	12.3	76.3	12.3	25.4	~11.5
CH_3Br	D_2	27.8	15.5	76.8	15.5	28.1	12.2
CD_3Br	H_2		7.0	74.1	7.0	29.9	10.9
CD_3Br	HD		10.1	74.6	10.1	32.0	~11.5
CD_3Br	D_2		12.7	75.0	12.7	33.9	12.2

[a] I in $^2P_{1/2}$ state. [b] I in $^2P_{3/2}$ state.

this work can be compared with the corresponding ratios obtained in the thermal reactions.[7] With hot CH_3, the ratio k_5/k_8 is 2.12, whereas for the thermal reaction at 25°, this ratio is 8.57. The ratios for CD_3 are k_{14}/k_{15} = 0.465 (hot radical) and 4.30 (thermal reaction).

There are relatively few other reactions of hot radicals for which isotope effects have been reported. With CH_3 and CD_3 produced by photolysis of methyl iodide at 254 nm, Doepker and Ausloos[5j] found $R_{CD_3H}/R_{CD_4} = R_{CH_4}/R_{CH_3D}$ = 1.31 for the methane produced by hydrogen abstraction from methyl iodide. Mains and Lewis[5m] obtained values of 1.48 and 1.43 for these same ratios, in the flash photolysis of methyl iodide. Doepker and Ausloos also measured the kinetic isotope effect for the reaction of CD_3 with CD_3CH_3 and found $R_{CH_3H}/R_{CD_3} = 0.95$. For the reaction of CD_3 with an equimolar mixture of C_4H_{10} and C_4D_{10}, they found R_{CD_3H}/R_{CD_4} = 1.25. All of these rate constant ratios are much closer to unity than those reported for similar hydrogen abstraction reactions in thermal systems.[22]

The customary theoretical formulation of kinetic isotope effects is based on activated complex theory, and is derived with the assumption that the reactants have a Boltzmann distribution of energies. Obviously, this approach is not suitable for the interpretation of hot atom or hot radical experiments, where values of rate constants (or reactive cross sections) for a specific reactant energy are needed. Moreover, a complete treatment of the isotope effect would also require consideration of the steady-state energy distribution for the hot reactant, since in any real experiment this will differ from that produced by photodissociation.

Such a detailed treatment does not, at present, seem feasible for the reactions considered here. However, we have tried to approach the problem at a level corresponding to that generally used in the explanation of kinetic isotope effects. This approach uses activated complex theory to calculate an average reactive cross section $\bar{S}_r(E)$ as a function of total energy E[41]

$$\bar{S}_r(E) = (\kappa h^2/8\pi\mu)[\epsilon_\ddagger(E)/\epsilon_1(E)]$$

In this expression, κ is the transmission coefficient, μ is the reduced mass of reactants, $\epsilon_1(E)$ is an energy density function for the reactants, and $\epsilon_\ddagger(E)$ is the number of internal states of the activated complex with total energy less than or equal to E.

We have introduced a further simplification by treating the methyl radical as a structureless mass, thus reducing the problem to that of an atom colliding with a diatomic molecule. Then the only contributions to $\epsilon_1(E)$ come from the one vibrational mode and doubly degenerate rotation of the hydrogen molecule. A direct count method was used to evaluate $\epsilon_1(E)$ for H_2 and D_2, from the expressions given in section IIIC of the paper by Morokuma, *et al.*[41a]

For the activated complex, we have used the actual six-atom moments of inertia for the doubly degenerate rotation and vibrational frequencies calculated for the "three-atom" complex, from force constants and interatomic distances obtained by the BEBO method.[7] At energies of interest in this work (≥20 kcal/mol), the completely classical expression[41a] for $\epsilon_\ddagger(E)$ was found to be a very good approximation, and it was used for the evaluation of $\bar{S}_r(E)$.

The results of these calculations are shown in Figures 9 and 10, together with the appropriate energy distributions for methyl radicals with internal energy calculated from the soft radical model and a distribution in center-of-mass energy calculated from the expressions given by Chantry.[37] The absolute values of these cross sections seem to be unreasonably large.

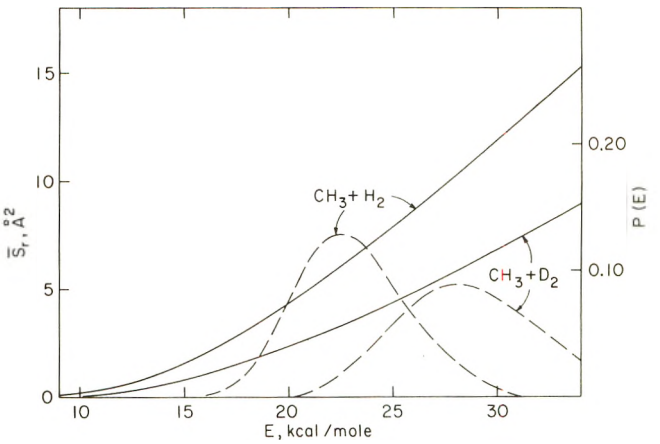

Figure 9. Excitation functions (solid lines) for the reactions $CH_3 + H_2$ and $CH_3 + D_2$, calculated from activated complex theory. Energy distribution (dashed lines) with E_{int}^{R} (15.3 kcal/mol) added to E_{CM} with a thermal distribution.

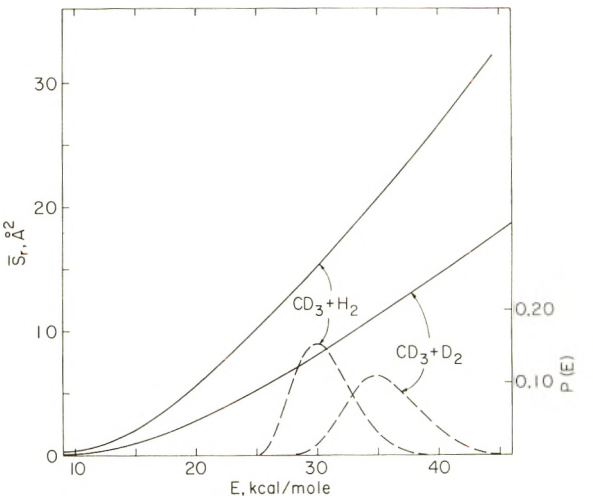

Figure 10. Excitation functions (solid lines) for the reactions $CD_3 + H_2$ and $CD_3 + D_2$, calculated from activated complex theory. Energy distribution (dashed lines) with E_{int}^{R} (24.9 kcal/mol) added to E_{CM} with a thermal distribution.

It is not clear how one calculates a rate constant using the excitation functions obtained from activated complex theory, because the cross section is not simply a function of translational energy. However, if the cross section is weighted in the usual way by the factor $P(E)\ (2E/\mu)^{1/2}$, the following rate constant ratios are obtained: $CH_3 + H_2/CH_3 + D_2 = 1.30$ and $CD_3 + H_2/CD_3 + D_2 = 1.79$. These do not agree very well with the experimental values, and in particular, the reversal between CH_3 and CD_3 is not predicted.

One can probably devise *ad hoc* excitation functions that can be combined with the energy distributions of Figures 9 and 10 to account for the observed results. However, it seems pointless to do this without more detailed knowledge of the energy partitioning in the formation of methyl radicals, and the relative roles of internal and translational energy in surmounting the energy barrier for reaction.

Acknowledgment. We thank Professor J. W. Root and Dr. C.-W. Tsao for communicating their results to us prior to publication, and for many helpful discussions. We also acknowledge helpful discussions with Drs. J. R. Barker, J. T. Muckerman, and M. D. Newton.

References and Notes

(1) This research sponsored by the U. S. Atomic Energy Commission.
(2) (a) T. Carrington, *J. Chem. Phys.*, **41**, 2012 (1964); (b) D. Kley and K. H. Welge, *ibid.*, **49**, 2870 (1968).
(3) (a) R. G. Gann and J. Dubrin, *J. Chem. Phys.*, **47**, 1867 (1967); (b) G. P. Sturm, Jr., and J. M. White, *ibid.*, **50**, 5035 (1970).
(4) (a) K. R. Wilson in "Chemistry of the Excited State," J. N. Pitts, Jr., Ed., Gordon and Breach, New York, N. Y., 1970, and references contained therein; (b) G. E. Busch, R. T. Mahoney, and K. R. Wilson, *IEEE J. Quantum Electron.*, **QE-6**, 171 (1970); (c) G. E. Busch, J. R. Cornelius, R. T. Mahoney, R. I. Morse, D. W. Schlosser, and K. R. Wilson, *Rev. Sci. Instrum.*, **41**, 1066 (1970); (d) R. J. Oldman, R. K. Sander, and K. R. Wilson, *J. Chem. Phys.*, **54**, 4127 (1971); (e) G. E. Busch and K. R. Wilson, *ibid.*, **56**, 3626, 3638, 3655 (1972); (f) S. J. Riley and K. R. Wilson, *Discuss. Faraday Soc.*, **53**, 132 (1972); (g) R. W. Diesen, J. C. Wahr, and S. E. Adler, *J. Chem. Phys.*, **50**, 3635 (1969).
(5) (a) R. D. Schultz and H. A. Taylor, *J. Chem. Phys.*, **18**, 194 (1950); (b) N. R. Davidson and T. Carrington, *J. Amer. Chem. Soc.*, **74**, 6277 (1952); (c) R. B. Martin and W. A. Noyes, *ibid.*, **75**, 4183 (1953); (d) F. P. Hudson, R. R. Williams, Jr., and W. H. Hamill, *J. Chem. Phys.*, **21**, 1894 (1953); (e) G. M. Harris and J. E. Willard, *J. Amer. Chem. Soc.*, **76**, 4678 (1954); (f) R. D. Souffie, R. R. Williams, Jr., and W. H. Hamill, *ibid.*, **78**, 917 (1956); (g) R. F. Pottie, W. H. Hamill, and R. R. Williams, Jr., *ibid.*, **80**, 4224 (1958); (h) R. H. Luebbe, Jr., and J. E. Willard, *ibid.*, **81**, 761 (1959); (i) C. D. Bass and G. C. Pimentel, *ibid.*, **83**, 3754 (1961); (j) R. D. Doepker and P. Ausloos, *J. Chem. Phys.*, **41**, 1865 (1964); (k) R. E. Rebbert and P. Ausloos, *ibid.*, **47**, 2849 (1967); **48**, 306 (1968); (l) R. A. Fass and J. E. Willard, *ibid.*, **52**, 1874 (1970); (m) G. J. Mains and D. Lewis, *J. Phys. Chem.*, **74**, 1694 (1970); (n) J. Saunders and D. S. Urch, *Chem. Phys. Lett.*, **8**, 277 (1971); (o) C.-W. Tsao and J. W. Root, *J. Phys. Chem.*, **76**, 308 (1972); (p) C.-W. Tsao and J. W. Root, *J. Amer. Chem. Soc.*, in press.
(6) R. W. Walker, *J. Chem. Soc. A*, 2391 (1968). Earlier work is reviewed here.
(7) J. S. Shapiro and R. E. Weston, Jr., *J. Phys. Chem.*, **76**, 1669 (1972).
(8) (a) R. J. Carter, W. H. Hamill, and R. R. Williams, Jr., *J. Amer. Chem. Soc.*, **77**, 6457 (1955); (b) R. M. Martin and J. E. Willard, *J. Chem. Phys.*, **40**, 3007 (1964); (c) C. C. Chou and R. S. Rowland, *ibid.*, **50**, 5133 (1969), and references cited therein.
(9) (a) R. E. Weston, Jr., and S. Ehrenson, *Chem. Phys. Lett.*, **9**, 351 (1971); (b) S. Ehrenson and M. D. Newton, *ibid.*, **13**, 24 (1972); (c) K. J. Morokuma and R. E. Davis, *J. Amer. Chem. Soc.*, **94**, 1060 (1972); (d) J. J. Kaufman, J. J. Harkins, and W. S. Koski, *Int. J. Quantum Chem.*, **1s**, 261 (1967).
(10) D. L. Bunker and M. Pattengill, *J. Chem. Phys.*, **53**, 3041 (1970); T. Valencich and D. L. Bunker, *Chem. Phys. Lett.*, **20**, 50 (1973).
(11) (a) F. Bruner and G. P. Cartoni, *J. Chromatogr.*, **18**, 390 (1965); (b) F. Bruner, G. P. Cartoni, and M. Possanzini, *Anal. Chem.*, **41**, 1122 (1969); (c) F. Bruner, G. P. Cartoni, and A. Liberti, *ibid.*, **38**, 298 (1966).
(12) (a) B. Budick, R. Novick, and A. Lurio, *J. Appl. Optics*, **4**, 229 (1965); (b) H. Hunziker, *J. Chem. Phys.*, **50**, 1288 (1969).
(13) (a) M. Zelikoff and L. M. Aschenbrand, *J. Chem. Phys.*, **22**, 1680, 1685 (1954); (b) G. A. Castellion and W. A. Noyes, Jr., *J. Amer. Chem. Soc.*, **79**, 290 (1957).
(14) R. M. Martin and J. E. Willard, *J. Chem. Phys.*, **40**, 2999 (1964).
(15) P. C. Kobrinsky and R. M. Martin, *J. Chem. Phys.*, **48**, 5728 (1968).
(16) A. A. Gordus and R. B. Bernstein, *J. Chem. Phys.*, **22**, 790 (1954).
(17) Note that the numbering of reactions and rate constants differs from that of ref 7.
(18) (a) R. T. K. Baker, M. Silbert, and R. Wolfgang, *J. Chem. Phys.*, **52**, 1120 (1970); (b) R. Wolfgang, *ibid.*, **39**, 2983 (1963); (c) P. J. Estrup and R. Wolfgang, *J. Amer. Chem. Soc.*, **82**, 2665 (1960); (d) D. Seewald, M. Gersh, and R. Wolfgang, *J. Chem. Phys.*, **45**, 3870 (1966); (e) R. N. Porter and S. Kunt, *ibid.*, **52**, 3240 (1970); (f) J. W. Root and F. S. Rowland, *J. Phys. Chem.*, **74**, 451 (1970); (g) R. Wolfgang, *ibid.*, **74**, 4601 (1970); (h) F. S. Rowland, *ibid.*, **74**, 4603 (1970).
(19) R. E. Weston and H. A. Schwarz, "Chemical Kinetics," Prentice-Hall, Englewood Cliffs, N. J., 1972, p 103.
(20) R. G. Gann and J. Dubrin, *J. Chem. Phys.*, **50**, 535 (1969).
(21) From the data[22] for the reaction $H + C_4H_{10}$ and an estimate of the effect of D substitution.
(22) A. F. Trotman-Dickenson and G. S. Milne, *Nat. Stand. Ref. Data Ser., Nat. Bur. Stand.*, **No. 9**, 6 (1967).
(23) A. Kuppermann and J. M. White, *J. Chem. Phys.*, **44**, 4352 (1966).
(24) (a) A. A. Westenberg and N. de Haas, *J. Chem. Phys.*, **47**, 1393 (1967); (b) B. A. Ridley, W. R. Schulz, and D. J. LeRoy, *ibid.*, **44**, 3344 (1966).
(25) M. Karplus and R. N. Porter, *Discuss. Faraday Soc.*, **44**, 164 (1968).
(26) From results[27] for $H + H_2$, averaged over rotational states.
(27) M. Karplus, R. N. Porter, and R. D. Sharma, *J. Chem. Phys.*, **43**, 3259 (1965).
(28) (a) P. D. Mercer and H. R. Pritchard, *J. Phys. Chem.*, **63**, 1468 (1959); (b) G. C. Fettis, J. H. Knox, and A. F. Trotman-Dickenson, *J. Chem. Soc.*, 1064 (1960).
(29) J. T. Muckerman, *J. Chem. Phys.*, **54**, 1155 (1971).
(30) (a) R. S. Mulliken, *J. Chem. Phys.*, **8**, 382 (1940); (b) K. Kimura and S. Nagakura, *Spectrochim. Acta*, **17**, 166 (1961).
(31) D_0, the bond dissociation energy at 0°K, is $D_{298} - 298\Delta C_P$. The last term is 1.3 kcal/mol,[41] and the recommended values of D_{298} are 55.5 ± 3[32] or 56.3 ± 1[33] kcal/mol.
(32) B. de B. Darment, *Nat. Stand. Ref. Data Ser., Nat. Bur. Stand.*, **No. 31**, 23 (1970).
(33) J. A. Kerr, *Chem. Rev.*, **66**, 465 (1966).
(34) P. Fink and C. F. Goodeve, *Proc. Royal Soc., Ser. A*, **163**, 592 (1937).
(35) C. C. Chou, P. Angelberger, and F. S. Rowland, *J. Phys. Chem.*, **75**, 2536 (1971).
(36) W. Braun, A. M. Bass, and M. Pilling, *J. Chem. Phys.*, **52**, 5131 (1970).
(37) P. J. Chantry, *J. Chem. Phys.*, **55**, 2746 (1971).
(38) L. Y. Tan, A. M. Winer, and G. C. Pimentel, *J. Chem. Phys.*, **57**, 4038 (1972).
(39) Private communication from Dr. M. D. Newton of this department.
(40) A. B. Callear and H. E. van den Bergh, *Chem. Phys. Lett.*, **5**, 23 (1970).
(41) (a) K. Morokuma, B. C. Eu, and M. Karplus, *J. Chem. Phys.*, **51**, 5193 (1969); (b) K. Morokuma and M. Karplus, *ibid.*, **55**, 63 (1971); (c) S. H. Lin, K. H. Lau, and H. Eyring, *ibid.*, **55**, 5657 (1971).

Intramolecular Photolytic Interactions of Aromatic Carboxylic Acids in Solution

Lalitha J. Mittal,[1a,b] J. P. Mittal,[1a] and E. Hayon*

Pioneering Research Laboratory, U. S. Army Natick Laboratories, Natick, Massachusetts 01760 *(Received April 30, 1973)*

The primary photolytic processes in aqueous solutions of ionized and nonionized phenylalkylcarboxylic acids and esters, $Ph(CH_2)_nCOOR$ (where R = H, CH_3, and C_2H_5 and n = 1, 2, and 3), at 20° were studied using the technique of flash photolysis. The main observed processes are $Ph(CH_2)_nCOOR \xrightarrow{h\nu}$ $PhCH_2\cdot + \cdot(CH_2)_{n-1}COOR$ (25) and $Ph\cdot + \cdot(CH_2)_nCOOR$ (26). No evidence was obtained for either photoionization or rupture of the $Ph(CH_2)_nCOO$–R bond. The nature of –R was, however, found to influence the relative importance of the two photoprocesses. The ratio ϕ_{26}/ϕ_{25} was found to be 0.7, 1.5, and 3.0, respectively, when R = H, CH_3, and C_2H_5. The major process observed in the photolysis of ionized phenylalkylcarboxylic acids was photoionization, leading to the production of e_{aq}^- and carbon dioxide: $Ph(CH_2)_nCOO^- \xrightarrow{h\nu} Ph(CH_2)_n\cdot + e_{aq}^- + CO_2$ (27) and $Ph\cdot + \cdot(CH_2)_nCOO^-$ (29). The quantum yield of process 27 was found to increase with increase in n, with ϕ_{27} ratios of 1.0:1.18:1.45 when n = 1, 2, and 3, respectively. The concentrations of the radicals in processes 25–27 and 29 were found to be directly proportional to the square of the incident light intensity, I^2, revealing the biphotonic nature of these processes in water at 20°. The effects of low concentrations of specific quenchers, such as ethyl pyruvate and Ni^{2+} ions, showed that the excited state precursors of these photoprocesses must be relatively long lived, probably the triplet excited states. Since under the experimental conditions used, optical excitation energy was absorbed initially only by the aromatic ring and the photoejected electron comes mainly from the $-COO^-$ group, intramolecular photolytic interactions are clearly indicated. Such interactions are probably enhanced if spatial configuration is favorable by increased electronic overlap and intersystem crossing.

Introduction

Considerable interest exists in the photochemistry of benzyl derivatives and, in particular, of phenylalkylcarboxylic acids. With the former compounds, $Ph(CH_2)_nX$, the interaction of the side chain on optical excitation of the $^1A_{1g} \rightarrow {}^1B_{2u}$ benzene absorption band has been found to be quite strong. Such interactions have been the subject of various studies by photochemists and spectroscopists. The interest in phenylalkylcarboxylic acids is a more particular case (X = COOH) and stems from the important role of the aromatic amino acids phenylalanine and tyrosine as spectroscopic probes for the study of polypeptides and proteins, and as major participants in their photochemistry.

The absorption and fluorescence spectra of a number of aromatic carboxylic acids have been examined at room temperature as a function of pH (see ref 2–4, and references cited therein). The observed changes in the intensity and in the vibronic structure of the $^1A_{1g} \rightarrow {}^1B_{2u}$ benzene absorption band have been attributed[2,3] to the inductive effect of the carboxyl group. The quenching of fluorescence due to the substituent X has been interpreted[3,4] in terms of an intramolecular charge-transfer interaction between the carboxyl group and the aromatic ring. The substituent is suggested to enhance spin–orbit coupling leading[4] to a quenching of fluorescence, enhancement of the intersystem crossing (ISC) rate constant and the phosphorescence yields, and a decrease in the natural phosphorescence lifetime.

Various mechanisms have been proposed for the photochemistry of aromatic carboxylic acids in solution (see ref 5 and 6, and references cited therein). Photoionization and the formation of benzyl radicals have been observed in aqueous solutions[5] at room temperature. While no direct evidence is available with regard to the nature of the excited state precursors in the photochemistry of $Ph(CH_2)_nCOOH$ compounds, it was suggested[5] that electron ejection occurs from the singlet excited state of these aromatic systems. This conclusion differs from that arrived at in more recent work where the photoionization of tyrosine[7,8] and the photoionization and photodissociation of phenylalanine[9,10] in water at 20° were shown to occur from the triplet excited state *via* a biphotonic process.

In this work, we report the results obtained on flash photolysis of phenylacetic acid, phenylpropionic acid, and methyl and ethyl phenylacetate in aqueous solutions. The effects of pH, light intensity, and specific quenchers on the transient species observed were examined in detail.

Experimental Section

The flash photolysis set-up[11] and the experimental conditions[12] used have been described elsewhere. Most of the work was carried out using flash intensities of ~2000 J. The light output from the flash lamps was varied by changing the charging voltage across the lamps, typically from ~17 to ~23 kV, at constant capacitance. The light output was checked and found to be directly proportional to the charging (voltage)^2 in the far-uv region (where optical excitation occurs).

Quartz optical cells of 20-cm path were used throughout. Solutions were prepared with triply distilled water and were degassed by bubbling with prepurified nitrogen gas. Appropriate solution cut-off filters were placed in the outer jacket of the optical cell. Solutions were buffered using perchloric acid, potassium hydroxide, and ~1 m*M* phosphate and borate.

The chemicals used were the best grade available commercially. Phenylacetic acid was obtained from MCB and phenylpropionic acid from K & K. The esters (Eastman and Aldrich) used were further purified by distillation.

All experiments were carried out in oxygen-free solutions at room temperature (~20°).

Results and Discussion

Unless stated otherwise, mainly the first absorption transition $^1A_{1g} \rightarrow {}^1B_{2u}$ of the benzene nucleus of the phenylalkylcarboxylic acids and esters studied was optically excited. This was done by using a 240-nm (15% aqueous acetic acid solution) cut-off filter in the outer jacket of the optical cell. Small but distinct differences exist[3] (~20% lower integrated intensity for the -COOH acids) between the absorption spectra of the ionized and nonionized carboxylic acids. The spectra of the esters are almost identical with those of the corresponding nonionized acids.

It should be clearly stated that, due to certain limitations of the flash photolysis technique, photolytic processes other than those observed and discussed below may also be occurring. However, due to lifetime (flash duration ~10 μsec) and spectral detection limitations, certain photolytic processes may not be observed.

Phenylacetic Acid. The flash photolysis of oxygen-free aqueous solutions of 2 mM phenylacetic acid (pK_a = 4.31) produced transient optical absorptions which are dependent upon the pH of the solution. Figures 1 and 2 show the transient spectra obtained at pH 2.2 and 6.3, respectively. The spectrum at pH 2.2 shows mainly the formation of the characteristic transient absorption of the benzyl $PhCH_2\cdot$ radical. A closer examination of the experimental curve and a comparison with the recently redetermined[13] absorption spectrum of $PhCH_2\cdot$ in water (dotted spectrum in Figure 1) reveals the presence of other absorbing transient species. The following primary photolytic processes can be considered.

$$PhCH_2COOH \xrightarrow{h\nu} \begin{cases} PhCH_2\cdot + \cdot COOH & (1) \\ Ph\cdot + \cdot CH_2COOH & (2) \\ PhCH_2\cdot + CO_2 + (e_{aq}^- + H^+) & (3) \end{cases}$$

Concomitant with the formation of $PhCH_2\cdot$ is the formation of $\cdot COOH$ radicals. The spectrum of this radical[14] has a λ_{max} 235 nm and ϵ_{235} 3×10^3 M^{-1} cm^{-1} and undergoes ionization with a pK_a ~1.4.[15] The spectrum of the basic form

$$\cdot COOH \rightleftharpoons \cdot CO_2^- + H^+ \quad (4)$$

is essentially indistinguishable[14] from that of the acid form. Its maximum could not be observed here due to the strong absorption by phenylacetic acid in this wavelength region. However, based on the known[13] extinction coefficients of the benzyl, ϵ_{318} 9.0×10^3 and ϵ_{307} 4.7×10^3 M^{-1} cm^{-1} and $\cdot COOH$ radicals, and assuming equimolar concentrations of $\cdot COOH$ and $PhCH_2\cdot$ (based on reaction 1), the absorption due to the contribution from $\cdot COOH$ has been derived and is shown in Figure 1. The sum of the absorptions of these two radicals can be seen *not* to account completely for the absorption of the experimental curve, particularly above 330 nm. It is suggested (see also below) that process 2 also occurs and that the residual absorption is due to the carboxylalkyl radical $\cdot CH_2COOH$. The spectrum of this radical has been determined,[14] λ_{max} 320 nm and ϵ_{320} 650 M^{-1} cm^{-1}. It undergoes an acid-base reaction

$$\cdot CH_2COOH \rightleftharpoons \cdot CH_2COO^- + H^+ \quad (5)$$

with a pK_a = 4.5.[14] The absorption of the $\cdot CH_2COO$ radical is red shifted and has[14] a λ_{max} 350 nm and ϵ_{350} 800 M^{-1} cm^{-1}.

The absorption of the phenyl radical, reaction 2, is not observed. In the gas phase, the Ph· radical is reported[16]

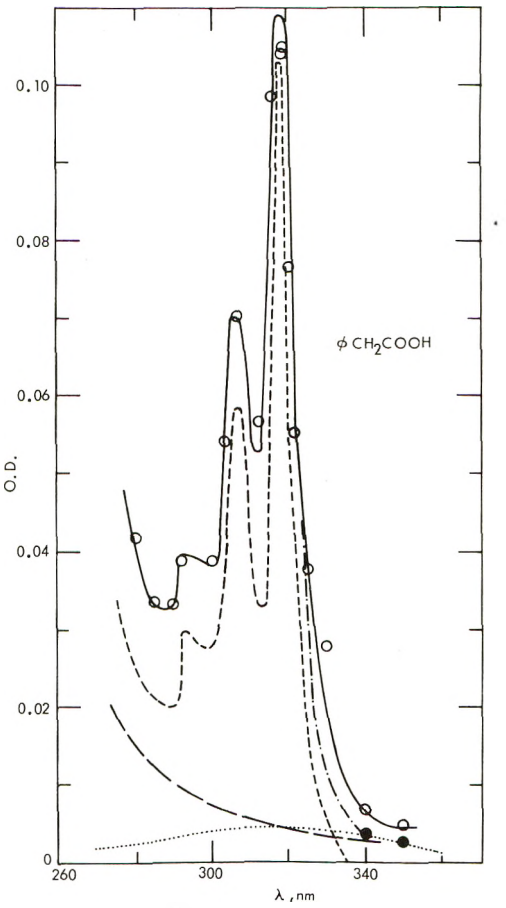

Figure 1. Transient spectrum produced in the flash photolysis of 2 mM phenylacetic acid at pH 2.2, N_2 (O). Spectrum of the $PhCH_2\cdot$ (----), the $\cdot CO_2H$ (--), and the sum of $PhCH_2\cdot$ plus $\cdot CO_2H$ (-·-·) used to synthesize the experimental curve is shown. The spectrum of the CH_2COOH radical (···) obtained by difference is also shown. A 240-nm cut-off filter was used.

to absorb at ~440 nm. A recent[17] indirect method indicated that the maximum is at 260 nm and ϵ 630 M^{-1} cm^{-1}, in aqueous solution. The absorption spectrum of phenyl in water was rechecked. The method utilized dissociative electron capture by chlorobenzene as a means of

$$PhCl + e_{aq}^- \longrightarrow Ph\cdot + Cl^-$$

generating phenyl radicals. A 5 mM PhCl aqueous solution was pulse radiolyzed at pH 9.2 in the presence of 1.5 M *t*-BuOH. The transient spectra were determined in argon (1 atm) and N_2O (1 atm) solutions. The "difference" spectrum is taken to be due to the Ph· radical. The spectrum was similar to the one recently reported,[17] with λ_{max} <270 nm and ϵ_{280} 400 M^{-1} cm^{-1}.

Based on the known extinction coefficients, and $[PhCH_2\cdot]$ = 0.57 μM, $[\cdot CH_2COOH]$ = 0.41 μM, it is interesting to note that $\phi_1/\phi_2 \sim 1.4$.

No evidence is presently available for the occurrence of process 3. Hydrated electrons could not be observed at our time resolutions (~10 μsec) due to the rapid reaction with H^+, with $k_6 = 2.3 \times 10^{10}$ M^{-1} sec^{-1} (ref 18)

$$e_{aq}^- + H^+ \longrightarrow H \quad (6)$$

However, if H atoms were produced *via* reaction 6, or directly, they would have added to the aromatic ring and produced a substituted cyclohexadienyl radical, with an absorption in the region ~320 nm. It is, therefore, concluded on the basis of available information that phenylacetic acid does not undergo photolysis *via* process 3.

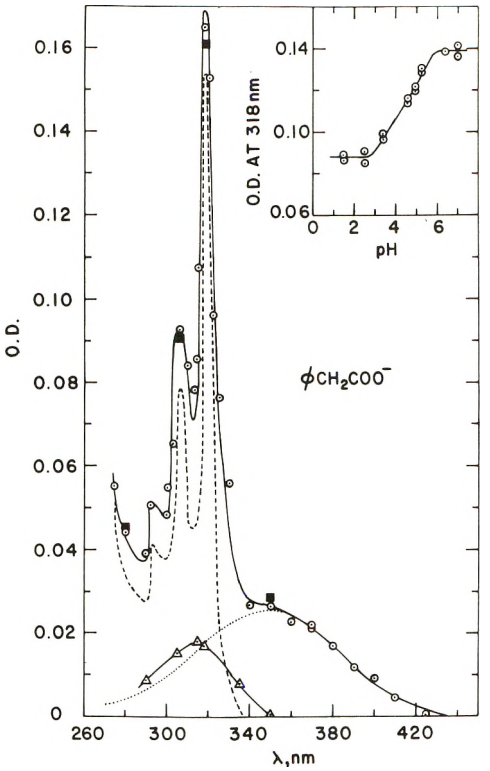

Figure 2. Transient spectrum produced in the flash photolysis of 2 m*M* phenylacetic acid at pH 6.3, N_2 (O) and in N_2O plus 1.0*M* *t*-BuOH (■). Spectrum of the $PhCH_2\cdot$ (----) and the $\dot{C}H_2COO^-$ (•••) radicals used to synthesize the experimental curve is shown. The insert shows change in absorbance at 318 nm with pH in N_2-saturated solutions. The spectrum of the transient produced in the presence of 5×10^{-2} *M* nickel perchlorate is shown (△); cut-off filter 240 nm.

The process

$$PhCH_2COOH \xrightarrow{h\nu} PhCH_2CO\cdot + OH$$

was suggested[6] to occur on photolysis in methanol solutions. No evidence for this process was observed in aqueous solutions. This was concluded on the basis of the absence of a change in the transient spectrum in presence of 1.0 *M* *tert*-butyl alcohol, an efficient scavenger[19] for OH radicals. The OH radical if produced would have added to the benzene ring to give the cyclohexadienyl radical, with a maximum at ~320 nm.

Phenylacetate Ion. The photochemistry of ionized phenylacetic acid in water produced a somewhat different and more intense transient absorption, Figure 2. The following primary processes are considered

$$PhCH_2COO^- \xrightarrow{h\nu} \begin{cases} PhCH_2\cdot + e_{aq}^- + CO_2 & (7) \\ Ph\cdot + \cdot CH_2COO^- & (8) \\ PhCH_2\cdot + \cdot COO^- & (9) \end{cases}$$

The characteristic absorption spectrum of e_{aq}^- with λ_{max} ~720 nm was observed. In order to slow down the decay kinetics of e_{aq}^-, since k (e_{aq}^- + $PhCH_2COO^-$) = 2.0×10^7 M^{-1} sec^{-1} (ref 20), the flash photolysis of 2×10^{-4} *M* phenylacetate at pH 9.2 was monitored at 700 and 318 nm, using a 240-cm cut-off filter. Good reproducible results were obtained under these conditions. Based on ϵ_{700} 1.8×10^4 M^{-1} cm^{-1} (ref 21) for e_{aq}^-, identical concentrations (0.17 μM) of e_{aq}^- and $PhCH_2\cdot$ radicals were obtained. These results confirm the occurrence of process 7. A similar experiment was carried out using a water filter, *i.e.*, a ~200-nm cut-off instead of 240 nm. Under these conditions the $^1A_{1g} \rightarrow {}^1B_{1u}$ as well as the $^1A_{1g} \rightarrow {}^1B_{2u}$ transitions are optically excited. Except for a threefold increase, equimolar concentrations of e_{aq}^- and $PhCH_2\cdot$ radicals were produced. The photoionization of phenylacetate probably produces initially the carboxylate radical $PhCH_2COO\cdot$ which breaks down to $PhCH_2\cdot$ and CO_2.

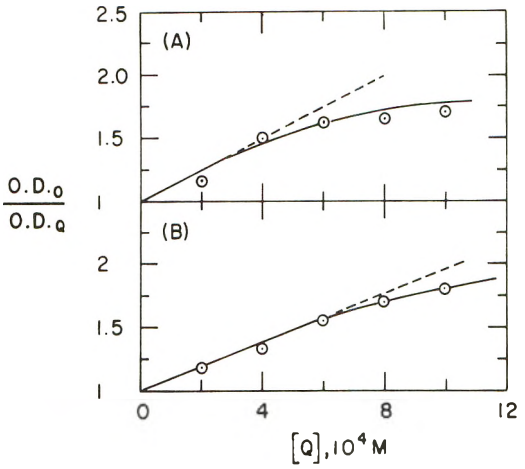

Figure 3. Quenching of the excited state of phenylacetic acid (5 m*M*) by ethyl pyruvate, as a function of the quencher concentration. Monitored at 318 nm; (A) at pH 6.8, 260-nm cut-off filter; (B) at pH 1.5, 250-nm cut-off filter.

The formation of $\cdot CH_2COO$ (process 8) can be seen in Figure 2 from the absorption spectrum of this radical,[14] with λ_{max} 350 nm. The experimental results do not appear to provide room for the occurrence of process 9; all the benzyl radicals are accounted for by the e_{aq}^- measured, process 7, and the experimental curve can be synthesized without any contribution from CO_2^- radicals.

The $\phi_8/\phi_7 \sim 1.8$, but $\phi_8/\phi_2 \sim 3.6$ indicating a much more efficient rupture of $Ph\text{-}CH_2COO^-$ compared to $Ph\text{-}CH_2COOH$. The dependence of the photochemistry of phenylacetic acid upon the state of protonation of the carboxyl group was determined by monitoring the absorption of $PhCH_2\cdot$ at 318 nm as a function of pH. The insert in Figure 2 shows the results obtained: a typical "titration" curve with a midpoint value of 4.4 ± 0.1. This value is in excellent agreement with the pK_a = 4.31 of the ground-state molecule.

Excited State Precursors. As mentioned in the Introduction, the nature of the excited states involved in the photodissociation and photoionization of phenylalkylcarboxylic acids in solution has not been established. To test whether triplet excited states are involved in the photodissociation process leading to the formation of benzyl radicals, two typical quenchers were added in low concentration. The addition of 5×10^{-2} *M* nickel perchlorate (does not absorb >230 nm) to 2 m*M* $PhCH_2COO^-$, pH 6.3, using a 240-nm cut-off filter, produced a relatively very weak and completely different transient absorption, see Figure 2, with λ_{max} ~315 nm. A similar spectrum was also obtained on flash photolysis in presence of N_2O (1 atm) and 1.0 *M* *t*-BuOH. This spectrum is similar to that of Ni^+ produced[22] from the reduction of Ni^{2+} by e_{aq}^-. In the present experiments it could be produced by energy transfer to Ni^{2+} followed by reduction of $*Ni^{2+}$ by H_2O.

Ethyl pyruvate has also been used as a quencher; its triplet energy level E_T is ~2.4 eV (65 kcal/mol).[23] The quenching of the benzyl radical was monitored at 318 nm, and Stern-Volmer plots are given in Figure 3 for results obtained on flash photolysis of phenylacetate at pH 6.8

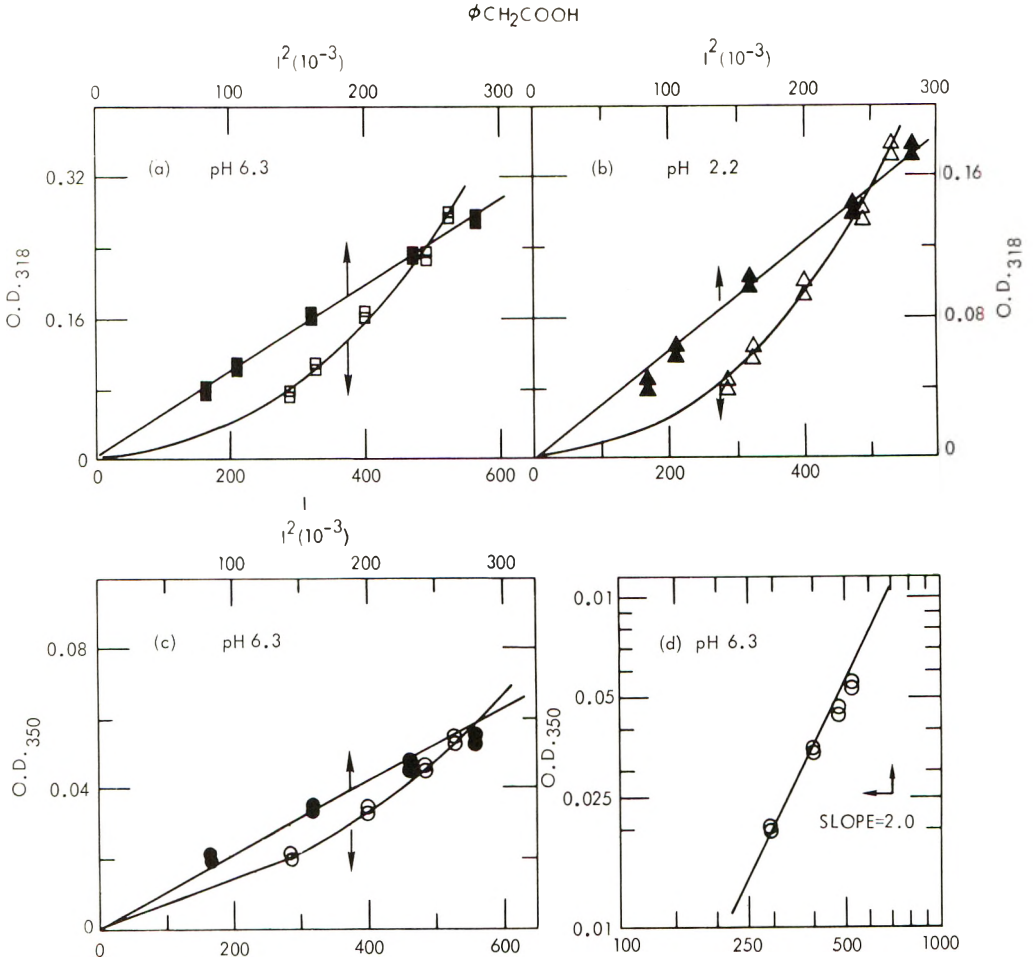

Figure 4. Dependence upon the light intensity (I and I^2) of the concentration of the transient species produced in the flash photolysis of 2 mM phenylacetic acid at different pH values and different wavelengths. A 240-nm cut-off filter was used.

TABLE I: Decay Kinetics of the Intermediates Produced on Flash Photolysis of Aromatic Carboxylic Acids in Oxygen-Free Aqueous Solutions

System[a]	pH	Second-order decay,[b] $2k/\epsilon$, cm sec^{-1}
Phenylacetic acid	2.2	$5.2 \pm 0.3 \times 10^5$
Phenylacetate ion	6.7	$3.1 \pm 0.2 \times 10^5$
Phenylpropionate ion	6.6	$4.7 \pm 0.2 \times 10^5$
Methyl phenylacetate	6.5	$3.0 \pm 0.3 \times 10^5$
Ethyl phenylacetate	6.7	$7.7 \pm 0.6 \times 10^5$

[a] 2 mM solutions of aromatic carboxylic acids and esters were used, and a 240-nm cut-off filter. [b] Decay monitored at 318 nm.

and phenylacetic acid at pH 1.5. Using appropriate cut-off filters, $\ll$5% of the exciting light is absorbed by ethyl pyruvate. These plots depart from linearity due to the formation of increasing amounts of a transient species (which absorbs at 318 nm) with increase in the quencher concentration. Energy transfer from $PhCH_2COO^-$ and $PhCH_2COOH$ to ethyl pyruvate produces a triplet excited state, which then gives rise to a transient species identical with that observed[24] by direct optical excitation of ethyl pyruvate in aqueous solution. From the tangents to these Stern–Volmer plots, a quenching constant of 1.25×10^3 and 9.0×10^3 can be derived at pH 6.8 and 1.5, respectively.

The lifetime of the singlet state of phenylacetic acid has not been determined, but is presumably similar to that of phenylpropionic acid, $\tau_S \sim 8$ nsec.[25] Phenylacetic acid has a $\phi_F \sim 0.04$,[4] identical with that from phenylpropionic acid.[25] Assuming a rate as high as $5 \times 10^{10}\ M^{-1}$ sec^{-1} for the quenching of the singlet excited states of phenylacetic acid and acetate by ethyl pyruvate, the results obtained (Figure 3) at $\geq 2 \times 10^{-4}\ M$ concentration of the quencher must be due to the quenching of a much longer-lived excited state, probably the triplet state.

The dependence of the concentration of the transient species produced upon the intensity of the exciting light (I) was examined. Figure 4 shows the results obtained. On monitoring processes 1 and 7 at 318 nm and process 8 at 350 nm, a linear dependence of $[PhCH_2\cdot]$ and $[\cdot CH_2COO^-]$ upon the square of the light intensity, I^2, was observed in all cases. The experimental results seem quite clear and indicate that (a) the photodissociation of $PhCH_2COOH$ to give $PhCH_2\cdot$ and $\cdot COOH$; (b) the photodissociation of $PhCH_2COO^-$ to give $Ph\cdot$ and $\cdot CH_2COO^-$; and (c) the photoionization of $PhCH_2COO^-$ to give $PhCH_2\cdot$, e_{aq}^- and CO_2, all are biphotonic processes. The lifetime of the triplet excited state precursors must be less than ~ 10 μsec (the lifetime of the exciting light flash), in order for them to absorb a second quanta of light.

Phenylpropionic Acid. The optical excitation of β-phenylpropionic acid in water at pH 2.0 was done without using a cut-off filter (*i.e.*, down to $\sim$200 nm), thus exposing both benzene transitions to light absorption. The transient absorption produced is shown in Figure 5. The main

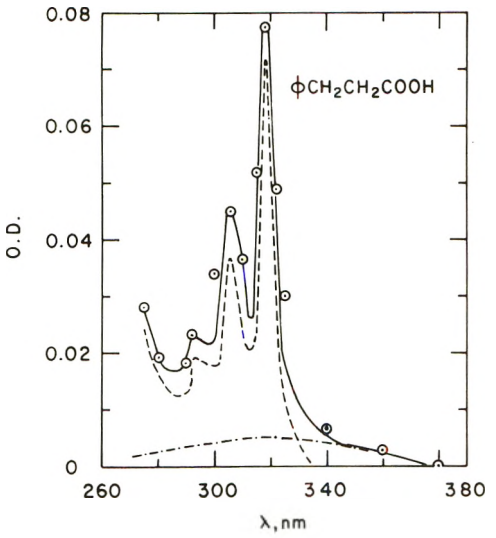

Figure 5. Transient spectrum produced in the flash photolysis of 2 m*M* β-phenylpropionic acid at pH 2.0, N_2 (O). Spectrum of the $PhCH_2\cdot$ (----) and the $\dot{C}H_2COOH$ (-·-·) radicals used to synthesize the experimental curve. No cut-off filter was used.

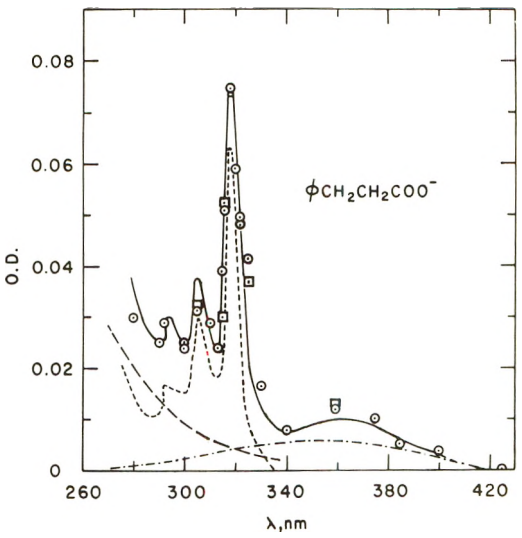

Figure 6. Transient spectrum produced in the flash photolysis of 2 m*M* β-phenylpropionic acid at pH 6.6, N_2 (O) and N_2O plus 1.0*M* *t*-BuOH (□). Spectrum of the $PhCH_2\cdot$ (----), CH_2COO^- (-·-·), and $PhCH_2CH_2\cdot$ (--) radicals used to synthesize the experimental curve. No cut-off filter was used.

species formed appears to be the $PhCH_2\cdot$ radical, with an equimolar concentration of the $\cdot CH_2COOH$ radical. The following primary processes are considered

$$PhCH_2CH_2COOH \xrightarrow{h\nu} \begin{cases} PhCH_2\cdot + \cdot CH_2COOH & (10) \\ PhCH_2CH_2\cdot + \cdot COOH & (11) \\ Ph\cdot + \cdot CH_2CH_2COOH & (12) \\ PhCH_2CH_2\cdot + CO_2 + H(\text{or } e_{aq}^- + H^+) & (13) \end{cases}$$

The experimental results demonstrate the occurrence of process 10 and the absence of process 11. The $PhCH_2CH_2\cdot$ radical starts absorbing[20] below ~340 nm, and the results do not allow for any absorption due to the $PhCH_2CH_2\cdot$ or the $\cdot COOH$ radicals. Process 12 is considered to be occurring even though no evidence for it can be provided. This is because both the Ph· and the $\cdot CH_2CH_2CO$ radicals[14] absorb below ~280 nm. For the same reasons and arguments mentioned above in the case of phenylacetic acid, process 13 does not appear to occur.

The photolysis of β-phenylpropionate ion differs in some respects from that of phenylacetate ion: there does not appear to be a marked dependence of the quantum yield of decomposition upon the ionization of the carboxyl group of phenylpropionic acid. The transient spectrum observed is shown in Figure 6. A strong absorption with λ_{max} ~720 nm due to e_{aq}^- was also observed. No absorption other than that of e_{aq}^- was previously[5] reported. The following photolytic processes can be considered

$$PhCH_2CH_2COO^- \xrightarrow{h\nu} \begin{cases} PhCH_2\cdot + \cdot CH_2COO^- & (14) \\ PhCH_2CH_2\cdot + \cdot CO_2^- & (15) \\ Ph\cdot + \cdot CH_2CH_2COO^- & (16) \\ PhCH_2CH_2\cdot + e_{aq}^- + CO_2 & (17) \end{cases}$$

The experimental spectrum given in Figure 6 has been synthesized to account for (a) equimolar concentrations of $PhCH_2\cdot$ and $\cdot CH_2COO^-$ radicals (process 14, based on the known[13,14] extinction coefficients of these radicals, and (b) equimolar concentrations of e_{aq}^- and $PhCH_2CH_2\cdot$ radicals (process 17), again based on the known[21,20] extinction coefficients and absorption spectra of these radicals. These calculations indicate that $\phi_{17}/\phi_{14} = 2.3$, *i.e.*, that photoionization of the β-phenylpropionate ion is more effective than the rupture of the $PhCH_2$-CH_2COO^- bond (see more below).

It can be seen in Figure 6 that a weak absorption in the 330–450-nm region has not been accounted for. In this wavelength region part of the transient produced was found to decay much faster with a half-life <40 μsec. A similar fast-decaying transient was also observed[10] on flash photolysis of phenylalanine at pH ~6.0. This short-lived absorption is tentatively assigned to the triplet-triplet absorption of the β-phenylpropionate ion.

No evidence appears for the formation of $\cdot CO_2^-$ (process 15). A similar conclusion was reached in the photolysis of the phenylacetate ion. These results cannot exclude the occurrence of process 16; indeed, the feeling is that it probably occurs. It is interesting to note that within 10%, $\phi_{10} \sim \phi_{14}$.

Methyl Phenylacetate. The flash photolysis of oxygen-free 2 m*M* aqueous solution of methyl phenylacetate was carried out at pH 6.0 using a 218-nm (10^{-2} *M* KBr) cut-off filter. The transient spectrum observed is shown in Figure 7. Three primary processes can be considered

$$PhCH_2COOCH_3 \xrightarrow{h\nu} \begin{cases} PhCH_2\cdot + \cdot COOCH_3 & (18) \\ Ph\cdot + \cdot CH_2COOCH_3 & (19) \\ e_{aq}^- + A & (20) \end{cases}$$

The benzyl radical is clearly produced in this system but no absorption due to the partner $\cdot COOCH_3$ could be observed. The $\cdot COOCH_3$ radical was also not observed[24] in the flash photolysis of aliphatic methyl esters. This was explained on the basis of the relatively short lifetime ($\tau \ll 10$ μsec) of this radical. It undergoes rapid unimolecular decomposition to give CO_2 and $\cdot CH_3$

$$\cdot COOCH_3 \longrightarrow CO_2 + \cdot CH_3 \quad (21)$$

The methyl radicals presumably absorb below ~220 nm, are relatively poor reactants, and under flash photolysis conditions probably recombine to produce ethane, C_2H_6.

Evidence for process 19 is available, as shown by the absorption spectrum of the $\cdot CH_2COOCH_3$ radicals, Figure 7. This radical has been reported previously,[26] has a λ_{max} 320 nm, and an ϵ_{320} 800 M^{-1} cm^{-1}. A quantum yield ratio of ϕ_{19}/ϕ_{18} ~ 1.5 was derived based on

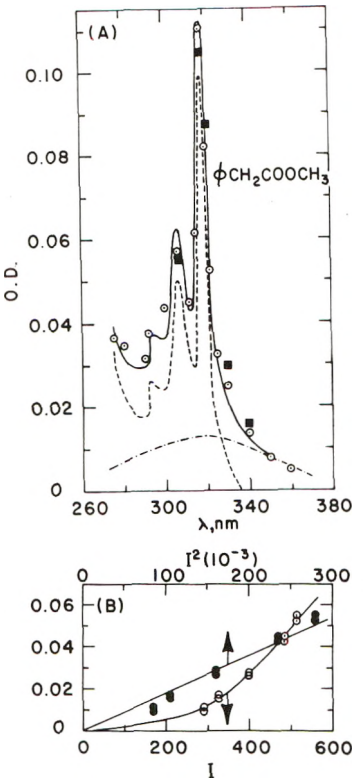

Figure 7. (A) Transient spectrum produced in the flash photolysis of 2 m*M* methyl phenylacetate at pH 6.0, N_2 (O) and in N_2O plus 1.0 *M* *t*-BuOH (■) using a 218-nm cut-off filter. Spectrum of the $PhCH_2\cdot$ (----) and the CH_2COOCH_3 (-·-·) radicals used to synthesize the experimental curve.

$[\cdot CH_2COOCH_3] = 0.81\ \mu M$ and $[PhCH_2\cdot] = 0.55\ \mu M$. These results indicate that the rupture $Ph\text{-}CH_2COOCH_3$ is considerably more efficient than $Ph\text{-}CH_2COOH$ (processes 19 and 2, *i.e.*, $(\phi_{19}/\phi_{18})_{ester} \gg (\phi_1/\phi_2)_{acid}$. No pH dependence was observed in the flash photolysis of $PhCH_2COOCH_3$.

No photoionization of this ester appears to occur (process 20) since the transient absorption produced (Figure 7) was the same in presence or absence of N_2O, an efficient scavenger for e_{aq}^-. These experiments were carried out in presence of 1.0 *M* *tert*-butyl alcohol in order to scavenge the OH radicals produced according to

$$e_{aq}^- + N_2O \longrightarrow N_2 + OH + OH^-$$

The electron adduct to methyl phenylacetate is expected[20] to absorb in the 300–330-nm region.

The absorbance at 318 nm was monitored as a function of the incident light intensity (I) from the flash lamps. A linear dependence upon the square of the light intensity, I^2, was found (see Figure 7). The transients produced from both processes 18 and 19 absorb at this wavelength. These results demonstrate that (a) the photolysis occurs *via* a biphotonic process, and (b) long-lived excited states are the precursors of these processes.

Ethyl Phenylacetate. The photochemistry of ethyl phenylacetate is qualitatively similar to that of methyl phenylacetate

$$PhCH_2COOC_2H_5 \xrightarrow{h\nu} \begin{cases} PhCH_2\cdot + \cdot COOC_2H_5 & (22) \\ Ph\cdot + \cdot CH_2COOC_2H_5 & (23) \\ e_{aq}^- + B & (24) \end{cases}$$

Processes 22 and 23 occur (see Figure 8), but no evidence for process 24 is available. The $\cdot COOC_2H_5$ radical also decays very fast to produce CO_2 and $\cdot C_2H_5$ radicals. The

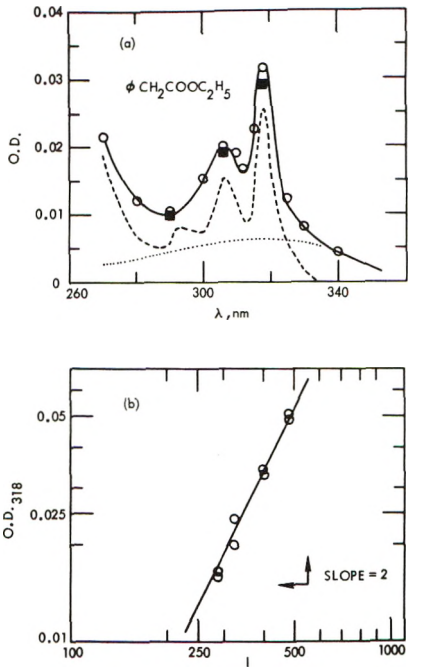

Figure 8. Transient spectrum produced in the flash photolysis of 2 m*M* ethyl phenylacetate at pH 6.7, N_2 (O), using a 240-nm cut-off filter. Spectrum of the $PhCH_2\cdot$ (----) and the $\cdot CH_2COOC_2H_5$ (·····) radicals used to synthesize the experimental curve. Dependence of OD_{318} upon the intensity (I) of the exciting light (curve b).

$\cdot CH_2COOC_2H_5$ radical is expected to have the same spectrum and extinction coefficient as the $\cdot CH_2COOCH_3$ radical.[26] The ratio $\phi_{23}/\phi_{22} \sim 3.0$, *i.e.*, process 23 is the predominant reaction. The corresponding ratios for methyl phenylacetate and phenylacetic acid are 1.5 and 0.7, respectively. Thus a marked dependence upon the nature of the substituent R in $PhCH_2COOR$ (where R = C_2H_5, CH_3, and H) can be noted for the photolytic rupture of the $Ph\text{-}CH_2COOX$ bond.

The dependence of the formation of processes 22 and 23 upon the light intensity was monitored at 318 nm. A linear dependence upon I^2 was found, see Figure 8, indicating that these processes are biphotonic and have a long-lived excited state, probably the triplet, as the precursor.

Conclusions

Similar primary photolytic processes were observed in aqueous solutions from nonionized phenylalkylcarboxylic acids and the corresponding esters

$$Ph(CH_2)_nCOOR \xrightarrow{h\nu} \begin{cases} PhCH_2\cdot + \cdot(CH_2)_{n-1}COOR & (25) \\ Ph\cdot + \cdot(CH_2)_nCOOR & (26) \end{cases}$$

where R = H or alkyl group, and n = 1 and 2. No evidence was obtained for either photoionization or rupture of the $Ph(CH_2)_nCOO\text{-}R$ bond. The nature of R, however, was found to have a considerable influence upon the relative importance of processes 25 and 26. For $PhCH_2COOR$ the ratio ϕ_{26}/ϕ_{25} was found to be 0.7, 1.5, and 3.0, respectively, when R = H, CH_3, and C_2H_5.

The fluorescence quantum yield ϕ_F at 300°K for $PhCH_2COOH$, $PhCH_2COO_2H_5$, and $PhCH_2CH_2COOH$ is ~0.04[4,25] and $\tau_F \sim 8$ nsec.[25] At 77°K in EPA or alcohol glasses these acids have a phosphorescence lifetime of ~5–7 sec[2,4] and a (0,0) band at 341 nm.[2] From absorption spectra and luminescence studies it was concluded[2-4] that the -COOR group enters into an intramolecular

charge-transfer interaction with the phenyl group, *e.g.*, fluorescence quenching was found[4] to be very pronounced in fluid media in contrast to rigid glasses where intramolecular relaxation processes are inhibited. In the flash photolysis experiments described above, the photodissociation processes 25 and 26 were found to occur *via* a long-lived excited state, probably the triplet state, in water at 20°. Furthermore, these processes were biphotonic. Since the duration of the flash was ~10 μsec, one must conclude that the triplet must be produced in times <10 μsec.

The photolysis of ionized phenylalkylcarboxylic acids does not lead to the corresponding process 25. Instead, the major reaction leads to photoionization (process 27). Process 27 was shown to be biphotonic and hence to involve a long-lived triplet excited state. Indeed both the photoionization and photodissociation reactions of $Ph(CH_2)_nCOO^-$ are biphotonic and occur from long-lived excited states.

$$Ph(CH_2)_nCOO^- \xrightarrow{h\nu} \begin{cases} Ph(CH_2)_n\cdot + e_{aq}^- + CO_2 & (27) \\ PhCH_2\cdot + \cdot(CH_2)_{n-1}COO^- & (28) \\ Ph\cdot + \cdot(CH_2)_nCOO^- & (29) \end{cases}$$

The quantum yield of process 27, as determined from the amount of e_{aq}^- produced at "zero time" after the flash,[27] was 1:1.18:1.45 when n = 1, 2, and 3, respectively. The above-mentioned results demonstrate (a) that the photoejected electron comes from the $-COO^-$ group, (b) that since the exciting energy is absorbed initially by the aromatic ring, intramolecular interactions of the triplet excited state must occur, and (c) that such an interaction is enhanced if spatial configuration is favorable by increased electronic overlap and intersystem crossing.

Intramolecular charge-transfer interactions have been suggested[2-4] to explain absorption and fluorescence results. Intramolecular excitation transfer between nonconjugated chromophores is known.[28] This possibility cannot be excluded, since the energy level of the biphotonically excited triplet $Ph(CH_2)_nCOO^-$ could be well above the triplet energy level of the $-COO^-$ group.

The pK_a values of triplet excited states of aromatic compounds are known to be close to the dissociation constants of the ground-state molecules.[29] The changes with pH in the photolytic processes observed are considered to result, however, from the change in the concentration of the nonionized or ionized forms of the phenylalkylcarboxylic acids.

References and Notes

(1) (a) Permanent address, Bhabha Atomic Research Center, Trombay, Bombay, India. (b) This work is based on a dissertation to be submitted in partial fulfillment of the Ph.D. Degree, University of Bombay, Bombay, India.
(2) H. J. Maria and S. P. McGlynn, *J. Chem. Phys.*, **52**, 3399 (1970).
(3) J. Tournon and M. A. El-Bayoumi, *J. Amer. Chem. Soc.*, **93**, 6396 (1971).
(4) J. Tournon and M. A. El-Bayoumi, *J. Chem. Phys.*, **56**, 5128 (1972).
(5) H. I. Joschek and L. L. Grossweiner, *J. Amer. Chem. Soc.*, **88**, 3261 (1966).
(6) T. O. Meiggs and S. I. Miller, *J. Amer. Chem. Soc.*, **94**, 1989 (1972).
(7) J. Feitelson and E. Hayon, *J. Phys. Chem.*, **77**, 10 (1973).
(8) J. Feitelson, E. Hayon, and A. Treinin, *J. Amer. Chem. Soc.*, **95**, 1025 (1973).
(9) L. J. Mittal, J. P. Mittal, and E. Hayon, *Chem. Phys. Lett.*, **18**, 319 (1973).
(10) L. J. Mittal, J. P. Mittal, and E. Hayon, *J. Amer. Chem. Soc.*, in press.
(11) L. Dogliotti and E. Hayon, *J. Phys. Chem.*, **71**, 2511 (1967); M. Langmuir and E. Hayon, *J. Phys. Chem.*, **71**, 3808 (1967).
(12) L. J. Mittal, J. P. Mittal, and E. Hayon, *Photochem. Photobiol.*, in press.
(13) J. P. Mittal and E. Hayon, *Nature (London)*, **240**, 20 (1972).
(14) P. Neta, M. Simic, and E. Hayon, *J. Phys. Chem.*, **73**, 4207 (1969).
(15) G. V. Buxton and R. M. Sellers, *J. Chem. Soc., Faraday Trans.*, **69**, 555 (1973).
(16) G. Porter and B. Ward, *Proc. Chem. Soc.*, 288 (1964); *Proc. Roy. Soc., Ser. A*, **287**, 457 (1965).
(17) B. Cercek and M. Kongshaug, *J. Phys. Chem.*, **74**, 4319 (1970).
(18) M. Anbar and P. Neta, *Int. J. Appl. Radiat. Isotopes*, **18**, 493 (1967).
(19) M. Simic, P. Neta, and E. Hayon, *J. Phys. Chem.*, **73**, 3794 (1969).
(20) J. P. Mittal and E. Hayon, to be submitted for publication.
(21) E. J. Hart and M. Anbar "The Hydrated Electron," Wiley-Interscience, New York, N. Y., 1970.
(22) J. H. Baxendale, E. M. Fielden, and J. P. Keene, *Proc. Roy. Soc.*, **286**, 320 (1965).
(23) G. S. Hammond, P. A. Leermakers, and N. J. Turro, *J. Amer. Chem. Soc.*, **83**, 2395 (1961).
(24) L. J. Mittal, J. P. Mittal, and E. Hayon, *J. Phys. Chem.*, **77**, 1482 (1973).
(25) J. Feitelson, *J. Phys. Chem.*, **68**, 391 (1964).
(26) M. Simic and E. Hayon, *Radiat. Res.*, **48**, 244 (1971).
(27) Experiments carried out at pH 9.2, 2×10^{-4} *M* $Ph(CH_2)_nCOO^-$, and a water filter, *i.e.*, both the $^1A_{1g} \rightarrow {}^1B_{2u}$ and the $^1A_{1g} \rightarrow {}^1B_{1u}$ transitions were optically excited.
(28) A. A. Lamola, P. A. Leermakers, G. W. Byers, and G. S. Hammond, *J. Amer. Chem. Soc.*, **87**, 2322 (1965); D. O. Conway and A. A. Baum, *J. Amer. Chem. Soc.*, **93**, 1153 (1971), and other references cited therein.
(29) E. Van der Donckt, *Progr. React. Kinet.*, **5**, 273 (1970).

Ionization Constants and Spectral Characteristics of Some Semiquinone Radicals in Aqueous Solution

P. S. Rao[1] and E. Hayon*

Pioneering Research Laboratory, U. S. Army Natick Laboratories, Natick, Massachusetts 01760 *(Received April 19, 1973)*

Publication costs assisted by Natick Laboratories

The ionization constants, absorption maxima, and extinction coefficients of the semiquinone radicals and radical anions of 12 quinones were determined. These were obtained in aqueous solutions in the presence of 1–3 *M* *tert*-butyl alcohol or isopropyl alcohol by electron e_{aq}^- attachment, using the technique of pulse radiolysis. Various benzoquinones, naphthaquinones, anthraquinones, diphenoquinone, epinephrine, and adrenalone were studied. The ionization constants range from 3.2 to 5.4. These values are correlated with the redox potentials of the corresponding quinones. The decay kinetics of some semiquinone radicals and radical anions were determined.

A large number of quinones are known[2] to occur in nature and to play an important part in oxidation–reduction reactions. The role of semiquinone radicals as active agents in biochemical electron transfer reactions has been indicated.[2,3] Recently, the kinetics in aqueous solutions of electron transfer processes from free radicals (leading to the oxidation or reduction of these free radicals) to various quinones has been studied.[4-10] It became apparent that basic information on the ionization constants, absorption spectra, and extinction coefficients of most semiquinone radicals in water was lacking, in spite of a recent investigation[11] on this subject. Reported below is a pulse radiolysis study aimed at obtaining this information. Twelve quinones were examined, including benzoquinones, naphthaquinones, anthraquinones, adrenalone, and diphenoquinine. These were selected on the basis of their redox potentials, ranging from E° [1] values of −0.266 to +0.534 V, and their relative solubilities in aqueous alcohol (1–3 *M*) solutions.

Experimental Section

The pulse radiolysis set-up used has been described elsewhere.[12] Single pulses of 2.3-MeV electrons of ~30 nsec duration were used. Due to the intense photochemical decomposition of quinones in solution, particular care was taken to carry out the experiments with minimum exposure to light. Appropriate glass filters were used to reduce the effect of the monitoring light from a 450-W xenon lamp, in addition to placing a synchronized shutter which opened for ~7–8 msec.

The quinones used were supplied by Eastman and by Aldrich, and most of them were recrystallized and/or sublimed. The quinones were initially dissolved in 1.0–3.0 *M* *tert*-butyl alcohol or isopropyl alcohol, as indicated, and then appropriate amounts of triply distilled water were added. Solutions were buffered using perchloric acid, potassium hydroxide, and ~1.0 m*M* phosphate or borate buffers.

Dosimetry was carried out[12] using KCNS solutions. The extinction coefficients were derived[12] based on $G(e_{aq}^-) = G(OH) = 2.8$. Experimental conditions of concentration and dose were chosen for 100% formation of the semiquinone radicals. The extinction coefficients derived by electron transfer from $(CH_3)_2COH$ radicals are low by ~10–15%, due to the formation of β radicals on reaction of OH radicals with isopropyl alcohol.

Results and Discussion

The semiquinone radicals were formed by the reaction of hydrated electrons, e_{aq}^- with quinones (Q)

$$e_{aq}^- + Q \longrightarrow \cdot Q^- \quad (1)$$

$$\cdot Q^- + H_2O \longrightarrow Q^-H^+ + OH^- \quad (2)$$

$$\cdot Q^- + H_3O^+ \longrightarrow \cdot Q^-H^+ + H_2O \quad (3)$$

Depending on the acid dissociation constant, the semiquinone radical anion can be protonated to give the corresponding radical, reactions 2 and 3. The OH radicals produced from the radiolysis of water were scavenged by *tert*-butyl alcohol or isopropyl alcohol

$$OH + (CH_3)_3COH \longrightarrow \cdot CH_2(CH_3)_2COH + H_2O \quad (4)$$

$$OH + (CH_3)_2CHOH \longrightarrow (CH_3)_2\dot{C}OH + H_2O \quad (5)$$

The radical produced in reaction 4 is relatively inert and was found not to react with the quinones examined. The acetone ketyl radical, however, reacts with the quinones producing $\cdot Q^-H^+$ radicals according to reaction 6

$$(CH_3)_2\dot{C}OH + Q \longrightarrow \cdot Q^-H^+ + CH_3COCH_3 \quad (6)$$

$$\cdot Q^-H^+ \rightleftharpoons \cdot Q^- + H^+ \quad (7)$$

with values of k_6 ranging from ~1.0 to 6.0 × 10^9 M^{-1} sec^{-1} (see ref 8). Under the experimental conditions used all the $(CH_3)_2\dot{C}OH$ radicals produced semiquinone radicals quantitatively according to reaction 6.

Typically, these experiments were carried out in 1–3 *M* *t*-BuOH or $(CH_3)_2CHOH$, 50–100 μM quinone, and argon (1 atm). Relatively low doses of 1–2 krads/pulse were used throughout.

Transient absorption bands were observed with maxima in the 400–450-nm region for $\cdot Q^-$ radicals, see Table I, except for 1,2-naphthaquinone, epinephrine, and adrenalone. Similarly, $\cdot Q^-H^+$ radicals showed maxima in the 370–425-nm region. In most cases, the semiquinone radicals and radical anions have other absorption bands in the uv or far-uv region (see *e.g.*, ref 6 and 13), but these have not been examined in detail.

TABLE I: Ionization Constants, Absorption Maxima, and Extinction Coefficients of Semiquinone Radicals $\cdot Q^-$ and Radical Anions $\cdot Q^- - H^+$ in Aqueous Solution[a]

No	Quinone	$E^{\circ\prime}$, V	pK_a[b]	$\cdot Q^-$ λ_{max}, nm	$\cdot Q^-$ ϵ, M^{-1} cm^{-1}	$\cdot Q^- - H^+$ λ_{max}, nm	$\cdot Q^- - H^+$ ϵ, M^{-1} cm^{-1}
1	Anthraquinone[c]	−0.266	5.3	395, 480	7.8×10^3, 7.3×10^3	375	1.1×10^4
2	Anthraquinone-1-sulfonate[e]	−0.218	5.4	400, 500	8.0×10^3, 8.0×10^3	385	1.2×10^4
3	2-Hydroxy-1,4-naphthaquinone[d]	−0.139	4.7	390	6.3×10^3	370	5.9×10^3
4	Menaquinone	+0.002	4.5	395	1.2×10^4	370	9.7×10^3
5	1,4-Naphthaquinone	+0.050	4.1	390	1.3×10^4	370	7.3×10^3
6	Duroquinone	+0.068	5.1	445	7.1×10^3	425	4.0×10^3
7	1,2-Naphthaquinone[d]	+0.143	4.8	265	4.0×10^4	<260	1.6×10^4
8	2,5-Dimethyl-*p*-benzoquinone	+0.176	4.6	440	6.8×10^3	415	3.6×10^3
9	*p*-Benzoquinone	+0.293	4.0[f]	425	7.2×10^3	415	4.5×10^3
10	Epinephrine[d]	+0.380	3.7	265	3.3×10^3	<260	1.3×10^3
11	Adrenalone[d]	+0.480	3.6	290	1.7×10^4	~280	1.0×10^4
12	Diphenoquinone[d]	+0.534	3.2	400	2.6×10^3	370	4.7×10^3

[a] Obtained in 1–2 *M* aqueous *t*-BuOH solutions, ϵ values good to ±10%, only main absorption bands usually given. [b] pK_a values better than ±0.2 units. [c] In 3.0 *M* isopropyl alcohol, ϵ values are ±20%. [d] Data corrected for depletion of the absorption due to the quinone at the appropriate wavelengths. [e] From ref 14. [f] From ref 11.

TABLE II: Decay Kinetics of Semiquinone Radicals in Aqueous Solution[a]

Quinone	Decay rate, $2k$, M^{-1} sec^{-1} [b] $\cdot Q^- - H^+$	$\cdot Q^-$
Anthraquinone-1-sulfonate[c]	1.6×10^9	
Menaquinone	1.3×10^9 (pH 3.0, 370 nm)	1.6×10^8 (pH 9.2, 395 nm)
1,4-Naphthaquinone	1.3×10^9 (pH 3.0, 370 nm)	1.0×10^8 (pH 9.2, 390 nm)
Duroquinone	7.2×10^8 (pH 3.0, 420 nm)	2.9×10^7 (pH 9.0, 440 nm)
p-Benzoquinone	1.2×10^9 (pH 2.6, 410 nm)	5.5×10^7 (pH 9.2, 430 nm)

[a] Determined in 1–3 *M* isopropyl alcohol. [b] Values in parentheses are the experimental conditions used in determining $2k$; values good to ±15%. [c] From ref 14.

Table I shows the absorption maxima and extinction coefficients of the semiquinone radicals studied. In all cases, the absorption of $\cdot Q^-$ radicals is red-shifted compared to that of $\cdot Q^- - H^+$ radicals. This is consistent with the general observation that the basic forms of free radicals absorb at lower energies compared to the acidic forms.

The semiquinone radicals and radical anions were found to decay by good second-order kinetics in aqueous 1–3 *M* isopropyl alcohol solutions. In 1–3 *M* *t*-BuOH solutions, the radicals appear to decay faster and the second-order kinetics was not good. Table II shows some of those rates. The semiquinone radical anions decay more slowly, with $2k \sim 1.5 \times 10^8$ M^{-1} sec^{-1} and the semiquinone radicals with $2k \sim 1.5 \times 10^9$ M^{-1} sec^{-1}.

The ionization constants of the semiquinone radicals were determined by monitoring the change in absorbance at a fixed wavelength (usually at the absorption maxima of the $\cdot Q^-$ radicals) as a function of pH. Typical titration curves were obtained and from the midpoint values the pK_a were derived. These are listed in Table I. The pK_a values of the semiquinone radicals of anthraquinone-1-sulfonate[14] and benzoquinone[11] were obtained from the literature. The ionization constant values ranged from 3.2 to 5.4. It appeared that a correlation existed between the pK_a values and the redox potential $E^{\circ\prime}$ (at pH 7.0) values of the quinones (taken from ref 15). Figure 1 shows a plot of pK_a *vs.* $E^{\circ\prime}$, with a least-squares line drawn across the values.

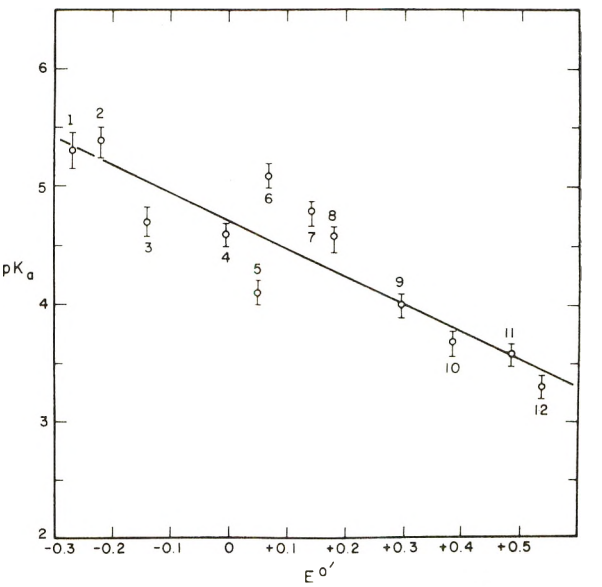

Figure 1. Plot of the ionization constants, pK_a, of semiquinone radicals in aqueous solution *vs.* the redox potential $E^{\circ\prime}$ of the corresponding quinones at pH 7.0 and ~22°. The numbers refer to the different quinones used and are given in Table I. The $E^{\circ\prime}$ values were taken from ref 15.

Various correlations have been shown between the redox potential of quinones and their half-wave reduction potential,[16] electron affinity,[17] energy of the highest occupied orbital (calculated[18] by LCAO-MO method), and heat of atomization between the quinone and the hydroquinone form (calculated[19] using the semiempirical SCF-MO pro-

cedure). The correlation presented in Figure 1 shows that the acidities of the semiquinone radicals increase with increase in the reduction potential of the quinones. It is interesting to note that similar correlation was recently found[20] between the basicities of a series of substituted anilines and the electrolytic oxidation potentials.

References and Notes

(1) Permanent address, Radiation Chemistry Section, C.S.M.C.R.I., Bhavnagar, India.
(2) "Biochemistry of Quinones," R. A. Morton, Ed., Academic Press, New York, N. Y., 1965.
(3) "Electron and Coupled Energy Transfer in Biological Systems," Vol. 1, T. E. King and M. Klingenberg, Ed., Marcel Dekker, New York, N. Y., 1971, Parts A and B.
(4) M. Simic and E. Hayon, *Int. J. Radiat. Biol.*, **22**, 507 (1972).
(5) M. Simic and E. Hayon, *Biochem. Biophys. Res. Commun.*, **50**, 364 (1973).
(6) E. Hayon and M. Simic, *J. Amer. Chem. Soc.*, **95**, 1029 (1973).
(7) P. S. Rao and E. Hayon, *Biochem. Biophys. Acta*, **292**, 516 (1973).
(8) P. S. Rao and E. Hayon, *Nature (London)*, **243**, 334 (1973).
(9) P. S. Rao and E. Hayon, *Biochem. Biophys. Res. Commun.*, **51**, 468 (1973).
(10) R. L. Willson, *Trans. Faraday Soc.*, **67**, 3020 (1971).
(11) R. L. Willson, *Chem. Commun.*, 1249 (1971).
(12) M. Simic, P. Neta, and E. Hayon, *J. Phys. Chem.*, **73**, 3794 (1969); J. P. Keene, E. D. Black, and E. Hayon, *Rev. Sci. Instrum.*, **40**, 1199 (1969).
(13) E. Hayon, T. Ibata, N. N. Lichtin, and M. Simic, *J. Phys. Chem.*, **76**, 2072 (1972).
(14) B. E. Hulme, E. J. Land, and G. O. Phillips, *J. Chem. Soc., Faraday Trans. 1*, **68**, 1992 (1972).
(15) "Handbook of Biochemistry," Chemical Rubber Publishing Co., Cleveland, Ohio, 1970, p J33.
(16) M. E. Peover, *J. Chem. Soc.*, 4540 (1962).
(17) G. Briegleb, *Angew. Chem., Int. Ed. Engl.*, **3**, 617 (1964).
(18) T. Fueno, T. Lee, and H. Eyring, *J. Phys. Chem.*, **63**, 1940 (1959).
(19) M. J. S. Dewar and N. Trinajstic, *Tetrahedron*, **25**, 4529 (1969).
(20) P. R. Jones, M. J. Drews, J. K. Johnson, and P. S. Wong, *J. Amer. Chem. Soc.*, **94**, 4594 (1972).

Electronic Absorption and Emission of Aromatic Hydroxycarbonium Ions[1]

Nicolae Filipescu,* Saroj K. Chakrabarti, and Peter G. Tarassoff

Department of Chemistry, The George Washington University, Washington, D. C. 20006

(Received January 15, 1973)

Publication costs assisted by the U. S. Atomic Energy Commission

The spectroscopic properties of representative aromatic hydroxycarbonium ions have been investigated and compared with those of the parent unprotonated carbonyl compounds. The energy levels, oscillator strengths, polarizations, and charge densities of the planar carbonium ions were calculated by a MO-SCF-CI procedure. Comparison of theoretical values with experimental quantities yielded satisfactory structural models for the cations. The aromatic ketones studied are readily soluble in sulfuric acid, are completely monoprotonated, and form very stable solutions. In contrast to the parent ketones, most hydroxycarbonium ions exhibited strong $\pi^* \rightarrow \pi$ fluorescence ($\phi_f > 0.5$) and less intense $\pi^* \rightarrow \pi$ phosphorescence.

Whereas the excited-state properties of carbonyl compounds have been extensively investigated both spectroscopically and photochemically,[2] those of their protonated derivatives, the hydroxycarbonium ions, have received much less attention mainly because the strongly acidic inorganic media required for the preparation of carbonium ions are less commonly employed by most spectroscopists and photochemists than the usual organic or aqueous solvents. Since many hydroxycarbonium ions are remarkably stable and since others are active photochemically,[3] they represent an important class of compounds of potentially high interest both in photochemistry and molecular electronic spectroscopy.

In this paper we report on the uv-visible absorption and emission spectra of selected aromatic carbonyl compounds dissolved in sulfuric acid or, at low temperatures, in sulfuric-acetic acid mixtures. The following representative ketones and lactones are grouped together in the present work: coumarin (C), xanthone (X), flavone (FLA), fluorenone (FLU), perinaphthenone (PN), di-*p*-methoxybenzophenone (DMB), and 2-acetonaphthone (2AN). These aromatic compounds were selected because they present common features that may allow valuable generalizations, because they yield stable and planar protonated derivatives which lend themselves both to accurate quantitative spectral measurements and to useful theoretical analysis, and because their spectroscopy and photochemistry in *non*acidic solvents has received previous attention.[4]

Results and Discussion

The ketones studied were readily soluble in sulfuric acid; 10^{-3} *M* standard solutions remained stable over extended periods (weeks). No significant spectral differences could be detected in samples in which atmospheric oxygen was partially or rigorously excluded. Since concentrated sulfuric acid is known to have oxidative properties and is a medium of choice in the preparation of a variety of aromatic free radicals, all our ketone solutions were examined in an esr spectrometer.[5] Absence of esr signal indicated that no paramagnetic species was present. Except for protonated coumarin, the other solutions did not exhibit significant photochemical changes when irradiated for several hours with a 500-W high-pressure Hg arc.

Absorption Spectra. The uv-visible absorption spectra of the seven hydroxycarbonium ions in sulfuric acid are compared to those of the respective parent ketones in 3-

methylpentane (3MP) in Figure 1. In sulfuric acid solutions diluted with 1:1 ethanol–water to 0.1 N H_2SO_4, the electronic absorption spectra of the ketones were consistent with the coexistence of both ketone molecules and respective hydroxycarbonium ions. This undoubtedly corresponds to a state of partial protonation of the carbonyl groups with the two absorbing species in dynamic equilibrium.

In sulfuric acid solution, most of the compounds exhibited a shift of the lowest-energy band toward longer wavelengths. For coumarin and flavone this red shift was not sufficient to cause visible absorption and consequently their H_2SO_4 solutions remained colorless. The others, however, became vividly colored from different shades of yellow and green for DMB, PN, X, and 2AN to purple for FLU.

The differences between the absorption spectra of the ketones in 3MP and those in H_2SO_4 are sufficiently pronounced to suggest that in pure acid the ketones exist only as the respective hydroxycarbonium ions, or, that there are no significant amounts of unprotonated carbonyl molecules in solution.

Theoretical Analysis of Absorption Spectra. On inspection, there seems to be no obvious correlation between the near-ultraviolet absorption bands of the ketones and those of their protonated derivatives. One should mention, however, that except for the usual n → π^* and π → π^* classification based on relative energies and extinction coefficients there has been no reported attempt to assign individual bands in the absorption spectra of the above ketones to specific electronic transitions. Therefore, we will not try in this paper to establish theoretical ketone–protonated ketone correlations; instead, we analyze the absorption spectra of the hydroxycarbonium ions independently. The results of this analysis will provide not only some reasonable agreement between calculated and experimental spectra but also additional significant information such as extent of π delocalization, whether mono- or diprotonation takes place (where hypothetically possible), and charge densities in ground and excited states (related to chemical and photochemical reactivities).

Method of Calculation. Energy levels, oscillator strengths, polarizations, and charge densities were derived *via* a π-electron calculation employing a semiempirical MO-SCF-CI procedure which included only singly excited configurations. The structures of all cations were considered planar with C–C and C–O distances of 1.40 Å, C=O 1.25 Å, and C–OH 1.36 Å. Within hexagonal cycles or in sp^2-hybridized atoms, the bond angles were taken to be 120°; for ether oxygen the bond angle was 114°. Slight variations in bond distances and angles did not alter significantly the calculated data. The following optimized parameters were used: valence-state ionization potentials for C^+ 8.26 eV, for O^+ 17.70 eV, and for O^{2+} 28.50 eV; one-center repulsion integral for C 11.13 eV, for O^+ 15.23 eV, and for O^{2+} 21.53 eV; both bond resonance integrals β_{CC} and β_{CO} were −2.37 eV. The two-center repulsion integrals were evaluated by the Mataga–Nishimoto approximation.[6] Self-consistency was reached after six or seven iterations. This method of calculation is known to give good results for evaluating spectral properties of heteroaromatic and nonalternant systems.[7] A modification to Bloor and Gilson's closed-shell SCF-CI program[8] was used on an IBM 360/50 computer.

Calculated values for singlet and triplet energy levels, oscillator strengths for transitions to and from the ground

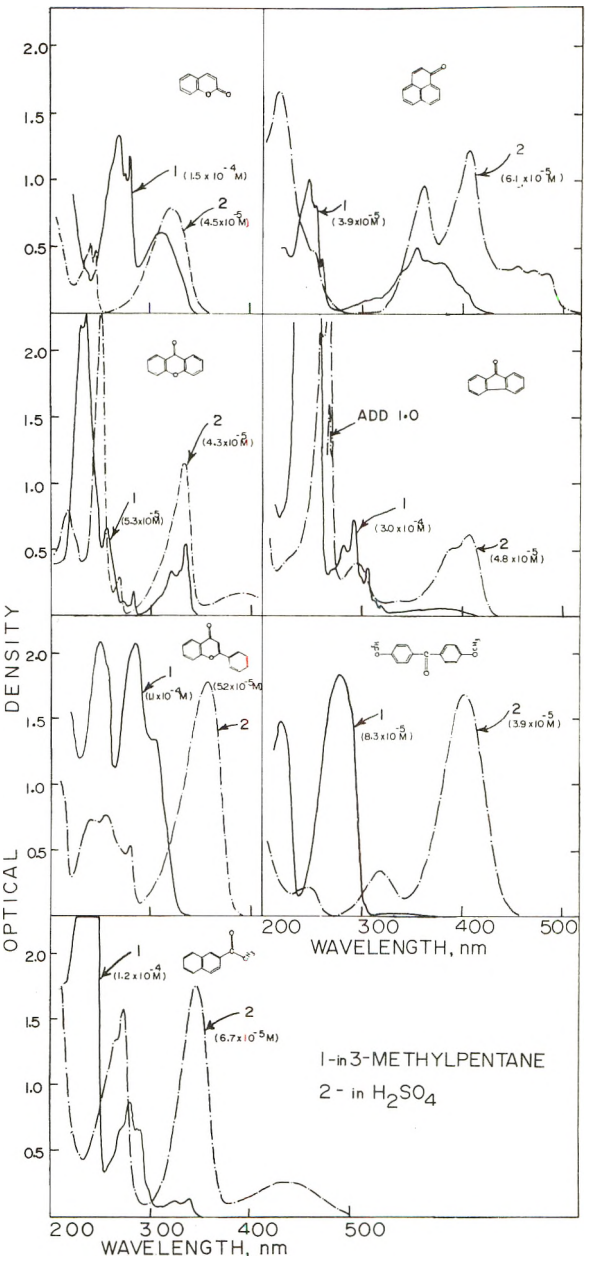

Figure 1. Absorption spectra of the selected aromatic ketones in 3MP and in sulfuric acid.

state, and polarizations are compared with experimental quantities in Table I. The values listed are those obtained for the configurations 1–7 shown in Figure 2.

The valence-bond structures have been purposely written as oxonium ions for **1**, **2**, and **3**, and carbonium ions for the remaining four. In fact the results of our calculations indicate that there is little π delocalization over the hydroxyl oxygen in the first three ions in contrast with the latter four. When the core of the exocyclic oxygen atom of **1**–**3** ions was included in the π-electron calculation the derived spectral values became unacceptable on comparison with experiment. For instance, if the OH oxygen in coumarinium ion is included in the delocalization with a total of 12 π electrons, then the energies of the first excited singlet state come out to be about 2 eV lower than the observed value. In addition, the calculated lowest triplet comes also unacceptably low compared to experimental values. On the other hand, the hydroxyl oxygens of cations **4**–**7** must be included in the MO calculation to obtain rea-

TABLE I: Comparison of Experimental and Calculated Spectral Parameters of Hydroxycarbonium Ions

ΔE_{calcd}, eV (nm)	f_{calcd}	Polarization[a]	ΔE_{obsd}, eV (nm)	f_{obsd}	Main configuration
			Coumarin (**1**)		
3.81 (325)[b]	0.59	11°	3.88 (319)	0.30	0.97 (5 → 6)
4.16 (297)[b]	0.08	108°	4.13 (300)	0.05	0.92 (4 → 6) + 0.32 (5 → 7)
5.80 (213)[b]	0.52	72°	5.14 (241)	0.20	0.94 (5 → 7)
6.49 (191)[b]	0.60	21°			0.99 (4 → 7)
2.38 (519)[c]		11°			0.97 (5 → 6)
3.48 (355)[c]		21°			0.94 (4 → 7)
3.67 (338)[c]		108°			0.94 (4 → 6)
4.65 (267)[c]		72°			0.97 (5 → 7)
			Xanthone (**2**)		
3.30 (375)[b]	0.29	90°	3.17 (390)	0.07	0.99 (7 → 8)
3.54 (350)[b]	0.65	0°	3.72 (333)	0.25	0.97 (6 → 8)
5.45 (227)[b]	1.07	180°	4.93 (251)	0.44	0.97 (7→ 9)
6.17 (200)[b]	1.52	90°	5.71 (217)		0.99 (6 → 9)
2.01 (620)[c]		90°	2.36 (525)		0.99 (7 → 8)
2.61 (474)[c]		0°			0.99 (6 → 8)
4.64 (267)[c]		180°			0.99 (7 → 9)
4.81 (257)[c]		90°			0.99 (6 → 9)
			Flavone (**3**)		
3.59 (345)[b]	0.92	8°	3.47 (357)	0.52	0.97 (8 → 9)
3.92 (316)[b]	0.21	54°	3.90 (318)	0.10	0.98 (7 → 9)
5.23 (237)[b]	1.2	68°	4.86 (255)	0.59	0.98 (8 → 10)
5.69 (217)[b]	0.85	168°			0.97 (7 → 10)
2.61 (475)[c]		6°	2.70 (447)		0.72 (7 → 9) − 0.33 (7 → 10)
2.74 (451)[c]		54°			0.79 (8 → 9) + 0.59 (7 → 10)
4.06 (305)[c]		68°			0.91 (8 → 10) + 0.40 (7 → 10)
5.08 (244)[c]		168°			0.85 (7 → 10) − 0.39 (8 → 10)
			Perinaphthenone (**5**)		
3.30 (376)[b]	0.75	64°	2.74 (452)	0.30	0.99 (7 → 8)
3.87 (320)[b]	0.27	164°	3.44 (360)	0.19	0.92 (6 → 8)
5.21 (238)[b]	1.2	176°	4.93 (251)		0.91 (7 → 9)
6.10 (203)[b]	0.59	121°	5.73 (216)		0.99 (6 → 9)
1.70 (731)[c]		61°			0.99 (7 → 8)
2.70 (459)[c]		162°			0.99 (6 → 8)
4.38 (283)[c]		164°			0.89 (7 → 9)
4.84 (256)[c]		95°			0.90 (6 → 9)
			9-Fluorenone (**4**)		
3.01 (411)[b]	0.31	15°	3.06 (406)	0.16	0.99 (6 → 7)
4.48 (276)[b]	0.00	45°	4.21 (344)	0.12	0.70 (6 → 8) − 0.70 (5 → 7)
5.31 (233)[b]	1.19	45°	4.65 (267)	0.77	0.70 (5 → 7) + 0.70 (6 → 8)
6.63 (187)[b]	0.28	127°			0.99 (5 → 8)
1.24 (1000)[c]		15°			0.96 (6 → 7)
3.28 (378)[c]		43°			0.68 (5 → 7) + 0.68 (6 → 8)
			4,4′-Dimethoxybenzophenone (**6**)		
3.88 (318)[b]	0.94	180°	3.60 (344)	0.29	0.99 (7 → 8)
4.11 (301)[b]	0.13	90°	4.24 (292)	0.09	0.98 (6 → 8)
6.31 (196)[b]	0.34	90°			0.98 (7 → 9)
6.38 (194)[b]	0.43	180°			0.99 (6 → 9)
2.97 (418)[c]		180°	2.75 (451)		0.99 (7 → 8)
3.36 (369)[c]		90°			0.99 (6 → 8)
5.24 (236)[c]		90°			0.99 (7 → 9)
5.39 (230)[c]		180°			0.99 (6 → 9)
			2-Acetonaphthone (**7**)		
3.43 (361)[b]	0.17	153°	2.96 (420)	0.08	0.95 (6 → 7)
4.25 (291)[b]	0.20	30°	3.66 (339)	0.30	0.81 (5 → 7) − 0.54 (6 → 8)
5.05 (245)[b]	1.56	44°	4.57 (271)	0.47	0.83 (6 → 8) + 0.55 (5 → 7)
5.57 (222)[b]	0.69	33°			0.97 (5 → 8)
2.30 (537)[c]		152°			0.89 (6 → 7) + 0.45 (6 → 8)
3.09 (401)[c]		44°			0.88 (6 → 8) − 0.44 (6 → 7)
3.53 (350)[c]		60°			0.98 (5 → 7)
4.44 (279)[c]		33°			0.98 (5 → 8)

[a] The angle made with respect to the direction of x axis. [b] Singlet state ($S_0 \rightarrow S_1$). [c] Triplet state ($S_0 \rightarrow T_1$).

sonable agreement with experimental spectral quantities. That protonation does not take place in the aromatic rings of the ketones was clearly shown by their nmr spectra in D_2SO_4 which showed no additional H splitting or H exchange.

The agreement between theoretical and experimental values in Table I is as good as any previously reported on aromatic and heteroaromatic molecules.

Charge Densities. The calculated charge densities for the ground and first excited singlets and the lowest triplet of the hydroxycarbonium ions are given in Figure 3. These values may prove valuable in estimating the reactivity of the cationic species in both the ground and the S_1 and T_1 states. Several interesting generalizations can be obtained from examination of the numerical values in Figure 3. For the hydroxycarbonium ions derived from DMB, 2AN, PN, and FLU which have no ether or lactone oxygen and which have substantial π delocalization over the hydroxyl oxygen, the electronic charge density increases slightly on going from the ground state to either the lowest singlet or lowest triplet excited states. On the other hand, the increase in density on the carbon atom adjacent to the OH increases substantially in the T_1 and S_1 states with somewhat higher values for the S_1 level. This behavior is common to all compounds in this study and is analogous to that of the unprotonated ketones in which the natural C → O polarity in the ground state has been shown to reverse to a considerable extent in the S_1 and T_1 states.[2] On those carbon atoms included in the aromatic ring system, there are changes in the electron density on going from ground to excited states; however, none of them comes close to those observed for the carbon atom attached to the hydroxyl group. For the ions containing an ether-linked oxygen, a consistent increase in electron density on that atom is observed in the S_1 and T_1 states when compared to the ground state.

Emission Spectra. The fluorescence, phosphorescence, and excitation spectra of four representative hydroxycarbonium ions are shown in Figure 4. Those of the remaining three have been omitted for the following reasons: FLU emits only a very weak, broad-band fluorescence in the red spectral region (~610 nm), which seems to be concentration dependent,[9] 2AN shows only intense fluorescence in a broad band between 500 and 600 nm, but no phosphorescence, and DMB emits fluorescence and phosphorescence similar to that of benzophenone.[10]

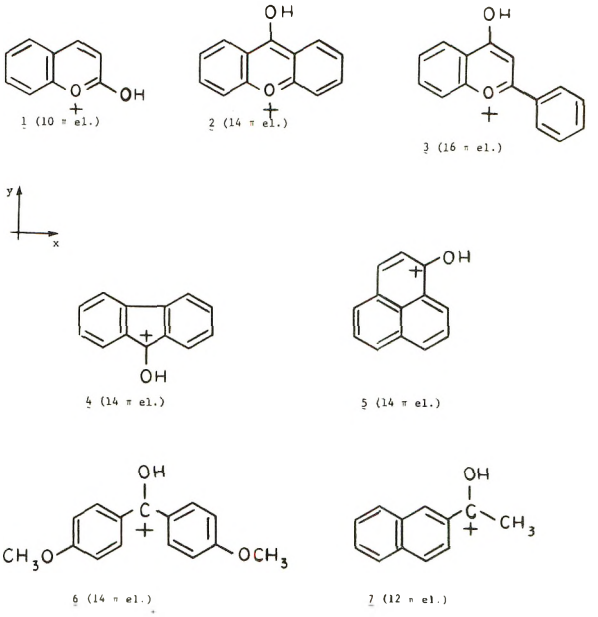

Figure 2. Hydroxycarbonium ions investigated.

The emission quantum yields and phosphorescence lifetimes of the hydroxycarbonium ions which exhibited both fluorescence and phosphorescence are given in Table II. The corresponding emission parameters of the parent carbonyl compounds determined under identical conditions in nonacidic solvent (3MP) are also included in Table II for comparison. While the ketones exhibit characteristic, short-lived $\pi^* \rightarrow n$ phosphorescence and virtually no fluorescence in 3MP, in acid, the respective cations, with the exception of coumarin,[11] emit significant fluorescence and weaker phosphorescence of 2–3-sec lifetime characteristic of $\pi^* \rightarrow \pi$ spin-forbidden transitions. The change in emitting state from n,π^* to π,π^* is readily understood since protonation takes place at the nonbonding electrons of the carbonyl oxygen. The decrease in phosphorescence quantum yield associated with protonation reflects a corresponding decrease in intersystem crossing efficiency. This, again, can be explained satisfactorily by analyzing the respective changes in energy levels both observed experimentally and derived theoretically. As expected, the S_1–T_1 gap is substantially larger in the cation (π,π^* states) than in the ketone (n,π^* states). This sizable dif-

TABLE II: Emission Spectral Parameters of the Ketones, Lactones, and Their Protonated Derivatives

Compound	λ_{fl}^{max}, nm (H_2SO_4/HOAc (3/1)) 77°K	298°K	ϕ_F	ϕ_P	ϕ_F/ϕ_P	τ_p, sec	τ_{fl}°, nsec
Coumarin	400	435	*a*	*a*	~0.20[c]		
			0.12[b]	0.84[b]	0.143	2.4 ± 0.10	5.0
Xanthone	425	458		0.689[a]			
			0.72[b]	0.12[b]	6.00	2.2 ± 0.10	34.0
Flavone	375	402	0.09[a]	0.697[a]	0.129		
			0.47[b]	0.36[b]	1.30	2.1 ± 0.10	4.0
Perinaphthenone	490	503		0.58[a]			
			0.82[b]				33.7
4,4′-Dimethoxybenzophenone	435	445		0.70[a]			
			0.626[b]	0.235[b]	2.66	2.80 ± 0.15	4.2
2-Acetonaphthone	490	537					
			0.690				38.0

[a] 3MP. [b] H_2SO_4/HOAc (3/1). [c] J. B. Gallivan, *Mol. Photochem.*, **2**, 191 (1970).

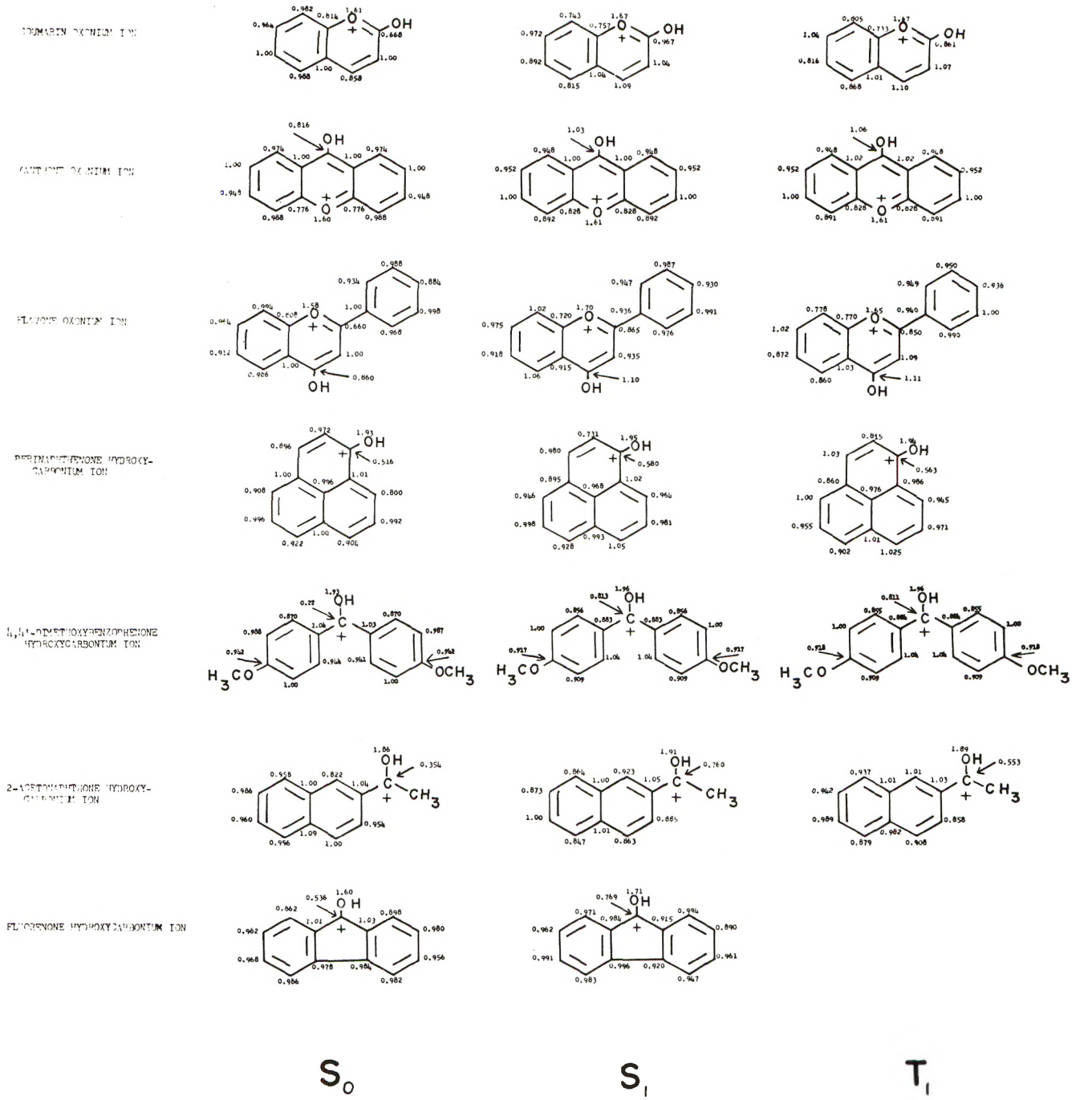

Figure 3. Calculated charge densities for the ground and first excited singlets and the lowest triplet of the hydroxycarbonium ions.

ference should decrease the spin-orbit coupling matrix element accordingly.

In addition, the theoretically derived T_2 state, which is known to be instrumental in intersystem crossing when properly located energetically with respect to S_1, seems to be distinctly higher than S_1 in the hydroxycarbonium ions which emit poorly or not at all from T_1 but lower in those exhibiting phosphorescence. Nevertheless, even in the latter, the T_2-mediated crossover does not seem to compensate for the larger effect of the increase in the S_1-T_1 gap. Consequently, the cations remain poorer phosphorescence emitters than their respective unprotonated ketones.

The fact that there was no detectable $\pi^* \rightarrow n$ phosphorescence in acidic glass and that $T_1 \rightarrow S_0$ emission was distinctly singly exponential seems to confirm the totally protonated state of dissolved ketone suggested by the absorption spectra.

The fluorescence maxima at ambient temperature and at 77°K and the calculated fluorescence lifetimes are also included in Table I. It is interesting that the hypsochromic shift in λ_{max} of fluorescence on going from room to liquid nitrogen temperature is quite sizable (20–25 nm). This, however, is not unexpected since both the cationic solute and the solvent are highly polar and this is reflected in ground-excited state differences in solvation and equilibrium configurations.

Polarization. The calculated polarizations corresponding to different singlet–singlet electronic transitions are given in Table I. The main feature of these derived values is that by comparison with experimental fluorescence–exci-

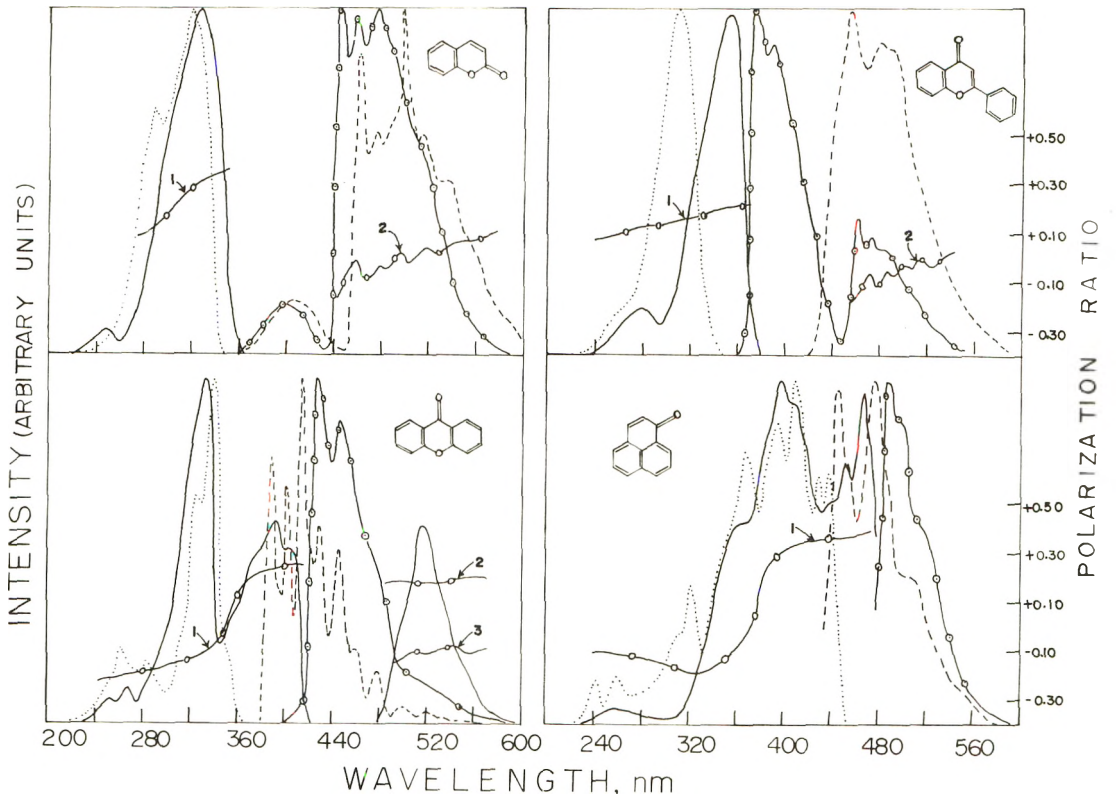

Figure 4. Emission, excitation, and polarization spectra of coumarin, xanthone, flavone, and perinaphthenone in rigid glass at 77°K. Solvents were 3MP for ketones and H_2SO_4–AcOH for their cations: fluorescence excitation of cation (——), and ketone (···); emission spectra of cation (–⊙–) and ketone (- - -); polarization spectra (–O–): 1, excitation; 2, fluorescence; and 3, phosphorescence.

tation polarization measurements shown in Figure 1, they confirm the validity of cationic configurations **1**–**7**. Possible structures other than those shown for **1**–**7** and diprotonated species considered in calculations failed grossly to agree with the experimental values. On the other hand, the calculations for species **1**–**7** gave a satisfactory overall consistency between calculated and experimentally measured quantities. For example, configuration **2** for protonated xanthone predicts theoretically that the first electronic transition should be short-axis and the second and third be long-axis polarized. In agreement with these predictions, the measured polarized fluorescence excitation spectrum shown in Figure 1 shows the first electronic transitions to be positively polarized while the second and third absorption bands are negatively polarized.

Figure 1 also shows the phosphorescence polarization curves of the hydroxycarbonium ions which emit phosphorescence. In general, these measurements indicate an out-of-phase polarization for the $0 \rightarrow 0$ bands of the $T_1 \rightarrow S_0$ emissions. As expected, this is characteristically associated with phosphorescence.

Conclusion

Aromatic ketones are readily soluble in acidic solvents such as sulfuric acid, are completely protonated, and yield very stable solutions of hydroxycarbonium ions. These ions exhibit quantitatively measurable fluorescence and phosphorescence. Being planar, they are very well suited for both theoretical and experimental studies in molecular spectroscopy and photochemistry.

Experimental Section

The selected ketones and lactones were purified by repeated recrystallization from appropriate solvents followed by vacuum sublimation. Fluorometric sulfuric and acetic acids were obtained from Matheson Coleman and Bell and 3-methylpentane from Phillips Petroleum Co.

When ketone solutions in pure sulfuric acid were cooled to 77°K, they formed a poor quality glass. In contrast, the samples dissolved in a mixture of sulfuric acid and acetic acid (3:1 by volume) yielded a clear rigid glass at 77°K. Since no significant differences could be detected in either the absorption or emission spectra on going from pure sulfuric to sulfuric–acetic acid mixtures, all quantum yields, lifetimes, and polarization measurements of the hydroxycarbonium ions at 77°K were carried out in sulfuric–acetic acid mixtures.

All samples were deaerated by passing pure dry nitrogen gas for 20 min before measurements. The emission spectra (both fluorescence and phosphorescence) were measured with the Perkin-Elmer Model MPF-2A fluorescence spectrophotometer with a 150-W xenon light source and the necessary phosphorescence accessories. The exciting and emission monochromators had 600 lines/mm gratings blazed at 3000 Å. An R106 photomultiplier was used for the blue region and an R136 for the red region. Two film type polarizers were used for the polarization measurements. Quartz tubes of 2 mm i.d., contained in a quartz dewar flask, were used for the low-temperature emission spectra. A 3-mm slit width (22 mμ band pass) in the excitation monochromator and a 2-mm slit width (15 mμ band pass) in the emission monochromator were normally used. Higher slit widths had to be used for recording emission of low intensity in a few cases. The emission was observed at right angle to the exciting beam. The recorded luminescence spectra were not corrected for instrument response.

The polarization of emission and its excitation was obtained by photoselection. The degree of polarization (P)

was calculated from the formula, $P = (I_{\parallel} - I_{\perp})/(I_{\parallel} + I_{\perp})$. All polarization graphs represent an average of at least four different measurements. The results were reproducible within ±6%.

Quantum yields of emission were measured relative to 9,10-diphenylanthracene whose fluorescence quantum yield was taken to be unity. Fluorescence quantum yields at room temperature were also checked with quinine bisulfate standard (ϕ_f = 0.55); the agreements were good. The results of several measurements agree within ±10%.

The phosphorescence lifetime measurements were made on the Perkin-Elmer fluorescence spectrophotometer with phosphorescence attachments and the decay curve was displayed on a Hewlett-Packard oscilloscope (Model 10175B).

All absorption spectra measurements were made using a Cary 15 recording spectrophotometer.

Acknowledgment. This work was supported in part by the Atomic Energy Commission under Contract No. AT-(40-1)-3797. The time made available by the University Computer Center and the partial support from the Research Committee of The George Washington University are also greatly acknowledged.

References and Notes

(1) Taken in part from the Ph.D. Dissertation of P. G. Tarassoff at George Washington University.
(2) See, for example, N. J. Turro, "Molecular Photochemistry," W. A. Benjamin, New York, N. Y., 1967.
(3) See, for example, N. Filipescu and J. W. Pavlik, *J. Amer. Chem. Soc.*, **92**, 6062 (1970).
(4) See, for example, (a) G. O. Schenk, I. von Wilucki, and C. H. Kranch, *Chem. Ber.*, **95**, 1409 (1962); (b) G. S. Hammond, C. A. Stout, and A. A. Lamola, *J. Amer. Chem. Soc.*, **86**, 3103 (1964); (c) H. Morrison, H. Curtis, and T. McDowell, *ibid.*, **88**, 5415 (1966).
(5) Modified Varian V-4502 esr spectrometer with 100-kHz modulation.
(6) M. Mataga and K. Nishimoto, *Z. Phys. Chem.*, **13**, 140 (1957).
(7) (a) F. L. Minn, J. P. Pinion, and N. Filipescu, *J. Phys. Chem.*, **75**, 1794 (1971); (b) M. Tichy and R. Zahradnik, *ibid.*, **73**, 534 (1969), and references therein.
(8) Quantum Chemistry Program Exchange, Indiana University, Program 71.3.
(9) This behavior of FLU seems to be related to its photochemical reactivity. The photochemical changes of FLU are currently under investigation.
(10) The emission of benzophenone in phosphoric acid has been mentioned briefly in R. Rusakowicz, G. W. Byers, and P. A. Leermakers, *J. Amer. Chem. Soc.*, **93**, 3263 (1971).
(11) The somewhat different behavior of coumarin does not seem to be related to the photoreactivity of the cation since the photoreaction is very inefficient ($\Phi < 10^{-4}$).

Binding of Methylmercury Chloride to the Model Peptide, *N*-Acetyl-L-cysteine. A Proton Magnetic Resonance Study[1a]

Paul G. Simpson,[1b] Ted E. Hopkins,[1b] and Rizwanul Haque*[1c]

Department of Chemistry and Department of Agricultural Chemistry and Environmental Health Sciences Center, Oregon State University, Corvallis, Oregon 97331 *(Received March 26, 1973)*

Publication costs assisted by the National Institutes of Health

The methylmercury ion CH_3Hg^+ is shown to form a 1:1 complex with the model peptide *N*-acetyl-L-cysteine as studied by proton magnetic resonance. Both the chemical shift of the CH_3Hg protons and the $J(^{199}Hg-CH_3)$ coupling constant decrease with the addition of *N*-acetyl-L-cysteine until an excess of peptide is present, whereupon they remain constant. The small $J(^{199}Hg-CH_3)$ coupling constant of 170 Hz for the complex is consistent with the formation of a covalent Hg–S bond. Two separate CH_2 peaks occur for the peptide–methylmercury mixtures corresponding to the CH_2 of the cysteine residue in the complex and free peptide; the latter occurs only in excess peptide. Broadening of the CH_2 doublets is interpreted as due to slow dissociation of the complex unassisted by protonation or chloride addition. The chemical shift of the CH_2 protons in the complex increases with increasing methylmercury:peptide molar ratio, indicating higher complex formation in excess methylmercury.

Mercury compounds are of great environmental concern in view of their occurrence in many biological samples. Methylmercury salts are of particular interest because of their high toxicity[2] and since they are formed in the environment from metallic inorganic and organic compounds of mercury.[3-5] Many mercury compounds form a stable Hg–S bond to sulfur-containing amino acids residues and are thus rather tightly bound to proteins in living systems.[6] Cysteine compares with the sulfhydryl group of serum albumin in its reaction with the methylmercuric ion, HC_3Hg^+,[6,7] and is expected to serve as a model for most sulfhydryl proteins. Proton magnetic resonance (pmr) has not been used to a great extent to determine the structure of Hg–amino acid residue complexes, but has been used by Kan and Li for Hg–nucleoside complexes.[8] Their investigations are also limited to Hg^{2+} ions in the nonaqueous solvent dimethyl sulfoxide.

In this communication we shall demonstrate the use of pmr for the study of the interaction of methylmercury chloride with the model peptide *N*-acetyl-L-cysteine. The

α-amino group was blocked with the acetyl group in order to eliminate its possible interaction with the methylmercury ion[6,9] which might complicate the results. The binding of the amino group to Hg is much weaker than that of the sulfhydryl group, and the interaction of the carboxylic group is even weaker.[6]

Experimental Section

Materials and Methods. Reagent grade methylmercury chloride was obtained from Strem Chemicals, Inc., Danvers, Mass. The blocked amino acid *N*-acetyl-L-cysteine was obtained from Cyclo Chemical Co., Los Angeles, Calif., supplied with the following data: % N 8.55 theoretical, 8.32 found; melting point 108–110°; chromatographically pure (tlc with $CHCl_3$:HAc, $CHCl_3$:MeOH and $CHCl_3$–acetone solvents). It was used without further purification. Solutions of freshly prepared material showed no impurities in the pmr spectra. However, aged solution did show impurities of ~10% in the pmr spectrum. Solutions of the mercury compound, amino acid, and mixtures were prepared by dissolving weighed quantities in D_2O. Pmr spectra were recorded at 100 MHz on a Varian HA 100 nmr spectrometer, interfaced with a Varian model C-1024 time-averaging computer. To obtain good spectra of these dilute solutions 25 to 200 scans were averaged. Chemical shifts were measured and reported with respect to sodium 2,2-dimethyl-2-silapentane-5-sulfonate (DSS) as an internal standard. The line width $\Delta\nu_{1/2}$ of the generally collapsed CH_2 doublet peak was calculated by the following equation[10]

$$\Delta\nu_{1/2} = \Delta\nu_{1/2}(\text{obsd}) - J(CH_2\text{-}CH)$$

where $\Delta\nu_{1/2}$(obsd) is the observed width at half-height of the doublet and $J(CH_2\text{-}CH)$ is the coupling constant. For consistency we used this method in those few cases where the doublet was not collapsed. All spectra were recorded at 31°. The estimated standard error of line width, chemical shift, and coupling constant measurements are 1, 1, and 3 Hz, respectively.

Results

The pmr spectrum of methylmercury chloride in D_2O (Figure 1a) shows a single methyl peak at 0.99 ppm downfield. A satellite doublet corresponding to the ^{199}Hg isotope (spin ½ and natural abundance 17%) having a coupling constant $J(^{199}Hg\text{-}CH_3)$ = 221 Hz appears around the methyl peak. The methylmercury salt did not show any concentration-dependent effect in either the chemical shift or the coupling constant of the methyl peak. Peaks of the satellite quartet due to ^{201}Hg with spin ⅜ (natural abundance 13.2%) were not observed. This may be due to line broadening caused by the large quadrupole moment of the ^{201}Hg isotope.

The pmr spectrum of the peptide in D_2O (Figure 1c) shows a sharp singlet at 2.08 ppm due to the methyl protons of the acetyl group, and a doublet due to the CH_2 protons at 2.97 ppm (J = 5 Hz). The COOH proton peak is not observable because of its rapid exchange with D_2O resulting in the formation of HDO (δ = 4.9 ppm). Due to this strong HDO peak the CH proton was not observable, although the CH sextet peak was observed in the solvent acetone. The NH proton peak was observed in H_2O (δ = 8.4 ppm, pH 2.2) and is broadened by the quadrupole moment of ^{14}N. This peak is absent in D_2O, indicating that exchange with D_2O has converted the NH to ND. Similarly, an NH proton peak for *N*-acetylglycine was observed in H_2O (δ = 8.3 ppm) but not in D_2O. The NH proton peak of *N*-methylacetamide has been reported in H_2O,[11] as well as the conversion of the amide's NH to ND in D_2O.[12] The pmr spectrum of the amino acid did not show any concentration dependence in the chemical shift of the CH_3 and CH_2 protons.

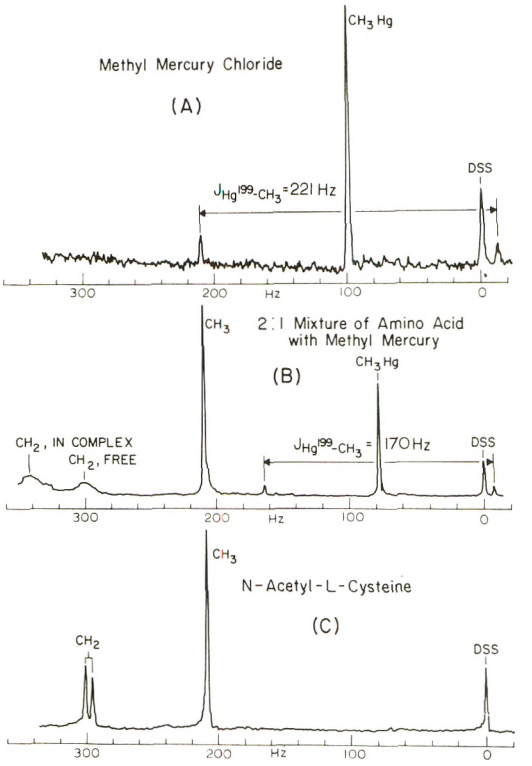

Figure 1. (A) The proton magnetic resonance spectrum of methylmercury chloride (6.9 m*M*). (B) The spectrum of a 2:1 molar ratio mixture of *N*-acetyl-L-cysteine with methylmercury chloride. The two separate CH_2 peaks correspond to equal amounts of free peptide and a 1:1 complex with methylmercury. (C) The spectrum of *N*-acetyl-L-cysteine (8.2 m*M*).

Addition of *N*-acetyl-L-cysteine to an approximate 75% saturated solution (6.9 m*M*, 1.7 mg/ml) or methylmercury chloride produced two separate peaks corresponding to the CH_2 protons, depending on the molar ratio of the amino acid to methylmercury. The new CH_2 peak (δ = 3.6–3.4 ppm) was observed in excess methylmercury. When the molar ratio of the amino acid to methylmercury exceeded 1:1 then the doublet at 2.97 ppm reappeared as a broad peak and became increasingly dominant and sharp as the amino acid concentration was increased. The CH_3 peak did not show any change in line width or chemical shift. The spectrum of a 2:1 molar ratio mixture is shown in Figure 1b.

The addition of the peptide to the methylmercury solution also produced changes in the chemical shift of the CH_3Hg protons as well as in the coupling constant $J(^{199}Hg\text{-}CH_3)$ (see Figure 1b). The methylmercury proton peak gradually shifted to high field as the concentration of the peptide was increased, with a final net chemical shift difference of 21 Hz as shown in Figure 2a. The coupling constant $J(^{199}Hg\text{-}CH_3)$ showed a drastic decrease from 221 to 170 Hz as the peptide concentration was increased (Figure 2b).

The new CH_2 proton peak showed a dependence on the peptide:mercury molar ratio in excess methylmercury

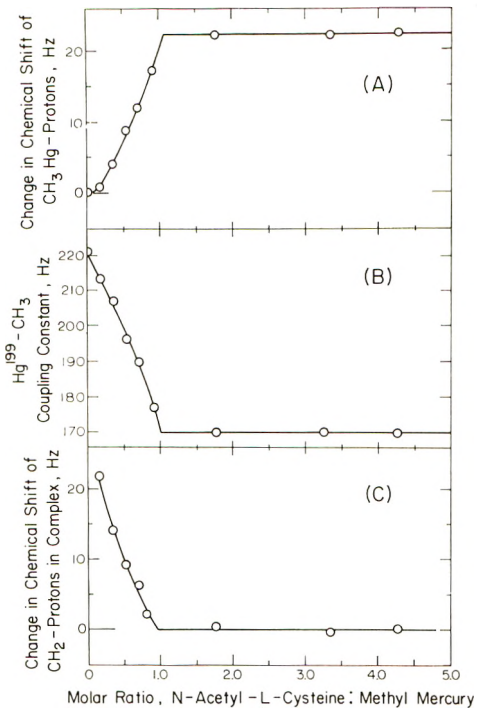

Figure 2. (A) The change in chemical shift of the CH_3Hg protons as a function of the molar ratio of *N*-acetyl-L-cysteine: methylmercury chloride mixtures. (B) The mercury–proton coupling constant as a function of the molar ratio. The coupling constant and chemical shift of the CH_3Hg protons in excess peptide indicate the formation of a covalent Hg–S bond in the complex. (C) The change in chemical shift of the CH_2 protons as a function of molar ratio, indicating the formation of higher complexes in excess CH_3HgCl.

(Figure 2c). Dilution of the 1:1 molar mixture did not show any shift of that peak or any other peak indicating that it was not a dilution effect.

Discussion

The changes in the pmr characteristics of the amino acid as well as the methylmercury chloride can be explained unequivocally on the basis of the binding of the methylmercury to *N*-acetyl-L-cysteine. The high affinity of Hg to S will favor a complex of type I. The formation of such a complex would produce the greatest change in the electronic environment for the CH_2 and the CH_3Hg protons.

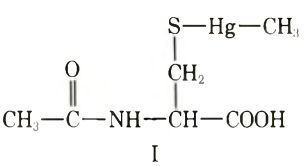

I

The shift of the bound CH_2 peak in excess CH_3Hg can be explained by the formation of higher complexes. These complexes could involve methylmercury binding to the carboxylic acid group of I. While such binding might be expected from estimated association constants for Hg with acetate,[6] it probably does not account for the large size of the shift of more than 20 Hz. Schwarzenbach and Schellenberg[13] report large association constants for the formation of $(CH_3Hg)_2S$ and $(CH_3Hg)_3S^+$. It is more likely then that the higher complexes involve two or more methylmercury groups bonded to the sulfur. The ratio of methylmercury groups to peptide in these higher complexes is not established; however, $(CH_3Hg)_2S^+CH_2R$ is favored over $(CH_3Hg)_3S^{2+}CH_2R$ because of the higher charge on the sulfur of the latter ion.

The formation of higher complexes is expected to affect the chemical shift of the CH_3Hg protons and the mercury–methyl coupling constants of the solutions with low peptide to methylmercury ratios, and thus it accounts for at least part of the definite curvature noticable in the lines connecting the first few points of Figures 2A and 2B. The experimental uncertainties and the number of species containing CH_3Hg groups preclude a detailed analysis of the curvature to determine equilibrium constants, and answering the related question of how sharp the break in the curve is at the equivalence point.

The changes in the coupling constant $J(^{199}Hg\text{-}CH_3)$ and chemical shift of the CH_3Hg protons by the addition of the peptide may be compared to the results of Hatton, Schneider, and Siebrand.[14] These workers found that $J(^{199}Hg\text{-}CH_3)$ in CH_3HgX type compounds is strongly dependent upon the substituent X. It varied from 233 Hz for X = ClO_4 to 104 Hz for X = CH_3. Apparently a strong covalent bond reduces the coupling constant significantly. The coupling constant for $(CH_3\text{-}Hg)_2S$ is 156 Hz which is in good agreement with the value of 170 Hz for the methylmercury–peptide complex. The chemical shift of the CH_3Hg protons also shows a dependence on the substituent X, ranging in pyridine from 0.17 ppm for X = ClO_4 to 1.11 ppm for X = CH_3; the value for $(CH_3\text{-}Hg)_2S$ is 0.75 ppm, again in good agreement with the value of 0.78 ppm observed for the methylmercury–peptide complex in D_2O. The change in the mercury proton coupling constant and proton chemical shift in organic mercury compounds may be used as a probe to study the nature and strength of their binding with peptides and biological macromolecules. However, it should be noted that when the organic mercury is bonded to slowly rotating macromolecules the proton resonance will be broadened. This would provide indirect evidence of binding. When the rotation is sufficiently fast, the resonance peak will be observable and its line width and chemical shift will indicate the strength and nature of the binding.

The observation of two separate peaks for the CH_2 protons indicates that the exchange of the peptide group from the bound to free-acid forms in solution is slow. The exchange may be expressed by the following chemical equilibria

$$CH_3Hg\text{-}SCH_2R \underset{k_{-1}}{\overset{k_1}{\rightleftharpoons}} CH_3Hg^+ + RCH_2S^- \qquad (1a)$$

$$CH_3Hg^+ + RCH_2S^- + H^+ + Cl^- \overset{K}{\rightleftharpoons} CH_3HgCl + HSCH_2R \qquad (1b)$$

The line width data may be used to describe the exchange process qualitatively.

$$CH_3Hg\text{-}SCH_2R + HSCH_2{}^*R \underset{k_{-2}}{\overset{k_2}{\rightleftharpoons}} CH_3Hg\text{-}SCH_2{}^*R + HSCH_2R \qquad (2)$$

The mean lifetimes of bound (τ_B) and free (τ_F) forms may be expressed[11] as

$$1/\tau_B = (1/C)\ dC/dt \qquad (3)$$

$$/\tau_F = (1/P)\ dP/dt \qquad (4)$$

Where C and P are the concentrations of the complex and free peptides, respectively. The derivatives, dC/dt and dP/dt, are for one-way exchange (rates of net change are

zero) and are related to appropriate rate constants as

$$dC/dt = k_1C + k_2CP \quad (5)$$

$$dP/dt = k_{-1}MA + k_2CP = k_1C + k_2CP = dC/dt \quad (6)$$

where M and A are the concentrations of CH_3Hg^+ and RCH_2S^-, respectively. Equations 5 and 6 are consistent with equilibria 1a and 2 being slow, rate determining and equilibrium 1b fast. If protonation of the complex, chloride addition or both preceded the rate-determining dissociation step, then k_1C would be replaced by $k_1C[H^+]$, $k_1C[Cl^-]$, or $k_1C[H^+][Cl^-]$, respectively. The observed line width at half-height ($\Delta\nu_{1/2}$) of a particular peak is related to the mean lifetime τ and the relaxation time T_2 as

$$\pi\Delta\nu_{1/2} = 1/T_2 = 1/T_2 = 1/T_2^* + 1/\tau$$

where T_2^* is the relaxation time due to field inhomogeneity and inherent relaxation in the absence of exchange.

If dissociation, (1), dominates the exchange rate, *i.e.*, if

$$k_1C \gg k_2CP$$

then

$$dC/dt = dP/dt = k_1C \quad (7)$$

and the exchange rates become

$$1/\tau_B = k_1 \quad (8)$$

$$1/\tau_F = k_1C/P \quad (9)$$

predicting constant broadening of the CH of the complex and decreasing broadening of the CH of the free peptide with increasing peptide. Different behavior is expected if exchange of the peptide moiety (2) dominates, *i.e.*, if

$$k_1C \ll k_2CP$$

In that case

$$dC/dt = dP/dt = k_2CP \quad (10)$$

and the exchange rates become

$$1/\tau_B = k_2P \quad (11)$$

$$1/\tau_F = k_1C \quad (12)$$

predicting a constant broadening of the CH_2 of the free peptide and an increasing broadening of the CH_2 of the complex with increasingly excess peptide.

The observed spectra for the mixtures with excess peptide behave according to eq 8 and 9 for exchange dominated by dissociation reaction 1. The net line widths of the CH_2 peaks of the free peptide are 5.8, 3.2 and 1.9 Hz for the 1.77, 3.35, and 4.27 molar ratio mixtures. For the peptide solution in which exchange does not occur $\Delta\nu_{1/2}(\text{obsd}) = 1/\pi T_2^* + J(CH_2\text{-}CH) = 7.7$ Hz. The net line widths are obtained by subtracting this value from $\Delta\nu_{1/2}(\text{obsd})$. These data yield values of $k_1 = P/C\tau_F$ of 14, 24, and 19 sec^{-1} consistent with eq 9 but not 12. The line width at half-height of the broad doublet CH_2 peak of the complex is constant for these mixtures ($\Delta\nu_{1/2}(\text{obsd}) =$ 12.8, 12.9, 12.9 Hz). Thus, while the absolute value of $1/\tau_B$ cannot be computed since the constants $1/T_2^*$ and $J(CH_2\text{-}CH)$ for the complex are not experimentally determined, it is constant, independent of free peptide concentration, and hence consistent with eq 8 but not 11. If we use the value of $1/\pi T_2^* + J(CH_2\text{-}CH) = 7.7$ of the free peptide as an estimate for the bound peptide, then we obtain

$$1/\tau_B = k_1 \simeq 16 \text{ sec}^{-1} \quad (13)$$

in good, perhaps fortuitous, agreement with the value obtained from the free peptide. In any case, the CH_2 peaks from both the bound and free peptides agree with eq 8 and 9 for exchange dominated by dissociation 1, not by exchange of the peptide moiety (2). Neither a 2.5-fold increase in $[H^+]$ nor a sixfold increase in $[Cl^-]$ had a noticeable effect on the line widths. Thus (7) is the rate law and in turn neither protonation nor chloride addition precedes rate-determining dissociation 1a.

The observation of one single peak for the CH_3Hg protons indicates that the exchange of these protons from bound to free forms is quite rapid. The methyl group, the whole methylmercury group, or both may be exchanging. Hatton, Schneider, and Siebrand[14] report that fast methyl exchange occurs for CH_3HgCl, CH_3HgBr, CH_3HgI, and CH_3HgSCN, but not for the more strongly bonded CH_3HgCN. The methylmercury–peptide complex I is probably similar to CH_3HgCN as suggested by their similar $J(^{199}Hg\text{-}CH_3)$ values of 170 and 178, respectively. The fast exchange giving a single CH_3Hg proton peak would then involve the methylmercury group as a whole. The shift of the bound CH_2 peak in excess CH_3Hg also supports the occurrence of this exchange mechanism. It should be pointed out that the above discussion on the exchange process is a qualitative one and further studies must be performed to get a quantitative picture.

Acknowledgments. We wish to thank Mrs. Yvonne Brander for her technical assistance in obtaining the spectra and Professor James Krueger for helpful discussions. This work was supported by Grant No. ES-00210 from the U. S. Public Health Service, a Grant-in-Aid of Research from Sigma Xi, and grants from the General Research Fund, Graduate School, and the Research Council, Oregon State University. This manuscript has been issued as Technical Paper No. 3615 from Oregon Agricultural Experiment Station.

References and Notes

(1) (a) Presented in part at 27th Northwest Regional Meeting of the American Chemical Society, Corvallis, Ore., June 1972. (b) Department of Chemistry. (c) Department of Agricultural Chemistry and Environmental Health Sciences Center.
(2) (a) A. Katz, *Crit. Rev. Environ. Contr.*, **2**, 517 (1972); (b) L. T. Kurland, S. N. Faro, and H. Siedler, *World Neurol.*, **1**, 170 (1960).
(3) S. Jensen and A. Jernelov, *Nature (London)*, **223**, 753 (1969).
(4) A. Jernelov in "Chemical Fallout," M. W. Miller and G. G. Berg, Ed., Charles C. Thomas, Springfield, Ill., 1969, p 68.
(5) J. M. Wood, F. Scott Kennedy, and C. G. Rosen, *Nature (London)*, **220**, 173 (1968).
(6) F. R. N. Gurd and P. E. Wilcox, *Advan. Protein Chem.*, **11**, 311 (1956), and the references cited therein.
(7) W. L. Hughes, Jr., *Cold Spring Harbor Symp. Quant. Biol.*, **14**, 79 (1950).
(8) L. S. Kan and N. C. Li, *J. Amer. Chem. Soc.*, **92**, 4823 (1970).
(9) J. Bjeruum in "Metal Ammine Formation in Aqueous Solution," Haase and Son, Copenhagen, 1941, pp 164–165, 286–295.
(10) O. Jardetzky and N. G. Wade-Jardetzky, *Mol. Pharm.*, **1**, 214 (1965).
(11) A. Berger, A. Loewenstein, and S. Meiboom, *J. Amer. Chem. Soc.*, **81**, 62 (1959).
(12) R. H. Barker and G. J. Boudreaux, *Spectrochem. Acta, Part A*, **23**, 727 (1967).
(13) G. Schwarzenbach and M. Schellenberg, *Helv. Chem. Acta*, **48**, 28 (1965).
(14) J. V. Hatton, W. G. Schneider, and W. Siebrand, *J. Chem. Phys.*, **39**, 330 (1963).

Configuration Coordinate Model for the Hydrated Electron. II. Jahn-Teller Splitting of the Excited State

M. Tachiya,*[1] Y. Tabata, and K. Oshima

Department of Nuclear Engineering, University of Tokyo, Tokyo, Japan *(Received February 9, 1973)*

The configuration coordinate model for the solvated electron is further developed. The configuration coordinate diagram for the hydrated electron is constructed by calculating the total energies of the hydrated electron under various orientational polarizations which are not necessarily spherically symmetric. Medium relaxation following an optical transition is discussed in terms of this diagram. The Jahn-Teller splitting of the excited state is predicted to be about 0.3 eV.

I. Introduction

In a previous paper[2] we presented a configuration coordinate model for the solvated electron. We constructed the configuration coordinate diagram for the hydrated electron by calculating the total energies of the hydrated electron under various orientational polarizations which are spherically symmetric. The orientational polarization under which the total energy for the ground state is minimum is probably spherically symmetric, however, the orientational polarization under which the total energy for the excited state is minimum probably is not. Thus the optical excitation of the solvated electron is followed by the distortion of the orientational polarization around the electron. The excited state, which is assumed to be the 2p state, is triply degenerate under the orientational polarization which is spherically symmetric. However, if the orientational polarization is distorted from spherical symmetry, the degeneracy of the excited state is removed and the Jahn-Teller splitting occurs.

In the present paper we construct the configuration coordinate diagram for the hydrated electron by calculating the total energies of the hydrated electron under various orientational polarizations which are not necessarily spherically symmetric. In terms of this diagram we discuss medium relaxation following an optical transition.

II. Theory

The total energy of the hydrated electron consists of the electronic energy and the polarization energy. The electronic energy E of the hydrated electron is obtained by solving the following Schrödinger equation

$$\left[-\frac{\hbar^2}{2m}\nabla^2 + V\right]\psi = E\psi \tag{1}$$

where V is the potential acting on the electron. If the orientational polarization at a point $\mathbf{r}'$ be $\mathbf{P}(\mathbf{r}')$, the potential is given by

$$V(\mathbf{r}) = -e\int \frac{\mathbf{P}(\mathbf{r}')\cdot(\mathbf{r}-\mathbf{r}')}{|\mathbf{r}-\mathbf{r}'|^3}\, d^3\mathbf{r}' \tag{2}$$

It is seen from eq 1 and 2 that the electronic energy E is a functional of the orientational polarization $\mathbf{P}(\mathbf{r})$. In the previous paper we considered only the orientational polarization which is spherically symmetric. In the present paper we consider not only the orientational polarization which is spherically symmetric but also the orientational polarization which is not.

We solve eq 1 approximately by using the variation method. If the wave function is normalized, the electronic energy is written as

$$E = \int \psi\left[-\frac{\hbar^2}{2m}\nabla^2 - e\int \frac{\mathbf{P}(\mathbf{r})\cdot(\mathbf{r}-\mathbf{r}')}{|\mathbf{r}-\mathbf{r}'|^3}\, d^3\mathbf{r}'\right]\psi\, d^3\mathbf{r} \tag{3}$$

As a trial wave function for the ground state we choose the following hydrogen-like 1s wave function

$$\psi_{1s} = (\lambda^3/\pi)^{1/2} \exp(-\lambda r) \tag{4}$$

The variational parameter λ is determined by the following condition

$$\partial E_{1s}/\partial\lambda = 0 \tag{5}$$

On the other hand, as a trial wave function for the excited state we choose the following hydrogen-like 2pz wave function

$$\psi_{2pz} = (\mu^5/\pi)^{1/2} r \exp(-\mu r) \cos\theta \tag{6}$$

The variational parameter μ is determined by the following condition

$$\partial E_{2pz}/\partial\mu = 0 \tag{7}$$

We assume that the polarization energy Π is given by[2]

$$\Pi = \gamma\int \mathbf{P}(\mathbf{r})^2\, d^3\mathbf{r} \tag{8}$$

where γ is a constant. In the previous paper we used 5.55 for the constant γ. The same value is used in the present paper.

The total energy F of the hydrated electron is given by

$$F = \int \psi\left[-\frac{\hbar^2}{2m}\nabla^2 - e\int \frac{\mathbf{P}(\mathbf{r})\cdot(\mathbf{r}-\mathbf{r}')}{|\mathbf{r}-\mathbf{r}'|^3}\, d^3\mathbf{r}'\right]\psi\, d^3\mathbf{r} + \gamma\int \mathbf{P}(\mathbf{r})^2\, d^3\mathbf{r} \tag{9}$$

Since the second term in eq 9 does not involve ψ, eq 5 is equivalent to

$$\partial F_{1s}/\partial\lambda = 0 \tag{10}$$

and eq 7 is equivalent to

$$\partial F_{2pz}/\partial\mu = 0 \tag{11}$$

If the orientational polarization $\mathbf{P}(\mathbf{r})$ is given, the total energy for the ground state can be calculated by use of eq 4, 9, and 10. The total energy for the excited state can be calculated by use of eq 6, 9, and 11.

III. Calculations and Results

A. Orientational Polarization under Which the Total Energy is Minimum. The orientational polarization under which the total energy is minimum is determined by the following condition

$$\delta F(\mathbf{P})/\delta \mathbf{P}(\mathbf{r}) = 0 \quad (12)$$

From eq 2 the orientational polarization is given by[3]

$$\mathbf{P}(\mathbf{r}) = -(1/4\pi e)\nabla V \quad (13)$$

Using eq 13, the total energy is rewritten as

$$F = \int \psi\left[-\frac{\hbar^2}{2m}\nabla^2 + V\right]\psi \, d^3\mathbf{r} + \frac{\gamma}{(4\pi e)^2}\int \nabla V \cdot \nabla V \, d^3\mathbf{r} \quad (14)$$

Equation 12 is equivalent to

$$\delta F(V)/\delta V(\mathbf{r}) = 0 \quad (15)$$

From eq 14 and 15 the following Euler equation is derived for the potential under which the total energy is minimum[5]

$$\frac{2\gamma}{(4\pi e)^2}\nabla^2 V - \psi^2 = 0 \quad (16)$$

The solution of eq 16 is given by

$$V(\mathbf{r}) = -\frac{2\pi e^2}{\gamma}\int \frac{\psi(\mathbf{r}')^2}{|\mathbf{r} - \mathbf{r}'|} \, d^3\mathbf{r}' \quad (17)$$

Using eq 16, eq 14 is rewritten as

$$F = \int \psi\left[-\frac{\hbar^2}{2m}\nabla^2 + \frac{1}{2}V\right]\psi \, d^3\mathbf{r}' \quad (18)$$

The total energy for the ground or excited state is obtained by substituting eq 4 or 6 into eq 17 and 18.

The total energy for the ground state is given by

$$F_{1s} = \frac{\hbar^2\lambda^2}{2m} - \frac{5\pi e^2\lambda}{8\gamma} \quad (19)$$

The total derivative of F_{1s} with respect to λ is written as

$$\frac{dF_{1s}}{d\lambda} = \frac{\partial F_{1s}}{\partial \lambda} + \frac{\delta F_{1s}}{\delta \mathbf{P}}\frac{\delta \mathbf{P}}{\delta \lambda} \quad (20)$$

Since $\partial F_{1s}/\partial\lambda = \delta F_{1s}/\delta \mathbf{P} = 0$ (eq 10 and 12), we have

$$dF_{1s}/d\lambda = 0 \quad (21)$$

From eq 19 and 21 we have

$$\lambda = \lambda_0 \equiv 5\pi/8\gamma a_0 \quad (22)$$

where a_0 is the Bohr radius. The total energy for the ground state is given by

$$F_{1s} = -\hbar^2\lambda_0^2/2m \quad (23)$$

From eq 17 the potential V_0 under which the total energy for the ground state is minimum is given by

$$V_0(\mathbf{r}) = -\frac{16\hbar^2\lambda_0^2}{5m}\left[\frac{1}{\lambda_0 r} - \left(\frac{1}{\lambda_0 r} + 1\right)\exp(-2\lambda_0 r)\right] \quad (24)$$

From eq 13 and 24 the orientational polarization $\mathbf{P}_0$ under which the total energy for the ground state is minimum is given by

$$\mathbf{P}_0(\mathbf{r}) = \frac{e\lambda_0^2}{2\gamma}\left[\frac{1}{\lambda_0^2 r^2} - \left(\frac{1}{\lambda_0^2 r^2} + \frac{2}{\lambda_0 r} + 2\right)\times \exp(-2\lambda_0 r)\right]\mathbf{e}_r \quad (25)$$

where $\mathbf{e}_r$ is the unit vector along the radial direction. The orientational polarization $\mathbf{P}_0(\mathbf{r})$ is shown in Figure 1. The orientational polarization under which the total energy for the ground state is minimum is spherically symmetric and pointing toward the origin. The potential $V_0(\mathbf{r})$ is shown in Figure 2. $V_0(\mathbf{r})$ is also spherically symmetric.

The total energy for the excited state is given by

$$F_{2pz} = \frac{\hbar^2\mu^2}{2m} - \frac{501\pi e^2\mu}{1280\gamma} \quad (26)$$

The total derivative of F_{2pz} with respect to μ is written as

$$\frac{dF_{2pz}}{d\mu} = \frac{\partial F_{2pz}}{\partial \mu} + \frac{\delta F_{2pz}}{\delta \mathbf{P}}\frac{\delta \mathbf{P}}{\delta \mu} \quad (27)$$

Since $\partial F_{2pz}/\partial\mu = \delta F_{2pz}/\delta \mathbf{P} = 0$ (eq 11 and 12), we have

$$dF_{2pz}/d\mu = 0 \quad (28)$$

From eq 26 and 28 we have

$$\mu = \mu_0 \equiv 501\pi/1280\gamma a_0 \quad (29)$$

The total energy for the excited state is given by

$$F_{2pz} = -\hbar^2\mu_0^2/2m \quad (30)$$

From eq 17 the potential V_1 under which the total energy for the excited state is minimum is given by

$$V_1(\mathbf{r}) = -\frac{1280\hbar^2\mu_0^2}{1503m}\left[\frac{6}{\mu_0 r} - \left(\frac{6}{\mu_0 r} + 9 + 6\mu_0 r + 2\mu_0^2 r^2\right)\exp(-2\mu_0 r) + (3\cos^2\theta - 1)\left\{\frac{9}{\mu_0^3 r^3} - \left(\frac{9}{\mu_0^3 r^3} + \frac{18}{\mu_0^2 r^2} + \frac{18}{\mu_0 r} + 12 + 6\mu_0 r + 2\mu_0^2 r^2\right)\times \exp(-2\mu_0 r)\right\}\right] \quad (31)$$

From eq 13 and 31 the orientational polarization $\mathbf{P}_1$ under which the total energy for the excited state is minimum is given by

$$\mathbf{P}_1(\mathbf{r}) = \frac{e\mu_0^2}{12\gamma}\left[\frac{6}{\mu_0^2 r^2} - \left(\frac{6}{\mu_0^2 r^2} + \frac{12}{\mu_0 r} + 12 + 8\mu_0 r + 4\mu_0^2 r^2\right)\exp(-2\mu_0 r) + (3\cos^2\theta - 1)\left\{\frac{27}{\mu_0^4 r^4} - \left(\frac{27}{\mu_0^4 r^4} + \frac{54}{\mu_0^3 r^3} + \frac{54}{\mu_0^2 r^2} + \frac{36}{\mu_0 r} + 18 + 8\mu_0 r + 4\mu_0^2 r^2\right)\exp(-2\mu_0 r)\right\}\right]\mathbf{e}_r + \frac{e\mu_0^2}{2\gamma}\sin\theta\cos\theta\left\{\frac{9}{\mu_0^4 r^4} - \left(\frac{9}{\mu_0^4 r^4} + \frac{18}{\mu_0^3 r^3} + \frac{18}{\mu_0^2 r^2} + \frac{12}{\mu_0 r} + 6 + 2\mu_0 r\right)\times \exp(-2\mu_0 r)\right\}\mathbf{e}_\theta \quad (32)$$

where $\mathbf{e}_\theta$ is the unit vector along the θ direction. The orientational polarization $\mathbf{P}_1(\mathbf{r})$ is shown in Figure 3. The orientational polarization under which the total energy for the excited state is minimum is not spherically symmetric. The variation of $\mathbf{P}_1(\mathbf{r})$ along $\theta = 0°$, $\theta = 45°$, and $\theta = 90°$ is shown in Figure 4. The potential $V_1(\mathbf{r})$ is shown in Figure 5. $V_1(\mathbf{r})$ is not spherically symmetric. The variation of $V_1(\mathbf{r})$ along $\theta = 0°$ and $\theta = 90°$ is shown in Figure 6.

B. Configuration Coordinate Diagram. The orientational polarization $\mathbf{P}(\mathbf{r})$ represents the configuration of the water molecules around the electron. It is possible to consider the hydrated electron as a kind of molecule. If the

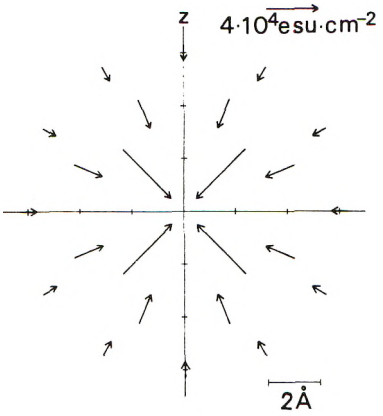

Figure 1. Orientational polarization $\mathbf{P}_0(\mathbf{r})$ under which the total energy for the ground state is minimum.

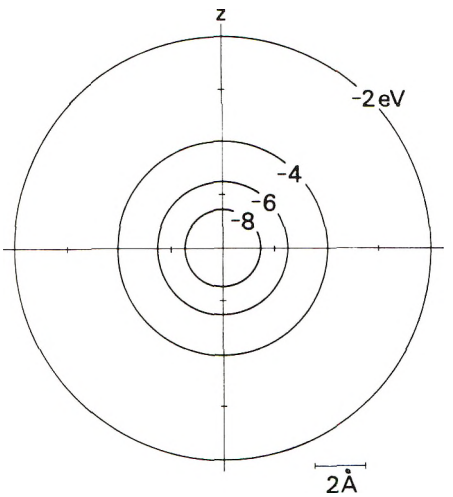

Figure 2. Potential $V_0(\mathbf{r})$ generated by the orientational polarization $\mathbf{P}_0(\mathbf{r})$.

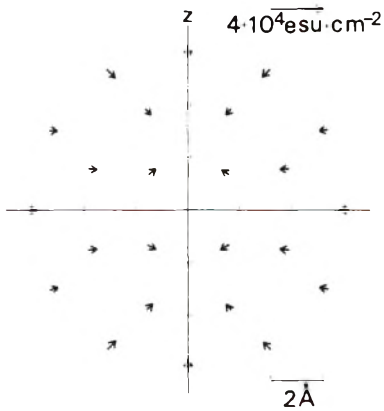

Figure 3. Orientational polarization $\mathbf{P}_1(\mathbf{r})$ under which the total energy for the excited state is minimum.

hydrated electron as a kind of molecule is compared with a diatomic molecule, the orientational polarization $\mathbf{P}(\mathbf{r})$ corresponds to the internuclear distance. The total energy of a diatomic molecule is a function of the internuclear distance. The configuration coordinate diagram for a diatomic molecule is obtained by plotting the total energy against the internuclear distance. But it is impossible to plot the total energy of the hydrated electron against the orientational polarization $\mathbf{P}(\mathbf{r})$ because the orientational polarization $\mathbf{P}(\mathbf{r})$ is not a number but a function. The total energy of the hydrated electron is a functional of the

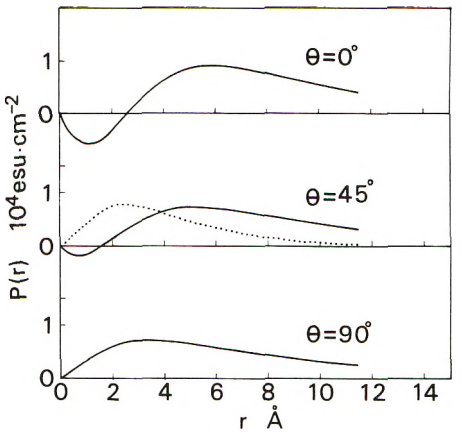

Figure 4. Variation of the orientational polarization $\mathbf{P}_1(\mathbf{r})$ along θ = 0, 45, and 90°. The full line denotes the radial component. The dotted line denotes the θ component.

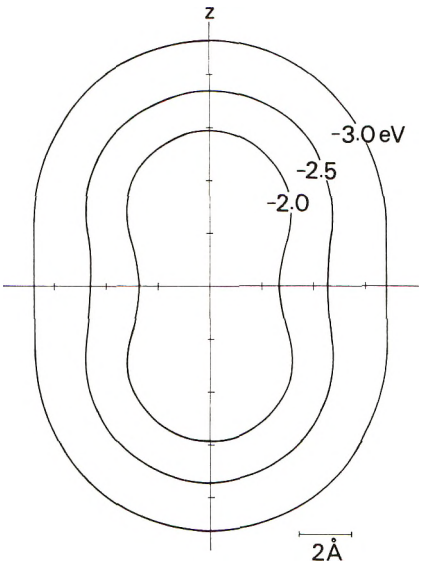

Figure 5. Potential $V_1(\mathbf{r})$ generated by the orientational polarization $\mathbf{P}_1(\mathbf{r})$.

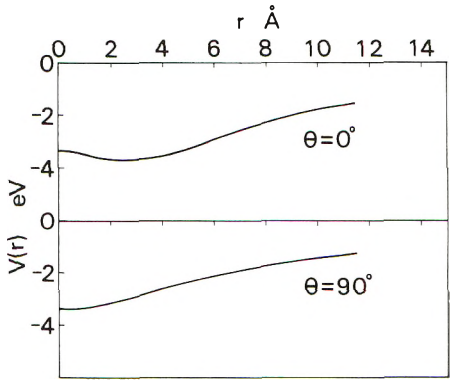

Figure 6. Variation of the potential $V_1(\mathbf{r})$ along θ = 0 and 90°.

orientational polarization $\mathbf{P}(\mathbf{r})$. In the present paper we calculate the total energies of the hydrated electron under various orientational polarizations represented by

$$\mathbf{P}_x(\mathbf{r}) = (1 - x)\mathbf{P}_0(\mathbf{r}) + x\mathbf{P}_1(\mathbf{r}) \qquad (33)$$

by varying x. We construct the configuration coordinate diagram for the hydrated electron by plotting the total energies against x.

The total energies for arbitrary x are calculated in the following way. The orientational polarization $\mathbf{P}_x(\mathbf{r})$ which

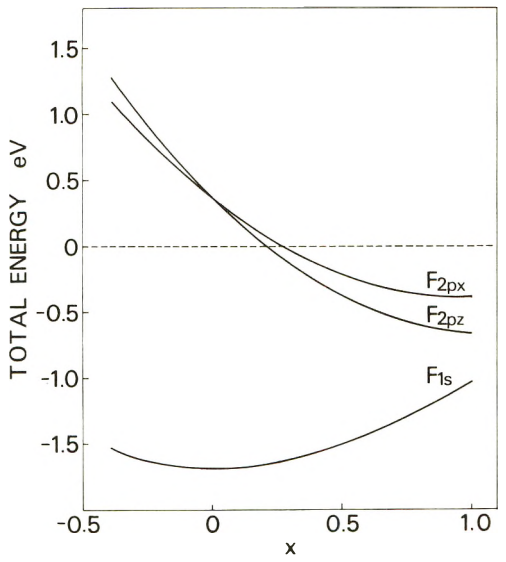

Figure 7. Configuration coordinate diagram for the hydrated electron. The abscissa x represents the orientational polarization $\mathbf{P}_x(\mathbf{r})$. For example, $x = 0$ represents $\mathbf{P}_0(\mathbf{r})$ in Figure 1. $x = 1$ represents $\mathbf{P}_1(\mathbf{r})$ in Figure 3.

corresponds to x is given by eq 33. The total energy for the ground state under $\mathbf{P}_x(\mathbf{r})$ is calculated by use of eq 4, 9, and 10. The total energy for the excited state under $\mathbf{P}_x(\mathbf{r})$ is calculated by use of eq 6, 9, and 11.

The excited state is triply degenerate under the orientational polarization $\mathbf{P}_0(\mathbf{r})$, which is spherically symmetric. But if the orientational polarization changes from $\mathbf{P}_0(\mathbf{r})$ toward $\mathbf{P}_1(\mathbf{r})$, which is not spherically symmetric, the degeneracy of the excited state is partially removed. The 2pz state branches off from the 2px and 2py states, which are still degenerate. The calculation of the total energy for the 2pz state is already described. The total energy for the 2px state is calculated in the following way. As a trial wave function for the 2px state we choose the following hydrogen-like 2px wave function

$$\psi_{2px} = (\nu^5/\pi)^{1/2} r \exp(-\nu r) \sin\theta \cos\varphi \quad (34)$$

The variational parameter ν is determined by the following condition

$$\partial F_{2px}/\partial\nu = 0 \quad (35)$$

The total energy for the 2px state is calculated by use of eq 9, 34, and 35.

The configuration coordinate diagram for the hydrated electron is shown in Figure 7. In Figure 7 the abscissa x represents the orientational polarization $\mathbf{P}_x(\mathbf{r})$ around the electron. For example, $x = 0$ represents the orientational polarization $\mathbf{P}_0(\mathbf{r})$ in Figure 1. $x = 1$ represents the orientational polarization $\mathbf{P}_1(\mathbf{r})$ in Figure 3. The total energy for the 1s state is minimum at $x = 0$, while the total energy for the 2pz state is minimum at $x = 1$. The energy difference between the 1s and 2p states at $x = 0$ is 2.0 eV. The energy difference between 1s and 2pz states at $x = 1$ is 0.4 eV, while the energy difference between the 2pz and 2px states at $x = 1$ is 0.3 eV.

IV. Discussions

As is obvious from Figure 7, the orientational polarization under which the total energy for the 2pz state is minimum is different from the orientational polarization under which the total energy for the 1s state is minimum. Thus the optical excitation of the hydrated electron from the 1s state to the 2pz state is followed by the change of the orientational polarization from $\mathbf{P}_0(\mathbf{r})$ to $\mathbf{P}_1(\mathbf{r})$. The orientational polarizations $\mathbf{P}_0(\mathbf{r})$ and $\mathbf{P}_1(\mathbf{r})$ are shown in Figures 1 and 3, respectively. The change of the orientational polarization from $\mathbf{P}_0(\mathbf{r})$ to $\mathbf{P}_1(\mathbf{r})$ implies the reorientation of the water molecules around the electron. Thus the optical excitation is followed by the reorientation of the water molecules around the electron. In the semicontinuum model the optical excitation is followed by the expansion of the cavity.[6]

It is also seen from Figure 7 that the total energy for the 2pz state at $x = 0$ is positive. Thus the optical excitation of the hydrated electron from the 1s state to the 2pz state may be followed by the vanishing of the orientational polarization around the electron and the liberation of the electron. In the measurement of the absorption spectrum of the trapped electron it has been found that the trapped electrons are partially bleached by the measuring light. This phenomenon may be explained by the mechanism described above.

The total energy for the 2pz state at $x = 1$ is negative. Thus, once the orientational polarization around the electron changes from $\mathbf{P}_0(\mathbf{r})$ to $\mathbf{P}_1(\mathbf{r})$, the 2pz state cannot autoionize. The radiative or nonradiative transition from the 2pz state to the 1s state occurs. If the radiative transition occurs, the emission will be observed in the infrared region.

In the case of optical excitation from the 1s state to the 2px or 2py state the orientational polarization around the electron does not change to $\mathbf{P}_1(\mathbf{r})$, which is distorted in the direction of the z axis. It changes from $\mathbf{P}_0(\mathbf{r})$ to the orientational polarization which is distorted in the direction of the x or y axis.

In the present paper we assume the excited state to be the 2p state. If the excited state were assumed to be the 2s state, no Jahn-Teller splitting would be found. On the other hand, if the excited state were assumed to be the 3d state, the type and magnitude of the Jahn-Teller splitting would be different from that found with the 2p state. Thus the results are dependent upon the assumptions that are made regarding the excited state.

In the present paper the variational calculation was carried out using trial wave functions which involve only one parameter. Thus the present results may be considered to be semiquantitative.

References and Notes

(1) Japan Society for the Promotion of Science. Postdoctoral Fellow 1973–1974.
(2) M. Tachiya, Y. Tabata, and K. Oshima, *J. Phys. Chem.*, **77**, 263 (1973).
(3) Equation 2 is rewritten as

$$V(\mathbf{r}) = e\int \frac{\mathrm{div}\ \mathbf{P}(\mathbf{r}')}{|\mathbf{r} - \mathbf{r}'|}\, d^3\mathbf{r}' \quad (i)$$

In general the vector field $\mathbf{P}(\mathbf{r})$ can be written as[4]

$$\mathbf{P}(\mathbf{r}) = \mathrm{grad}\ \varphi(\mathbf{r}) + \mathrm{rot}\ \mathbf{A}(\mathbf{r}) \quad (ii)$$

where the scalar potential $\varphi(\mathbf{r})$ and the vector potential $\mathbf{A}(\mathbf{r})$ are given by

$$\varphi(\mathbf{r}) = -\int \frac{\mathrm{div}\ \mathbf{P}(\mathbf{r}')}{4\pi|\mathbf{r} - \mathbf{r}'|}\, d^3\mathbf{r}' \quad (iii)$$

and

$$\mathbf{A}(\mathbf{r}) = \int \frac{\mathrm{rot}\ \mathbf{P}(\mathbf{r}')}{4\pi|\mathbf{r} - \mathbf{r}'|}\, d^3\mathbf{r}' \quad (iv)$$

respectively. We assume that the orientational polarization $\mathbf{P}(\mathbf{r})$ is rotationless. Then eq ii reduces to

$$\mathbf{P}(\mathbf{r}) = \text{grad } \varphi(\mathbf{r}) \qquad (v)$$

From Eq i, iii, and v eq 13 is derived.

(4) See P. M. Morse and H. Feshbach, "Methods of Theoretical Physics," McGraw-Hill, New York, N. Y., 1953, p 52.

(5) See, for example, R. Courant and D. Hilbert, "Methods of Mathematical Physics," Vol. 1, Interscience, New York, N. Y., 1953, Chapter IV.

(6) D. A. Copeland, N. R. Kestner, and J. Jortner, *J. Chem. Phys.*, **53**, 1189 (1970).

Application of a New Equation Based on Enthalpies of Formation and Ionization Potentials to the Problem of the Nature of Bonding in Weak Molecular Complexes

Manjit S. Sambhi

Department of Chemistry, University of Malaya, Kuala Lumpur, Malaysia *(Received March 12, 1973)*

Publication costs assisted by Department of Chemistry, University of Malaya

The existence of molecular complexes is generally inferred from the formation constants and enthalpies of formation data. The enthalpy of formation can arise from charge transfer and other forces. These other forces include coulombic, induction, dispersion, and exchange repulsion forces. The relative contributions of charge transfer and other energies to the enthalpy of formation has been a topic of considerable interest. An equation based on theoretical relationships and employing enthalpies of formation and ionization potentials can provide useful information about the nature of bonding in weak molecular complexes. The application of this equation to $b\pi$–$a\pi$ and $b\pi$–$a\sigma$ complexes is discussed.

Introduction

Mulliken[1] used a valence-bond treatment to describe the interaction of electron donor (D) and an electron acceptor (A) to form a molecular complex (D,A). The ground and the excited state of the complex can be described by the wave functions

$$\psi_N = a\psi_0(D,A) + b\psi_1(D^+\text{-}A^-)$$

and

$$\psi_E = a^*\psi_1(D^+\text{-}A^-) - b^*\psi_0(D,A)$$

The term ψ_0 refers to the no-bond wave function and corresponds to the structure in which the bonding results from coulombic, induction, dispersion, and exchange repulsion forces, while the dative-bond wave function ψ_1 corresponds to the structure where an electron has been transferred from D to A. Resonance between the no-bond and the dative structures in the ground state provides additional stability over the usual stability attributed to forces in the no-bond structure. This additional force contributing to the stability of the molecular complex is called a charge-transfer force. The coulombic, induction, and dispersion forces are attractive, while the exchange repulsion works against them, giving a total net force in the no-bond structure which might be either negative or, if the charge-transfer forces are strong enough, even zero or positive. The coefficients a and b in the ground-state wave function measure the relative contributions of the normalized no-bond and charge-transfer wave functions.

Drago and Wayland[2] have proposed a four parameter equation to correlate the enthalpy data in gas phase or poorly solvating media while Dewar and Thompson[3] attempted to ascertain the no-bond and charge-transfer character of molecular complexes from formation constant data.

We have developed an equation based on theoretical relationships derived by Mulliken[1] and Briegleb[4] which can provide useful information on the nature of bonding in molecular complexes. The equation uses enthalpies of formation ($\Delta H°$) of complexes and ionization potentials (I_D) of donors and the application of this equation to $b\pi$–$a\pi$ and $b\pi$–$a\sigma$ molecular complexes is discussed.

Theory

The ground-state energy (E_N) of a complex can be written as

$$E_N = R_N + E_0 = \Delta H°$$

where R_N is the resonance energy due to interaction between the no-bond and dative structures and E_0 is the energy change due to other interactions when the donor and acceptor come together. The energy of the excited state (E_E) can be represented as

$$E_E = I_D - E_A + E_C + R_E = E_1 + R_E$$

where E_1 is the energy of the dative structure, E_A is the electron affinity of the acceptor, E_C is mainly the coulombic attractive energy associated with the dative structure, and R_E is the resonance energy arising from the admixture of the no-bond and the dative structures.

For weak molecular complexes[5] E_N and E_E are given by the expressions

$$E_N = -\frac{\beta_0^2}{E_1 - E_0} + E_0$$

and

$$E_E = + \frac{\beta_1^2}{E_1 - E_0} + E_1$$

where β_0 and β_1 are resonance integrals. The enthalpy of formation for weak molecular complexes is then

$$\Delta H^\circ = - \frac{\beta_0^2}{E_1 - E_0} + E_0 = R_N + E_0 \quad (1)$$

Now $(E_1 - E_0) = I_D - E_A + E_C - E_0$, hence from eq 1

$$\Delta H^\circ = - \frac{\beta_0^2}{I_D - E_A + E_C - E_0} + E_0$$

and if $(E_A - E_C + E_0)$ can be designated by C_1, then

$$\Delta H^\circ = - \frac{\beta_0^2}{I_D - C_1} + E_0 \quad (2)$$

The difference in enthalpies of formation of two complexes is given by

$$\Delta H^\circ_2 - \Delta H^\circ_1 = - \frac{\beta_{02}^2}{I_{D2} - C_{12}} + E_{02} + \frac{\beta_{01}^2}{I_{D1} - C_{11}} - E_{01} \quad (3)$$

where subscripts 1 and 2 refers to complexes 1 and 2, respectively. Equation 3 can be written in the form

$$-(\Delta H^\circ_2 - \Delta H^\circ_1) = \frac{(\beta_{02}^2 I_{D1} - \beta_{01}^2 I_{D2})}{(I_{D2} - C_{12})(I_{D1} - C_{11})} - \frac{(\beta_{02}^2 C_{11} - \beta_{01}^2 C_{12})}{(I_{D2} - C_{12})(I_{D1} - C_{11})} - (E_{02} - E_{01}) \quad (4)$$

It has been shown[6] that for weak molecular complexes

$$h\nu_{CT} = I_D - C_1 + \frac{C_2}{I_D - C_1} \quad (5)$$

where $h\nu_{CT}$ refers to the energy of the absorption maximum, $C_1 = (E_A - E_C + E_0)$, and $C_2 = \beta_0^2 + \beta_1^2$. If for a series of complexes with a given acceptor C_1 and C_2 are reasonably constant, then a plot of $h\nu_{CT}$ against I_D should follow eq 5. Such plots were obtained by Briegleb[4] and C_1 and C_2 can be evaluated and β_0 can be approximated from C_2 by assuming reasonable values of S_{01} and $(E_1 - E_0)$.[5] The substitution of C_1 and β_0 obtained by this procedure directly into eq 2 can lead to erroneous estimations of R_N and E_0 particularly if the values of S_{01} and $(E_1 - E_0)$ assumed are significantly different from the true values of the complexes. Mulliken and Person[5] have critically discussed the empirical procedure required to obtain C_1 and β_0 and have pointed out that these parameters can be expected to be reasonably constant if the donors are closely related. We will only use the empirical values of C_1 in the application of our equation.

Let us now assume that there are sets of complexes with the same acceptor which have β_0 as constant. This makes $\beta_{01} = \beta_{02}$. For complexes of related donors it is easily verified that $(\beta_{02}^2 C_{11} - \beta_{01}^2 C_{12}) \ll (I_{D2} - C_{12})(I_{D1} - C_{11})$ and this makes the second term in eq 4 approximately 0. Equation 4 now becomes

$$-(\Delta H^\circ_2 - \Delta H^\circ_1) = \frac{\beta_0^2 (I_{D1} - I_{D2})}{(I_{D1} - C_{11})(I_{D2} - C_{12})} - (E_{02} - E_{01}) \quad (6)$$

where β_{01} and β_{02} have been replaced by β_0. If we now compute the differences in enthalpies of formation of complexes with reference to an arbitrary chosen standard complex, then 6 takes the form

$$-(\Delta H^\circ_N - \Delta H^\circ_S) = \frac{\beta_0^2 (I_{DS} - I_{DN})}{(I_{DS} - C_{1S})(I_{DN} - C_{1N})} - (E_{0N} - E_{0S}) \quad (7)$$

Subscript S refers to the standard complex and subscript N refers to any complex in the series where N = 1, 2, 3, 4... corresponding to different complexes. A complex incorporating a donor with the highest I_D and having numerically the highest ΔH°, *i.e.*, smallest $-\Delta H^\circ$, is a convenient standard to choose. The term $(I_{DS} - C_{1S})$ now becomes constant. An average value of C_1 obtained from eq 5 can be used for C_{1S} and C_{1N}. If for a number of complexes in the series the term $(E_{0N} - E_{0S})$ is reasonably constant, then a plot of $-(\Delta H^\circ_N - \Delta H^\circ_S)$ against $(I_{DS} - I_{DN})/(I_{DN} - C_{1N})$ should yield a linear plot with a gradient of $\beta_0^2/(I_{DS} - C_{1S})$ and an intercept of $-(E_{0N} - E_{0S})$. The information derived from the gradients and intercepts of such plots can provide useful information to the relative contributions of R_N and E_0 to ΔH° of weak molecular complexes. Although the indicated procedure has involved several assumptions which cannot be exactly correct, it seems reasonable that they are sufficiently valid so that the results are significant.

The application of eq 7 to $b\pi$-$a\pi$ and $b\pi$-$a\sigma$ complexes will now be discussed.

Application of Eq 7 and Discussion

Equation 7 is strictly applicable to complexes in the vapor phase as it is based on the theoretical description of Mulliken[1,5] for interaction between isolated donor and acceptor molecules. Spectrophotometric and thermodynamic data are not readily available for complexes in the vapor phase, while a vast amount of data have accumulated for complexes in solution. It has been shown for several donor-acceptor systems that enthalpies measured in weakly polar solvent will differ by constant amount from those measured in a poorly solvating medium,[7,8] and we have, therefore, used the approximation

$$(\Delta H_N - \Delta H_S)_{vap} \approx (\Delta H_N - \Delta H_S)_{sol}$$

for all $b\pi$-$a\pi$ and $b\pi$-$a\sigma$ complexes examined here.

For tetracyanoethylene aromatic hydrocarbon complexes[9] a red shift of 1000–3000 cm^{-1} occurs for charge-transfer absorption maxima (λ_{max}) on going from vapor phase to solution. This would imply that $h\nu_{CT(vap)} = kh\nu_{CT(sol)}$ where k is a constant >1. The $b\pi$-$a\pi$ and $b\pi$-$a\sigma$ complexes examined here have generally λ_{max} in the region of 300–600 mμ, and if we take an average red shift of 2000 cm^{-1} for λ_{max} on going from vapor phase to solution, then k is in the region 1.06–1.15. Thus, C_1 obtained from $h\nu_{CT}$ solution values would not be very different from C_1 obtained from $h\nu_{CT}$ vapor-phase values and these were used without any modification for the $b\pi$-$a\pi$ and $b\pi$-$a\sigma$ complexes examined. This means that the gradients obtained from plots based on eq 7 are slightly affected but not the intercepts.

(A) $b\pi$-$a\pi$ Complexes

(i) 1,3,5-Trinitrobenzene (TNB) Complexes. The ΔH° data for the TNB complexes were obtained from ref 4 while the I_D data were obtained from ref 4, 5, and 10. A value of 5.00 eV for C_1 found for $b\pi$-TNB complexes[4] was used for C_{1S} and C_{1N}. The benzene complex forms a con-

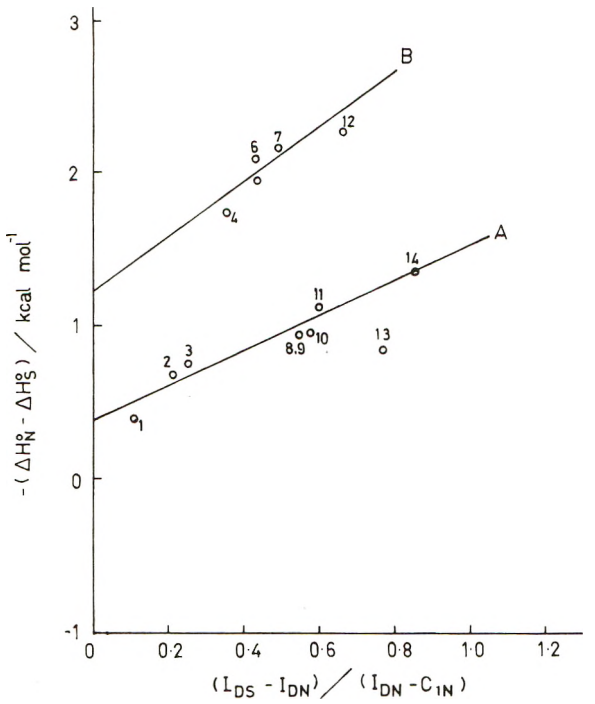

Figure 1. $-(\Delta H^{\circ}_N - \Delta H^{\circ}_S)$ *vs.* $(I_{DS} - I_{DN})/(I_{DN} - C_{1N})$ plot for TNB complexes of Table I. The numbers refer to complexes as designated in Table I.

TABLE I: Data for a Plot of $-(\Delta H^{\circ}_N - \Delta H^{\circ}_S)$ *vs.* $(I_{DS} - I_{DN})/(I_{DN} - C_{1N})$ for TNB Complexes[a]

Donor	I_D, eV	$(I_{DS} - I_{DN})/(I_{DN} - C_{1N})$	$-\Delta H^{\circ}$, kcal mol^{-1}	$\Delta H^{\circ}_N - \Delta H^{\circ}_S$, kcal mol^{-1}
Benzene (S)	9.24	0	0.45	0
Toluene (1)	8.82	0.11	0.86	0.41
p-Xylene (2)	8.48	0.22	1.12	0.67
Mesitylene (3)	8.40	0.25	1.21	0.76
Naphthalene (4)	8.12	0.36	2.20	1.75
1-Methylnaphthalene (5)	7.96	0.43	2.41	1.96
2-Methylnaphthalene (6)	7.96	0.43	2.56	2.11
Phenanthrene (7)	7.85	0.49	2.63	2.18
o-Toluidine (8)	7.75	0.54	1.39	0.94
m-Toluidine (9)	7.75	0.54	1.39	0.94
Aniline (10)	7.70	0.57	1.35	0.90
p-Toluidine (11)	7.65	0.60	1.58	1.13
Anthracene (12)	7.55	0.66	2.74	2.29
Diphenylamine (13)	7.40	0.77	1.31	0.86
N,N-Dimethylaniline (14)	7.30	0.84	1.82	1.37

[a] Solvent: chloroform. $C_{1S} = C_{1N} = 5.00$ eV. The donors are designated by numerals given in parentheses.

venient standard as it has highest I_D and numerically the highest ΔH°. Table I gives the necessary data for Figure 1.

Figure 1 shows that two reasonable straight lines (A and B) were obtained with average gradients of 4.91×10^{-2} and 7.86×10^{-2} eV, respectively. The gradients yield $\beta_0 = -0.46$ and -0.58 eV for lines A and B, respectively.

The values of β_0 of -0.46 and -0.58 eV are in agreement with values discussed for $b\pi$–$a\pi$ complexes calculated from the empirical constant $C_2 = \beta_0^2 + \beta_1^2$ and assuming that S_{01} is approximately 0.1.[5] As the benzene complex was chosen as the standard, one should ideally have obtained lines A and B of the same value of gradient, but this minor difference may be attributed to the uncertainties in ΔH° data or that C_1 varies over a small range. Mulliken and Person[5] have discussed the trial-and-error procedure necessary to evaluate C_1 from a plot of $h\nu_{CT}$ and I_D data. They have emphasized the rather large limits of the value of C_1 obtained. Briegleb[4] used one curve to fit all the $h\nu_{CT}$ and I_D data and it may be necessary to use separate curves for different series of complexes as was done in the case of primary, secondary, and tertiary amine complexes.[11]

The resonance energy R_N can be evaluated by the expression

$$R_N = -\beta_0^2/(I_D - C_1)$$

The average value of $I_D - C_1$ for complexes of lines A and B is approximately 3 eV, and if we take the average β_0 for the complexes we obtain R_N in the region of -1.6 and -2.5 kcal mol^{-1}. These values are of the same magnitude or greater than the ΔH° values.

The intercept of line A is 0.4 kcal mol^{-1} and this implies that for complexes represented by line A, the E_{0N} is 0.4 kcal mol^{-1} more negative than for the benzene complex. The E_{0S} contribution to ΔH° of the benzene complex cannot be evaluated by this method, but if we make the drastic assumption that all of ΔH° for the benzene complex is E_{0S}, then E_{0N} for the complexes of line A becomes $-0.45 - 0.40 = -0.85$ kcal mol^{-1}. This means that the minimum R_N varies from approximately 20 to 50% of ΔH° for these complexes. The contribution of R_N to ΔH° is in accord with the findings of other authors.[12-14]

The intercept of line B is 1.2 kcal mol^{-1} and using the same reasoning as above, one can obtain $E_{0N} = -1.2 - 0.45 = -1.65$ kcal mol^{-1}. This means that approximately a minimum of 20–30% of ΔH° for the complexes of line B can be assigned to R_N.

Since E_0 for these complexes does not account for all of ΔH° even when R_N is assumed zero for the benzene complex, it seems justifiable to assume that R_N for the benzene complex also is not zero, and thus R_N is probably higher than estimated above for these complexes.

The term E_{0N} being more negative than E_{0S} is consistent with the view that dipole–dipole interactions which are present in the substituted benzene complexes are absent in the benzene complex and that donors of line B are more polarizable than benzene. It is to be expected that only complexes of closely related donors would have β_0 and C_1 reasonably constant and it is significant that complexes of line A are of related substituted benzene donors while complexes of line B are of donors consisting of two or three six-membered aromatic rings, and thus having common structural and dimensional properties.

(ii) 1,3,5-Trinitrobenzene Complexes Repeated. The ΔH° data for complexes have now been obtained from nmr chemical shifts[15] and are more negative than the values shown in Table I. The I_D data are from ref 5 and 10 and $C_{1S} = C_{1N} = 5.00$ eV as before. The benzene complex again forms a convenient standard and Table II shows the relevant data necessary for Figure 2.

A reasonable linear plot is obtained as shown in Figure 2. The gradient is 1.4×10^{-1} eV and yields $\beta_0 = -0.77$ eV which is higher than the value of β_0 obtained from Figure 1 and gives R_N in the region of -4.6 kcal mol^{-1}.

The intercept of the plot is 0 kcal mol^{-1} and if we assume as before (see i) that R_N for the benzene complex is zero, then E_{0N} for the complexes cannot be greater than -1.9 kcal mol^{-1} and possibly less in view of the evidence obtained from Figure 1. This means that the minimum

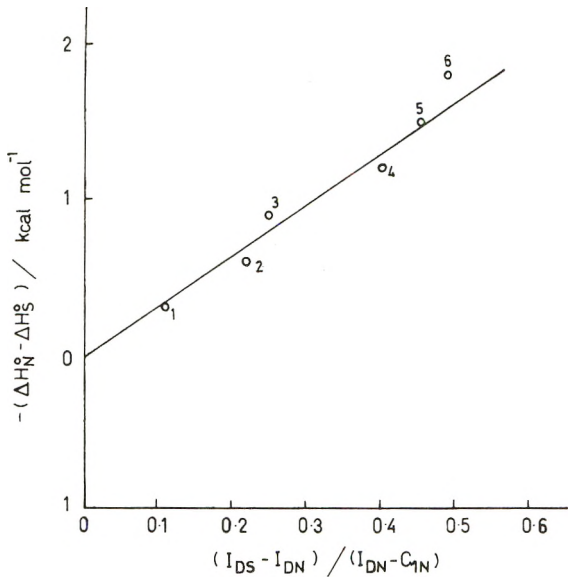

Figure 2. $-(\Delta H^{\circ}_N - \Delta H^{\circ}_S)$ *vs.* $(I_{DS} - I_{DN})/(I_{DN} - C_{1N})$ plot for TNB complexes of Table II. The numbers refer to complexes as designated in Table II.

TABLE II: Data Required for a Plot of $-(\Delta H^{\circ}_N - \Delta H^{\circ}_S)$ *vs.* $(I_{DS} - I_{DN})/(I_{DN} - C_{1N})$ for TNB Complexes[a]

Donors	I_D, eV	$(I_{DS} - I_{DN})/(I_{DN} - C_{1N})$	$-\Delta H^{\circ}$, kcal mol^{-1}	$\Delta H^{\circ}_N - \Delta H^{\circ}_S$, kcal mol^{-1}
Benzene (S)	9.24	0	1.9	0
Toluene (1)	8.82	0.11	2.2	0.3
p-Xylene (2)	8.48	0.22	2.5	0.6
Mesitylene (3)	8.40	0.28	2.8	0.9
Durene (4)	8.03	0.40	3.1	1.2
Pentamethylbenzene (5)	7.92	0.45	3.4	1.5
Hexamethylbenzene (6)	7.85	0.49	3.7	1.8

[a] Solvent: carbon tetrachloride $C_{1S} = C_{1N} = 5.00$ eV. The donors are designated by numerals given in parentheses.

R_N contribution to ΔH° of the complexes varies from approximately 20 to 50%.

(iii) Chloranil Complexes. The ΔH° data were obtained from ref 4 and the I_D data are from ref 4, 5, 10, and 16. The benzene complex forms a convenient standard and a value of 5.70 eV for C_1 obtained by Briegleb[4] was used for C_{1S} and C_{1N}. Table III gives the relevant data necessary for Figure 3.

Figure 3 shows that the points are scattered and that no satisfactory plot can be obtained. This is not unexpected since eq 7 based on the original simple form of Mulliken's theory[5] may be roughly valid in the case of complexes formed from simple molecules, but it ignores the necessity of considering the stabilization of the ground state of a complex by more than one charge-transfer state, and other complications which can occur in some cases.[5] In particular, the number of important charge-transfer states (with differing $h\nu_{CT}$) should increase with the number of condensed rings in polynuclear aromatic hydrocarbons. Hence, use of the $h\nu_{CT}$ for the longest wavelength charge-transfer bond, and also the use of the minimum ionization potential, in connection with I_D and C_1 and β_0^2 of eq 7 should become increasingly unsatisfactory if the equation is used to compare molecules with varying numbers of condensed rings and resulting in the failure to find a suitable plot to fit the points in Figure 3.

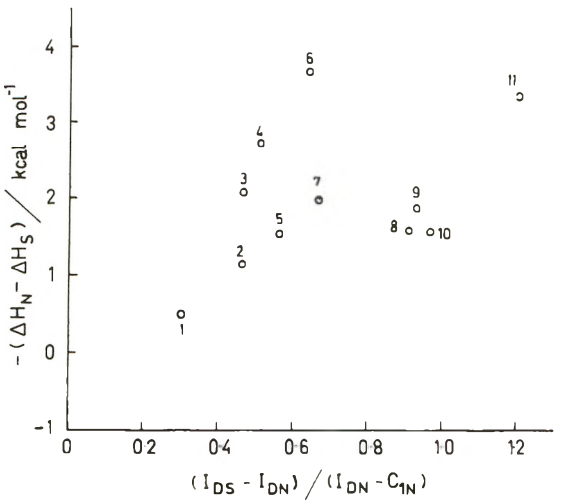

Figure 3. $-(\Delta H^{\circ}_N - \Delta H^{\circ}_S)$ *vs.* $(I_{DS} - I_{DN})/(I_{DN} - C_{1N})$ plot for chloranil complexes of Table III. The numbers refer to complexes as designated in Table III.

TABLE III: Data Required for a Plot of $-(\Delta H^{\circ}_N - \Delta H^{\circ}_S)$ *vs.* $(I_{DS} - I_{DN})/(I_{DN} - C_{1N})$ for Chloranil Complexes[a]

Donors	I_D, eV	$(I_{DS} - I_{DN})/(I_{DN} - C_{1N})$	$-\Delta H^{\circ}$, kcal mol^{-1}	$\Delta H^{\circ}_N - \Delta H^{\circ}_S$, kcal mol^{-1}
Benzene (S)	9.24	0	1.65	0
Biphenyl (1)	8.40	0.31	2.15	0.50
Naphthalene (2)	8.12	0.46	2.80	1.15
Triphenylene (3)	8.10	0.48	3.75	2.10
Durene (4)	8.03	0.52	4.40	2.75
Stilbene (5)	7.95	0.57	3.20	1.55
Hexamethylbenzene (6)	7.85	0.65	5.35	3.70
Phenanthrene (7)	7.85	0.65	3.65	2.00
Anthracene (8)	7.55	0.91	3.25	1.60
1,2-Benzanthracene (9)	7.53	0.93	3.55	1.90
Pyrene (10)	7.50	0.97	3.25	1.60
Dimethylaniline (11)	7.30	1.21	5.05	3.40

[a] Solvent: carbon tetrachloride. $C_{1S} = C_{1N} = 5.70$ eV. The donors are designated by numerals given in parentheses.

(B) *b*π-*a*σ *Complexes*

(i) Iodine Complexes. The ΔH° data for the complexes were obtained from ref 4 while the I_D data were obtained from ref 5 and 10. The benzene complex was chosen as the standard and a value of 5.20 eV for C_1 found for *b*π-*a*σ complexes[4] was used for C_{1S} and C_{1N}. The data necessary for Figure 4 are shown in Table IV.

We have assumed that ΔH° for the iodine complexes of toluene and o-xylene are of the same magnitude in carbon tetrachloride and *n*-hexane, since these are solvents with poor solvating action.

Figure 4 shows a reasonably linear plot and the average gradient is 2.215×10^{-1} eV which yields $\beta_0 = -0.95$ eV. This is in the range of values recommended for *b*π-I_2 complexes[5] and R_N obtained from this is in the region of -4.8 kcal mol^{-1}. The intercept is -0.3 kcal mol^{-1} and if we assume that R_N for the benzene complex is zero, then E_{0N} for the complexes cannot be greater than 1.0 kcal mol^{-1}. This means that the minimum R_N contribution to ΔH° of the complexes varies from 40 to 70%. This evaluation of E_0 and R_N is only applicable to the resting model of the complexes[5] where the axis of the iodine molecule is parallel to the plane of the benzene ring. However, if the

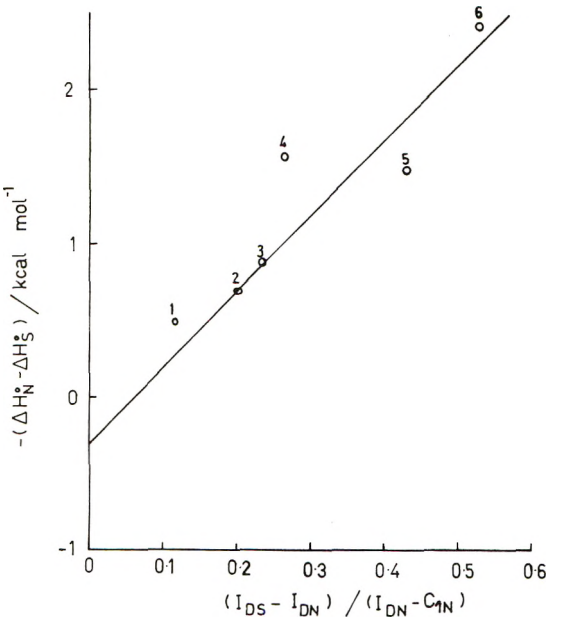

Figure 4. $-(\Delta H^{\circ}_N - \Delta H^{\circ}_S)$ *vs.* $(I_{DS} - I_{DN})/(I_{DN} - C_{1N})$ plot for iodine complexes of Table IV. The numbers refer to complexes as designated in Table IV.

TABLE IV: Data Required for a Plot of $-(\Delta H^{\circ}_N - \Delta H^{\circ}_S)$ *vs.* $(I_{DS} - I_{DN})/(I_{DN} - C_{1N})$ for Iodine Complexes[a]

Donors	I_D, eV	$(I_{DS} - I_{DN})/(I_{DN} - C_{1N})$	$-\Delta H^{\circ}$, kcal mol^{-1}	$\Delta H^{\circ}_N - \Delta H^{\circ}_S$, kcal mol^{-1}
Benzene (S)	9.24	0	1.30	0
Toluene (1)	8.82	0.12	1.80	0.50
o-Xylene (2)	8.56	0.20	2.00	0.70
p-Xylene (3)	8.48	0.23	2.18	0.88
Mesitylene (4)	8.40	0.26	2.86	1.56
Durene (5)	8.03	0.43	2.78	1.48
Hexamethylbenzene (6)	7.85	0.52	3.73	2.43

[a] $C_{1S} = C_{1N} = 5.2$ eV. The donors are designated by numerals given in parentheses. Solvent for complexes 1 and 2 is *n*-hexane and for the other complexes it is carbon tetrachloride.

axial model which has the iodine molecule standing above the plane of the benzene ring with its axis along the latter's sixfold symmetry axis is more or less correct, then the proper I_D and C_1 values used in eq 7 would be changed. This would mean that $I_{DN} - C_{1N}$ might be changed considerably while $I_{DS} - I_{DN}$ might not be much affected. The result would very likely be merely to increase the slope in Figure 4.

Conclusion

If for a series of complexes with the same acceptor β_0 and $(E_{0N} - E_{0S})$ are reasonably constant, then a plot of $-(\Delta H^{\circ}_N - \Delta H^{\circ}_S)$ *vs.* $(I_{DS} - I_{DN})/(I_{DN} - C_{1N})$ should be reasonably linear. An average value of C_1 obtained from the $h\nu_{CT}$ *vs.* I_D plot[4] was used for C_{1S} and C_{1N}. The gradient yields β_0 and the intercept of $-(E_{0N} - E_{0S})$.

It is found that β_0 is on the average -0.6 and -0.95 eV for $b\pi$-$a\pi$ and $b\pi$-$a\sigma$ complexes, respectively. The R_N calculated from the average β_0 value is generally greater or of the same magnitude as ΔH° of the complexes. The intercept $-(E_{0N} - E_{0S})$ provides an estimation of the relative contributions of R_N and E_0 to ΔH°. The E_{0S} contribution to ΔH° of an arbitrary chosen standard complex cannot be evaluated by this method, but if we make that assumption that R_N for the standard complex is zero, then the minimum R_N contribution to ΔH° of the complexes can be determined. The benzene complex was chosen as the standard complex in all cases discussed and we find that the minimum R_N contribution to ΔH° of $b\pi$-$a\pi$ and $b\pi$-$a\sigma$ complexes varies from 20 to 50% and 40 to 70%, respectively. This is in accord with the views of other authors[12-14,17] and does not subscribe to the view that charge-transfer forces are absent in weak molecular complexes.

References and Notes

(1) R. S. Mulliken, *J. Amer. Chem. Soc.*, **74**, 811 (1952).
(2) R. S. Drago and B. B. Wayland, *J. Amer. Chem. Soc.*, **87**, 3571 (1965).
(3) M. J. S. Dewar and C. C. Thompson, Jr., *Tetrahedron Suppl.*, **7**, 97 (1966).
(4) G. Briegleb, "Elektronen-Donator-Acceptor-Komplexes," Springer-Verlag, Berlin, 1961.
(5) R. S. Mulliken and W. B. Person, "Molecular Complexes: A Lecture and Reprint Volume," Wiley, New York, N. Y., 1969.
(6) S. H. Hastings, J. L. Franklin, J. C. Schiller, and F. A. Matsen, *J. Amer. Chem. Soc.*, **75**, 2900 (1953).
(7) R. S. Drago, M. S. Nozari, and G. C. Vogel, *J. Amer. Chem. Soc.*, **94**, 90 (1972).
(8) M. S. Nozari and R. S. Drago, *J. Amer. Chem. Soc.*, **94**, 6877 (1972).
(9) M. Kroll, *J. Amer. Chem. Soc.*, **90**, 1097 (1968).
(10) R. Foster, "Organic Charge-Transfer Complexes," Academic Press, London, 1969.
(11) H. Yada, J. Tanaka, and S. Nagakura, *Bull. Chem. Soc. Jap.*, **33**, 1660 (1960).
(12) M. W. Hanna, *J. Amer. Chem. Soc.*, **90**, 285 (1968).
(13) J. L. Lippert, M. W. Hanna, and P. J. Trotter, *J. Amer. Chem. Soc.*, **91**, 4035 (1969).
(14) R. J. W. Le Fevre, D. V. Radford, and P. J. Stiles, *J. Chem. Soc. B*, 1297 (1968).
(15) R. Foster, C. A. Fyfe, and M. I. Foreman, *Chem. Commun.*, 913 (1967).
(16) G. Briegleb, *Angew. Chem., Int. Ed. Engl.*, **3**, 617 (1964).
(17) R. S. Mulliken and W. B. Person, *J. Amer. Chem. Soc.*, **91**, 3409 (1969).

Hydrogen-Bonded Species of Acetic Acid in Inert Solvents[1]

Mark A. Goldman[2] and Merle T. Emerson*[3]

Department of Chemistry, The Florida State University, Tallahassee, Florida 32306 and the Department of Chemistry, University of Alabama at Huntsville, Huntsville, Alabama 35807 *(Received October 27, 1972; Revised Manuscript Received May 14, 1973)*

Publication costs assisted by the School of Science and Engineering, University of Alabama in Huntsville

The nmr chemical shift of the acid proton of acetic acid in CCl_4 has been investigated. The observed chemical shift can be quantitatively explained by assuming that acetic acid is present as an equilibrium mixture of monomers, cyclic dimers, linear dimers, and linear polymers. The temperature dependence of these equilibria is also studies. Low-temperature chemical shift measurements in cyclopentane support this model and corroborate the assignment of the chemical shift of the cyclic dimer.

Introduction

Beckmann[4] postulated the existence of a monomer–dimer equilibrium in order to explain the anomalous freezing point depressions of solutions of carboxylic acids in inert solvents. Since this early work, acetic acid has been extensively studied[5] and the presence of a monomer–dimer equilibrium has been corroborated. Using electron diffraction, Karle and Brockway[6] concluded that in the gas phase acetic acid exists as a cyclic dimer.

Based on a model assuming only a simple monomer–dimer equilibrium, several attempts to measure this hydrogen-bonding equilibrium constant have resulted in a considerable range of values.[7-11] The magnitude of the equilibrium constant obtained from infrared intensity data decreases rapidly with increase of acetic acid concentration.[8-10] These constants are two orders of magnitude larger than that obtained by sonic relaxation measurements.[11]

It is well known that the concentration dependence of the nmr chemical shift can be used to study hydrogen-bonding systems.[12] Huggens, Pimentel, and Shoolery[13] first studied the nmr shift of acetic acid in CCl_4. This work was extended by Reeves[14,15] and others.[16,17] It was found that concentration dependence of the acid proton chemical shift cannot be accounted for quantitatively by a simple monomer–cyclic dimer equilibrium. One must conclude that other hydrogen-bonded species are present in solution. The observation of long chain linear polymers in crystalline acetic acid[18] along with cyclic dimers in the gas phase[6] lead one to postulate that acetic acid in the liquid state is composed of a mixture of monomers, cyclic dimers, and linear polymers (*i.e.*, that the liquid state can be described as an equilibrium mixture of the gas and solid states). Recently, infrared and Raman evidence indicating the presence of chain polymers has been reported.[19-21]

The purpose of this work is to provide a quantitative model for solutions of acetic acid in inert solvents. It will be shown that the chemical shift of the acid proton can be accounted for quantitatively by equilibria between monomers, cyclic dimers, linear dimers, and linear polymers.[22] The temperature dependence of the nmr shifts allows one to obtain ΔH values for these equilibria.

Theory

If we postulate the existence of linear polymers, as well as monomers and cyclic dimers, the simplest expression for the chemical shift δ would be

$$\delta = f_E\delta_E + f_1\delta_1 + f_c\delta_c \tag{1}$$

where f_E is the fraction of nonhydrogen-bonded acid protons found on the chain polymer ends,[23] f_1 is the fraction of acid protons forming hydrogen bond linkages in the chain polymers, and f_c is the fraction of hydrogen-bonded protons in cyclic dimers. The δ_E, δ_1, and δ_c are, respectively, the characteristic chemical shifts of end protons, internal hydrogen bonding protons and hydrogen bonded protons in cyclic dimers.

The existence of monomers, cyclic dimers, and chain polymers can be accounted for by considering two equilibrium processes

$$AH + AH \overset{K_c}{\rightleftharpoons} (AH)_{2c} \tag{2}$$

and

$$AH + (AH)_i \overset{K_p}{\rightleftharpoons} (AH)_{i+1} \tag{3}$$

where the first equilibrium involves the formation of a cyclic dimer from two monomeric acid units and the second involves the addition of a monomer unit to an existing polymer of i units to form an $i + 1$ unit polymer.

The use of a single equilibrium constant for all polymer growth equilibria is not adequate. Using statistical arguments, it has been shown[24,25] that the equilibrium constant for two monomers bonding together to form a linear dimer should be different from that for a monomer adding to an n-mer ($n \geq 2$). Therefore, the equilibrium constants for the above reactions should be modified as follows

$$K_c = \frac{[(AH)_{2c}]}{[AH]^2} = \frac{\chi_c}{\chi_1^2} \tag{4a}$$

$$K_l = \frac{[AH\cdot AH]}{[AH]^2} = \frac{\chi^2}{\chi_1^2} \tag{4b}$$

$$K = \frac{[(AH)_{i+1}]}{[(AH)_i][AH]} = \frac{\chi_{i+1}}{\chi_i\chi_1} \tag{4c}$$

χ_c is the mole fraction of cyclic dimer, χ_1 the mole fraction of monomer and χ_i is the mole fraction of linear polymer of length i. Expressions for the mole fraction of each of the constituents can be obtained in terms of the mole fraction of the monomer by solving the set of simultaneous equilibrium expressions (4). Thus

$$\chi_c = K_c\chi_1^2 \tag{5a}$$

and

$$\chi_i = K_l K^{i-2} \chi_1^{\,i} = (K_l/K_2)(K\chi_1)^i \tag{5b}$$

In order to obtain an expression for χ_1 in terms of the equilibria constants, it is necessary to use a mass balance relationship for the total acetic acid in the solution. The amount of solvent in each solution also is needed since the mole fraction of each species is dependent on the solvent concentration. The mole fraction of solvent present is given by

$$\chi_s = \eta_s/\eta_T$$

where η_s is the number of moles of solvent[26] and η_T is the total moles of all species present. We can now write

$$\frac{\eta_s}{\eta_T} + \chi_c + \sum_{i=1}^{\infty} \chi_i = 1 \tag{6}$$

The mass balance equation for the acetic acid is

$$\frac{\eta^0_m}{\eta_T} = \sum_{i=1}^{\infty} (i)\chi_i + 2\chi_c \tag{7}$$

where η^0_m is the total number of moles of acetic acid molecules in a solution.

It can be easily shown that

$$\sum_{i=2}^{\infty} \chi_i = \frac{K_l y^2}{K^2(1-y)} \tag{8}$$

and

$$\sum_{i=2}^{\infty} (i)\chi_i = \frac{K_l y^2(2-y)}{K^2(1-y)^2} \tag{9}$$

where $y = K\chi_1$. Upon combining eq 6 and 7, we obtain

$$\frac{\eta^0_m}{\eta_s + \eta^0_m} = \frac{Ky(1-y)^2 + 2K_c y^2(1-y)^2 + K_l y^2(2-y)}{K^2(1-y)^2 + K_c y(1-y)^2 + K_l y^2} \tag{10}$$

Upon expansion, eq 10 yields a fourth-degree polynomial of y in terms of η^0_m, η_s and the three equilibrium constants K, K_l, and K_c.

$$y^4 + \frac{\eta_s(K - 4K_c - K_l) - \eta^0_m(2K_c - K + K_l)}{(2\eta_s + \eta^0_m)K_c} y^3 + \frac{2\eta_s(K_c + K_l - K) - \eta^0_m(K(K+2) - K_c - K_l)}{(2\eta_s + \eta^0_m)K_c} y^2 + \frac{K[\eta_s + \eta^0_m(2K+1)]}{(2\eta_s + \eta^0_m)K_c} y - \frac{\eta^0_m K^2}{(2\eta_s + \eta^0_m)K_c} = 0 \tag{11}$$

If one has available values for the equilibria constants, the monomer concentration can be obtained by solving eq 11. The concentration of cyclic dimer and linear polymers can then be obtained from eq 5a and 5b.

The problem to be solved is more complex than this since we want to find the set of equilibria constants and chemical shifts which will most closely reproduce the observed dependence of the chemical shift on the concentration of acetic acid. In order to accomplish this it is necessary to have expressions for the fractions of the various types of protons which contribute to the chemical shift in eq 1. These are easily obtained from the values of χ_1, χ_i, and χ_c, such that

$$f_E = \frac{\sum_1^{\infty} \chi_i}{2\chi_c + \sum_1^{\infty} (i)\chi_i} = \frac{Ky + K_l y^2/(1-y)^2}{2K_c y^2 + Ky + K_l y^2(2-Y)/(1-y)^2} \tag{12a}$$

$$f_I = \frac{\sum_2^{\infty} (i-1)\chi_i}{2\chi_c + \sum_1^{\infty} (i)\chi_i} = \frac{K_l y^2/(1-y)^2}{2K_c y^2 + Ky + K_l y^2(2-y)/(1-y)^2} \tag{12b}$$

$$f_c = \frac{2\chi_c}{2\chi_c + \sum_1^{\infty} (i)\chi_i} = \frac{2K_c y^2}{2K_c y^2 + Ky + K_l y^2(2-y)/(1-y)^2} \tag{12c}$$

We can now assume trial values for the equilibria constants, solve eq 11 for y, and calculate values for f_E, f_I, and f_c. However, we still need values of δ_E, δ_I, and δ_c in order to complete eq 1. Thus, with a trial set of f's it is simple to devise a least-squares method for obtaining the best values of δ_E, δ_I, and δ_c for placing in eq 1. These data are then calculated for the total concentration range covered and a measure of the fit to experimental observation is obtained.

The δ's and fit (R^2) are obtained in the following manner. Let us define

$$R^2 = \sum_j (\delta_j^{\text{obsd}} - \delta_j^{\text{calcd}})^2 \tag{13}$$

where δ_j^{obsd} is the observed chemical shift for the jth solution and δ_j^{calcd} is the value calculated *via* eq 1. The δ_E, δ_I, and δ_c are those values which minimize the value of R^2. It is not possible to obtain an analytic expression for R^2 in terms of equilibria constants; however, it is possible to obtain a least-squares set of equilibria constants by repeating the above procedure for several sets of constants until the set is found which gives the smallest value for R^2.

The macroscopic mole fraction of acetic acid of a particular sample may also be calculated. The mole fraction is defined as

$$\chi_A = \frac{\sum_1^{\infty} n_i + n_c}{\sum_1^{\infty} n_i + n_c + n_s} \tag{14a}$$

Making use of eq 8 and the definition of mole fraction gives

$$\chi_A = \chi_1 + \frac{K_l y^2}{K^2(1-y)} + K_c \chi_1^{\,2} \tag{14b}$$

This is the value plotted in the following graphs.

Experimental Section

Mueller and Rose[27] have shown that traces of water can greatly affect the chemical shift of the acid proton. It has also been shown[28] that samples prepared in a drybox give a noticeably spurious upfield shift compared to those prepared on a vacuum system. Thus, elaborate precautions are necessary to assure the dryness of any samples used.

Acetic acid used in this work was purified as follows. Reagent grade acetic acid was mixed with acetic anhydride in a 5:1 ratio. Solid potassium permanganate was then added slowly to the mixture, with stirring, over a period of several days until the purple color was no longer discharged. The liquid was vacuum distilled to separate the acid from the nonvolatile residue. The mixture was

then fractionally distilled using a 1-m column packed with glass beads. The middle fraction (bp 118°) was collected over vacuum-dried anhydrous sodium acetate. Final purification consisted of several passages through a continuous-flow solid–liquid zone refiner.[29,30] The acid was then stored under vacuum at −25° over anhydrous sodium acetate. All transfers were performed on a vacuum line using standard high-vacuum techniques.

Reagent grade CCl_4 was dried by refluxing for 1 day in a Soxhlet extractor using 4A Molecular Sieve. The dried CCl_4 was stored over P_2O_5 in an evacuated flask. Spectral grade cyclopentane was used without further purification except for degassing on a vacuum line. It was stored under vacuum over "dri-Na" (J. T. Baker Chemical Co.). Tetramethylsilane was used without further purification.

Nmr samples were prepared by vacuum transfer of each component into evacuated 5-mm nmr tubes. The tubes were attached to the transfer line[30] in such a way as to permit the evacuated tube to be removed and weighed on an analytical balance. Thus, the weight of each substance in the sample was known. After the solution preparation was completed, the evacuated sample was frozen with liquid nitrogen and the tube was sealed[31] and pulled off the vacuum system.

A Varian A-60 nmr spectrometer equipped with a variable temperature probe was employed. The side-band modulation method was used for determining chemical shifts. The acetic acid methyl–TMS shift for the CCl_4 samples was also measured. It was found to be virtually constant (123 Hz) over the entire concentration range. Because of the closeness of the methyl group and cyclopentane resonances, only the acid proton to TMS shift was measured for the cyclopentane samples. The temperature of the probe was ascertained using either ethylene glycol or methanol standards obtained from Varian Associates.[32]

The poor temperature regulation on the A-60 is most likely the main source of error in the chemical shift measurements. The chemical shift measurement is probably accurate to ±0.25 Hz. Therefore, if one considers a range of 0.5 Hz to be experimental error, the R^2 for the 28 samples could have a value of up to 7.0 and still be within experimental error. All R^2 values were found to be with this value.

Results and Discussion

Figure 1 shows the dependence of the acid proton chemical shift on concentration at three temperatures in CCl_4. It is quite obvious that more than a simple monomer–cyclic dimer equilibrium must be present to give curves of this complexity.

A minimum value for R^2 is not a sufficient boundary condition to determine the appropriate values of the equilibrium constants as several sets of K's give R^2 within that expected for the estimated experimental errors. Additional criteria are then needed to determine the correct set of K's. These criteria are as follows: (1) a self-consistent set of chemical shifts at all temperature (*i.e.*, the value of the chemical shift should be independent of temperature, and therefore the same values should be derived at all three temperatures); (2) the value of δ_c should be reasonably close to that indicated by low-temperature chemical shift studies in cyclopentane (see discussion below); (3) the value of ΔH for the formation of a given type of H bond should be independent of temperature.[33]

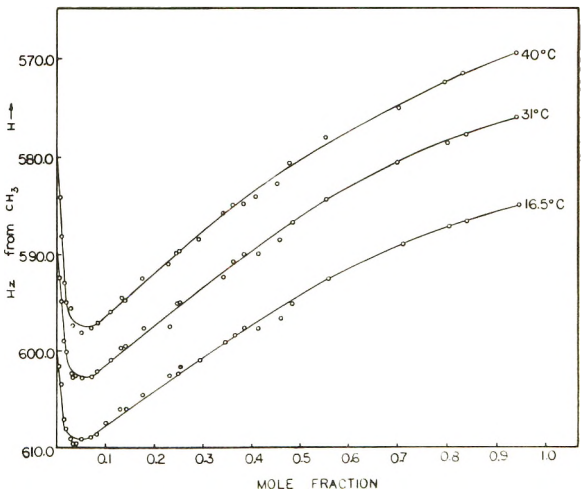

Figure 1. Dependence of acid proton chemical shift on mole fraction in CCl_4. Solid line shows least-squares fit.

TABLE I: Equilibria Constants

Temp, °C	K, $(mf)^{-1}$	K_l, $(mf)^{-1}$	K_c, $(mf)^{-1}$
16.5	59.0	1130	3550
31.0	44.0	650	1850
40.0	37.5	475	1250

TABLE II: Enthalpy (kcal/mol)

ΔH	−3.5
ΔH_l	−6.6
ΔH_c	−8.0

TABLE III: Chemical Shift[a]

Temp, °C	δ_c	δ_I	δ_E
16.5	663	596	400
31.0	665	583	398
40.0	666	576	397
Av shift	665	585	398

[a] In Hz, downfield from CH_3.

The values of the equilibria constants that meet these criteria and best reproduce these curves are shown in Table I. The values of ΔH, derived from the plots of ln K *vs.* $1/T$, are shown in Table II. These enthalpy of reaction values should be considered as estimates since a rather limited temperature range has been studies.

Previous studies have yielded both temperature-dependent[16,27,28,34] and temperature-independent[14,15] values for the chemical shift. The values of the chemical shifts of the three types of protons present are listed in Table III. The cyclic dimer has the greatest downfield shift, the internal protons are found upfield of the cyclic dimer, and the end protons, not involved in H bonding, are found the furthest upfield.

A plot of shift *vs.* temperature for several dilute samples in cyclopentane is shown in Figure 2. It thus appears that one form of the acid (cyclic dimer) tends to predominate at low temperatures. This is in agreement with our calculations which show that the amount of cyclic dimer increases as the temperature decreases (see Figure 3). Unfortunately, the temperature was not accurately known at

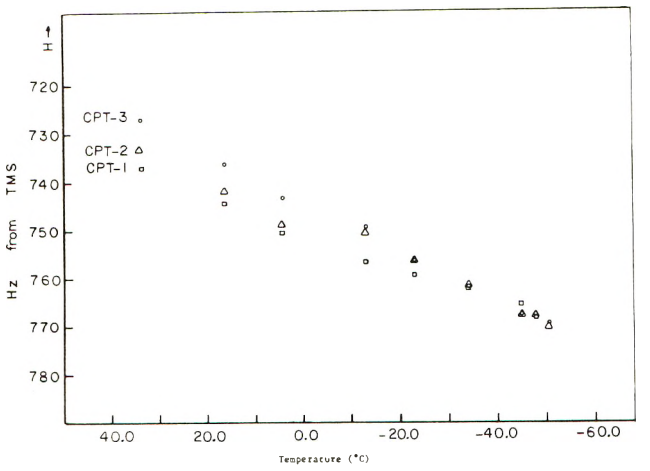

Figure 2. Acid proton chemical shift *vs.* temperature in cyclopentane. For cyclopentane samples CPT-1, 2, 3.

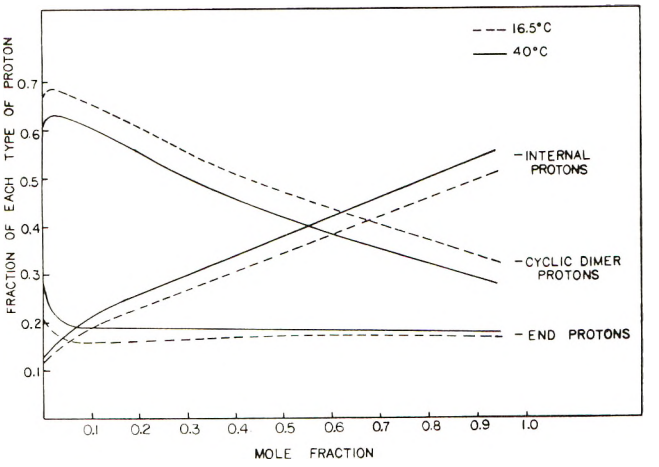

Figure 3. Variation of acid proton type with total mole fraction of acetic acid.

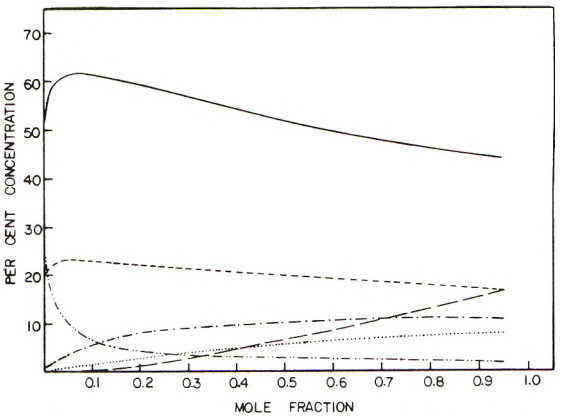

Figure 4. Per cent of various species relative to total mole fraction at 40.0°, where % of χ_i = χ_i/χ_A × 100: ——, cyclic dimer; — · · —, monomer; - - - - - -, linear dimer; — · —, trimer; · · · · · ·, tetramer; — —, sum of species larger than tetramer.

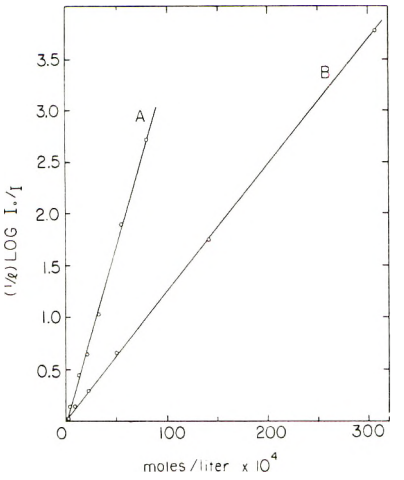

Figure 5. Beer's law plot of infrared intensity data of Barrows and Yerger (ref 9) for acetic acid monomer and cyclic dimer *vs.* the concentrations of monomer and cyclic dimer calculated from this model: A, monomer (vertical scale is expanded by a factor of 10); B, cyclic dimer.

the lower temperatures; thus, a reliable extrapolation cannot be made. However, the fact that the three curves have different slopes and converge at near the value predicted for the cyclic dimer is indicative that the interpretation is correct.

The variation of f_c, f_I, and f_E with the mole fraction of acetic acid at 16.5 and 40.0° is shown in Figure 3. As expected, upon dilution the average length of a polymer decreases; this is shown by the decrease in the fraction of internal protons. As more and more linear dimer is formed (*i.e.*, as the average length of the polymers approaches two), more and more cyclic dimers will be formed from it and therefore the amount of cyclic dimer will increase as shown. Upon further dilution, the cyclic dimer will then decrease forming monomers, with a corresponding increase in end protons. This is more fully illustrated in Figure 4 where the amount of each species present at 40° is shown.

The question of the uniqueness of the values of the equilibrium constants and chemical shifts must be considered. Unfortunately, the relationship between the observed chemical shift and the equilibrium constants is much too complex to permit the direct calculation of error limits or correlation coefficients.[35] However, uncertainty limits can be estimated from the change in the magnitude of R^2 as the value of each equilibrium constant is varied. From these data, we estimate that the uncertainty in the value of each equilibrium constant is about ±10%. A much more complete statistical analysis of the chemical shifts can be carried out since the observed shift is a linear function of f_c, f_I, and f_E (there are only two independent variables since $f_c + f_I + f_E = 1$). The correlation coefficient for δ_c with δ_{obsd} and δ_I with δ_{obsd} have been evaluated and found to fall within a range of 0.95 to 0.99.

It should be pointed out that one simplifying assumption was introduced in order to make the quantitative treatment feasible; that is, the equilibrium constant for the addition of a monomer unit to a polymer chain is assumed to be independent of chain length. This is obviously not a completely valid assumption but appears to be a reasonable approximation since a good fit of the experimental data is obtained at all temperatures and concentrations. The value of the polymerization equilibrium constant that we obtain is, therefore, a weighed average of the individual polymerization constants.

The second question that must be considered is that of the validity of the model used in this work. The strongest arguments in support of this model are that: (1) it takes into account the previously identified hydrogen-bonded species of acetic acid; and (2) the calculations fit the ex-

perimental data to within the limits of the accuracy of the experimental results. Simpler models that have been used have not adequately predicted the experimental facts.

A test of the validity of our model can be made by reexamining literature data obtained using a different type experimental measurement. The infrared work of Barrows and Yerger[9] was selected because all concentration data needed for our calculations were given. The integrated band intensities obtained by Barrows and Yerger[9] are shown in Figure 5 plotted against the monomer and cyclic dimer concentrations calculated *via* eq 11 and 5. The intensities follow Beer's law over the entire concentration range. Using a simple monomer-dimer equilibrium Barrows and Yerger found it necessary to postulate a rapidly changing equilibrium constant. This anomaly is obviously a result of neglecting of the linear polymer.

Finally, the large discrepancy between the equilibrium constant obtained by sonic relaxation measurements[11] and infrared intensity measurements[9] can now be explained. The equilibrium constant obtained by sonic relaxation[11] agrees well with the constant we obtain for the addition of a monomer to a linear polymer. This is quite reasonable since the monomer-polymer equilibrium has the smallest ΔH and would be expected to cause sound absorption at the lowest frequency. Only qualitative agreement should be inferred since the value of the equilibrium constant depends upon the process assumed in its calculation (monomer-dimer equilibrium was assumed in the original work[11]).

Conclusion

It is quite evident then, that the presence of linear polymers is a significant aspect of acetic acid solutions, even at low concentrations, and should be taken into consideration when interpreting experimental results.

It should also be noted that the proposed model is not restricted to dilute solutions only, but it reproduces the experimental shift *vs.* concentration curve (Figure 1) over the entire range of concentrations and can be used successfully to interpret previous unexplained results obtained by other methods (*e.g.*, see ref 9) quantitatively. It also allows one to describe completely the system under observation in terms of the exact amount of each species present.

Acknowledgment. The support of the Florida State University Computing Center and the E.I. DuPont Company for award of a teaching fellowship (to M. A. G.) is greatly appreciated. We also wish to thank Dr. S. Cohen for many helpful discussions and Miss G. Doubrava for assistance in writing the least-squares portion of the computer program.

References and Notes

(1) Presented at the 157th National Meeting of the American Chemical Society, Minneapolis, Minn., April 1969.
(2) Taken in part from a dissertation presented by M. A. Goldman in partial fulfillment of the requirements for the degree of Doctor of Philosophy at the Florida State University, 1969. Present address, National Oceanic and Atmospheric Administration, Mauna Loa Observatory, Hilo, Hawaii 96720.
(3) Correspondence concerning this work should be directed to the University of Alabama in Huntsville.
(4) E. Beckmann, *Z. Phys. Chem.*, **6**, 444 (1890).
(5) G. Allen and E. F. Caldin, *Quart. Rev.*, **7**, 255 (1953), and references therein.
(6) J. Karle and L. O. Brockway, *J. Amer. Chem. Soc.*, **66**, 574 (1944).
(7) M. D. Taylor, *J. Amer. Chem. Soc.*, **73**, 315 (1951).
(8) J. T. Harris, Jr., and M. E. Honbs, *J. Amer. Chem. Soc.*, **76**, 1419 (1954).
(9) J. M. Barrows and E. A. Yerger, *J. Amer. Chem. Soc.*, **76**, 5248 (1954).
(10) J. Wenograd and R. A. Spurr, *J. Amer. Chem. Soc.*, **79**, 5844 (1957).
(11) E. Freedman, *J. Chem. Phys.*, **21**, 1784 (1953).
(12) J. T. Arnold and M. E. Packard, *J. Chem. Phys.*, **19**, 1608 (1951); H. S. Gutowsky and A. Saika, *ibid.*, **21**, 1688 (1953).
(13) C. M. Huggins, G. C. Pimentel, and J. N. Shoolery, *J. Phys. Chem.*, **60**, 1311 (1956).
(14) L. W. Reeves and W. G. Schneider, *Trans. Faraday Soc.*, **54**, 314 (1958).
(15) L. W. Reeves, *Trans. Faraday Soc.*, **55**, 1684 (1959).
(16) J. C. Davis, Jr., and K. S. Pitzer, *J. Phys. Chem.*, **64**, 886 (1960).
(17) A. Capalbi, C. Franconi, B. Pisce, and M. Tosato, *Sci. Tec.*, **5**, 126 (1961).
(18) R. E. Jones, and D. H. Templeton, *Acta Crystallogr.*, **11**, 484 (1958).
(19) J. Lascombe, M. Haurie, and M. Josien, *J. Chim. Phys.*, **59**, 1233 (1962).
(20) L. Bellamy, R. Lake, and R. Pace, *Spectrochim. Acta*, **19**, 443 (1963).
(21) M. Haurie, A. Novak, and M. Lecomte, *C. R. Acad. Sci., Ser. C*, **264**, 694 (1967).
(22) Recently, M. Servantou, J. Biais, and B. Lemanceau, *J. Chim. Phys.*, **67**, 800 (1970), have published the results of a similar attempt to obtain values for hydrogen bonding equilibria constants for acetic acid solutions. Their assumed models are somewhat different from the one we are presenting and only orders of magnitude were obtained for the equilibrium constants.
(23) It is assumed that the chemical shift of the monomer is the same as that for a nonhydrogen-bonded end proton and is therefore included within f_E.
(24) L. Sarolea-Mathot, *Trans. Faraday Soc.*, **49**, 8 (1953).
(25) N. D. Coggeshall and E. L. Saier, *J. Amer. Chem. Soc.*, **73**, 5414 (1951).
(26) Tetramethylsilane, used as an internal standard, is assumed to be part of the solvent in computing η_S.
(27) N. Muller and P. Rose, *J. Phys. Chem.*, **69**, 2564 (1965).
(28) N. Muller and O. R. Hughs, *J. Phys. Chem.*, **70**, 3975 (1966).
(29) J. P. Oliver and J. B. De Roos, Wayne State University, private communication.
(30) M. Goldman, Ph.D. Dissertation, Florida State University, 1969, p 19.
(31) It was noted that if a leak developed in sealing the tube, the sample gave an anomalous upfield shift at all concentrations. This was probably due to the pickup of trace amounts of water (see ref 26 and 27). Such samples were immediately discarded.
(32) Publication No. 87-100-110, Varian Associates (Preliminary Instruction Manual, V-6057, Variable Temperature System for A-60 Analytical Spectrometers), Palo Alto, Calif.
(33) F. Daniels and R. Alberty, "Physical Chemistry," Wiley, New York, N. Y., 1956, Chapter 7.
(34) N. Muller and R. Reiter, *J. Chem. Phys.*, **43**, 3265 (1965).
(35) P. R. Bevington, "Data Reduction and Error Analysis for the Physical Sciences," McGraw-Hill, San Francisco, Calif., 1969, Chapters 8–11.

Thermodynamics of Electrolytes. II. Activity and Osmotic Coefficients for Strong Electrolytes with One or Both Ions Univalent

Kenneth S. Pitzer* and Guillermo Mayorga

Inorganic Materials Research Division of the Lawrence Berkeley Laboratory and Department of Chemistry, University of California, Berkeley, California 94720 *(Received February 5, 1973)*

Publication costs assisted by the U. S. Atomic Energy Commission

The system of equations developed in the first paper of this series is successfully applied to the available free energy data at room temperature for 227 pure aqueous electrolytes with one or both ions univalent. The experimental data are represented substantially within experimental error from dilute solutions up to an ionic strength varying from case to case but typically 6 *M*. Where the data extend to high concentration, three parameters are evaluated for each solute, but one of these has negligible effect and is omitted if there are data only for the dilute range. This yields a very compact set of tables from which these important and useful properties can be reproduced. These parameters will also be of importance in treating mixed electrolytes. A simplified graphical presentation is given for activity coefficients of 1-1 electrolytes. In most cases the new equations are fitted to the osmotic coefficient data as recommended by Robinson and Stokes but for hydroxides, zinc halides, hydrogen halides, and a few other cases we have based our evaluation on the original data from several sources. The implications of our parameters are also discussed in terms of solvent structure and interionic forces.

It is the twofold purpose of this research to represent as compactly and as accurately as possible the very extensive array of experimental data on the thermodynamic properties of single aqueous electrolytes at room temperature and to interpret the resulting parameters in terms of interionic forces. In the first paper[1] of this series (cited hereafter as I) the theoretical aspects were considered in order to guide the selection of equations which reproduce the measured properties substantially within experimental accuracy, which are compact and convenient in that only a very few parameters need be tabulated for each substance and the mathematical calculations are simple, which have appropriate form for mixed electrolytes as well as for a single solute, and whose parameters have physical meaning as far as possible. Choices were made between several possible forms of equations on the basis of accuracy of representation of the experimental data for several solutes.

In this paper we present the results for single electrolytes which show no association. Also included are several solutes which are said, on the basis of some properties, usually conductance, to show some association, but whose thermodynamic properties are fitted satisfactorily by the same equations used for nonassociating electrolytes. In later papers we expect to treat single electrolytes showing moderate association as well as mixed electrolytes.

Equations and General Parameters

The equations chosen in I differ from those generally used heretofore in several respects, but most important is the ionic strength dependence of the second virial coefficient. This was shown to be justified theoretically by a simple derivation in which the Debye-Hückel radial distribution is substituted into the osmotic pressure equation of statistical mechanics, although it was also noted that the more complex theory of Mayer[2] previously had indicated such a dependence. This same simple derivation also led to a different form for the long-range electrostatic term which was found to be empirically superior to the conventional Debye-Hückel form derived by a charging process (instead of the osmotic pressure equation).

The pertinent equations for single electrolytes for the excess Gibbs energy G^{ex}, the osmotic coefficient φ, and the activity coefficient γ are as follows

$$(G^{ex}/n_w RT) = f^{(Gx)} + m^2(2\nu_M\nu_X)B_{MX}^{Gx} + m^3[2(\nu_M\nu_X)^{3/2}]C_{MX}^{Gx} \quad (1)$$

$$\varphi - 1 = |z_M z_X| f^{\varphi} + m\left(\frac{2\nu_M\nu_X}{\nu}\right)B_{MX}^{\varphi} + m^2\frac{2(\nu_M\nu_X)^{3/2}}{\nu}C_{MX}^{\varphi} \quad (2)$$

$$\ln\gamma = |z_M z_X| f^{\gamma} + m\left(\frac{2\nu_M\nu_X}{\nu}\right)B_{MX}^{\gamma} + m^2\frac{2(\nu_M\nu_X)^{3/2}}{\nu}C_{MX}^{\gamma} \quad (3)$$

where ν_M and ν_X are the numbers of M and X ions in the formula and z_M and z_X give their respective charges in electronic units; also $\nu = \nu_M + \nu_X$, while n_w is the number of kg of solvent and m is the conventional molality. The other quantities have the form

$$f^{Gx} = -A_\varphi(4I/b)\ln(1 + bI^{1/2}) \quad (4)$$

$$f^{\varphi} = -A_\varphi\frac{I^{1/2}}{1 + bI^{1/2}} \quad (5)$$

$$f^{\gamma} = -A_\varphi\left[\frac{I^{1/2}}{1 + bI^{1/2}} + \frac{2}{b}\ln(1 + bI^{1/2})\right] \quad (6)$$

$$B_{MX}^{Gx} = \beta_{MX}^{(0)} + \frac{2\beta_{MX}^{(1)}}{\alpha^2 I}[1 - e^{-\alpha I^{1/2}}(1 + \alpha I^{1/2})] \quad (7)$$

$$B_{MX}^{\varphi} = \beta_{MX}^{(0)} + \beta_{MX}^{(1)}e^{-\alpha I^{1/2}} \quad (8)$$

$$B_{MX}^{\gamma} = 2\beta_{MX}^{(0)} + \frac{2\beta_{MX}^{(1)}}{\alpha^2 I}[1 - e^{-\alpha I^{1/2}}(1 + \alpha I^{1/2} - (1/2)\alpha^2 I)] \quad (9)$$

$$C_{MX}^{Gx} = (1/2)C_{MX}^{\varphi} \quad (10)$$

$$C_{MX}^{\gamma} = (3/2)C_{MX}^{\varphi} \quad (11)$$

Note that the superscripts Gx, φ, and γ are labels (not exponents). Also I is the ionic strength, $\frac{1}{2}\Sigma m_i z_i^2$, and A^{φ} is the Debye–Hückel coefficient for the osmotic function, $[\frac{1}{3}(2\pi N_0 d_w/1000)^{1/2}(e^2/DkT)^{3/2}]$, which has the value 0.392 at 25° for water. In order to maintain simple equations for mixed electrolytes, b must remain the same for all solutes and in I the value 1.2 was selected; also the value $\alpha = 2.0$ was found to be satisfactory for all solutes considered in this paper. For each substance the two parameters $\beta_{MX}^{(0)}$ and $\beta_{MX}^{(1)}$ define the second virial coefficient and C_{MX}^{φ} defines the third virial coefficient which is usually very small and sometimes completely negligible. If necessary to fit unusual behavior, one could add to the second virial coefficient further terms of the same form but with different values of α and β, but this was not required for the present work.

The numerical factors, such as $(2\nu_M\nu_X)$, multiplying the second and third virial coefficients in eq 1-3 are needed in order to retain the simple meaning that the virial coefficients represent the short-range interaction of pairs and triplets of ions, respectively. In eq 2 and 3 the quantities $(2\nu_M\nu_X/\nu)$ and $2(\nu_M\nu_X)^{3/2}/\nu$ are both unity for a symmetrical MX electrolyte. For convenience in working with single electrolytes, we shall tabulate $\frac{4}{3}\beta^{(0)}$, $\frac{4}{3}\beta^{(1)}$, and $(2^{5/2}/3)C_{\varphi}$ for 2-1 electrolytes and the corresponding quantities for other types, but these numerical factors must be removed before the virial coefficients are used in work with mixed electrolytes.

While eq 1-11 are quite simple and should be used by anyone desiring accurate values of the thermodynamic properties, we recognize that for many purposes a rough estimate of the activity coefficient will suffice. Since we shall see that there is a close relationship between $\beta^{(1)}$ and $\beta^{(0)}$ and that C^{φ} is usually very small, one can make a reasonably good estimate of the activity coefficient from $\beta^{(0)}$ alone. For this purpose we present a large graph with curves of γ for various values of $\beta^{(0)}$ from which one can visually interpolate values of the activity coefficient directly for 1-1 electrolytes.

Evaluation of Parameters

Robinson and Stokes critically reviewed the available data in their classic papers and in the various editions of their book. In most cases we have accepted the tables of osmotic coefficients in the second (revised) edition of their book[3] and evaluated by least squares the best values of $\beta^{(0)}$, $\beta^{(1)}$, and C^{φ} which are listed in Tables I-IX. Also listed are the maximum molality for which agreement is attained to 0.01 in φ or for which data are available, and the standard deviation of fit. In Tables IV, V, VII, VIII, and IX the data seemed less accurate, and the departures from ideal behavior are greater; hence the allowable error in φ was increased to 0.02 (and to 0.03 for the 5-1 type salt $K_5P_3O_{10}$).

The last column in the tables gives the reference, three to Robinson and Stokes book, or to a more recent literature source.[4-60] The symbol "t" indicates that several references are involved and these are identified either in the text, in Table X, or in formulas in parentheses after the journal citations. In the preceding column the letters a, b, and c indicate high, intermediate, and low accuracy, re-

Table I: Inorganic Compounds of 1-1 Type.

	$\beta^{(0)}$	$\beta^{(1)}$	C^{Φ}	Max. m	σ	ref.
HCl	0.1775	0.2945	0.00080	6	a	t
HBr	.1960	.3564	.00827	3	a	t
HI	.2362	.392	.0011	3	b	t
$HClO_4$	.1747	.2931	.00819	5.5	.002	3
HNO_3	.1119	.3206	.0010	3	.001	3
LiCl	.1494	.3074	.00359	6	.001	3
LiBr	.1748	.2547	.0053	2.5	.002	3
LiI	.2104	.373	---	1.4	.006	3
LiOH	.015	.14	---	4	c	t
$LiClO_4$	.1973	.3996	.0008	3.5	.002	3
$LiNO_2$	.1336	.325	-.0053	6	.003	4
$LiNO_3$	.1420	.2780	-.00551	6	.001	3
NaF	.0215	.2107	---	1	.001	3
NaCl	.0765	.2664	.00127	6	.001	3
NaBr	.0973	.2791	.00116	4	.001	3
NaI	.1195	.3439	.0018	3.5	.001	3
NaOH	.0864	.253	.0044	6	b	t
$NaClO_3$	.0249	.2455	.0004	3.5	.001	3
$NaClO_4$	.0554	.2755	-.00118	6	.001	3
$NaBrO_3$	-.0205	.1910	.0059	2.5	.001	3
NaCNS	.1005	.3582	-.00303	4	.001	3
$NaNO_2$	.0641	.1015	-.0049	5	.005	4
$NaNO_3$	.0068	.1783	-.00072	6	.001	3
NaH_2PO_4	-.0533	.0396	.00795	6	.003	3
NaH_2AsO_4	-.0442	.2895	---	1.2	.001	3
$NaBO_2$	-.0526	.1104	.0154	4.5	.004	5
$NaBF_4$	-.0252	.1824	.0021	6	.006	5
KF	.08089	.2021	.00093	2	.001	3
KCl	.04835	.2122	-.00084	4.8	.0005	t
KBr	.0569	.2212	-.00180	5.5	.001	3
KI	.0746	.2517	-.00414	4.5	.001	3
KOH	.1298	.320	.0041	5.5	b	6
$KClO_3$	-.0960	.2481	---	0.7	.001	3
$KBrO_3$	-.1290	.2565	---	0.5	.001	3
KCNS	.0416	.2302	-.00252	5	.001	3
KNO_2	.0151	.015	.0007	5	.003	7
KNO_3	-.0816	.0494	.00660	3.8	.001	3
KH_2PO_4	-.0678	-.1042	---	1.8	.003	3
KH_2AsO_4	-.0584	.0626	---	1.2	.003	3
$KPtF_6$	-.163	-.282	---	0.5	.001	8
RbF	.1141	.2842	-.0105	3.5	.002	9
RbCl	.0441	.1483	-.00101	5	.001	3
RbBr	.0396	.1530	-.00144	5	.001	3
RbI	.0397	.1330	-.00108	5	.001	3
$RbNO_2$	.0269	-.1553	-.00366	5	.002	4
$RbNO_3$	-.0789	-.0172	.00529	4.5	.001	3
CsF	.1306	.2570	-.0043	3.2	.002	9
CsCl	.0300	.0558	.00038	5	.002	t
CsBr	.0279	.0139	.00004	5	.002	3
CsI	.0244	.0262	-.00365	3	.001	3
CsOH	.150	.30	---	---	b	t
$CsNO_3$	-.0758	-.0669	---	1.4	.002	3
$CsNO_2$	.0427	.060	-.0051	6	.004	4
$AgNO_3$	-.0856	.0025	.00591	6	.001	3
$TlClO_4$	-.087	-.023	---	0.5	.001	3
$TlNO_3$	-.105	-.378	---	0.4	.001	3
NH_4Cl	.0522	.1918	-.00301	6	.001	3
NH_4Br	.0624	.1947	-.00436	2.5	.001	10
NH_4ClO_4	-.0103	-.0194	---	2	.004	11
NH_4NO_3	-.0154	.1120	-.00003	6	.001	3

Table II: Salts of Carboxylic Acids (1-1 Type).

Li Acetate	0.1124	0.2483	-.00525	4	.001	3
Na Formate	.0820	.2872	-.00523	3.5	.001	3
Na Acetate	.1426	.3237	-.00629	3.5	.001	3
Na Propionate	.1875	.2789	-.01277	3	.001	3
NaH Malonate	.0229	.1600	-.00106	5	.002	3
NaH Succinate	.0354	.1606	.00040	5	.001	3
NaH Adipate	.0472	.3168	---	0.7	.001	3
K Acetate	.1587	.3251	-.00660	3.5	.001	3
KH Malonate	-.0095	.1423	.00167	5	.004	3
KH Succinate	.0111	.1564	.00274	4.5	.002	3
KH Adipate	.0419	.2523	---	1	.001	3
Rb Acetate	.1622	.3353	-.00551	3.5	.001	3
Cs Acetate	.1628	.3605	-.00555	3.5	.001	3
Tl Acetate	.0082	.0131	-.00127	6	.001	3

Table III: Tetraalkylammonium Halides

Me_4NF	0.2677	0.2265	0.0013	3	.002	37
Et_4NF	.3113	.6155	.0349	2	.002	37
Pr_4NF	.4463	.4090	.0537	2	.002	37
Bu_4NF	.6092	.402	-.0281	1.7	.005	37
Me_4NCl	.0149	-.083	.0057	3.4	.005	38
Et_4NCl	.0336	-.153	.0084	3	.002	38
Pr_4NCl	.1065	-.354	.0098	2.5	.002	38
Bu_4NCl	.2058	-.464	-.0588	2.5	.001	38
Me_4NBr	-.0363	-.201	.0084	3.5	.004	38
Et_4NBr	-.0457	-.448	.0135	4	.001	38
Pr_4NBr	.0108	-.826	.0078	3.5	.003	38
Bu_4NBr	-.0558	-.579	-.0010	4.5	.007	38
Me_4NI	.0345	-.585	---	0.3	.003	38
Et_4NI	-.1930	-.599	.0401	2	.007	38,39
Pr_4NI	-.2839	-.863	---	0.5	.005	38

See text for meaning of a, b, c, t.

Table IV: Sulfonic Acids and Salts (1-1 Type)
(SA = sulfonic acid; S = sulfonate)

	$\beta^{(0)}$	$\beta^{(1)}$	C^{ϕ}	Max. m	σ	ref.
Methane SA	0.1298	0.629	0.0052	4	---	40
Li methane S	.1320	.271	-.0030	4	---	40
Na methane S	.0787	.274	-.0024	4	---	40
K methane S	.0581	.165	-.0046	4	---	40
NH_4 methane S	.0661	.191	-.0041	4	---	40
Me_4N methane S	.1458	.168	-.0043	4	---	40
Et_4N methane S	.1548	.090	-.0034	4	---	40
Bu_4N methane S	.2145	.235	-.0392	4	---	40
Ethane SA	.1536	.341	-.0056	4	---	40
Li ethane S	.1799	.319	-.0118	4	---	40
Na ethane S	.1316	.374	-.0082	4	---	40
K ethane S	.0965	.250	-.0074	4	---	40
NH_4 ethane S	.1142	.179	-.0114	4	---	40
Me_4N ethane S	.1796	.083	-.0116	4	---	40
Et_4N ethane S	.1805	.075	-.0040	4	---	40
Bu_4N ethane S	.1827	.445	-.0374	4	---	40
Benzene SA	.0526	.445	.0036	5	.002	41
Li benzene S	.1134	.466	-.0075	4.5	.002	41
Na benzene S	.0842	.351	-.0181	2.5	.001	41
p-toluene SA	-.0366	.281	.0137	5	.002	3
Li p-toluene S	.0189	.399	.0046	4.5	.004	3
Na p-toluene S	-.0344	.396	.0043	4	.003	3
K p-toluene S	-.0985	.453	.0122	3.5	.002	3
2,5 Me_2benzene SA	-.0965	.141	.0210	4.5	.01	3
Li 2,5 Me_2benzene S	-.0098	.361	.0039	3.5	.002	41
Na 2,5 Me_2benzene S	-.0277	.228	---	1	.005	41
p-Et benzene SA	-.1736	.435	.0383	2	.007	3
Li p-Et benzene S	-.1438	.804	.0317	5	.01	41,42
Na p-Et benzene S	-.2240	.895	.0355	2.5	.01	41,42
Mesitylene SA	-.2209	.248	.0432	2	.01	41
Li Mesitylene S	-.1998	.871	.0456	2	.004	41
Na Mesitylene S	-.2018	.767	---	1	.003	41

Table V: Additional 1-1 Type Organic Salts

Choline Cl	.0457	-.196	.0008	6	.004	43
Choline Br	-.0066	-.227	.0036	6	.004	43
Me_3BzNCl	-.0821	-.178	.0162	3.5	.01	43
Me_3BzNBr	-.1517	-.545	.0187	3	.01	43
$Me_2OEtBzNCl$	-.0879	-.343	.0134	4	.01	43
$Me_2OEtBzNBr$	-.1518	-.778	.0177	3	.01	43
$(HOC_2H_4)_4NF$	.0938	.128	-.0030	4	.001	44
$(HOC_2H_4)_4NBr$	-.0474	-.259	.0106	3	.002	44
Me_3SCl	.0314	-.184	.0023	6	.005	45
Me_3SBr	-.0228	-.245	.0044	6	.004	45
Me_3SI	-.0601	-.604	.0006	3	.01	45
Bu_3SCl	.0726	-.245	-.0099	6	.01	45
Bu_3SBr	-.0803	-.616	.0053	6	.01	45

Table VI: Inorganic Compounds of 2-1 Type.

	$\frac{4}{3}\beta^{(0)}$	$\frac{4}{3}\beta^{(1)}$	$2^{\frac{5}{2}}C^{\phi}$	Max. m	σ	ref.
$MgCl_2$	0.4698	2.242	0.00979	4.5	.003	3
$MgBr_2$	.5769	2.337	.00589	5	.004	3
MgI_2	.6536	2.4055	.01496	5	.003	3
$Mg(ClO_4)_2$	.6615	2.678	.01806	2	.002	3
$Mg(NO_3)_2$	.4895	2.113	-.03889	2	.003	3
$CaCl_2$	.4212	2.152	-.00064	2.5	.003	3
$CaBr_2$	.5088	2.151	-.00485	2	.002	3
CaI_2	.5839	2.409	-.00158	2	.001	3
$Ca(ClO_4)_2$	.6015	2.342	-.00943	2	.005	3
$Ca(NO_3)_2$	.2811	1.879	-.03798	2	.002	3
$SrCl_2$	.3810	2.223	-.00246	4	.003	3
$SrBr_2$	.4415	2.282	.00231	2	.001	3
SrI_2	.5350	2.480	.00501	2	.001	3
$Sr(ClO_4)_2$	.5692	2.089	-.02472	2.5	.003	3
$Sr(NO_3)_2$	.1795	1.840	-.03757	2	.002	3
$BaCl_2$	.3504	1.995	-.03654	1.8	.001	3
$BaBr_2$	.4194	2.093	-.03009	2	.001	3
BaI_2	.5625	2.249	-.03286	1.8	.003	3
$Ba(OH)_2$	.229	1.60	---	0.1	---	36
$Ba(ClO_4)_2$	.4819	2.101	-.05894	2	.003	3
$Ba(NO_3)_2$	-.043	1.07	---	0.4	.001	3
$MnCl_2$	.4363	2.067	-.03865	2.5	.003	3
$FeCl_2$	.4479	2.043	-.01623	2	.002	3
$CoCl_2$	.4857	1.967	-.02869	3	.004	3
$CoBr_2$	.5693	2.213	-.00127	2	.002	3
CoI_2	.695	2.23	-.0088	2	.01	3
$Co(NO_3)_2$	.4159	2.254	-.01436	5.5	.003	3
$NiCl_2$	.4639	2.108	-.00702	2.5	.002	3
$CuCl_2$	.4107	1.835	-.07624	2	.003	3
$Cu(NO_3)_2$	.4224	1.907	-.04136	2	.002	3
$ZnCl_2$	.3469	2.190	-.1659	1.2	.006	t
$ZnBr_2$	.6213	2.179	-.2035	1.6	.007	t
ZnI_2	.6428	2.594	-.0269	0.8	.002	t
$Zn(ClO_4)_2$	.6747	2.396	.02134	2	.003	3
$Zn(NO_3)_2$	.4641	2.255	-.02955	2	.001	3
$Cd(NO_3)_2$	.3820	2.224	-.04836	2.5	.002	3
$Pb(ClO_4)_2$	.4443	2.296	-.01667	6	.004	3
$Pb(NO_3)_2$	-.0482	0.380	.01005	2	.002	3

Table VI: Inorganic Compounds of 2-1 Type (Continued)

	$\frac{4}{3}\beta^{(0)}$	$\frac{4}{3}\beta^{(1)}$	$2^{\frac{5}{2}}C^{\phi}$	Max. m	σ	ref.
UO_2Cl_2	0.5698	2.192	-.06951	2	.001	3
$UO_2(ClO_4)_2$	.8151	2.859	.04089	2.5	.003	3
$UO_2(NO_3)_2$	.6143	2.151	-.05948	2	.002	3
Li_2SO_4	.1817	1.694	-.00753	3	.002	3
Na_2SO_4	.0261	1.484	.00938	4	.003	3
$Na_2S_2O_3$	.0882	1.701	.00705	3.5	.002	3
Na_2CrO_4	.1250	1.826	-.00407	2	.002	3
Na_2CO_3	.2530	1.128	-.09057	1.5	.001	3
Na_2HPO_4	-.0777	1.954	.0554	1	.002	3
Na_2HAsO_4	.0407	2.173	.0034	1	.001	3
K_2SO_4	.0666	1.039	---	0.7	.002	3
K_2CrO_4	.1011	1.652	-.00147	3.5	.003	3
$K_2Pt(CN)_4$	.0881	3.164	.0247	1	.005	53
K_2HPO_4	.0330	1.699	.0309	1	.002	3
K_2HAsO_4	.1728	2.198	-.0336	1	.001	3
Rb_2SO_4	.0772	1.481	-.00019	1.8	.001	3
Cs_2SO_4	.1184	1.481	-.01131	1.8	.001	3
$(NH_4)_2SO_4$	.0545	0.878	-.00219	5.5	.004	3
cis$[Co(en)_2NH_3NO_2](NO_3)_2$	-.0928	0.271	---	0.6	.002	54
tr.$[Co(en)_2NH_3NO_2](NO_3)_2$	-.0901	.249	---	.8	.002	54
cis$[Co(en)_2NH_3NO_2]Cl_2$	-.0327	.684	.0121	2.8	.005	54
tr.$[Co(en)_2NH_3NO_2]Cl_2$	.0050	.695	.0066	2.4	.005	54
cis$[Co(en)_2NH_3NO_2]Br_2$	-.1152	.128	.0158	1	.004	54
tr.$[Co(en)_2NH_3NO_2]Br_2$	-.0912	.424	.0223	2.4	.005	54
cis$[Co(en)_2NH_3NO_2]I_2$	-.1820	.594	---	0.6	.004	54
tr.$[Co(en)_2NH_3NO_2]I_2$	-.1970	1.003	---	.3	.003	54

Table VII: Organic Electrolytes of 2-1 Type
(SA = Sulfonic acid; S = Sulfonate)

m-Benzenedi SA	0.5611	2.637	-.0463	1.6	.004	55
Li_2 m-Benzenedi S	.5464	2.564	-.0622	2.5	.004	55
Na_2 m-Benzenedi S	.3411	2.698	-.0419	3	.004	55
4,4'bibenzyldi SA	.1136	2.432	.0705	2	.01	3,t
Li_2 4,4'bibenzyldi S	.1810	1.755	.0462	1.2	.007	55
Na_2 4,4'bibenzyldi S	.0251	1.969	---	0.4	.01	55
Na_2 fumarate	.3082	1.203	-.0378	2	.003	3
Na_2 maleate	.1860	0.575	-.0170	3	.004	3

Table VIII: 3-1 Electrolytes

	$\frac{3}{2}\beta^{(0)}$	$\frac{3}{2}\beta^{(1)}$	$3^{\frac{3}{2}}C^{\phi}$	Max. m	σ	ref.
$AlCl_3$	1.0490	8.767	.0071	1.6	.005	3
$SrCl_3$	1.0500	7.978	-.0840	1.8	.005	3
YCl_3	0.9599	8.166	-.0587	1.8	.007	3
$LaCl_3$	.9158	8.231	-.0831	1.8	.007	3
$CeCl_3$	.9187	8.227	-.0809	1.8	.01	3
$PrCl_3$	.9030	8.181	-.0727	2	.006	3
$NdCl_3$	.9175	8.104	-.0737	1.8	.007	3
$SmCl_3$	.9330	8.273	-.0728	1.8	.01	3
$EuCl_3$	.9370	8.385	-.0687	1.8	.007	3
$CrCl_3$	1.1046	7.883	-.1172	1.2	.005	3
$Cr(NO_3)_3$	1.0560	7.777	-.1533	1.4	.004	3
$Ga(ClO_4)_3$	1.2381	9.794	.0904	2	.008	3
$InCl_3$	-1.68	-3.85	---	0.01	---	t
Na_3PO_4	.2672	5.777	-.1339	0.7	.003	3
Na_3AsO_4	.3582	5.895	-.1240	0.7	.001	3
K_3PO_4	.5594	5.958	-.2255	0.7	.001	3
$K_3P_3O_9$	.4867	8.349	-.0886	0.8	.004	60
K_3AsO_4	.7491	6.511	-.3376	0.7	.001	3
$K_3Fe(CN)_6$	.5035	7.121	-.1176	1.4	.003	3
$K_3Co(CN)_6$	.5603	5.815	-.1603	1.4	.008	3
$Co(en)_3Cl_3$	.2603	3.563	-.0916	1	.003	t
$Co(en)_3(NO_3)_3$	.1882	3.935	---	0.3	.01	58
$Co(en)_3(ClO_4)_3$	.1619	5.395	---	0.6	.007	59
$Co(pn)_3(ClO_4)_3$	.2022	3.976	---	0.3	.003	58

Table IX: 4-1 and 5-1 Electrolytes

4-1 Solute	$\frac{8}{5}\beta^{(0)}$	$\frac{8}{5}\beta^{(1)}$	$\frac{16}{5}C^{\phi}$	Max. m	σ	ref.
$ThCl_4$	1.622	21.33	-.3309	1	.006	3
$Th(NO_3)_4$	1.546	18.22	-.5906	1	.01	3
$Na_4P_2O_7$	0.699	17.16	---	0.2	.01	60
$K_4P_2O_7$	.977	17.88	-.2418	0.5	.01	60
$K_4Fe(CN)_6$	1.021	16.23	-.5579	0.9	.008	3
$K_4Mo(CN)_8$	0.854	18.53	-.3499	0.8	.01	3
$K_4W(CN)_8$	1.032	18.49	-.4937	1	.005	53
$Me_4NMo(CN)_8$	.938	15.91	-.3330	1.4	.01	53

5-1 Solute	$\frac{5}{3}\beta^{(0)}$	$\frac{5}{3}\beta^{(1)}$	$5^{\frac{3}{2}}C^{\phi}$			
$Na_5P_3O_{10}$	1.869	36.10	-1.630	0.4	.01	60
$K_5P_3O_{10}$	1.939	39.64	-1.055	0.5	.015	60

See text for meaning of a, b, c, t.

TABLE X: Standard Potentials of Cells

Cell	E°	Ref
$H_2\|HCl(m)\|AgCl, Ag$	0.2224	12
	0.2232	13
$H_2\|HCl(m)\|Hg_2Cl_2, Hg$	0.2681_5	14
$H_2\|HBr(m)\|Hg_2Br_2, Hg$	0.1392	15
$H_2\|HBr(m)\|AgBr, Ag$	0.0710	16, 17
	0.0709	18
$H_2\|HI(m)\|AgI, Ag$	−0.1522	20
$Zn, Hg\|ZnCl_2(m)\|AgCl, Ag$	0.9845	46
$Zn, Hg\|ZnBr_2(m)\|AgBr, Ag$	0.8333	49
$Zn, Hg\|ZnI_2(m)\|AgI, Ag$	0.6097	51
$In\|InCl_3(m)\|AgCl, Ag$	0.5600	57

spectively, in cases where some or all of the experimental data are other than isopiestic measurements.

In evaluating parameters, various weighting schemes were used in order to fit the experimental points within their estimated uncertainty to as high a concentration as possible.

In a number of cases the basic data are not isopiestic measurements but rather cell potentials. Ordinarily we then used these experimental potential values to evaluate our parameters in a manner that also allowed readjustment of the standard cell potential. The resulting standard cell potentials are given in Table X.

Occasionally there are data of several types available for a given solute, and in several cases special procedures were used giving appropriate weights to various data in obtaining best values of the parameters.

The third virial coefficient is omitted in cases where the experimental data do not extend to high enough concentration (usually 2 M) to require that term. Additional details and comments on these evaluations are given elsewhere.[61]

The present values supercede those given in paper I, although there is no significant difference (after an inadvertant error is corrected[1]).

Hydroxides

In contrast to most other cases there are special difficulties in obtaining reliable values of activity coefficients for hydroxides. Data from two types of galvanic cell are available.

A $\quad Pt, H_2|MOH(m')|M_xHg|MOH(m'')|H_2, Pt$

B $\quad Pt, H_2|MOH(m_a)MX(m_b)|AgX, Ag$

where M_xHg indicates an amalgam electrode in cell A and X indicates either Cl or Br in cell B.

Amalgam electrode cells were employed by both Harned and Akerlof and their respective collaborators. Although the amalgam electrodes are troublesome, these investigators have used them successfully in other types of cells where the results can be checked from independent sources. The reaction for cell A involves transfer of solvent as well as solute, hence the equation for the potential includes both the activity and osmotic coefficients

$$E = \frac{RT}{F}\left[2\ln\frac{\gamma''m''}{\gamma'm'} + 0.036(m''\varphi'' - m'\varphi')\right] \quad (12)$$

Since both activity and osmotic coefficients can be expressed in terms of $\beta^{(0)}$, $\beta^{(1)}$, etc., we have evaluated these quantities directly by least squares from the original cell potentials. The values for Li, Na, K, and Cs hydroxides presented in Table I come from measurements of amalgam cells but with weighting of data influenced by the measurements of type B cells as discussed below. In the case of sodium hydroxide, the isopiestic measurements of Stokes[24] were used along with cell potentials.

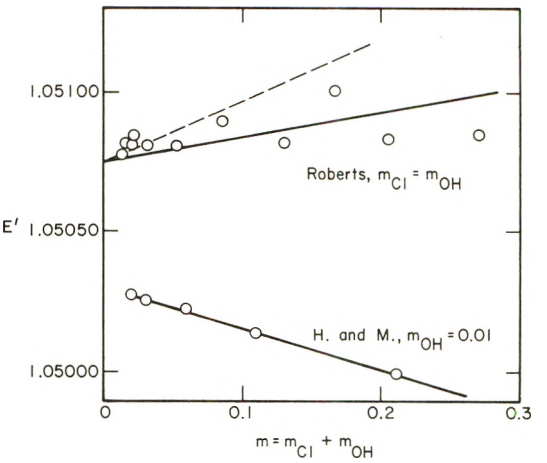

Figure 1. Cell potentials for NaOH–NaCl solutions; see eq 15 and accompanying text for details.

In 1955 Guggenheim and Turgeon[25] showed that, with certain assumptions, the activity coefficients of these hydroxides could also be evaluated from the existing measurements of cells of type B. Since the solutions in these cells are mixed electrolytes, the analysis in general involves additional terms for the interaction of ions of like charge, but Guggenheim and Turgeon accepted Brønsted's principle of specific interaction and ignored these terms. We now have good evidence that such terms are not negligible; hence, we must develop equations for these cell potentials on an adequate basis. First we express the potential for a cell of type B

$$E = E^\circ - \frac{RT}{F}\left[\ln K_w - 0.036(\varphi m) - \ln\frac{m_b}{m_a} - \ln\frac{\gamma_{X^-}}{\gamma_{OH^-}}\right] \quad (13)$$

where $m = m_a + m_b$ and K_w is the ionization constant for the solvent. Since we shall confine our use of data from this type of cell to solutions below 0.3 M, we shall ignore terms related to the third virial coefficient. Also the osmotic coefficient may be estimated with more than sufficient accuracy for the small term $0.036(\varphi m)$. The activity coefficient term may be expanded by substitution of either eq 41 and 42 or of 23, 27, 28, and 32 of paper I to yield

$$\ln(\gamma_{X^-}/\gamma_{OH^-}) = 2m\{(B_{MX}^{\gamma} - B_{MX}^{\varphi}) - (B_{MOH}^{\gamma} - B_{MOH}^{\varphi}) + (2y-1)\theta_{X,OH}\} \quad (14)$$

where $y = m_a/m$ and terms in C and ψ have been dropped as indicated above. Also we note that $B^{\gamma} - B^{\varphi} = B^{Gx}$ as defined in eq 56 of I or eq 7 of this paper.

For the particular case $y = \frac{1}{2}$ which requires $m_a = m_b$, the last term in eq 14 disappears; then we can write

$$E' = E + \frac{RT}{F}\ln\frac{m_b}{m_a} = E^\circ - \frac{RT}{F}[\ln K_w - 0.036(\varphi m) + 2m(B_{MOH}^{Gx} - B_{MX}^{Gx})] \quad (15)$$

Roberts[26] measured cells of type B with NaCl–NaOH solutions and $m_a = m_b$. His results are shown in the upper portion of Figure 1. The solid line is calculated from the

values of $\beta^{(0)}$ and $\beta^{(1)}$ derived for NaOH from the data of Akerlof and Kegeles[27] for type A cells together with isopiestic data (above 2 M) and parameters for NaCl from Table I. Type A cells with NaOH were also measured by Harned and Hecker[28] and their results lead to the dashed line on Figure 1. It is apparent that the Akerlof and Kegeles curve agrees satisfactorily with the data of Roberts whereas the Harned and Hecker curve departs significantly in this concentration range. It did not seem worthwhile to attempt to improve the constants evaluated from Akerlof and Kegeles' data, and they are included in Table I for NaOH.

The remaining series of experiments with type B cells all hold m_a fixed, usually at 0.01 M, and vary m_b. The results of Harned and Mannweiler[29] for NaOH–NaCl solutions are shown in the lower portion of Figure 1. In these experiments m_a = 0.01 M; hence the value of E' at m = 0.02 M should agree with that of Roberts. The difference of 0.5 mV seems large, and standard cell calibration errors appear to be the only plausible explanation. Our primary interest, however, is in the slopes of the curves, and the difference in slopes gives the value of $\theta_{Cl,OH}$. This may be seen by substituting eq 14 in 13. The result from Figure 1 is $\theta_{Cl,OH} = -0.047$.

For the other alkali metals it seems best to consider the difference in potential for a given cell of type B from that of the corresponding cell with NaOH–NaCl or NaOH–NaBr solution of the same m_a and m_b. This has the effect of cancelling the term in $\theta_{Cl,OH}$ or $\theta_{Br,OH}$. In most cases there are experimental potentials from the same laboratory for each cell of the pair but there is no difficulty in interpolating the values for the sodium cells when necessary. The difference in potential for such a pair of cells is

$$E_{M^+} - E_{Na^+} = \frac{RT}{F}\left[\ln\left(\frac{\gamma_{OH^-}}{\gamma_{X^-}}\right)_{M^+} - \ln\left(\frac{\gamma_{OH^-}}{\gamma_{X^-}}\right)_{Na^+}\right] \quad (16)$$

if we substitute the appropriate expressions cited above for the activity coefficients, we obtain

$$mB_{MOH}{}^{Gx} + \delta = \left(\frac{F}{2RT}\right)(E_{M^+} - E_{Na^+}) + m(B_{MCl}{}^{Gx} + B_{NaOH}{}^{Gx} - B_{NaCl}{}^{Gx}) \quad (17)$$

Here we have added a term δ to allow for the possibility of small differences in standard cell calibration between series of experiments carried out of different times, such as apparently arose in the experiments with NaOH–NaCl, or for differences between the AgX,Ag electrodes used in different series. Presumably δ is a very small constant for any series. The parameters for the alkali halides are taken from Table I. The results, which are discussed in detail elsewhere,[62] yield good agreement with data from type A cells for KOH and CsOH. There are small but troublesome conflicts among data for LiOH and further experiments are needed to resolve them.

The data[36] for type B cells with $Ba(OH)_2$–$BaCl_2$ solutions were also evaluated by equations modified as required for the double charge on the cation.

Behavior of Second Virial Coefficients

The values of $\beta^{(0)}$ and $\beta^{(1)}$ are plotted in Figures 2–5. Considering first Figure 2, we note that the values for most inorganic salts, acids, and bases of 1–1 type fall in a rather narrow band. This is not unexpected since $\beta^{(0)}$ and $\beta^{(1)}$ depend on the same properties of the ions and the solvent although we shall see that these properties are

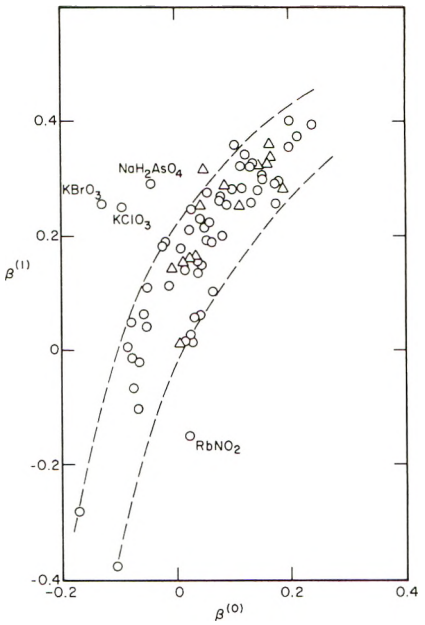

Figure 2. The relationship of $\beta^{(1)}$ to $\beta^{(0)}$ for 1–1 electrolytes. Inorganic solutes appear as circles and carboxylate salts as triangles.

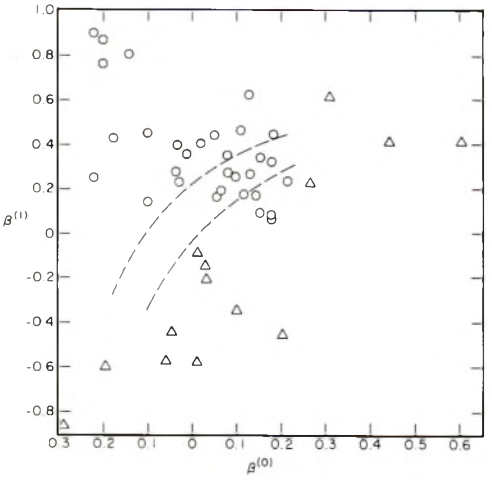

Figure 3. The relationship of $\beta^{(1)}$ and $\beta^{(0)}$ for organic electrolytes of 1–1 type. Sulfonates and sulfonic acids appear as circles and tetraalkylammonium halides as triangles. The dashed curves here show the region similarly designated on Figure 2.

weighted somewhat differently for the two parameters. Careful consideration of several solutes where measurements are precise and numerous indicates that the small but finite range of $\beta^{(1)}$ values for a given $\beta^{(0)}$ is real.

The organic electrolytes in Figure 3 and the higher valence types in Figures 4 and 5 show greater scatter but a clear trend of $\beta^{(1)}$ with $\beta^{(0)}$ is still apparent. These relationships are considered further in the Discussion.

A Convenient Approximation

For many purposes only a rough estimate of an activity coefficient is needed. Since $\beta^{(1)}$ has been shown to be determined within rather narrow limits if $\beta^{(0)}$ is known and the effect of the third virial coefficient is small, a convenient approximation becomes possible. Figure 6 shows the activity coefficient as a function of molality for 1–1 electrolytes for a series of values of $\beta^{(0)}$. In each case $\beta^{(1)}$ was given a value in the middle of the band in Figure 1, and C^{φ} was neglected.

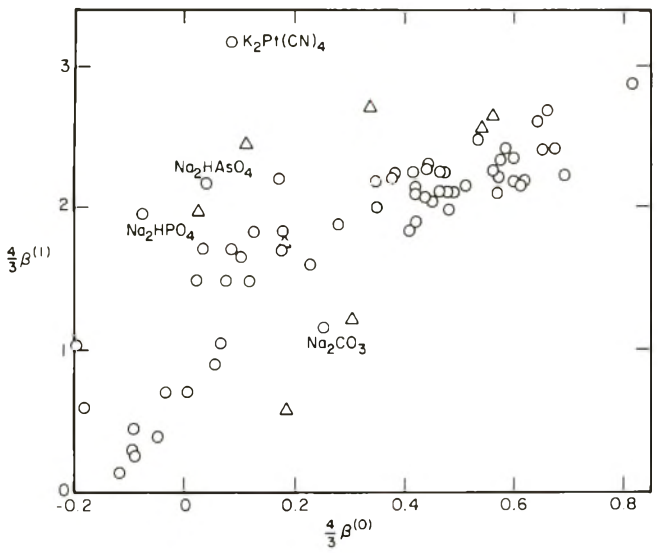

Figure 4. The relationship of $\beta^{(1)}$ to $\beta^{(0)}$ for 2–1 electrolytes. Inorganic solutes appear as circles while those with organic groups as triangles.

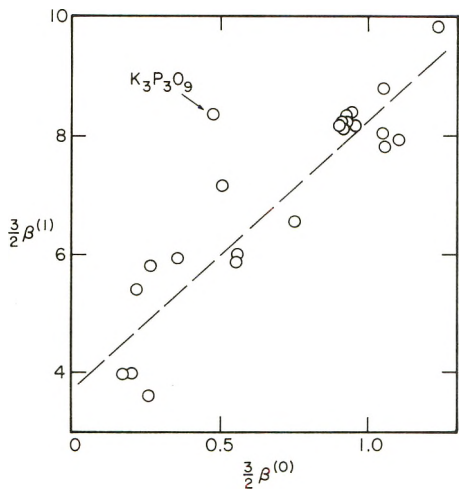

Figure 5. The relationship of $\beta^{(1)}$ to $\beta^{(0)}$ for 3–1 electrolytes.

By taking the value of $\beta^{(0)}$ from Tables I–V and interpolating between the appropriate curves on Figure 6, one can read directly an approximate value of the activity coefficient for any 1–1 electrolyte.

Similar graphs could, of course, be prepared for higher valence types, but the more extreme departures from unity of these activity coefficients reduces the utility of this procedure. Hence such graphs are omitted.

Discussion

First it is interesting to note that the equations, originally selected on the basis of their effectiveness in representing the properties of 1–1 and 2–1 electrolytes, proved to be equally effective for 3–1, 4–1, and even 5–1 type solutes. While the maximum molality values are lower for the high valence types, the maximum ionic strengths are about the same as for 1–1 and 1–2 solutes.

Let us now turn from our emphasis on convenient and accurate representation of data for thermodynamic purposes to the interpretation of the results in terms of interionic forces. In I it was shown that B^{φ} is a second virial coefficient arising from short-range forces between pairs of ions although its interpretation is complicated by the

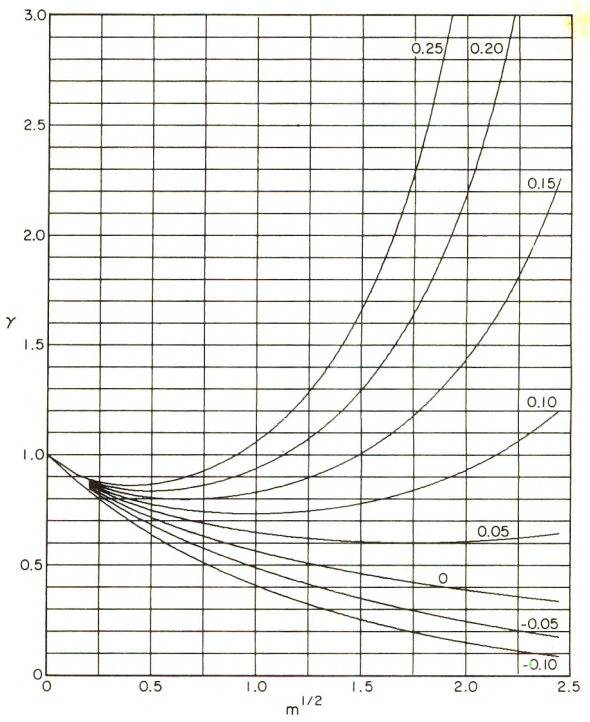

Figure 6. Activity coefficients for 1–1 electrolytes by the approximate method. The value of $\beta^{(0)}$ for each curve is indicated.

presence of the term for long-range electrostatic forces and the ionic strength dependence of the radial distribution functions. Thus much of the discussion will be qualitative in nature.

The second virial coefficient may be either positive or negative depending on the net predominance of repulsive or attractive short-range forces, respectively. Also the second virial coefficient for an electrolyte is a weighted mean of the interactions of pairs of ions with signs ++, +−, and −−, and it was shown in I that the relative weighting of +− interactions is greatest at low ionic strength. At higher ionic strength, the ++ and −− terms become more important but never equal to the weight of the +− interaction. Since multiply charged ions of the same sign will rarely approach one another closely, we can expect that the ++ or −− terms for such ions will be even smaller than for singly charged ions of the same sign and same size.

In view of this difference in weighting of +− compared to ++ and −− interactions, it is possible to determine two parameters for the short-range binary interactions of a single electrolyte (but only two). In our formulation these are $\beta^{(0)}$ and $\beta^{(1)}$. Ramanathan and Friedman[63] included more parameters in their model but, in accordance with these ideas, found that only two could be evaluated from osmotic or activity data and that any others had to be set to zero or to some other arbitrary value unless they were known from different sorts of measurements.

The simplest molecular model presenting effectively two parameters is one of rigid spherical ions of varying size. The thermodynamic properties depend primarily on the sum of radii for unlike ions ($R_+ + R_-$) but there is a secondary dependence on the absolute magnitude of the difference $|R_+ - R_-|$. The excluded volumes depend on the cubes of the distances of closest approach; hence, we expect a larger repulsive effect for like-charged ions when there is a difference in size. Rasaiah and Friedman[64]

TABLE XI: Rigid Sphere Models

$R_+ + R_-$, Å	$\lvert R_+ - R_- \rvert$, Å	$\beta^{(0)}$	$\beta^{(1)}$
2.90	1.64	0.1043	0.0200
2.90	0	0.0773	0.0497
2.76	0.86	0.0734	0.0188
4.6	0	0.3221	0.1431
4.6	1.0	0.3506	0.1063

made statistical calculations for this model, and we evaluated our parameters to fit several of their examples; the results are in Table XI and pertain to aqueous solution at room temperature. We see that for constant $(R_+ + R_-)$ a shift from equal to unequal sized ions increases $\beta^{(0)}$ and decreases $\beta^{(1)}$; thus it moves a point on Figure 2 downward and to the right. While no combination of the available examples corresponds exactly to a change of $\beta^{(1)}$ with $\beta^{(0)}$ constant, the comparison of the third line with the second line of Table XI approaches this case and indicates the approximate reduction in $(R_+ + R_-)$ required for a particular increase in $|R_+ - R_-|$.

While it is formally possible to discuss the parameters we have obtained for real electrolytes in terms of ionic hard-core radii, this does not seem promising. The ambiguity between the radius of the simple ion and the solvated ion is well known. Also there seems to be no correlation of the parameters in Table I with the expectations based upon ionic radii determined from crystals.

In their model for the intermolecular potential Ramanathan and Friedman[63] assumed electrostatic and repulsive terms based upon independent knowledge of charges and of radii in crystals and then evaluated empirically coefficients of a term, first introduced by Gurney,[65] which can be considered to represent the net effect of solvation, dispersion forces, and any other effects of similar range. Our results support this general concept that the second virial coefficients for electrolytes are best discussed in terms of a combination of repulsive radii determined from crystals or other sources and slightly longer range forces which arise from solvation effects, from dispersion forces, and in some cases also from such other effects as would arise from permanent dipoles or multipoles (for example, with OH^- or NO_3^-). The contribution of each of these various types of short-range forces to ++ and −− interactions will not follow the same relationship as its contribution to +− interactions; hence $\beta^{(1)}$ will not be exactly determined by $\beta^{(0)}$. But the relationship is complex, and we do not expect any simple pattern related to ionic size.

In Figures 2-5 we have noted that in each case the points for most solutes fall in a band with positive slope; this indicates that these short-range forces follow similar patterns for ++ and −− as compared to +− interionic interactions. In some cases the points outside these bands are individually labeled. Thus in Figure 2 the point for $RbNO_2$ falls below the band while the points for other nitrites are within but near the lower boundary of the band. Since these data for nitrites do not appear to be of very high accuracy, it is probable that $RbNO_2$ is not really anomalous. The results for all nitrites, however, indicate more repulsive or less attractive forces between pairs of nitrite ions than is typical for most anions. Corresponding statements can be made about the labeled points above the band with the conclusion that like ion interactions are less repulsive or more attractive than normal for BrO_3^-, ClO_3^-, and $H_2AsO_4^-$.

It is not surprising that the magnitude of these effects is greater for the salts involving large organic groups shown in Figure 3. For the electrolytes involving multiply charged ions in Figures 4 and 5 it is surprising that the points farthest from the principal band involve only the very common univalent ions Na^+ and K^+ which cannot be the cause of the deviation since most salts with these ions are normal. Thus the short-range forces between pairs of multiply charged ions must be responsible. In all cases the ions are polyatomic with the negative charge distributed among several peripheral atoms; hence it is not too surprising that they approach one another close enough for short-range forces to have some effect.

The location of a given point along the band for that type of electrolyte is, of course, the more important factor, and it will be discussed in terms of the value of $\beta^{(0)}$. This quantity is determined primarily by the short-range forces between ions of opposite charge. Our results show various trends of interest, but many of these have been discussed previously by Gurney[65] and Frank[66] among others. These authors emphasize a classification of both cations and anions with respect to a tendency to enhance or to disrupt the solvent structure. Then it is shown that the activity coefficient curves, or our β values, are the higher the more dissimilar are the ions in this respect and the lower the more similar they are.

We find that the multiply charged cations are readily added to this system. Then the most "structure-making" ions are the smaller multiply charged ions with the sequence Mg^{2+}, Ca^{2+}, Sr^{2+}, Ba^{2+}, Li^+, Na^+, K^+ continuing to the "structure-breaking" ions Rb^+ and Cs^+. The corresponding anion sequence is OH^-, F^-, Cl^-, Br^-, I^-, ClO_4^- wherein we have added perchlorate as the most "structure-breaking" ion to those usually given heretofore.

The divalent ions Zn^{2+}, Mg^{2+}, Ca^{2+}, and Sr^{2+} each have $\beta^{(0)}$ values in increasing order for Cl^-, Br^-, I^-, and ClO_4^-; while for Ba^{2+} as for Li^+ the values for ClO_4^- drop between Br^- and I^-. For other simple divalent cations the data are less extensive but there seems to be no contradiction of this pattern. The complex but compact ion UO_2^{2+} also follows this trend, but large cobalt complex ions show the opposite sequence and may be classified as "structure breakers."

When one ion is of intermediate character, for example, Na^+ or K^+, then the sequence may be irregular. For potassium there is a smooth trend of $\beta^{(0)}$ from OH^- down through F^- to Cl^- and then back upward for Br^- and I^-. But for sodium, the hydroxide and perchlorate both take intermediate values. Hydrogen ion in strong acids is a "structure maker" with properties close to those of Li^+. The sulfate ion appears to fall between F^- and Cl^-; its $\beta^{(0)}$ values drop from Li^+ to Na^+ and then rise through K^+, Rb^+, and Cs^+.

The $\beta^{(0)}$ values for nitrates are relatively low in all cases regardless of the structure making or breaking character of the cation. This suggests some tendency toward ion pair formation as is also indicated by spectroscopic data in several cases. Lemley and Plane[67] report a particularly complete spectral study for zinc nitrate while Peleg[68] reports a similar study of magnesium nitrate; these authors refer to work on other nitrates.

The electrolytes involving ClO_3^-, BrO_3^-, $H_2PO_4^-$, $H_2AsO_4^-$, BO_2^-, BF_4^-, and PF_6^- all have low $\beta^{(0)}$ values, but data are available for only one or two cations in most cases. Presumably these large anions are structure

breakers and in addition tend toward ion pair formation as do nitrates. Nevertheless, their behavior is well represented by or equations, and it is not necessary to assume incomplete dissociation.

It has been noted previously that acetate is a weak "structure maker," and our results agree. The values for nitrite follow those for chlorides rather closely; hence nitrite is a weak "structure breaker." The electrolytes involving large organic ions have been measured recently, and the papers presenting these results are accompanied in most cases by discussions making use of recent theory; hence we shall not comment further on these cases.

Bromley[69] has independently developed a system of representation and estimation for activity coefficients of strong electrolytes, and we have enjoyed discussions with him. His system, although developed simultaneously, may be described as a simplification of the present system. The third virial coefficient is omitted, and the second virial coefficient is modified into a form, still dependent on ionic strength, but with a single parameter B. This is, in effect, a relationship between our $\beta^{(1)}$ and $\beta^{(0)}$. He further shows that his B values can be approximated from two parameters for each ion B_M and δ_M or B_X and δ_X by the equation

$$B = B_M + B_X + \delta_M\delta_X$$

Structure-making cations have positive δ_M while structure breakers have negative δ_M. For anions the signs are reversed with structure makers having negative δ_X, and the struture breakers having positive δ_X. Thus the last term gives the effect just discussed in which $\delta_M\delta_X$ is the more positive the more dissimilar are pairs of ions with respect to this quality and is negative for pairs in which both ions have the same characteristic (either structure making or structure breaking).

Although less accurate than our equations, Bromley's system is quite effective and will be useful for many purposes. He also compares his results with a somewhat similar system of Meissner and Tester.[62]

Electrolytes of the 2-2 type and others involving ion pairing will be treated in a subsequent paper. Also we are proceeding to calculations for mixed electrolytes based upon the constants here obtained; indeed the convenience of our equations as applied to mixed electrolytes was a primary incentive for this work.

Acknowledgment. This research was sponsored by the U. S. Atomic Energy Commission.

Supplementary Material Available. Additional details concerning the evaluation of data for individual solutes will appear following these pages in the microfilm edition of this volume of the journal. Photocopies of the supplementary material from this paper only or microfiche (105 × 148 mm, 20× reduction, negatives) containing all of the supplementary material for the papers in this issue may be obtained from the Journals Department, American Chemical Society, 1155 16th St., N.W., Washington, D. C. 20036. Remit check or money order for $4.00 for photocopy or $2.00 for microfiche, referring to code number JPC-73-2300.

References and Notes

(1) K. S. Pitzer, *J. Phys. Chem.*, **77**, 268 (1973). In Table I the entries for 2-1 and 1-2 electrolytes should be reduced by the factor ¾ for $\beta^{(0)}$ and $\beta^{(1)}$. Also eq 50 should have a plus rather than a minus sign before $\beta^{(1)}$, and on p 276 ψ(Na,K,NO$_3$) = −0.0012.
(2) J. E. Mayer, *J. Chem. Phys.*, **18**, 1426 (1959).
(3) R. A. Robinson and R. M. Stokes, "Electrolyte Solutions," 2nd ed, revised, Butterworths, London, 1965.
(4) N. P. Chekhunova, P. J. Protsenko, and L. N. Venerovskaya, *Russ. J. Phys. Chem.*, **43**, 1158 (1969).
(5) R. F. Platford, *Can. J. Chem.*, **47**, 2271 (1969).
(6) G. Akerlof and P. Bender, *J. Amer. Chem. Soc.*, **70**, 2366 (1948).
(7) N. P. Chekhunova and P. I. Protsenko, *Russ. J. Phys. Chem.*, **41**, 2266 (1967).
(8) R. A. Robinson, J. M. Stokes, and R. M. Stokes, *J. Phys. Chem.*, **65**, 542 (1961).
(9) H. Ti Tien, *J. Phys. Chem.*, **67**, 532 (1963).
(10) A. K. Covington and D. E. Irish, *J. Chem. Thermodyn.*, **17**, 175 (1972).
(11) O. E. Esval and S. Y. Tyree, *J. Phys. Chem.*, **66**, 940 (1962).
(12) H. S. Harned and R. W. Ehlers, *J. Amer. Chem. Soc.*, **55**, 2179 (1933).
(13) G. Akerlof and J. W. Teare, *J. Amer. Chem. Soc.*, **59**, 1855 (1937).
(14) S. R. Gupta, G. J. Hills, and D. J. Ives, *Trans. Faraday Soc.*, **53**, 1874 (1963).
(15) S. R. Gupta, G. J. Hills, and D. J. Ives, *Trans. Faraday Soc.*, **53**, 1886 (1963).
(16) H. S. Harned, A. S. Keston, and J. G. Donelson, *J. Amer. Chem. Soc.*, **58**, 989 (1936).
(17) W. J. Bierman and R. S. Yamasaki, *J. Amer. Chem. Soc.*, **77**, 241 (1955).
(18) H. B. Hetzer, R. A. Robinson, and R. G. Bates, *J. Phys. Chem.*, **66**, 1423 (1962).
(19) H. S. Harned and R. A. Robinson, *Trans. Faraday Soc.*, **37**, 302 (1941): (HI).
(20) H. B. Hetzer, R. A. Robinson, and R. G. Bates, *J. Phys. Chem.*, **68**, 1929 (1964).
(21) H. S. Harned and M. A. Cook, *J. Amer. Chem. Soc.*, **59**, 1290 (1937): (KCl).
(22) T. Shedlovsky and D. A. MacInnes, *J. Amer. Chem. Soc.*, **59**, 503 (1937): (KCl).
(23) (a) T. Mussini, P. Longlin, and G. Riva, *J. Chem. Thermodyn.*, **4**, 591 (1972); (b) R. A. Robinson and D. A. Sinclair, *J. Amer. Chem. Soc.*, **56**, 1830 (1934): (CsCl).
(24) R. H. Stokes, *J. Amer. Chem. Soc.*, **67**, 1689 (1945).
(25) E. A. Guggenheim and J. C. Turgeon, *Trans. Faraday Soc.*, **51**, 747 (1955).
(26) E. J. Roberts, *J. Amer. Chem. Soc.*, **52**, 3877 (1930).
(27) G. Akerlof and G. Kegeles, *J. Amer. Chem. Soc.*, **62**, 620 (1940).
(28) H. S. Harned and J. C. Hecker, *J. Amer. Chem. Soc.*, **55**, 4838 (1933).
(29) H. S. Harned and G. E. Mannweiler, *J. Amer. Chem. Soc.*, **57**, 1873 (1935).
(30) H. S. Harned and W. J. Hamer, *J. Amer. Chem. Soc.*, **55**, 2194, 4496 (1933): (KOH).
(31) H. S. Harned and M. A. Cook, *J. Amer. Chem. Soc.*, **59**, 496 (1937): (KOH).
(32) H. S. Harned and O. E. Schupp, Jr., *J. Amer. Chem. Soc.*, **52**, 3886, 3892 (1930): (CsOH).
(33) H. S. Harned and F. E. Swindells, *J. Amer. Chem. Soc.*, **48**, 126 (1926): (LiOH).
(34) H. S. Harned and H. R. Copson, *J. Amer. Chem. Soc.*, **55**, 2206 (1933): (LiOH).
(35) H. S. Harned and J. G. Donelson, *J. Amer. Chem. Soc.*, **59**, 1280 (1937): (LIOH).
(36) H. S. Harned and C. G. Geary, *J. Amer. Chem. Soc.*, **59**, 2032 (1937).
(37) W. Y. Wen, S. Saito, and C. Lee, *J. Phys. Chem.*, **70**, 1244 (1966).
(38) S. Lindenbaum and G. E. Boyd, *J. Phys. Chem.*, **68**, 911 (1964).
(39) V. E. Bower and R. A. Robinson, *Trans. Faraday Soc.*, **59**, 1717 (1963).
(40) H. P. Gregor, M. Rothenberg, and N. Fine, *J. Phys. Chem.*, **67**, 1110 (1963).
(41) O. D. Bonner and O. C. Rogers, *J. Phys. Chem.*, **64**, 1499 (1960).
(42) S. Lindenbaum and G. E. Boyd, *J. Phys. Chem.*, **71**, 581 (1967).
(43) G. E. Boyd, A. Schwarz, and S. Lindenbaum, *J. Phys. Chem.*, **70**, 821 (1966).
(44) W. Y. Wen and S. Saito, *J. Phys. Chem.*, **69**, 3569 (1965).
(45) S. Lindenbaum, *J. Phys. Chem.*, **72**, 212 (1968).
(46) G. Scatchard and R. F. Tefft, *J. Amer. Chem. Soc.*, **52**, 2272 (1930).
(47) R. A. Robinson and R. H. Stokes, *Trans. Faraday Soc.*, **36**, 740 (1940): ($ZnCl_2$).
(48) Calculated from the Gibbs energy values of D. D. Wagman, *et al.*, *Nat. Bur. Stand. (U. S.), Tech. Note*, **No. 270-3** (1968): ($ZnCl_2$).
(49) R. H. Stokes and J. M. Stokes, *Trans. Faraday Soc.*, **41**, 688 (1945).
(50) R. H. Stokes, J. M. Stokes, and R. A. Robinson, *Trans. Faraday Soc.*, **40**, 533 (1944): ($ZnBr_2$).
(51) R. G. Bates, *J. Amer. Chem. Soc.*, **60**, 2983 (1938).
(52) R. M. Stokes, *Trans. Faraday Soc.*, **41**, 12 (1945): (ZnI_2).
(53) K. O. Groves, J. L. Dye, and C. H. Brubaker, *J. Amer. Chem. Soc.*, **82**, 4445 (1960).
(54) W. L. Masterton, T. L. Munnelly, and L. H. Berka, *J. Phys. Chem.*, **71**, 942 (1967).
(55) O. D. Bonner and O. C. Rogers, *J. Phys. Chem.*, **65**, 981 (1961).
(56) D. J. Karl and J. L. Dye, *J. Phys. Chem.*, **66**, 550 (1962): ($Co(en)_3Cl_3$).

(57) A. K. Covington, M. A. Hakeem, and W. F. K. Wynne-Jones, *J. Chem. Soc.*, 4394 (1963).
(58) R. A. Wynveen, J. L. Dye, and C. H. Brubaker, *J. Amer. Chem. Soc.*, **82**, 4441 (1960).
(59) C. H. Brubaker and T. E. Haas, *J. Phys. Chem.*, **65**, 866 (1961).
(60) G. Miller and A. S. Porter, *Trans. Faraday Soc.*, **63**, 335 (1967).
(61) Additional details concerning the evaluation of data for individual solutes are given in Lawrence Berkeley Laboratory Report No. LBL-1434 and will also appear as supplementary material. See paragraph at end of paper regarding supplementary material.
(62) H. P. Meissner and J. W. Tester, *Ind. Eng. Chem., Process Des. Develop.*, **11**, 128 (1972).
(63) P. S. Ramanathan and H. L. Friedman, *J. Chem. Phys.*, **54**, 1086 (1971).
(64) J. C. Rasaiah and H. L. Friedman, *J. Chem. Phys.*, **48**, 2742 (1968); **50**, 3965 (1969).
(65) R. W. Gurney, "Ionic Processes in Solution," McGraw-Hill, New York, N. Y., 1953, Chapter 16.
(66) H. S. Frank, *Z. Phys. Chem. (Leipzig)*, **228**, 364 (1965).
(67) A. T. G. Lemley and R. A. Plane, *J. Chem. Phys.*, **57**, 1648 (1972).
(68) M. Peleg, *J. Phys. Chem.*, **76**, 1019 (1972).
(69) L. A. Bromley, *AIChE J.*, **19**, 313 (1973).

Ionization and Electron Transfer Reactions in Linde Type Y Zeolites

Paul H. Kasai* and Roland J. Bishop, Jr.

Union Carbide Corporation, Tarrytown Technical Center, Tarrytown, New York 10591 *(Received May 21, 1973)*

Publication costs assisted by the Union Carbide Corporation

When type Y zeolite is exposed to Na vapor and subsequently to oxygen, Na_4^{3+} centers and O_2^- radicals are formed. Cu(II) and Ni(II) ions exchanged into type Y zeolite undergo electron transfer reactions with absorbed NO and NO_2 gases. These observations are discussed in terms of the ionizing power of the zeolite originating from the spacious and asymmetric arrangement of the crystalline charges.

Introduction

A great deal of effort has been made toward an understanding of the structures and the properties of various zeolites.[1] Zeolites are crystalline alumininosilicates, and their empirical formula may be given as $Na_m(AlO_2)_m \cdot (SiO_2)_n$. A representative value of the ratio m/n for the Linde type Y zeolite is 1/2.4. When it is completely dehydrated, the structural aspects of each zeolite can be considered in two parts: the three-dimensional framework structure of polyanion $[(AlO_2)_m(SiO_2)_n]^{m-}$, and the positions of the cations, Na^+, dictated by the potential field of the framework. The well-known "molecular sieve" property of zeolite is rendered by the large interconnecting channels and cages outlined by the framework. One of the most important consequences of such a structural feature is that many, if not all, of the cations are located near the "inner surface" of these void spaces. These cations are hence shielded only on one side, and by reason of symmetry, many of the negative charges of the polyanionic framework are also shielded unevenly. Thus, anhydrous zeolites can be viewed as "expanded" ionic crystals, having very irregular and extremely spacious arrangements of the ions. The dimension of the large cages in the type Y zeolite, for example, is ~13 Å in diameter. The crystallinity of the material, however, must impose a periodic pattern in a larger scale. One should then realize that the total crystalline energy (the Madelung energy of the crystal) can be greatly increased by filling these intracrystalline void spaces with properly arranged polarized species or additional cations and/or anions.

Recently we have reported on our electron spin resonance (esr) study of the interaction between nitric oxide (NO) and Linde's type Y zeolites.[2] We proposed and substantiated an occurrence of an electron transfer reaction (1) within the zeolite.[3] Although NO has a relatively low

$$NO + NO_2 \longrightarrow NO^+ + NO_2^- \qquad (1)$$

ionization potential (9.25 eV), and NO_2 has a large electron affinity (4 eV), the envisaged reaction (1) as such is an endothermic process. We proposed that the endorthermicity is offset by a gain in the Madelung energy of the crystal resulting from a proper arrangement of the additional ions produced. The process is schematically illustrated in Figure 1. This ionizing property, inherent to the original structure of dehydrated zeolites, should become even more pronounced when the usual monovalent Na^+ ions are replaced by divalent cations. We have thus come to view (anhydrous) zeolites, and particularly those exchanged with multivalent cations, as extremely powerful "solid-state ionizing solvents."

The purpose of this report is to reexamine the formations of Na_4^{3+} centers and O_2^- radicals in type Y zeolites from this new perspective, and to present several more examples of ionization phenomena, and facile electron transfer processes involving Cu(II) and Ni(II) ions in type Y zeolite. NO and NO_2 were used as electron donors and acceptors.

Experimental Section

Laboratory-synthesized iron-free type Y zeolite was used throughout the experiment. The notation (Na^+)-Y will be used to designate this Linde type Y zeolite, and (K^+)-Y, (Ni^{2+})-Y, and (Cu^{2+})-Y to designate the Y zeolite with the indicated cations prepared from (Na^+)-Y by

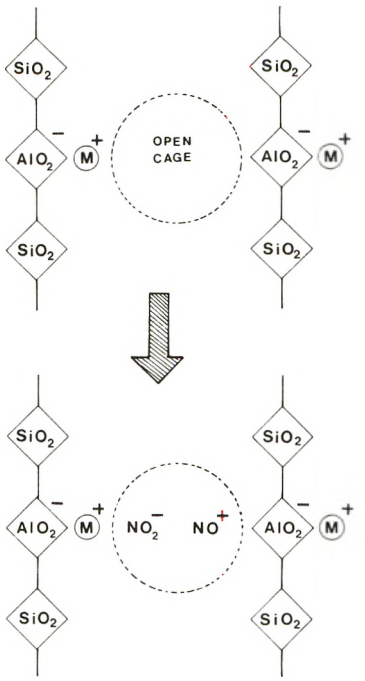

Figure 1. A schematic representation of irregular and extremely spacious arrangement of the polyanionic framework $[(AlO_2)_m(SiO_2)_n]^{m-}$ and the cations in dehydrated zeolite (upper figure). A gain in the ionic, crystalline energy should be realized when the void spaces are filled with properly arranged additional cations and/or anions (lower figure).

the standard exchange process. For those zeolites with divalent cations, the degrees of exchange attained were ~70%.

Zeolites were activated in esr sample tubes at 500° for 6 hr connected to a vacuum manifold maintained at 1×10^{-3} mm. A desired amount of gas such as NO, monitored by a pressure reading, was introduced into the esr tubes through the vacuum manifold.

All the esr measurements were done at liquid nitrogen temperature (77°K) using a X-band spectrometer. The microwave frequency locked to the loaded sample cavity was 9.09 GHz.

Results and Discussions

Ionization of Na Atoms. Formation of Na_4^{3+} Centers in Na-Y Zeolite. Perhaps the most dramatic and simplest example of the ionization process is that of Na atoms in (Na^+)-Y. When (Na^+)-Y was exposed to Na vapor at 300~500°, its color changed from white to bright red. The colored material was found to exhibit an esr spectrum consisting of 13 hyperfine components (Figure 2A).[4] The intensity pattern is that expected from the hyperfine interaction with four equivalent nuclei with $I = 3/2$. The same signal had been observed earlier in γ-ray irradiated (Na^+)-Y and was attributed to an electron trapped in a cage shared among four Na^+ ions, hence the notation Na_4^{3+} center.[5] The amount of Na_4^{3+} centers created by irradiation is in the order of 10^{17}~10^{18}/g, and these centers are destroyed when the sample is heated above 200°. The concentration of Na_4^{3+} centers produced by Na vapor amounted to $\sim 10^{21}$/g, corresponding to one electron in each α cage of the Y zeolite.[6] Spontaneous formation of the center by this "stoichiometric" amount at temperature above 200° can be best understood in terms of ionization of Na atoms induced by the electrolytic property of the zeolite.

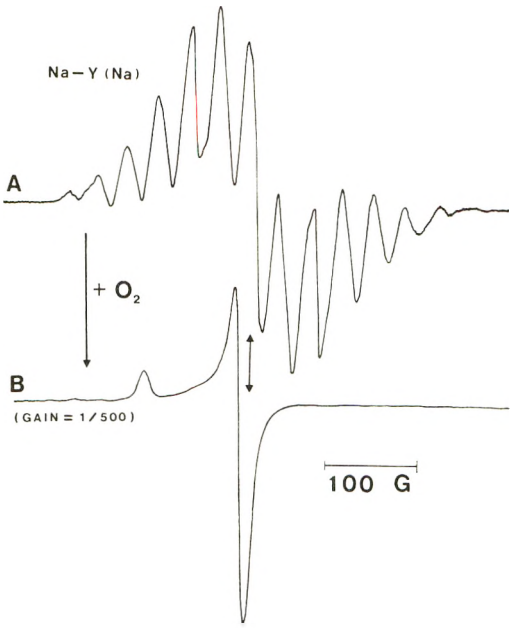

Figure 2. The esr spectrum of Na_4^{3+} centers (A), produced by exposing (Na^+)-Y to Na vapor, changes instantaneously to that of O_2^- radicals (B) when exposed to oxygen. The arrow indicates the position corresponding to $g = 2.00$.

$$Na \longrightarrow Na^+ + e^-$$

Formation of O_2^- Radicals in (Na^+)-Y with Na_4^{3+} Centers. When (Na^+)-Y treated with Na vapor was subsequently exposed to oxygen, the red colored material became instantly white, the esr signal due to Na_4^{3+} centers disappeared, and a new signal possessing a characteristically anisotropic g tensor appeared (Figure 2B and 4A). The oxygen induced signal was found to be identical with that seen when (Na^+)-Y was irradiated with γ-ray in the presence of oxygen, and had been assigned to O_2^- radical attached to Na^+ ion.[5] Being a $^2\pi$ radical, a well-defined esr signal of O_2^- can be expected only when the degeneracy of the valence π orbitals is lifted. Shown in Figure 3 is a schematic representation of the valence orbital levels of O_2^- molecule subjected to the electric field of a Na^+ ion in a manner depicted in the figure. The g tensor of an O_2^- radical whose π orbital degeneracy is lifted has been treated by Kanzig and Cohen.[7] For the case $\Delta > \delta \gg \lambda$ where λ is the spin orbit coupling constant of an oxygen atom, it can be shown that

$$g_x = g_e - (\lambda/\delta)^2 + (\lambda^2/\delta\Delta) \quad (2a)$$

$$g_y = g_e + (2\lambda/\Delta) - (\lambda/\delta)^2 - (\lambda^2/\delta\Delta) \quad (2b)$$

$$g_z = g_e + (2\lambda/\delta) \quad (2c)$$

Here $g_e = 2.0023$ represents the value for a free electron. Comparison of eq 2 with the g tensor assessed in Figure 4A leads to the following assignment: $g_x = g_1 = 2.0016$, $g_y = g_2 = 2.0066$, and $g_z = g_3 = 2.113$. For the particular orientation of O_2^- relative to the Na^+ ion depicted in Figure 3, one notes that the Na^+ ion is at the nodal plane of the antibonding π_x^* in which the unpaired electron resides. In this situation the largest hyperfine interaction with ^{23}Na nucleus is expected in the direction of y axis. If, on the other hand, the Na^+ ion is closer to one of the oxygen atoms, delocalization of the unpaired electron into the $3p_x$ orbital of the sodium atom occurs, and the largest hy-

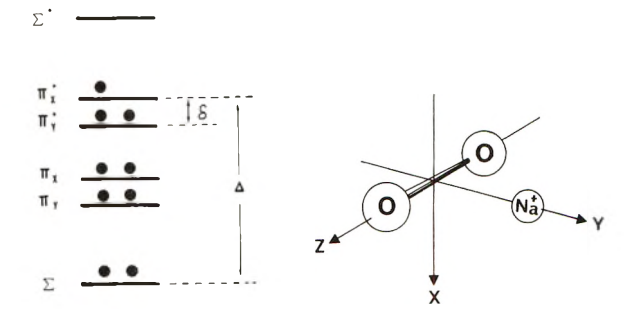

Figure 3. Valence orbital energy levels of O_2^- attached to Na^+ in the configuration shown.

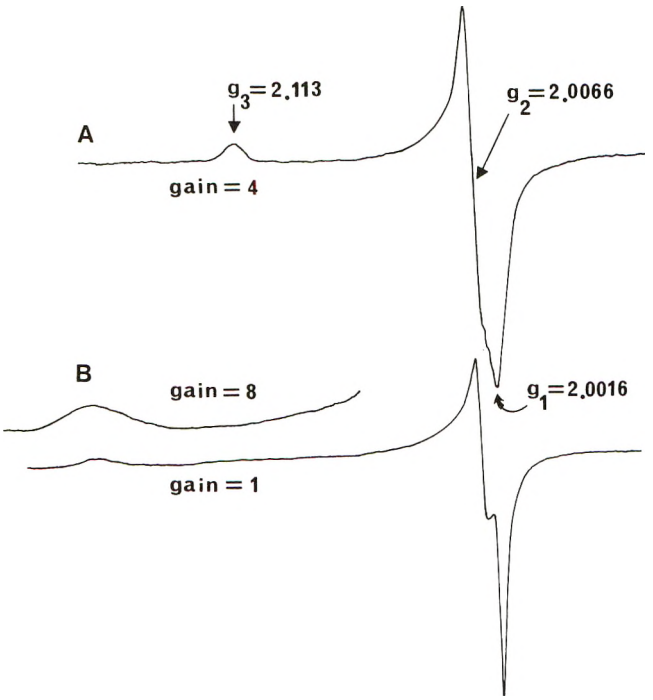

Figure 4. Esr spectra of O_2^- radicals created in (Na^+)–Y containing ionized Na atoms (A) and (K^+)–Y containing ionized K atoms (B).

perfine interaction is expected along the x axis.[8] Shown in Figure 4B is the esr spectrum obtained when (K^+)–Y reduced by K vapor is exposed to oxygen. The nuclear spins of both ^{23}Na (natural abundance = 100%) and ^{39}K (natural abundance = 93%) are 3/2. However, the magnetic moment of ^{23}Na is 2.22 nuclear magneton, while that of ^{39}K is only 0.39 nuclear magneton. The esr spectrum of O_2^- associated with K^+ is almost identical with that of O_2^- associated with Na^+, except that the signal of the former in the g_2 ($= g_y$) region is much sharper than that of the latter. In fact, one can almost recognize a quartet feature in the g_y region of the O_2^-–Na^+ spectrum. These observations are quite consistent with the orientation shown in Figure 3, and indicate the prevalence of the interaction of ionic nature between the superoxide ion O_2^- and the associated cation Na^+ or K^+.

An important aspect we must realize is that the generation of O_2^- radicals by exposing (Na^+)–Y containing ionized Na atoms to oxygen molecules is equivalent to incorporating a well-known oxide, alkali superoxide, in its ionized state.

$$NaO_2 \longrightarrow Na^+ + O_2^-$$

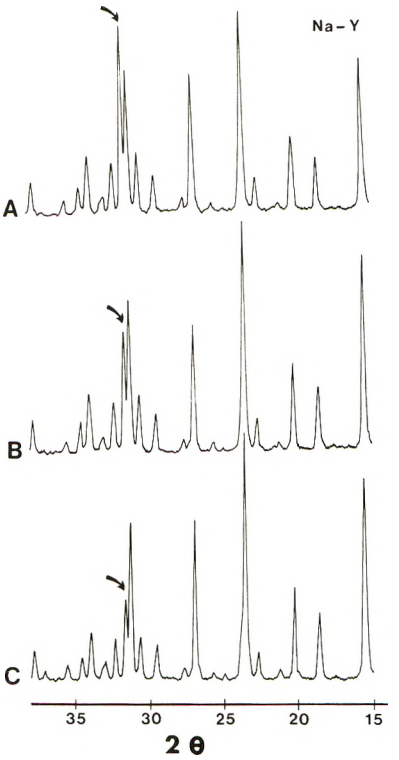

Figure 5. X-Ray powder patterns of anhydrous mixture of (Na^+)–Y and NaCl (10 wt %) obtained from the fresh mixture (A) and after successive heat treatment at 350 (B) and 500° (C) for 24 hr, respectively. The arrows indicate the NaCl peak (2,0,0) at 31.7°.

Dissolution of NaCl into Zeolites. In ref 2 we reported that when a slurry of (Na^+)–Y or (Ba^{2+})–Y containing 10 wt % of NaCl was activated to 500°, the X-ray powder pattern of the resulting material showed no trace of NaCl phase, but only that of the zeolite. We concluded that NaCl was occluded within the zeolitic cages in an ionized state, and attributed the result to the ionizing property of the zeolite.

To demonstrate that this is indeed a thermodynamically favored process, we decided to examine the effect of heating an anhydrous mixture of thoroughly activated zeolite and NaCl powders. Figure 5 shows a lower angle section (2θ = 15~35°) of the X-ray (Cu K_α) powder patterns obtained from (Na^+)–Y containing 10 wt % of NaCl. The zeolite was preactivated at 500° overnight, and mixed thoroughly with dried NaCl in a drybox. The X-ray powder pattern of the mixture was then examined prior to the heat treatment, and after successive heat treatments at 350 and 500° for 24 hr, respectively. In the 2θ range covered, the only prominent peak due to NaCl crystal is the (2,0,0) peak at 31.7° indicated by the arrows. All other peaks belong to the powder pattern of the Y zeolite. These patterns clearly demonstrate that, while the crystallinity of the zeolite stays virtually unchanged throughout the heat treatment, the NaCl phase disappears gradually as the sample is heated. The melting point of NaCl is 801°. One may thus conclude that, once the diffusion point is reached, NaCl begins to "dissolve" into zeolite cages in an ionized form, arranging themselves in a manner that would maximize the total crystal energy of the zeolitic system. 10 wt % of NaCl corresponds to approximately three Na^+–Cl^- ion pairs per α cage.

Reduction of Cu(II)-Zeolite by NO. Because of a high second ionization potential of Cu atom (20.34 eV), Rich-

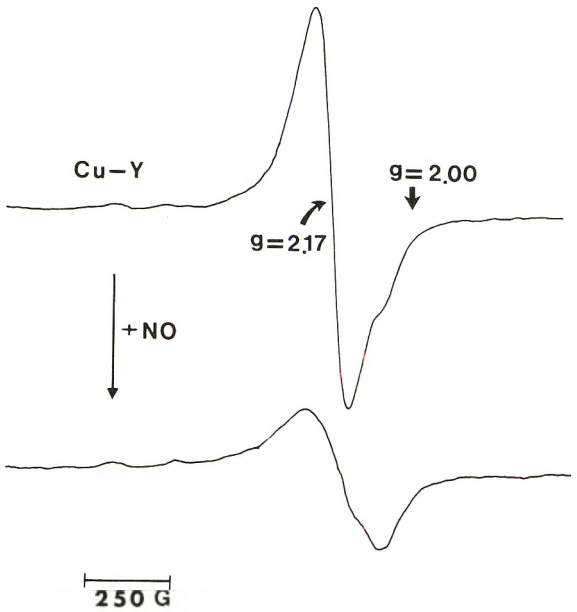

Figure 6. Esr spectra of activated (Cu^{2+})–Y observed before and after exposure to NO.

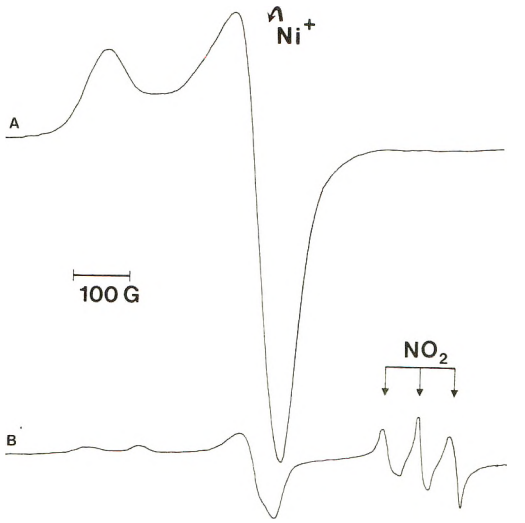

Figure 7. (A) Esr spectrum of (Ni^+, NO^+)–Y. (B) Esr spectrum of the above sample after it had been exposed to NO_2 and heated at 200° for 10 min.

ardson suggested that Cu^{2+} ions in zeolite should be the most vulnerable to a reductive reaction.[9] He had examined the extent of this reducibility by adsorbing anthracene on various cation-exchanged zeolites, and monitoring the esr signal of anthracene cation radicals produced. Although (Cu^{2+})–Y produced the largest amount of the cation radicals, he had to conclude that only a small fraction of Cu^{2+} ions were reducible. We suggested that a small number of Cu^{2+} ions were reduced because of pore clogging caused by a strong adherance of the initially produced large cations to the framework.[2] Although the ionization potential of NO (9.25 eV) is much higher than that of anthracene (7.55 eV), because of its smaller size, NO should be able to penetrate the zeolite throughout. If the gain in the crystalline energy in going from a divalent cation form, (Cu^{2+})–Y, to a monovalent cation form, (Cu^+, NO^+)–Y, is sufficiently large, exposure of (Cu^{2+})–Y to NO gas should result in the reduction of a substantial fraction, if not all, of the Cu^{2+} ions in the zeolite.

Figure 6 shows the esr spectra of activated (Cu^{2+})–Y observed before and after exposure to NO gas (0.75 atm). The Cu^{2+} ion signal decreased dramatically, spontaneously, and instantaneously, the moment the sample was exposed to NO at room temperature. We propose to attribute the change to the electron transfer reaction promoted by the electrolytic property of zeolite.

$$(Cu^{2+})\text{–Y} + NO \longrightarrow (Cu^+, NO^+)\text{–Y}$$

Consistently with the proposed reaction, only a trace amount of NO signal was observed, even though it was supplied in excess.

Recently, Gallezot, *et al.*,[10] have made an X-ray diffraction study of dehydrated $[Cu^{2+}(75\%)]$–Y, and reported that 75% of Cu^{2+} ions are at site I′, a semiexposed site, and the remaining at site I, a completely shielded position. The esr spectrum of Figure 6 can be recognized as a superposition of a broad symmetric signal at $g = 2.17$, and an asymmetric spectrum characteristic of Cu^{2+} ions immobilized in a distorted field. We assert that the broad, symmetric signal is due to Cu^{2+} ions at site I′, the signal of which is narrowed by an exchange process as suggested by Chao and Lunsford.[11] The latter asymmetric signal is assigned to Cu^{2+} ions at site I. Figure 6 shows that only those ions at site I′ have been reduced.

The reduction of Cu^{2+} ions in (Cu^{2+})–Y by NO has also been reported by Naccache, *et al.*[12] They attributed the reaction, however, to the formation of the Cu^+NO^+ complex. We believe the reaction is promoted by the energy gain resulting from a decrease of the internal charge separation when the divalent form of zeolite (Cu^{2+})–Y is converted to the monovalent form (Cu^+, NO^+)–Y. The doubly charged complex Cu^+NO^+ could hardly be stable within the dehydrated zeolitic framework, where many negatively charged units $(AlO_2)^-$ are left unattended by the cations.

Electron Transfer Reactions in (Ni^{2+})–Y. In our previous report,[2] we showed that a substantial amount ($\sim 10^{20}$/g) of Ni^+ ions are produced when (Ni^{2+})–Y is exposed to NO gas. The result is again attributed to the electron transfer process caused by the ionizing power of the zeolite.

$$(Ni^{2+})\text{–Y} + NO \longrightarrow (Ni^+, NO^+)\text{–Y}$$

Figure 7 shows the esr spectrum of (Ni^+, NO^+)–Y prepared by the method described above, and the spectrum of the same sample after it had been exposed to NO_2 (0.75 atm), and heated at 200° for 10 min. A near total disappearance of the Ni^+ signal, and a small amount of the NO_2 signal in the heated sample is attributed to the following reaction

$$(Ni^+, NO^+)\text{–Y} + NO_2 \longrightarrow (Ni^{2+}, NO^+, NO_2^-)\text{–Y}$$

Oxidation of Cu^+ Ions by NO_2. Examples of electron transfer reactions discussed above suggest that NO_2 alone may be able to act as an oxidizing agent within zeolite cages. Indeed, Naccache, *et al.*, observed that Cu^+ ions produced in (Cu^{2+})–Y by treatment with CO at 500° are reoxidized to Cu^{2+} ions when exposed to NO_2.[12] We also prepared (Cu^+)–Y by this technique. It appeared white and gave no esr signal. When NO_2 was added to this sample at room temperature, the esr signal of Cu^{2+} was restored instantaneously to its original intensity. We may thus write

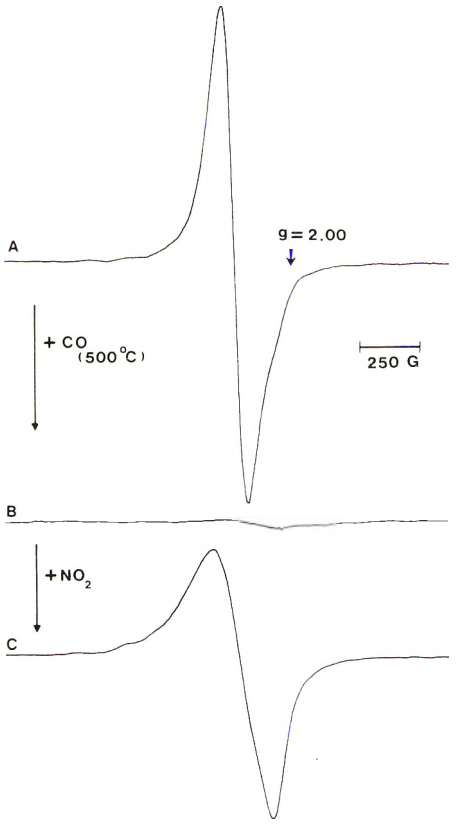

Figure 8. Esr spectra obtained (A) from freshly activated (Cu^{2+})-Y, (B) after it had been reduced by CO, and (C) after the reduced sample had been exposed to NO_2.

$$(Cu^{+})\text{-Y} + NO_2 \longrightarrow (Cu^{2+}, NO_2^{-})\text{-Y}$$

The sequence of spectra is shown in Figure 8. It is interesting to note that, unlike the reduction by NO at room temperature, the reduction by CO at 500° results in the reduction of all the Cu^{2+} ions in the zeolite. Furthermore, the spectrum of the reoxidized sample indicates that all the cupric ions are now immobilized in a distorted crystal field experiencing little, if any, exchange narrowing. The CO treatment at 500° must have resulted in the relocation of the Cu ions at site I, and possibly those at site I′, to the more exposed sites such as site II. The presence of NO_2^- ions near the Cu^{2+} ions should minimize the exchange coupling, as well as the motional narrowing. One must also note the total absence of the NO_2 signal although it was added in excess. The abundant presence of Cu^{2+}-NO_2^- ion pairs within the large cavities must be preventing the entrance of additional NO_2 molecules.

Summary and Concluding Remarks

The reactions presented and discussed in this report are

$$Na \longrightarrow Na^+ + e^-$$
$$NaO_2 \longrightarrow Na^+ + O_2^-$$
$$NaCl \longrightarrow Na^+ + Cl^-$$
$$Cu^{2+}(\text{or } Ni^{2+}) + NO \longrightarrow Cu^{+}(\text{or } Ni^{+}) + NO^+$$
$$Cu^{+}(\text{or } Ni^{+}) + NO_2 \longrightarrow Cu^{2+}(\text{or } Ni^{2+}) + NO_2^-$$

As written, most of these reactions are endothermic processes. Yet each one of these has been found or indicated to proceed with amazing facility within the zeolitic crystal. The most notable feature common to all of these reactions is that they result in an increase in the number of cations and/or anions within the zeolite cages. As stated earlier, a proper arrangement of these additional charged species within the periodically situated void spaces should result in an increase of the crystalline Madelung energy. We assert it is this gain in the crystalline energy which offsets the endothermicity of these reactions.

Catalytic properties of Y-type zeolites for a variety of organic reactions are well known, and have been the subjects of many investigations.[13] The observed activity has been attributed to the electric field associated with the exposed cations, to the acidity of the hydroxyl groups incorporated within the structure, or to the combined effect of both. We believe one of the most important, if not the important, properties of zeolite responsible for the observed catalytic activity is this ionizing or polarizing power rendered within its structure by a macroscopic property of the crystal, the Madelung energy.

References and Notes

(1) See, for example, the Proceeding of the Second International Conference on Molecular Sieve Zeolites, Worcester, Mass., Sept 1970.
(2) P. H. Kasai and R. J. Bishop, Jr., *J. Amer Chem. Soc.*, **94**, 5560 (1972).
(3) NO_2, in this particular case, is a product of a disproportionation reaction $4NO \rightarrow N_2O + N_2O_3$ (= $NO + NO_2$). W. E. Addison and R. M. Barrer, *J. Chem. Soc.*, 757 (1955).
(4) J. A. Rabo, C. L. Angell, P. H. Kasai, and V. Schomaker, *Discuss. Faraday Soc.*, **41**, 328 (1966).
(5) P. H. Kasai, *J. Chem. Phys.*, **43**, 3322 (1965).
(6) For the structures of zeolites, see a review article by J. V. Smith in ref 1.
(7) W. Kanzig and M. H. Cohen, *Phys. Rev. Lett.*, **3**, 509 (1959).
(8) For an analysis of hyperfine structure of an esr spectrum, see, for example, P. W. Atkins and M. C. R. Symons, "The Structure of Inorganic Radicals," Elsevier, Amsterdam, 1967.
(9) J. T. Richardson, *J. Catal.*, **9**, 172 (1967).
(10) P. Gallezot, Y. B. Taarit, and B. Imelik, *C. R. Acad. Sci., Ser. C*, **272**, 261 (1971).
(11) C. C. Chao and J. H. Lunsford, *J. Chem. Phys.*, **57**, 2890 (1972).
(12) C. Naccache, M. Che, and Y. B. Taarit, *Chem. Phys. Lett.*, **13**, 109 (1972).
(13) See, for example, a review article by J. A. Rabo and M. L. Poutsma in ref 1.

Conversion of Amorphous Calcium Phosphate to Microcrystalline Hydroxyapatite. A pH-Dependent, Solution-Mediated, Solid–Solid Conversion

Adele Ludin Boskey* and Aaron S. Posner

Hospital For Special Surgery, Cornell University Medical College, New York, New York 10021 *(Received January 8, 1973)*

Publication costs assisted by the National Institutes of Health

The rate of formation of microcrystalline hydroxyapatite from amorphous calcium phosphate has been studied at constant temperature as a function of the pH of the mediating solution; the effect of temperature on this conversion was observed in systems maintained at pH 8. The extent of reaction, determined by X-ray diffraction analysis of per cent crystallinity, was verified by titrimetric measurements. The rate of formation of crystalline material is characterized by a sigmoid plot of weight per cent crystallinity *vs.* time. The transformation kinetics, which can be described by a "first-order" rate law, is a function only of the pH of the mediating solution at constant temperature. A solution-mediated, autocatalytic mechanism is proposed which fits the experimental observations and explains the metastability of the amorphous material. Activation energies are reported for both the transformation process and the onset of nucleation.

Introduction

Synthetic crystalline hydroxyapatite, $Ca_{10}(PO_4)_6(OH)_2$, has been studied extensively as an analog of bone mineral.[1-3] The reaction of calcium and dibasic phosphate salts in neutral or basic solution has as its final product this crystalline hydroxyapatite. During the precipitation of the crystalline material, a precursor phase is formed which is amorphous to X-ray diffraction.[4] This phase has been shown to be structurally and chemically distinct from hydroxyapatite. Calculations assuming the amorphous phase consisted of individual or groups of individual hydroxyapatite unit cells were incapable of explaining the observed diffraction pattern.[5] Chemical analysis[6] of the precursor phase indicated this noncrystalline phase is a hydrated calcium phosphate ($Ca_3(PO_4)_2 \cdot xH_2O$) of calcium to phosphorus ratio 3/2 as compared to the 5/3 ratio found in hydroxyapatite. This distinct amorphous phase converts, in the presence of water, to microcrystalline hydroxyapatite.

The lifetime of the metastable amorphous precursor in aqueous solution was reported[7] to be a function of the presence of certain macromolecules and interfering ions, pH, viscosity, ionic strength, and temperature. A preliminary study[8] of the kinetics of conversion of metastable amorphous calcium phosphate to hydroxyapatite indicated that at high pH the rate of conversion was proportional to the amount of hydroxyapatite already formed, suggesting that the conversion was proceeding autocatalytically. This paper describes a more detailed experimental study on the effect of pH and temperature on the rate of formation of microcrystalline hydroxyapatite.

Experimental Section

Synthesis of Amorphous Calcium Phosphate. The amorphous calcium phosphate (ACP) used in this study was prepared by mixing 300 ml of prebuffered 0.04 *M* calcium salt (chloride or nitrate) with 0.036 *M* prebuffered dibasic phosphate salt (ammonium, sodium, or potassium) in 400 ml of constantly stirred 0.15 *M* buffer. All solutions were thermally equilibrated at 26° before mixing. Tris(hydroxymethylaminomethane–HCl (Tris) and ammonia–ammonium chloride buffers were used for the pH ranges 6.8–9 and 9–10, respectively. The amorphous precursor was either removed (see below) immediately after mixing, or left in contact with the mother liquor for the kinetic study.

Kinetic Study. All constant temperature studies were made at 26 ± 1°. The relative humidity of the room was kept below 51% to prevent conversion of the dried ACP during handling by reaction with water in the atmosphere. Two classes of experiments were carried out: in one the amorphous material, after precipitation, was left in contact with its mother liquor, and in the other a weighed portion of dried ACP, sieved through 100 mesh, was added, with or without seed crystals, to a fixed volume of 0.15 *M* buffer. In certain experiments 0.2–0.3 g/l. of hydroxyapatite (HA) seeds were added to the solution along with 0.7–0.8 g/l. of ACP at the initial mixing time. Four sets of seed crystallites of increasing sizes were prepared by heating ACP for 1 hr in buffer at a 60, 70, and 80°, respectively. The effect of varying each of a number of parameters while maintaining the others at constant level was considered. The parameters involved were (a) the composition of the buffer, (b) the pH of the mediating solution, (c) the nature of the ions other than calcium and phosphate in solution, (d) the use of nonaqueous solutions, (e) the slurry concentration (weight of ACP per liter), (f) the specific surface area of the amorphous precursor, (g) the stirring rate, and (h) the absence of carbonate from the mediating solutions (carbonate-free solutions were maintained by bubbling nitrogen through preboiled solutions). In addition to the above experiments, which were performed in a constant volume of 1 l., experiments using minimal amounts of buffer so as to have high slurry concentrations were carried out using a constant slurry volume of 1.5 ml with slurry concentrations ranging from 4 to 1000% by weight.

The time reaction coordinate was defined as the total time the amorphous material had remained in contact with the aqueous solution. In all experiments involving large slurry volumes, 100-ml aliquots were removed at

preselected times, the pH of the slurry was determined, and the solid was washed and filtered through medium millipore filters. Equal volumes of cold ammoniated water and acetone (or methanol) were used to quench the reaction. The acetone wash was repeated until a dry free-flowing powder was obtained. The time of completion of the acetone wash was recorded as the time reaction coordinate. Dried materials were sieved through 100 mesh and stored in a vacuum desiccator.

At a given time t, the extent of reaction, *i.e.*, the fraction of ACP converted (α), is equivalent to the weight fraction of hydroxyapatite present in the slurry. The extent of reaction was determined by an X-ray diffraction method, described in detail elsewhere.[8,9] In this method the integrated intensity of an X-ray diffraction peak characteristic of the crystalline material is compared to the integrated intensity of a 100% crystalline sample of the same material of similar particle size. The reliability of this X-ray method for determining the fraction of crystalline hydroxyapatite in a given sample has been confirmed using mechanical mixtures of amorphous and apatitic calcium phosphate. An independent check of the X-ray determined reaction coordinates was made by maintaining nonbuffered solutions of ACP in water at constant pH by the addition of base. In this titrimetric method α was defined as the number of moles of base added at time t relative to the number of moles required for complete conversion.

The temperature dependence of the transformation was studied at pH 8 at 10, 26, 37, and 48°, respectively; both the titrimetric and X-ray analysis methods were used to follow the course of the transformation. Temperatures from 26 to 48° were maintained to ±0.1° inside the reaction flask using a proportional temperature control with an internal probe. The experiment at 10° was conducted entirely in a constant temperature room adjusted to that temperature.

The calcium ion concentration, as determined by atomic absorption spectroscopy, was monitored as a function of time during the conversion at pH 8 but only measured after 15 min and 24 hr at other pH values. Precipitate-free solutions for these analyses were obtained from 50-ml aliquots either by filtering through fine millipore filters or centrifuging at 4° and 60 rpm.

The specific surfaces of ACP samples prepared at different pH values were determined from small angle scattering measurements by Porod's method.[10]

Results

Figure 1 illustrates the typical pH-dependent conversion curves (26°) obtained in these studies. The total time required for the amorphous to crystalline transformation to reach completion increases with increasing pH. As can be seen from the agreement of points obtained under different experimental conditions, the observed conversion paths were independent of (a) the nature of buffer, (b) the type of univalent ions in solution, or (c) whether the amorphous material was left in contact with the mother liquor or filtered, dried, and added to fresh buffer. Bubbling nitrogen through the solution to prevent the uptake of carbon dioxide shifted, but did not alter, the shape of the curve. The shift can be attributed to the high mixing speed caused by the nitrogen bubbler. The figure shows the excellent agreement between the reaction coordinates obtained from X-ray analysis and titration experiments.

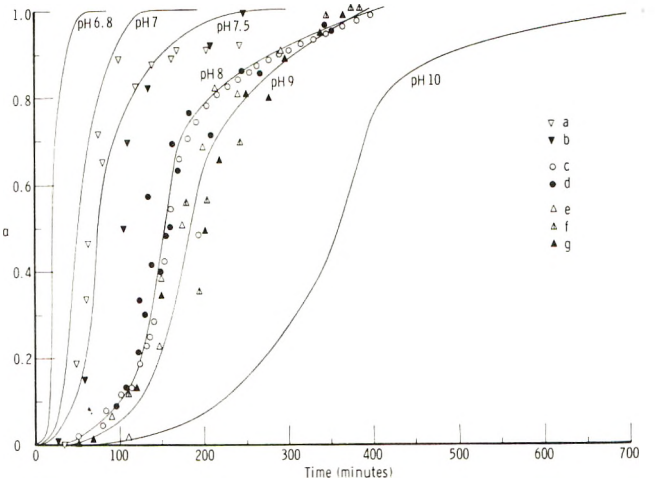

Figure 1. Effect of solution conditions on the transformation of ACP to HA as represented by α, extent of the conversion reaction, *vs.* time. Lines represent best fit of all X-ray data at each pH when $CaCl_2$ and $(NH_4)_2HPO_4$ are mixed together in Tris buffer (pH 6.8–9), or NH_4OH–NH_4Cl buffer (pH 10), and reaction allowed to proceed in presence of mother liquor. Data points shown are as follows: (a) pH 7.5, K_2HPO_4 substituted for $(NH_4)_2HPO_4$; (b) pH 7.5, Na_2HPO_4 for $(NH_4)_2HPO_4$; (c) pH 8.0, α calculated from NaOH titration; (d) pH 8.0, α calculated from X-ray data; in both c and d dry ACP was added to reaction solution, the data points shown here start at the proliferation period; e, f, and g represent reactions at pH 9 where as in a and b, initially precipitated ACP is left in contact with mother liquor throughout reaction; (e) carbonate-free solution, again, corrected for difference in induction time; (f) $Ca(NO_3)_2$ substituted for $CaCl_2$; (g) NH_4OH-NH_4Cl instead of Tris buffer.

The sigmoid curves shown in Figure 1 are typical of solid-state reactions involving nucleation.[11] As in the others, these curves can be divided into three sections: an "induction period" where no change in the extent of reaction is apparent; a rapid "proliferation period," marked by a rapid increase in the extent of reaction per unit time; and a gradual "tapering off" period, when the rate of the transformation slows appreciably. Only the proliferation period can be subjected to kinetic treatment.[11] As can also be seen from the curves, an increase in pH leads to an increase in both the induction time and the amount of time spent in the proliferation period of the reaction.

In the constant temperature experiments, the pH was the only solution variable which affected the half-life, $t_{1/2}$; the latter was defined as the amount of time required for half of the amorphous material to convert to crystalline after the completion of the induction period. The stirring rate, slurry concentration, and particle size altered the induction time, but these factors did not change the transformation half-life. The induction time was determined graphically as the point of intersection of the time axis with the tangent to the steepest part of the proliferation curve.[12] The conversion started sooner in the presence of faster stirring, smaller amorphous particles, and/or a greater concentration of amorphous particles.[13]

The amorphous particles remain stable in ethanol or acetone, and convert more slowly in a 50% acetone solution than they do in pure buffer. This corroborates the earlier view[8] that the reaction is solution mediated, or at least accelerated by the presence of water. The increase in the rate of conversion with increased water to solid ratio up to 400:1 further illustrates the necessity for water in this conversion.

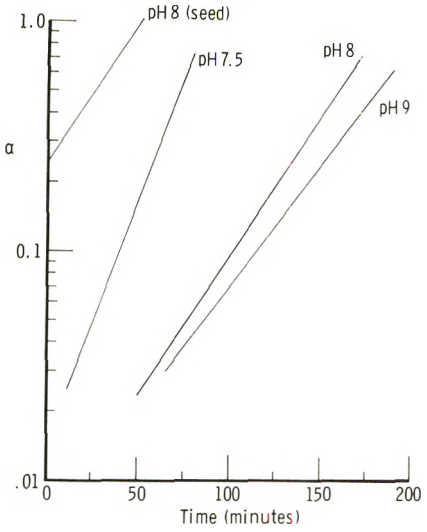

Figure 2. Kinetics of conversion during the proliferation period at selected pH values. Lines represent least-squares best fit of all data obtained at the given pH. In seed experiment, 23 wt % of HA was added at time zero.

TABLE I: Rate Constants as a Function of pH for the Autocatalytic Transformation of Amorphous Calcium Phosphate to Hydroxyapatite

pH	Weight % HA seeds (seed size, Å[a])	Rate constants		Av size at $\alpha = 1$, Å[a]
		k_0	k_1, min^{-1}	
6.8	0	2.7×10^{-4}	0.376	172
7.0	0	1.6×10^{-3}	0.129	170
7.0	0	1.1×10^{-3} [b]	0.125[b]	
7.5	0	8.3×10^{-3}	0.056	166
8.0	0	3.4×10^{-3}	0.0321	163
8.0	0	3.2×10^{-4} [b]	0.0317[b]	
8.0	19.51 (222)	0.195	0.0319	198[c]
8.0	27.81 (256)	0.275	0.0320	243[c]
8.0	20.12 (163)	0.202	0.0318	163[c]
8.0	25.30 (249)	0.254	0.0319	237[c]
9.0	0	3.5×10^{-3}	0.0266	160
10.0	0	9.4×10^{-3}	0.0132	157

[a] Particle size in largest (c-axis) dimension as determined by X-ray line broadening. [b] Titration data. [c] This figure includes seed size. Comparison with mechanical mixtures suggests that size of newly formed HA is the same as in unseeded experiments at same pH.

The kinetic treatment leading to the linear plots shown in Figure 2 indicated that the transformation was first order, or autocatalytic,[14] with the rate of formation of new crystals proportional to the number of crystals already present. Representative semilogarithmic plots are shown for unseeded conversions at pH 7.5, 8, and 9 and for the reaction at pH 8 in the presence of 23% hydroxyapatite seeds. The data on these curves correspond to the proliferation period, and closely fit equation: $d\alpha/dt = k_0 + k_1\alpha$. Table I lists values for k_0 and k_1, calculated by the method of least squares from conversion data at a number of pH values where α was determined by both the titration and X-ray methods. In each seeding experiment, the calculated value of k_0 was equal to the weight per cent crystalline seeds added at the start of the transformation. In the nonseeding experiments, k_0 was always very small.

The average hydroxyapatite crystallite sizes included in Table I were determined from X-ray diffraction line broadening analysis[15] assuming the contribution of strain to be negligible. In the nonseeded experiment, the average crystallite size in the c-axis direction remained a constant for a given pH as the conversion proceeded. In the seeding experiments, the crystal size observed at the end of the transformation corresponded to a weighted size-average of the unchanged apatite seed crystals (20%) and the newly formed hydroxyapatite crystals (80%). Studies of mechanical mixtures of large seed crystals and hydroxyapatite prepared at the pH of the experiment confirmed this view and thus suggested that no appreciable growth of seed crystals was taking place during the transformation.

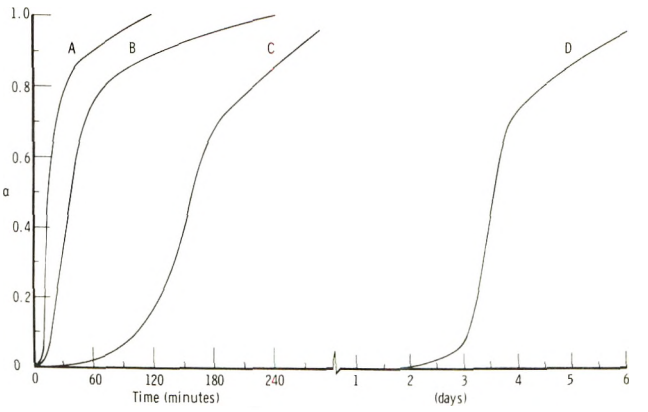

Figure 3. Effect of temperature on the rate of conversion of ACP to HA at pH 8. Lines represent best fit of combined X-ray and titration data: A = 48°, B = 37°, C = 26°, and D = 10°.

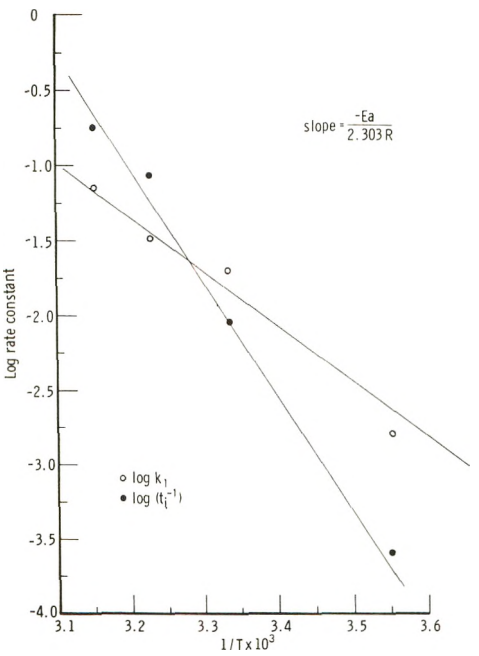

Figure 4. Arrhenius plots for the conversion of ACP to HA at pH 8: closed circles, logarithmic reciprocal induction time *vs.* reciprocal absolute temperature; open circles, logarithmic first-order rate constants *vs.* reciprocal absolute temperature.

Figure 3 shows the effect of temperature on the rate of the conversion at pH 8. An increase in temperature results in both a shortening of the induction time and an increase in the rate of crystal proliferation. The first-order rate constants calculated from these observations were used to prepare the Arrhenius plot shown in Figure 4. The activation energy for the conversion itself was 16.4 kcal/mol, while the activation energy associated with the induction

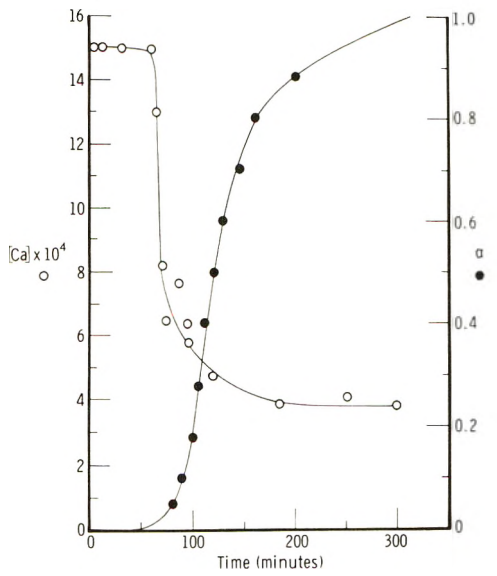

Figure 5. Kinetics of ACP to HA transformation; 1 g of ACP of specific surface 56 m^2/g was added to 1 l. of pH 8 buffer. Plotted here are (left) calcium concentration (moles/liter × 10^4) *vs.* time and (right) extent of reaction (% crystallinity), α, *vs.* time.

TABLE II: Average Degree of Supersaturation,[a] S, during the Induction Time of the ACP to HA conversion

pH of mediating solution	S^b	t_i, min	S^c	T_i, min
7.0	9.1	15	11	6
8.0	5.7	15	5.7	14
9.0	5.1	15	3.2	35
10.0	1.3	15	1.1	45

[a] Degree of supersaturation here defined as calcium concentration at time, t_i divided by the solution calcium concentration after 24 hr. [b] Solutions buffered by Tris or NH_4OH–NH_4Cl. [c] Solution maintained at constant pH by addition of NaOH or HCl.

period was approximately 33 kcal/mol. The latter was calculated using the induction time (t_i) as a rate constant for each temperature.

Figure 5 provides insight into how the observed solubility (measured as calcium ion concentration) parallels the onset of the conversion.[13] Similar to earlier results,[4] this figure shows that after the amorphous material has been added to the buffer, the calcium concentration rises, levels off slowly, and falls as the ACP conversion proceeds. The rate at which the solution calcium concentration levels off at constant temperature and the level attained before conversion is a function of the factors affecting the induction time: slurry concentration, specific surface of the amorphous particles, and the pH. Table II illustrates the fact that decreasing the pH increases the solution supersaturation; the latter was defined as the concentration of calcium in the solution at a given time divided by the calcium concentration after 24 hr.

Discussion

The sigma-shaped curves observed for this transformation are comparable to those observed for similar amorphous to crystalline conversions[16-19] and are characteristic of reactions involving nucleation and crystal proliferation. The theory of these processes, treated elsewhere,[20,21] states that they consist of the formation of a stable primary crystalline nucleus and the subsequent growth and proliferation of the crystalline material. An induction period, when no formation of crystalline material is observed, is characteristic of such reactions. It is during this period that a critical supersaturation is attained, with subsequent formation of the primary nuclei. In the case of the ACP to HA transformation the induction period includes additionally the time required for the amorphous calcium phosphate to dissolve and, thus, is a function of all factors related to the solubility of ACP. Thus, the induction time is decreased by using smaller ACP particles, a higher ACP slurry concentration, aqueous rather than nonaqueous solutions, lower pH, and higher temperature all of which decrease the time required for some critical degree of supersaturation to be reached.

It is not within the scope of this paper to deal with the detailed nature of the initial nucleation of hydroxyapatite. Some indication of the energy barrier which must be overcome in order to form the first nucleus was obtained from the study of the temperature dependence of the conversion. The effect of increasing the temperature was to decrease the induction time by both increasing the solubility of the ACP and providing additional energy needed to form a stable primary nucleus. The activation energy of 33 kcal/mol associated with this induction period indicates the energy barrier which must be overcome to produce the first stable nucleus and, as stated, includes the energy associated with the dissolution of the amorphous calcium phosphate. When seed crystals were added to the solution along with the ACP they served as primary nuclei and the transformation proceeded without an induction period. Thus, in the seeding experiments there was no measurable induction period activation energy suggesting that the energy associated with the dissolution of the ACP is relatively small and the activation energy measured for the nonseeded experiments is essentially that required to overcome the barrier to nucleation. Thus, the rate-limiting step in the overall conversion is the formation of the initial HA nuclei.

Important to this study is the mechanism of transformation once the initial nuclei are present. The rate of production of crystalline material during this proliferation period is proportional to the fraction of crystalline material already present. This process is said to be autocatalytic since it accelerates itself by the production of additional crystalline nuclei. The mechanism of autocatalysis is not clearly understood and explanations such as branching, three dimensional growth of compact nuclei, and growth along dislocation lines have been proposed.[11] Two observations suggest that the mechanism here cannot be exclusively one of crystal growth: (a) the restricted growth of HA crystals observed throughout the conversion reaction and (b) the fact that the seeding of the slurry with HA crystallites of greater size than normally obtained at the experimental pH and temperature did not lead to the development of larger crystals. The activation energy usually observed for crystal growth is relatively low, *i.e.*, 0–5 kcal/mol,[22] compared to the 16.4 kcal/mol value observed for the proliferation period. This suggests that this period is not simply one of crystallite growth but one in which new nuclei are constantly formed in conjuntion with the seed crystals of preexisting nuclei. Finally, at constant temperature, the first-order rate constant for the autocatalytic process (k_1) is only a function of the pH of the mediating solution. At lower pH the degree of supersatura-

tion is higher (Table II) and, thus, the rate constant, as predicted,[21] is greater.

The decrease in rate of reaction observed as completion nears is not fully understood, however, a theoretical treatment has attributed this "tapering off" to the coalescing of the nuclei already in solution.[11] In the case of zeolite A the rate decrease toward the end of the transformation has been attributed to a decrease in concentration of some unidentified stable intermediate.[16] The first study of the first transformation of ACP to hydroxyapatite in an unbuffered solution did not show such tapering off.[8] In that report the pH drop resulting from the uptake of hydroxyl ions from an unbuffered solution may well have caused a continuous increase in the rate constant, obscuring the tapering effect. In the present study nuclear aggregation plus a decrease in the degree of supersaturation of the mediating solution may have contributed to the reduction in the rate of transformation.

Conclusion

In the experiments reported above, the transformation of amorphous calcium phosphate to hydroxyapatite is solution mediated and depends upon the conditions which regulate both the dissolution of amorphous calcium phosphate and the formation of the preliminary hydroxyapatite nuclei. The rate of the autocatalytic proliferation, at a given temperature, is a function only of the solution pH, and does not vary with differing preparative techniques or solution conditions. Thus, it is only the induction period which is altered by the reaction parameters, and, at a given pH, the section of the sigmoid curve beyond the induction period remains the same regardless of the reaction conditions. The variables which affect the length of the induction period (pH, particle size, slurry composition, and the nonaqueous nature of the solution) are parameters which can be used to stabilize the metastable amorphous precursor.

Studies using X-ray diffraction[22] and infrared absorption spectroscopy[23] have indicated that mature bone mineral is composed of an amorphous calcium phosphate and a poorly crystallized apatitic phase. This apatitic phase is believed to be related to, but not identical with, hydroxyapatite.[2] Early bone mineral is richer in the amorphous than in the apatitic phase, while the reverse is true in mature bone.[23] The mechanism which account for the *in vivo* stabilization of the amorphous phase and the transformation of this phase as the bone matures remains to be elucidated. However, the results in this paper reveal ways in which the amorphous material is stabilized and indicate the importance pH control has on the interplay between the amorphous and crystalline phases.

Acknowledgment. This work is supported, in part, by Grants No. DE-01945 and AM-05414 from the National Institutes of Health. Publication No. 82 from the Laboratory of Ultrastructural Biochemistry.

The authors are grateful to Tajudeen Kashimawo and Joseph Pober for the technical assistance in this study.

Supplementary Material Available. A listing of induction time, half-life, and extent of conversion after 4 and 24 hr as a function of various solution conditions will appear in Table III and variations in solution calcium concentration during the conversion of amorphous calcium phosphate to hydroxyapatite will appear in Table IV following these pages in the microfilm edition of this volume of the journal. Photocopies of the supplementary material from this paper only or microfiche (105 × 148 mm, 20× reduction, negatives) containing all of the supplementary material for the papers in this issue may be obtained from the Journals Department, American Chemical Society, 1155 16th St., N. W., Washington, D. C. 20036. Remit check or money order for $3.00 for photocopy or $2.00 for microfiche, referring to code number JPC-73-2313.

References and Notes

(1) J. C. Elliott, *Calcif. Tissue Res.*, **3**, 293 (1969).
(2) A. S. Posner, *Physiol. Rev.*, **49**, 760 (1969).
(3) M. J. Dallemagne and L. J. Richelle, "Biological Mineralization," I. Zipkin, Ed., Wiley, New York, N.Y., in press.
(4) E. D. Eanes, I. H. Gillessen, and A. S. Posner, *Nature (London)*, **208**, 365 (1965).
(5) A. Bienenstock and A. S. Posner, *Arch. Biochem. Biophys.*, **124**, 604 (1968).
(6) J. D. Termine and A. S. Posner, *Calcif. Tissue Res.*, **1**, 8 (1967).
(7) J. D. Termine, R. A. Peckauskas, and A. S. Posner, *Arch. Biochem. Biophys.*, **140**, 318 (1970).
(8) E. D. Eanes and A. S. Posner, *Trans. N. Y. Acad. Sci.*, **28**, 233 (1965).
(9) L. E. Alexander and H. P. Klug, *Anal. Chem.*, **20**, 886 (1948).
(10) G. Porod, *Kolloid Zh.*, **124**, 83 (1951); **125**, 51, 109 (1952).
(11) L. G. Harrison, "Comprehensive Chemical Kinetics," Vol. 2, C. H. Banford and C. F. H. Tipper, Ed., Elsevier, Amersterdam, 1969, p 377.
(12) H. E. Lundager Madsen, *Acta Chem. Scand.*, **24**, 1677 (1970).
(13) See paragraph at end of paper regarding supplementary material.
(14) T. P. Melia and W. P. Moffitt, *Ind. Eng. Chem., Fundam.*, **3**, 313 (1964).
(15) H. P. Klug and L. E. Alexander, "X-Ray Diffraction Procedures for Polycrystalline and Amorphous Materials," Wiley, New York, N. Y., 1954, pp 491–511.
(16) J. Schlichtkrull, *Acta Chem. Scand.*, **11**, 439 (1957).
(17) A. C. T. Hsu, *AIChE J.*, **17**, 1311 (1971).
(18) G. T. Kerr, *J. Phys. Chem.*, **70**, 1047 (1966).
(19) A. E. Nielsen, *Acta Chem. Scand.*, **12**, 951 (1958).
(20) J. D. O'Rourke and R. A. Johnson, *Anal. Chem.*, **27**, 1969 (1955).
(21) A. G. Walton, "The Formation and Properties of Precipitates," Wiley-Interscience, New York, N. Y., 1967, Chapter I.
(22) R. A. Harper and A. S. Posner, *Proc. Soc. Exptl. Biol. Med.*, **122**, 137 (1966).
(23) J. D. Termine and A. S. Posner, *Science*, **153**, 1523 (1966).

Kinetics of Binding of Pyrophosphate to Magnesium Ions

R. C. Patel[1] and R. S. Taylor

Max Planck Institute for Biophysical Chemistry, Department of Biochemical Kinetics, D3400 Göttingen-Nikolausberg, West Germany
(Received February 26, 1973)

Publications costs assisted by the Max Planck Institute for Biophysical Chemistry

The kinetics of binding of pyrophosphate to magnesium ions have been studied by the temperature-jump technique as a function of pH at 25.0° and 1.0 *M* ionic strength. Only one relaxation time in the time range 10–1000 μsec was observed. A faster proton transfer effect was observed but not investigated. To explain the kinetic data it was necessary to consider three parallel substitution pathways involving the species $P_2O_7^{4-}$, $HP_2O_7^{3-}$, and $H_2P_2O_7^{2-}$, where these reactions were coupled by rapid proton transfer between the phosphate species. The equilibrium constant for the formation of a new complex $MgH_2P_2O_7$ was determined, as well as the rate constants for the forward and reverse processes in the substitution reactions. The forward rate constants are $k_1(P_2O_7^{4-}) = 7.1 \times 10^7\ M^{-1}\ sec^{-1}$, $k_2(HP_2O_7^{3-}) = 5.1 \times 10^6\ M^{-1}\ sec^{-1}$, and $k_3(H_2P_2O_7^{2-}) = 5.4 \times 10^5\ M^{-1}\ sec^{-1}$. The values of these constants are compared with those observed in other magnesium substitution reactions. No evidence for a significant acceleration of the rate of water loss for highly charged ligands was found and it was concluded that an SN1 mechanism adequately describes the substitution processes.

Introduction

The ability of highly charged ligands to increase the water substitution rate of metal ions has been proposed by Hammes and Morrell[2] for the cobalt (as compared to nickel) interactions with pyrophosphate and tripolyphosphate. The authors consider that this effect will be most marked for metal ions which have weakly bonded water ligands. Thus labile metal ions such as manganese and magnesium which have no crystal field stabilization energy associated with them might be expected to show similar effects. To this end the reaction of magnesium with pyrophosphate has been investigated over the pH range 3.65–8.65, where three different protonated forms of the ligand are known to be important.[3]

Although binding constants have been determined for pyrophosphate and tripolyphosphate with many metal ions[4] kinetic studies have been performed only with cobalt and nickel,[2,5] despite the fact that pyrosphosphate and especially its interaction with magnesium is of fundamental biochemical importance,[5a] not least since the species $[MgP_2O_7]^{2-}$ has recently been shown to be a substrate for phosphatase enzymes,[7] while pyrophosphate itself is a competitive inhibitor. The importance of magnesium interactions with phosphate containing species is not restricted to inorganic phosphates but runs through the whole range of organic phosphates such as mononucleotides and nucleic acids.[8-12] The kinetics of binding of ATP and ADP to magnesium have been investigated previously by other workers.[13-15] The binding site for magnesium in these processes is certainly the phosphate entity, since nmr studies have indicated no significant binding to the nucleoside base within nucleic acids or their constituent monomers.[16,17]

Kinetically magnesium is fairly well understood; ligand binding can be explained in terms of the Eigen–Tamm mechanism[18a] and the experimental water substitution rate[18b] is consistent with this. A comparison with published data should therefore be possible, although the necessity of using an ionic strength of 1.0 *M* due to the low stability of the MgH_2PO_7 complex makes such comparisons less meaningful.

The complexity of the mechanism presented here necessitates the use of a computer to evaluate required concentrations etc. Although the full mechanism is not needed to explain the data under all conditions, at least two of the three reaction pathways have significant contributions to the rate law, except at the lowest pH.

Experimental Section

In this study all experiments were carried out at 25.0° and 1.0 *M* ionic strength made up with tetramethylammonium chloride. The materials used, tetrasodium pyrophosphate decahydrate and magnesium chloride hexahydrate (Merck, Darmstadt) were of analytical reagent grade. Tetramethylammonium chloride (Th. Schuchardt, Munchen; reagent grade) was recrystallized from isopropyl alcohol.

The temperature-jump technique has been described previously.[19] In this study the temperature was raised by 4.0° by a discharge of 33 kV through a 5×10^{-8} F capacitor. Since the reaction itself had no color change it was necessary to couple the process to an acid–base indicator system. Six different indicators were used, each indicator being chosen to work at one pH in the study, which covers five pH units. The indicators used were Metacresol Purple, Phenol Red, and Bromocresol Green (Merck), Chlorophenol Red and Bromothymol Blue (Fluka AG), and Bromophenol Blue (Schuchardt). Sufficient indicator was present to give an optical density of approximately 0.8 at the wavelength of maximum absorption of the indicator anion (500–600 nm). After preparation the pH of the solutions was adjusted using standard 0.1 or 1.0 *M* potassium hydroxide or hydrochloric acid solutions (Merck). The solutions were then filtered through Millipore filters placed in the T-jump cell (capacity ~6 ml) and then outgassed under mild vacuum to prevent cavitational artifacts on discharge. A typical oscilloscope trace is shown in Figure

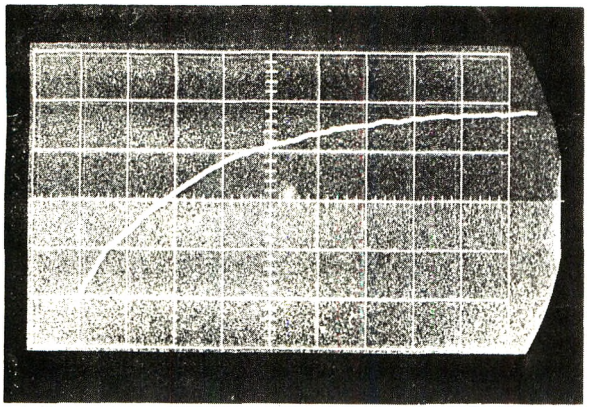

Figure 1. Typical oscilloscope trace for reaction of magnesium and pyrosphosphate at 25° and unit ionic strength: pH 6.75, $C_M = 2 \times 10^{-4}$ *M*, $C_L = 2 \times 10^{-4}$ *M*, $C_{In} = 4 \times 10^{-5}$ *M*, vertical scale = 2.0% transmission, horizontal scale = 1 msec, τ = 235 μsec.

1. All the traces obtained were characterized by single relaxation times.

The acid dissociation constants of the indicators were determined spectrophotometrically by the log ratio method[20] using a Beckman DK2A recording spectrophotometer, the pH being measured using a Polymetron (SA Glattbrugg) Type 42D pH meter with a Metrohm type EA152 combined electrode. The meter was standardized using Merck Titrisol standard buffers pH 3.0–9.0 at a pH close to the literature pK_a for the indicator at low ionic strength.[21] Nitrogen was bubbled through all solutions before, and over the surface during, the pH measurement, to prevent effects due to dissolved carbon dioxide.

The stock solutions of tetramethylammonium chloride (2 *M*) and magnesium chloride (5 and 0.5 *M*) were standardized by an ion-exchange procedure which has been described elsewhere.[22] The pyrophosphate stock concentration (*ca.* 0.2 *M*) was determined by pH titration. This stock solution was then adjusted to pH 10.3 and stored under refrigeration. Under these conditions stability is assured.[23] More dilute solutions (*ca.* 10^{-2} *M*) were made freshly each day by dilution of this stock.

The stability constant for the magnesium dihydrogen pyrophosphate complex was determined at 25.0° and μ = 1.00 in the following way. A solution of sodium pyrophosphate at pH ~2 (50 ml, 0.05 *M*) was titrated with magnesium chloride (4.27 *M*) in 50-μl increments. Any resulting change in pH (after correction for dilution effects, which are small since the volume increments of the magnesium chloride solution were 0.1% of the total volume) must be due to the formation of $MgH_2P_2O_7$, because the calculated concentrations of $MgHP_2O_7^-$ and $MgP_2O_7^{2-}$ [24] could give rise to no pH change under these conditions.

The calculation of K_3 is described in the next section. The pH meter for this experiment was standardized at pH 1.09 (0.1 *M* HCl) and checked at pH 2.10 (0.01 *M* HCl, 0.09 *M* KCl).

Results

The necessary constants, defined in terms of metal and ligand concentrations and hydrogen ion activities, which are presented in Table I, relating to the binding of pyrophosphate to magnesium under the conditions of this study have been determined previously by other workers,[3,24] with the exception of the formation constant, K_3,

TABLE I: Association Constants for Various Pyrophosphate Species with Hydrogen Ion (Log K_H) and Magnesium Ion (Log K_M) at 25.0° and 1.0 *M* Ionic Strength (Tetramethylammonium Chloride)

Ligand	Log K_H	Ref	Log K_M	Ref
$P_2O_7^{4-}$	8.93	3	5.41	24
$HP_2O_7^{3-}$	6.13	3	3.06	24
$H_2P_2O_7^{2-}$	1.81	3	1.33	This work
$H_3P_2O_7^-$	0.82	3		
$MgP_2O_7^{2-}$	6.58	3, 24	2.34	24
$MgHP_2O_7^-$	4.40	This work		

for the dihydrogenphosphato complex with magnesium which was found to be important at low pH. The equilibrium relationships used in this study are as follows, where $H_nL^{(4-n)-}$ represent the pyrophosphate species and $MH_nL^{(2-n)-}$ represent the complexes formed.

$$K_{A1} = [HL^{3-}]/\{H^+\}[L^{4-}] \quad (1)$$

$$K_{A2} = [H_2L^{2-}]/\{H^+\}[HL^{3-}] \quad (2)$$

$$K_{A3} = [H_3L^-]/\{H^+\}[H_2L^{2-}] \quad (3)$$

$$K_{A4} = [H_4L]/\{H^+\}[H_3L^-] \quad (4)$$

$$K_1 = [ML^{2-}]/[M^{2+}][L^{4-}] \quad (5)$$

$$K_2 = [MHL^-]/[M^{2+}][HL^{3-}] \quad (6)$$

$$K_3 = [MH_2L]/[M^{2+}][H_2L^{2-}] \quad (7)$$

In order to solve the relaxation data it is also necessary to consider two nonindependent protonation equilibria as well as the indicator protonation equilibria. The constants relating to these are

$$K_{MA} = [MHL^-]/[ML^{2-}]\{H^+\} = K_2K_{A1}/K_1 \quad (8)$$

$$K_{MB} = [MH_2L]/[MHL^-]\{H^+\} = K_3K_{A2}/K_2 \quad (9)$$

and in general form

$$K_{In} = [HIn]/\{H^+\}[In^-] \quad (10)$$

where HIn represents the undissociated indicator and In^- its anion. A different indicator was required at each pH.

The value of K_3 was obtained in the following way. It can be shown that at pH between 1 and 2 the only ligand species of importance are H_4L, H_3L^-, H_2L^{2-}, and, since pH changes significantly on addition of metal ions, MH_2L. The species MHL^-, ML^{2-}, HL^{3-}, etc., are all much less than 1% total ligand under these conditions.

The relationships between the species present are shown in eq 3, 4, and 7. The mass balance equations necessary are

$$C_M = [M^{2+}] + [MH_2L] \quad (11)$$

$$C_L = [H_2L^{2-}] + [H_3L^-] + [H_4L] + [MH_2L] \quad (12)$$

$$C_H - [H^+] = 4[H_4L] + 3[H_3L^-] + 2[H_2L^{2-}] + 2[MH_2L] \quad (13)$$

where C_M, C_L, and C_H are the total concentrations of metal, ligand, and hydrogen ions added. By consideration of the species in solution before the addition of any metal ions it can be shown that

$$[H^+] = \frac{\{H^+\}}{H_0}\left(C_H - \left(\frac{(4K_{A4}K_{A3}H_0^2 + 3K_{A3}H_0 + 2)C_L}{(K_{A4}K_{A3}H_0^2 + K_{A3}H_0 + 1)}\right)\right) \quad (14)$$

Here H_0 and $\{H^+\}$ represent the activities of hydrogen ion

TABLE II: Spectral Properties and Protonation Constants for the Indicators Used in This Study, Determined at 25.0° and 1.0 *M* Ionic Strength (Tetramethylammonium Chloride)

Indicator	pH of kinetic study where indicator was used	$\lambda_{max}^{In^-}$, nm	Log K_{In}
Bromophenol Blue	3.65	592	3.51
Bromocresol Green	4.65	615	4.27
Chlorophenol Red	5.65	575	5.88
Bromothymol Blue	6.65	615	6.88
Phenol Red	7.65	558	7.50
Metacresol Purple	8.65	580	8.32

as determined by pH measurements before and after the addition of magnesium ion, respectively.

On the addition of metal ions the pH decreases, and these changes are given by eq 15, obtained by substituting eq 3, 4, 7, 11, and 12 into eq 13 and rearranging

$$C_L = (1 + K_{A3}\{H^+\} + K_{A4}K_{A3}\{H^+\}^2)\alpha + K_3C_M\alpha/(1 + K_3\alpha) \quad (15)$$

where $\alpha = ((C_H - [H^+]) - 2C_L)/(2K_{A4}K_{A3}\{H^+\}^2 + K_{A3}\{H^+\})$, and $[H^+]$ is given by eq 14. Equation 15 can thus be arranged to give

$$K_3 = (C_L - \beta\alpha)/\alpha((C_M - C_L) + \beta\alpha) \quad (16)$$

where $\beta = (K_{A3}K_{A4}\{H^+\}^2 + K_{A3}\{H^+\} + 1)$. Thus K_3 can be calculated for each value of C_M. At 25.0° and μ = 1.0 *M* (NMe_4Cl), C_L = 0.050 *M*, C_M = 0.004–0.050 *M*, the value of K_3 is 21.4 M^{-1}. At higher metal concentrations (≥0.1 *M*) the value of K_3 becomes somewhat higher due to ionic strength differences.

The spectrophotometrically determined protonation constants, K_{In}, for the indicators used in this study, together with λ_{max} for the indicator anions are given in Table II.

The temperature-jump study was carried out between pH 3.65 and 8.65. Under these conditions the following mechanism, eq 17–18, is comprehensive, although not all

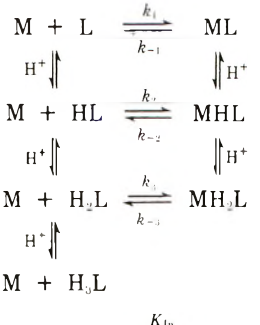

(17)

$$H^+ + In^- \rightleftharpoons HIn \quad (18)$$

the pathways have a significant contribution at every pH. (The charges of the species have been omitted for simplification.) The vertical equilibria are established rapidly and the horizontal ones more slowly. However, these slower processes give rise to only one relaxation time since they are coupled by the rapid protonation equilibria.[19] The equilibrium relationships between these species are given by eq 1–10.

The rate law derived from such a mechanism thus contains six terms when it covers the whole pH range studied. It can be written

$$-d[M]/dt = (k_1[L] + k_2[HL] + k_3[H_2L])[M] - (k_{-1}[ML] + k_{-2}[MHL] + k_{-3}[MH_2L]) \quad (19)$$

Expressing the concentration [X] of each species by the sum of its equilibrium concentration $[\bar{X}]$ and its deviation from this equilibrium value $\delta[X]$

$$[X] = \bar{[X]} + \delta[X] \quad (20)$$

the rate equation can be linearized for relaxation conditions ($\delta[X]/\bar{[X]} \ll 1$) and written in the form

$$\frac{1}{\tau} = \frac{-d(\ln \delta[M])}{dt} = k_1\left(\bar{[L]} + \bar{[M]}\frac{\delta[L]}{\delta[M]} - \frac{1}{K_1}\frac{\delta[ML]}{\delta[M]}\right) + k_2\left(\bar{[HL]} + \bar{[M]}\frac{\delta[HL]}{\delta[M]} - \frac{1}{K_2}\frac{\delta[MHL]}{\delta[M]}\right) + k_3\left(\bar{[H_2L]} + \bar{[M]}\frac{\delta[H_2L]}{\delta[M]} - \frac{1}{K_3}\frac{\delta[MH_2L]}{\delta[M]}\right) \quad (21)$$

or in more general form

$$\frac{1}{\tau} = \sum_{n=1}^{3} k_n\left(\bar{[H_{n-1}L]} + \frac{\bar{[M]}}{\delta[M]}\right)\left(\delta[H_{n-1}L] - \frac{\delta[MH_{n-1}L]}{K_n}\right) \quad (22)$$

where τ is the relaxation time. By using the mass balance conditions for total metal (C_M), total ligand (C_L) (eq 23 and 24), and total hydrogen ion (eq 25), eq 1–9, and the differential forms of the equilibrium expressions (eq 26–30) one can express the δ functions on the right-hand side of eq 21 in terms of equilibrium constants and equilibrium concentrations

$$\delta[M] + \delta[ML] + \delta[MHL] + \delta[MH_2L] = 0 \quad (23)$$

$$\delta[L] + \delta[HL] + \delta[H_2L] - \delta[M] = 0 \quad (24)$$

$$\delta[H] + \delta[HIn] + \delta[MHL] + \delta[HL] + 2\delta[MH_2L] + 2\delta[H_2L] - \delta[OH] = 0 \quad (25)$$

Since at pH >7 $[OH^-] > [H^+]$; $\delta[OH] = (-Kw\delta[H]/[H^+]^2)$ where Kw is the ionic product of water.

$$\delta[H_2L] = \bar{[H]}K_{A2}\delta[HL] + \bar{[HL]}K_{A2}\delta[H] \quad (26)$$

$$\delta[HL] = \bar{[H]}K_{A1}\delta[L] + \bar{[L]}K_{A1}\delta[H] \quad (27)$$

$$\delta[MH_2L] = \bar{[H]}K_{MB}\delta[MHL] + \bar{[MHL]}K_{MB}\delta[H] \quad (28)$$

$$\delta[MHL] = \bar{[H]}K_{MA}\delta[ML] + \bar{[ML]}K_{MA}\delta[H] \quad (29)$$

$$\delta[HIn] = \bar{[In]}K_{In}\delta[H]/(1 + \bar{[H]}K_{In}) \quad (30)$$

The derived δ ratios, omitting concentration brackets in δ functions for clarity, are as follows

$$\frac{\delta L}{\delta M} = +1\Big/\left[1 + \frac{\bar{[H]}K_{A1}}{[1 - \bar{[L]}K_{A1}(\delta H/\delta HL)]} \times \left(1 + K_{A2}\left(\bar{[H]} + \bar{[HL]}\frac{\delta H}{\delta HL}\right)\right)\right] \quad (31)$$

$$\frac{\delta ML}{\delta M} = -1\Big/\left[1 + \frac{\bar{[H]}K_{MA}}{[1 - \bar{[ML]}K_{MA}(\delta H/\delta MHL)]} \times \left(1 + K_{MB}\left(\bar{[H]} + \bar{[MHL]}\frac{\delta H}{\delta MHL}\right)\right)\right] \quad (32)$$

$$\frac{\delta HL}{\delta M} = +1\Big/\left[1 + \frac{1}{[H]}\left(\frac{1}{K_{A1}} - \bar{[L]}\frac{\delta H}{\delta HL}\right) + K_{A2}\left(\bar{[H]} + \bar{[HL]}\frac{\delta H}{\delta HL}\right)\right] \quad (33)$$

TABLE III: Relaxation Data for the Reaction of Magnesium Ions with Pyrophosphate as a Function of pH at 25.0° and 1.0 *M* Ionic Strength (Tetramethylammonium Chloride)

$10^4 \times C_M$, *M*	$10^4 \times C_L$, *M*	$10^5 \times C_{In}$, *M*	pH	No. of runs	$10^{-4}/\tau_{obsd}$, sec^{-1}	$10^{-4}/\tau_{calcd}$, sec^{-1}
430.0	86.0	3.62	3.65	3	4.67	4.42
860.0	85.0	3.58	3.65	2	6.45	6.46
1290.0	84.0	3.56	3.65	2	8.20	8.55
100.0	100.0	4.66	4.65	2	3.63	3.32
20.0	20.0	3.50	4.65	4	2.15	1.94
50.0	20.0	3.50	4.65	3	2.96	2.51
200.0	20.0	3.50	4.65	3	3.97	3.81
450.0	20.0	3.50	4.65	3	4.78	5.51
4.00	4.00	3.76	5.65	4	0.95	0.83
10.0	4.00	3.76	5.65	4	1.25	1.16
20.0	10.0	3.76	5.65	2	1.56	1.54
50.0	10.0	3.76	5.65	3	2.22	2.46
2.00	2.00	2.40	6.65	3	0.44	0.50
5.00	2.00	2.40	6.65	3	0.61	0.70
10.0	2.00	2.40	6.65	3	1.07	1.01
20.2	2.00	2.40	6.65	3	1.42	1.49
30.5	2.00	2.40	6.65	1	2.35	2.00
0.30	0.30	1.00	7.65	3	0.182	0.171
0.50	0.50	2.00	7.65	1	0.68	0.75
1.00	1.00	4.00	7.65	3	0.253	0.270
2.00	1.00	4.00	7.65	2	0.300	0.365
2.00	2.00	4.00	7.65	4	0.425	0.420
3.00	1.00	4.00	7.65	2	0.455	0.468
3.00	3.00	4.00	7.65	3	0.540	0.530
4.00	2.00	4.00	7.65	4	0.559	0.598
6.00	3.00	4.00	7.65	5	0.680	0.755
6.00	6.00	4.00	7.65	3	0.758	0.730
0.20	0.20	5.02	8.65	2	0.111	0.095
0.50	0.50	5.02	8.65	2	0.171	0.149

$$\frac{\delta MHL}{\delta M} = -1\Big/\left[1 + \frac{1}{[H]}\left(\frac{1}{K_{MA}} - \overline{[ML]}\frac{\delta H}{\delta MHL}\right) + K_{MB}\left(\overline{[H]} + \overline{[MHL]}\frac{\delta H}{\delta MHL}\right)\right] \quad (34)$$

$$\frac{\delta H_2L}{\delta M} = +1\Big/\left[1 + \frac{1}{K_{A2}[\overline{[H]} + \overline{[HL]}(\delta H/\delta HL)]} \times \left(1 + \frac{1}{\overline{[H]}}\left(\frac{1}{K_{A1}} - \overline{[L]}\frac{\delta H}{\delta HL}\right)\right)\right] \quad (35)$$

$$\frac{\delta MH_2L}{\delta M} = -1\Big/\left[1 + \frac{1}{K_{MB}[\overline{[H]} + \overline{[MHL]}(\delta H/\delta MHL)]} \times \left(1 + \frac{1}{\overline{[H]}}\left(\frac{1}{K_{MA}} - \overline{[ML]}\frac{\delta H}{\delta MHL}\right)\right)\right] \quad (36)$$

where

$$\frac{\delta H}{\delta HL} = -\frac{(\beta' K_{A1}\overline{[H]}(2 + K_{MA}\overline{[H]}) - \alpha'(1 + 2K_{A1}\overline{[H]}))}{K_{A1}[(\overline{[H]} + \delta' + \overline{[MHL]} + 2\overline{[L]})(2 + \alpha' + K_{MA}\overline{[H]}) + 2\gamma'(2 + K_{MA}\overline{[H]})]}$$

$$\frac{\delta H}{\delta MHL} = \frac{\alpha' K_{MA}}{(\alpha'\overline{[ML]} - \overline{[H]})(\gamma' + \beta'(\delta HL/\delta H))}$$

$$\alpha' = K_{MA}\overline{[H]}(1 + 2K_{MB}\overline{[H]})$$

$$\beta' = 1 + 2K_{A2}\overline{[H]}$$

$$\gamma' = 2\overline{[MH_2L]} + \overline{[MHL]} + \overline{[H_2L]} - \overline{[L]}$$

$$\delta' = \overline{[HIn]}/(1 + K_{In}\overline{[H]}) + Kw/\overline{[H]}$$

In Figure 2 the fractions, X/C_L, of various ligand and complex species are shown as a function of pH.

The relaxation eq 21 can now be written

$$1/\tau = k_1\Sigma(A) + k_2\Sigma(B) + k_3\Sigma(C) \quad (37)$$

where the Σ terms are the functions of the δ ratios (eq 31–36) and equilibrium concentrations as shown in eq 21.

The values of k_1, k_2, and k_3 and hence k_{-1}, k_{-2}, and k_{-3} were obtained by a three parameter fit of $1/\tau$ values to the Σ terms with the aid of a Univac 1108 computer. This procedure has been described elsewhere.[25] The values of τ were averaged for several experiments and are accurate to ±10%. The experimental and calculated values of $1/\tau$ are presented in Table III. The rate constants are tabulated in Table IV. Although it was necessary to make allowance for the presence of a small amount of ligand present as an ion pair, especially at low pH, this

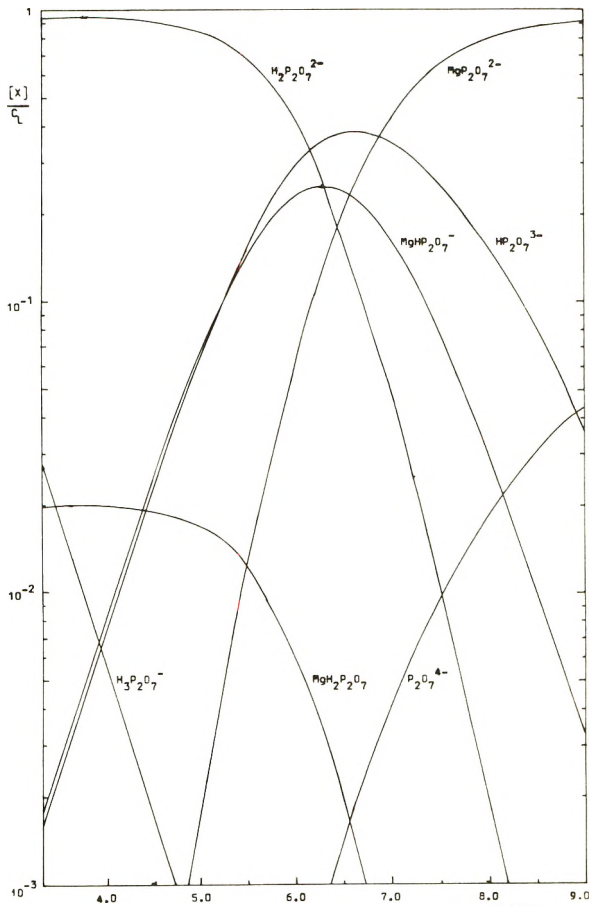

Figure 2. Fraction of total pyrophosphate present as various species, (X), at $C_M = C_L = 10^{-3}$ *M*, as a function of pH at 25.0° and 1.0 *M* ionic strength (tetramethylammonium chloride).

TABLE IV: Kinetic Data for the Reaction of Magnesium Ions with Pyrophosphate over the pH Range 3.65–8.65 at an Ionic Strength of 1.0 *M* (Tetramethylammonium Chloride) and 25.0°

Reaction pathway	Forward rate constant, M^{-1} sec^{-1}	Reverse rate constant, sec^{-1}
$Mg^{2+} + P_2O_7^{4-}$	$k_1 = 7.0 \times 10^7$	$k_{-1} = 2.8 \times 10^2$
$Mg^{2+} + HP_2O_7^{3-}$	$k_2 = 5.3 \times 10^6$	$k_{-2} = 4.8 \times 10^3$
$Mg^{2+} + H_2P_2O_7^{2-}$	$k_3 = 5.4 \times 10^5$	$k_{-3} = 2.5 \times 10^4$

TABLE V: Comparison of Experimental Rate Constants and Experimental and Calculated Values of Ion-Pairing Constants for Magnesium Complexation Reactions at 25.0°

Ligand	k_f, M^{-1} sec^{-1}	K_{0S}^{obsd}, M^{-1} [a]	K_{0S}^{calcd}, M^{-1}	μ, M	Ref
SO_4^{2-}	1.0×10^5 [b]				18a
$S_2O_3^{2-}$	1.0×10^5 [b]				18a
CrO_4^{2-}	1.0×10^5 [b]				
HF	6.0×10^4 [c]	0.6	0.4	0.4	26
OxH [d]	1.3×10^4	0.15	0.4	0.1	39, 40
F^-	5.5×10^4 [c]	0.55	1.6	0.4	26
Ox^- [d]	6.0×10^5	6.0	2.1	0.1	39, 40
IDA^{2-} [e]	1.4×10^6 [c]	14	12	0.11	26
$ADPH^{2-}$	1.0×10^6	10	9 [f]	0.1	14, 15
$H_2P_2O_7^{2-}$	5.4×10^5	5.4	13	1.0	This work
ADP^{3-}	3.0×10^6	30	30 [f]	0.1	14, 15
ADP^{3-}	8.0×10^6 [c]	80	30 [f]	0.1	6
CDP^{3-}	8.0×10^6 [c]	80	30 [f]	0.1	6
$HP_2O_7^{3-}$	5.1×10^6	53	80	1.0	This work
$HP_2O_7^{3-}$	8.1×10^6 [c]	81	30 [f]	0.1	6
$ATPH^{3-}$	3.0×10^6	30	30 [f]	0.1	13
HTi^{3-} [g]	6.0×10^6 [c]	60	66	0.1	41
ATP^{4-}	1.2×10^7	120	90 [f]	0.1	13
ATP^{4-}	1.8×10^7 [c]	180	90 [f]	0.1	6
CTP^{4-}	1.8×10^7 [c]	180	90 [f]	0.1	6
$HP_3O_{10}^{4-}$	1.8×10^7 [c]	180	90 [f]	0.1	6
$P_2O_7^{4-}$	7.1×10^7	700	450	1.0	This work

[a] $K_{0S}^{obsd} = k_f/k_0$ (water substitution rate). [b] First-order rate constant, k_0 (sec^{-1}). [c] k_f, corrected to 25.0°. [d] Ox = oxine = 8-hydroxyquinoline. [e] IDA = iminodiacetate. [f] K_{0S}^{calcd}, corrected for K^+ ion pairing. [g] Ti = Tiron = 1,2-dihydroxybenzene-4,5-disulphonate.

had only a small and probably not significant effect (<10%) on the rate constants obtained.

Discussion

In order to decide if any acceleration of the substitution process has occurred in the system under study, it is necessary to be able to compare the observed rate constant with that expected from the Eigen mechanism. This mechanism gives a second-order rate constant which is equal to the product of an ion pairing constant and the water substitution rate.[18a] If acceleration occurs the second-order rate constant will be higher than expected. By comparing the ion-pairing constants, calculated with the aid of a simple model (K_{0S}^{calcd}), with the ratio of the second-order rate constant to the water substitution rate (K_{0S}^{obsd}), any acceleration will be revealed in a significantly larger value of the latter (greater than a factor of 3–5), compared to the former.

Acceleration of the substitution processes such as that observed by Hammes[2] is unlikely to be due simply to a medium effect, where the rate of water loss is enhanced by the interaction of the medium ions with coordinated water. For magnesium at least a value of the water substitution rate has been obtained at very low ionic strength[18a,26] and a value for the water exchange rate at ~ 12 m.[18b] The latter is only ~ 5 times faster than the former, despite the very different methods of measurement.

The normal method of calculating ion-pairing constants is to use the method of Fuoss[27] and Eigen.[28] The ion-pairing constant is given by

$$K_{0S} = (4\pi N a^3/3000)e^{-U(a)/kT} \qquad (38)$$

$$U(a) = \frac{Z_1 Z_2 e^2}{aD} - \frac{Z_1 Z_2 e^2}{D(1 + \chi a)}$$

$$\chi^2 = 8\pi N e^2 \mu \, 1000 \, Dkt$$

where μ is the ionic strength, N is Avogadro's number, a is the distance of closest approach of the ions, Z_1 and Z_2 are the charges of the ions, e is the electron charge, k is the Boltzmann constant, T is the absolute temperature, and D is the macroscopic dielectric constant.

The values obtained from this equation with $\mu = 0.1$ are in good agreement (within a factor of 3) with those estimated from ligand and water substitution rates at the same ionic strength, although at this ionic strength the Debye-Hückel law is no longer valid. In fact eq 38 must be modified when considering data at high ionic strengths. This is best achieved by the use of the Davies eq 39[29] to calculate the activity coefficients of individual ions (γ_i).

$$\log \gamma_i = -0.5 Z_i^2 \left(\frac{\sqrt{\mu}}{1 + \sqrt{\mu}} - 0.3\mu \right) \qquad (39)$$

For a reaction $A^{n+} + B^{m-} \rightleftharpoons C^{(m-n)-}$

$$K_{0S} = \frac{K_{0S}^{\circ} \gamma_A \gamma_B}{\gamma_C} = K_{0S}^{\circ} \eta(\gamma_i) \qquad (40)$$

where K_{0S}° is the value of the ion-pairing constant at zero ionic strength and the values of γ_i are calculated by eq 39. The Davies equation[29] has been used with great success in calculating activity coefficients for even highly charged ions up to an ionic strength 0.1 M. It can be used up to an ionic strength of 0.7 M[30] but it must be realized that the ion-pairing constants calculated in this way cannot be expected to be very accurate since at higher ionic strengths specific ionic interactions give rise to equilibrium constants which are dependent not only on charge but also on the nature of the ion itself.[31] However, the authors feel justified in using this approach since the calculated and observed ion-pairing constants are quite close. It may be pointed out here that second-order rate constants for substitution reaction of the same ligand with nickel(II) at

both low and high ionic strengths are not significantly different even with a charge product of −6.[32]

The authors considered that it might be instructive to compare the results with those for other Mg^{2+} reactions. Before direct comparison can be made, however, it is necessary to modify some of the data which have been obtained previously by other workers either because the temperature was not 25° or because ion pairing between reacting and medium ions was not at that time suspected.

The binding of alkali metal ions to nucleotides has been thoroughly investigated in the last few years. The early values for the binding constant between potassium ions and ATP were in the range 10–15 M^{-1}.[3,33-36] More recently a value of 200 M^{-1} has been obtained using an ion specific electrode technique.[37,38] However, this value is a thermodynamic one since activity coefficient corrections have been made. The ion-pairing constants for the species ATP^{4-}, $ATPH^{3-}$, ADP^{3-}, and $ADPH^{2-}$ have been calculated at $\mu = 0.1$ M (K^+)[6] from literature values of the binding constants at different ionic strengths[8,35] and the values of activity coefficients obtained using the Davies eq 39.

The corrected ion-pairing constant for magnesium and the above species is therefore

$$K_{0S}^{\text{calcd}} = K_{0S}/(1 + K_{K^+}^{Z}[K^+]) \qquad (41)$$

where $K_{K^+}^{Z}$ is the binding constant for potassium ions to species of charge Z. At 25.0° and $\mu = 0.1$ M values of $K_{K^+}^{-2} = 3\ M^{-1}$, $K_{K^+}^{-3} = 12\ M^{-1}$, and $K_{K^+}^{-4} = 32\ M^{-1}$ can be calculated.

To correct the rate constants obtained at other temperatures in some studies to 25° the temperature dependence of the reactions was assumed to be the same as that observed for the substitutions of oxinate,[39] *i.e.*, $\Delta H^* = 12.3$ kcal/mol. The values of K_{0S}^{calcd} and k_f for many systems are shown in Table IV.

It can be seen that the agreement between derived and calculated values for the ion-pairing constants (K_{0S}^{obsd} and K_{0S}^{calcd}) is satisfactory, not only for the reactions investigated here but also in other systems, thus implying that there is no acceleration of the substitution process even for highly charged ligands. However, for the reaction of magnesium with pyrophosphate species in the present study a small increase may be concealed by the uncertainty in the values of the ion-pairing constants calculated. There is some support for this though it is indirect, since the ratio of rates of the forward reactions for successive charge products is 11, whereas the Davies equation predicts only 6. However, due to the uncertainty in the K_{0S} values calculated, the authors consider that the results favor an S_N1 type mechanism and do not feel that there is sufficient justification for invoking acceleration in rate due to high ligand charge.

Although Hammes and Morrell[2] have produced some evidence that such accelerations can occur it is possible that their mechanism is not complete since they do not consider species such as $CoH_2P_2O_7$, $NiH_2P_2O_7$, etc., which may, in the light of the results obtained here, be important. The pH range investigated in their study (5.7–6.1) is not sufficiently wide in view of the relatively low accuracy of relaxation experiments to determine whether such species are important.

Acknowledgment. R. S. T. would like to thank the Royal Society (London) and R. C. P. the Alexander-von-Humboldt-Stiftung for the award of postdoctoral Fellowships. The authors are most grateful to Dr. H. Diebler for useful discussion and Professor M. Eigen for his interest in this work, as well as for providing facilities to complete this project.

References and Notes

(1) Present address, Department of Chemistry, University of Oklahoma, Norman, Okla. 73069.
(2) G. G. Hammes and M. L. Morrell, *J. Amer. Chem. Soc.*, **86**, 1497 (1964).
(3) S. M. Lambert and J. I. Watters, *J. Amer. Chem. Soc.*, **79**, 4262 (1957).
(4) See, for example, J. Bjerrum, G. Schwarzenbach, and L. G. Sillen, *Chem. Soc., Spec. Publ.*, **No. 17** (1964); 1st Suppl., **No. 25** (1970).
(5) (a) M. J. Schlesinger and M. J. Coon, *Biochim. Biophys. Acta*, **41**, 30 (1960). (b) While this paper was in preparation, another paper dealing in part with the magnesium–pyrophosphate reaction[6] came to the authors' attention. However this study, carried out at constant pH, concerns the reaction only of the monoprotonated form of the ligand.
(6) C. M. Frey, J. L. Banyasz, and J. Stuehr, *J. Amer. Chem. Soc.*, **94**, 9198 (1972).
(7) (a) P. R. V. Nayndu and P. L. Miles, *Biochem. J.*, **119**, 29 (1969); (b) A. A. Baykov, E. A. Braga, and S. M. Avaeva, *FEBS Lett.*, **21**, 80 (1972).
(8) R. Phillips, *Chem. Rev.*, **66**, 501 (1966).
(9) R. M. Izatt, J. J. Christensen, and J. H. Rytting, *Chem. Rev.*, **71**, 439 (1971).
(10) W. E. C. Wacker, *Ann. N. Y. Acad. Sci.*, **162**, 717 (1969).
(11) C. Sander and P. O. P. T'So, *J. Mol. Biol.*, **55**, 1 (1971).
(12) H. Krakauer, *Biopolymers*, **10**, 2459 (1971).
(13) H. Diebler, M. Eigen, and G. G. Hammes, *Z. Naturforsch. B*, **15**, 554 (1960).
(14) M. Eigen and G. G. Hammes, *J. Amer. Chem. Soc.*, **82**, 5951 (1960).
(15) M. Eigen and G. G. Hammes, *J. Amer. Chem. Soc.*, **83**, 2786 (1961).
(16) M. Cohn and T. R. Hughes, *J. Biol. Chem.*, **237**, 176 (1962).
(17) (a) G. G. Hammes, A. E. Maciel, and J. S. Waugh, *J. Amer. Chem. Soc.*, **83**, 2394 (1961); (b) J. A. Happe and M. Morales, *ibid.*, **88**, 2077 (1966).
(18) (a) M. Eigen and K. Tamm, *Z. Electrochem.*, **66**, 93, 107 (1962); (b) J. Neely and R. Connick, *J. Amer. Chem. Soc.*, **92**, 3476 (1970).
(19) M. Eigen and L. de Maeyer in "Technique in Organic Chemistry," Vol. VIII/2, 2nd ed, A. Weissberger, Ed., Interscience, New York, N. Y., 1963, p 904 *et seq.*
(20) H. Diehl and F. Lindstrom, *Anal. Chem.*, **31**, 414 (1959).
(21) See "Data for Biochemical Research," Dawson, Elliot, Elliot, and Jones, Ed., Clarendon Press, Oxford, 1969, p 623.
(22) R. S. Taylor, Ph.D. Thesis, University of Leeds, 1970.
(23) J. D. Crowther and A. E. R. Westman, *Can. J. Chem.*, **32**, 42 (1954).
(24) S. M. Lambert and J. I. Watters, *J. Amer. Chem. Soc.*, **79**, 5606 (1957).
(25) T. S. Dowling, Ph.D. Thesis, University of Maryland, Colllege Park, Md., 1972.
(26) H. Diebler, M. Eigen, G. Ilgenfritz, G. Maass, and R. Winker, *Pure Appl. Chem.*, **20**, 93 (1969).
(27) R. Fuoss, *J. Amer. Chem. Soc.*, **80**, 5059 (1958).
(28) M. Eigen, *Z. Phys. Chem. (Frankfurt am Main)*, **1**, 176 (1954).
(29) C. W. Davies, "Ion Association," Butterworths, London, 1962, p 39.
(30) C. J. Nyman and R. A. Plane, *J. Amer. Chem. Soc.*, **82**, 5787 (1960).
(31) R. A. Robinson and R. H. Stokes, "Electrolyte Solutions," Revised 2nd ed, Butterworths, London, 1959, p 491.
(32) J. C. Cassatt and R. G. Wilkins, *J. Amer. Chem. Soc.*, **90**, 6045 (1968).
(33) N. C. Melchior, *J. Biol. Chem.*, **208**, 615 (1954).
(34) W. J. O'Sullivan and D. D. Perrin, *Biochemistry*, **3**, 18 (1964).
(35) R. M. Smith and R. A. Alberty, *J. Phys. Chem.*, **60**, 180 (1956).
(36) J. Botts, A. Chashin, and H. L. Young, *Biochemistry*, **4**, 1788 (1965).
(37) M. S. Mohan and G. A. Rechnitz, *J. Amer. Chem. Soc.*, **92**, 5839 (1970).
(38) G. A. Rechnitz and M. S. Mohan, *Science*, **168**, 1460 (1970).
(39) D. N. Hague, S. R. Martin, and M. S. Zetter, *J. Chem. Soc., Faraday Trans. 1*, **68**, 37 (1972).
(40) D. N. Hague and M. Eigen, *Trans. Faraday Soc.*, **62**, 1236 (1966).
(41) K. Kustin and K. O. Watkins, *Inorg. Chem.*, **3**, 1706 (1964).

Surface-Chemical Properties of Highly Fluorinated Compounds Containing Oxygen in the Aliphatic Chain

Marianne K. Bernett and W. A. Zisman*

Laboratory for Chemical Physics, Naval Research Laboratory, Washington, D. C. 20375 *(Received February 28, 1973)*

Publication costs assisted by the Naval Research Laboratory

Two series of liquids with the formulae $CF_3CF_2CF_2[OCF(CF_3)CF_2]_nOCHCF_3$, where n is 1, 2, 3, or 4, and $CF_3CF_2CF_2[OCF(CF_3)CF_2]_xOCF_2CF_3$, where $x > n$ but not necessarily an integer, were studied for selected surface-chemical properties. Surface tensions were found to be remarkably low (starting from 12.7 dyn/cm at 25°); interfacial tensions with water and selected organic liquids were high. Atomic and bond parachors for fluorine in such highly fluorinated organic compounds were significantly lower than previously established values for alkyl mono- or trifluorides. Spreading ability of drops of any of these liquids on the clean surface of bulk water or the above-mentioned organic liquids, in the absence of functional or hydrophilic adsorbing groups, was determined to be a function of the free surface and interfacial energies, expressed as spreading coefficients or equilibrium spreading pressures. Although in these polymers the oxygen atoms are ether oxygens, they are modified by the neighboring fluorine atoms to be more stable and nonhydrophilic. Thin films of the oxyperfluoropropylenes, spread on horizontal smooth solid surfaces, had a critical surface tension of wetting of 20 dyn/cm at 25°. Several of the lower polymers of the oxyperfluoropropylenes exhibited marked ability to displace surface-chemically organic liquids which had previously coated glass or stainless steel surfaces.

Introduction

Highly fluorinated organic compounds are distinguished by unusually low surface energies which characterize the liquids by their high surface activity and spreading ability, and the solids by the large contact angles when wetted by numerous liquids. In a 1966 review on the surface chemistry of organic fluorochemicals, Jarvis and Zisman[1] explained that the extreme surface properties of perfluoroaliphatic compounds arise from the extraordinarily weak field of force existing in the vicinity of covalently bonded fluorine atoms and their neighbors. They also stated that the extent of their surface activity in liquids (or adsorptivity on liquids) was dependent on the organophobic–organophilic balance of the fluorochemical molecule with respect to the solvent (or substrate liquid).

Since the time of the review, studies of organic fluorochemicals have continued along two main avenues: (i) additional areas in surface chemical properties were explored, such as spreading pressures,[2] or the ability to displace liquids from solid surfaces[3,4] and (ii) structurally new compounds and polymers were synthesized by various sources and were made available. These studies have progressed to the stage where an investigation of selective surface chemical properties of such a structurally different material seemed highly desirable; it would demonstrate whether the properties peculiar to organic fluorochemicals are altered appreciably by a major molecular modification as, for instance, the incorporation of another constituent in the aliphatic chain. The results of such an investigation can unify the recent advances with the established knowledge and point to further areas of exploration.

Experimental Materials

Ideally suited for this study was a series of homologous aliphatic polyether fluorocarbons, made available by the Du Pont Co. The four low-molecular weight compounds of this series had the general IUPAC name α(perfluoropropyl)-ω-(1,1,1,2-tetrafluoroethoxy)poly[oxy(perfluoro-1,2-propylene)] and the formula $CF_3CF_2CF_2[OCF(CF_3)CF_2]_n$-$OCHFCF_3$, where poly and n stand for 1, 2, 3, or 4.[5] The colorless liquids had a purity of 99.9% for the monomer and dimer, 99% for the trimer, and 98% for the tetramer, and were used as received. Table I lists conveniently abbreviated code names for each liquid, along with selected physical properties. Boiling point, density (d) at 25°, and critical temperature (T_c) are given as determined by the producer for the now commercially available materials.[5]

Another set of seven liquids with the general formula $CF_3CF_2CF_2[OCF(CF_3)CF_2]_xOCF_2CF_3$ are polymers with molecular weights ranging from about 2000 to 7000 (each polymer being a mixture) and distinguished from the OPFP series only by being capped by a fluorine instead of a hydrogen atom on the ω terminal. These liquids are known commercially as Krytox 143 fluorinated oils[6] and will be referred to here by that name. Code names, viscosities, and densities, as supplied by Du Pont, are shown in Table II. The polymers were used in the experiments without further purification.

Surface Tension and Eötvos Constant

Surface tensions (γ_{LV}) of the OPFP and Krytox series were measured by the ring method with a Cenco du Nouy interfacial tensiometer using the Fox and Chrisman correction factors.[7] All measurements were carried out at 25° and 45% relative humidity and are given in Tables I and II.

The Eötvos constant (K) for the OPFP series was calculated from the equation

$$K = \gamma_{LV}(M/d)^{2/3}/(T_c - T - 6) \quad (1)$$

where M is the molecular weight of the respective liquid

TABLE I: Physical Properties of Oxyperfluoropropylene Liquids $CF_3CF_2CF_2[OCF(CF_3)CF_2]_nOCHFCF_3$

n	Code	Bp, °C	d^{25}, g/ml	T_c, °C	γ_{LV}^{25}, dyn/cm	K, (eq 1)
1	OPFP-1	104.4	1.658	218.3	12.7	2.85
2	OPFP-2	152.3	1.723	263.2	13.8	3.00
3	OPFP-3	193.8	1.763	295.2	14.5	3.20
4	OPFP-4	224.2	1.792	322	14.9	3.35

TABLE II: Physical Properties of Krytox Liquids $CF_3CF_2CF_2[OCF(CF_3)CF_2]_xOCF_2CF_3$

Code	Viscosity^{25}, cS[a]	d^{25}, g/ml[a]	γ_{LV}^{25}, dyn/cm
Krytox AZ	32	1.86	16.5
Krytox AA	74	1.88	17.2
Krytox AY	100	1.88	17.3
Krytox AB	200	1.89	17.4
Krytox AX	300	1.90	17.5
Krytox AC	600	1.90	17.9
Krytox AD	1000	1.91	18.6

[a] From ref 6.

and T(°C) is the temperature at which the experiments were performed. Each value of K (Table I) is much higher than the value of 2.1 usually obtained for unassociated liquids and for molecules of roughly spherical structure. Thus, not only do the K values correspond to linear structures, but also the larger K values with larger n indicate these are progressively more elongated molecules; this would be predicted of such increasingly linear polymers even if some random coiling did occur, especially if n becomes greater than 4.

Parachors

Molecular parachors of the OPFP compounds calculated from molecular weight, surface tension, and density are

$$P = (M/d)\gamma^{1/4} \quad (2)$$

much lower than those calculated by using Quayle's[8] or Vogel's[9] values of atomic and structural parachors (Table III). Earlier observations of parachors for highly fluorinated organic compounds[10,11] have noted a similar discrepancy, caused by the large fluorine parachors of 25.5 or 26.1 reported by Quayle and Vogel, respectively.

Using recently published surface tension data on a group of highly purified fully fluorinated n-alkanes,[2] we determined the molecular parachors of n-C_6F_{14} through n-C_9F_{20}. These, in turn, along with Vogel's atomic parachor of 8.6 for carbon,[12] resulted in an average value of 22.5 for the atomic parachor of fluorine, in excellent agreement with earlier observations.[10,11] The (C–F) bond parachor, as obtained by Vogel's type of calculation,[13,14] $(2n + 2)(C\text{–}F) = C_nF_{2n+2} + (2n + 2)(C\text{–}H)$, gave an average value of 24.6, which is in fairly good agreement with 25.4 obtained earlier from highly fluorinated compounds,[10] but much lower than the values by Vogel which he calculated to be 28.9 from the n-alkyl fluorides[13,15] or 26.3 from the trifluoroacetates.[14] Molecular parachors of the oxyperfluoropropylenes as computed using the (C–F) bond value of 24.6, closely agreed with our values calculated from eq 2 (Table III, last column).

TABLE III: Calculated Parachor Values

Compd	Eq 2	Quayle's atomic increments[a]	Vogel's bond increments[b]	Computed bond increments
OPFP-0[c]	332.9	361.9	345.0	326.3
OPFP-1	514.3	558.4	536.4	507.5
OPFP-2	691.4	755.5	727.8	688.7
OPFP-3	867.3	952.5	919.2	869.9
OPFP-4	1041.3	1149.6	1110.6	1051.1

[a] Reference 8. [b] Reference 9. [c] d^{25} = 1.538 g/ml, γ_{LV}^{25} = 10.4 dyn/cm.[5]

We can therefore state that atomic or bond parachors for fluorine in highly fluorinated organic compounds are lower than those in the alkyl monofluorides, or even the trifluorides, where the three fluorines are attached to the same terminal carbon atom. Gibling[16] had stated that the volume contribution of any atom is not constant but varies according to the nature of the other atoms with which it is linked and that allowance should be made for the interference of the nonlinked atoms. Obviously, having many bulky fluorine atoms attached in close proximity to a carbon chain alters the volume contribution considerably from that of a single fluorine atom attached to a hydrocarbon chain. Fluorine atoms attached to carbon atoms which, in turn, are linked to an ether oxygen, also greatly increase the stability of the ether linkage. The electronic configuration of the oxygen is altered to change the behavior of the atom from hydrophilic to nonhydrophilic.

Critical Surface Tension of Wetting (γ_c)

Duplex films of each OPFP liquid were prepared by permitting several drops of the liquid to spread over the horizontal smooth surface of either an acid-cleaned soda-lime glass slide or a freshly flamed disk of platinum and unidirectionally wiping off the excess liquid with clean, Whatman filter paper. The remaining film was thick enough to display interference colors but not thick enough to form a depression when a drop of the wetting liquid was placed upon it. The advancing contact angle (θ) of each sessile drop of a pure, freshly percolated liquid was measured on the film by use of a contact angle goniometer;[17] with a few exceptions, reproducibility of θ was ±2°.

When cos θ of each member of a homologous series of liquids on a smooth, clean, solid, low-energy surface is plotted against γ_{LV} for each of those liquids, a straight line results; the intercept at cos θ = 1 (θ = 0°) is referred to as the critical surface tension of wetting (γ_c) for that particular surface.[17] Figure 1 shows the cos θ *vs.* γ_{LV} graph obtained for n-alkanes on a film of OPFP-2 but, since contact angles of any one n-alkane on films of OPFP 2, 3, or 4 were close enough to one another to fall within the range of reproducibility, the graph represents the average of all three oxyperfluoropropylenes. The γ_c of 20 dyn/cm obtained for these liquid films is slightly higher than the γ_c of solid polymers whose surface constitutions, although comparable in molecular arrangements, are comprised solely of fluorocarbon groupings, such as in polytetrafluoroethylene (γ_c = 18.5 dyn/cm),[17] polyhexafluoropropylene (γ_c = 16.2–17.1 dyn/cm),[18] and copolymers of the two in various molar proportions (γ_c = 17.8–19.0 dyn/cm).[19] Except for the presence of oxygen atoms in the fluorocarbon chain, the surface structure of the oxyperflu-

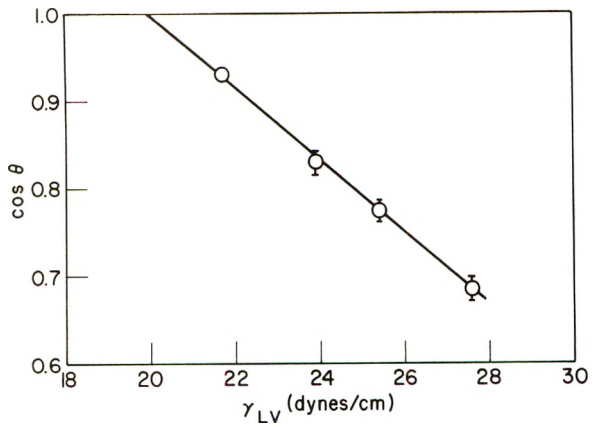

Figure 1. Wetting of *n*-alkanes on thin films of OPFP-2, OPFP-3, or OPFP-4 spread on glass at 25°.

oropropylenes resembles most that of the polyhexafluoropropylene by virtue of the pendant $-CF_3$ group in the repeating unit. It is known that the γ_c value of a hydrocarbon is increased by the introduction of oxygen atoms into the uppermost surface.[20-22] Our results show that the γ_c value of a fluorocarbon surface also is increased by the introduction of oxygen atoms.

We do not know the exact contribution, such as location or orientation, of the fluoroether group in the surface of the adsorbed film at the particular state observed. We assume, though, that ether oxygens bonded to fully fluorinated carbon atoms may act very differently from conventional ether oxygens bonded to hydrogen-linked carbon atoms and therefore modify the properties of compounds. Close proximity of fluorinated carbon atoms to functional groups has large effects upon these groups as shown, for instance, by the greatly increased stability of the whole perfluorodialkyl ether molecule.

Spreadability on Bulk Liquids

For spreadability studies, the surface of triply distilled water was covered with a duplex film of indicator oil (oxidized petroleum oil) whose surface pressure could be adjusted from about 2 to 11 dyn/cm by observation of the interference colors.[23] A small drop of the respective oxyperfluoropropylene specimen on the tip of a clean fine platinum wire was touched to the center of the film-covered water, and the spreading behavior was observed by the action of the indicator oil.

OPFP-1 rapidly spread and vanished from the surface. That the rapid disappearance of the drop was caused by the evaporation of the spread monolayer and not by the dissolution of OPFP-1 in the water was ascertained by observing the effect of a drop of OPFP-1 suspended above the water surface coated with the indicator oil; the volatile vapor molecules escaping from the suspended drop adsorbed on the liquid surface and forced away the indicator oil film to create a hole; this action continued until the drop either completely evaporated from the platinum tip, or until it was placed upon the surface, where it then spread and quickly disappeared. OPFP-2 acted less rapidly than OPFP-1, while OPFP-3 spread over the entire water surface, but remaining thicker in the center as indicated by the interference fringes on the advancing periphery. OPFP-4 spread very slowly, and the bulk of the drop remained as a lens that could be contracted or expanded with the surface pressure exerted by the film of the indicator oil. Liquids of the Krytox series did not spread but stayed on the surface as a lens with a well-defined but small contact angle. The results of the Krytox liquids can be compared but not fully equated with those of the OPFP series because the number of monomers, x, is not a well-defined number and the ω terminal is chemically somewhat different. However, the generalization can be made that spreadability decreases with increasing n (or x) until eventually a limiting value of n (or x) will be reached which will prevent spreading.

For observation of spreadability on organic liquids, the indicator oil was replaced by fine particles of clean Teflon. All four OPFP liquids spread on substrates of hexadecane and on propylene carbonate, the speeds decreasing with increasing n. In the Krytox series, all liquids spread on propylene carbonate, although the speed of spreading decreased with increasing molecular weight; a drop of Krytox AD enlarged to a thin lens which could be expanded and contracted by expanding or compressing the surface pressure of the indicator oil. On hexadecane, only the members below the molecular weight of Krytox AB would spread.

Harkins Spreading Coefficients, Interfacial Tensions, and Equilibrium Spreading Pressures

When a drop of a liquid "b" is placed on the surface of another liquid "a," the spreading behavior of this system can be expressed by the initial value of the Harkins spreading coefficient S_{ba}

$$S_{ba} = (\gamma_a - \gamma_b) - \gamma_{a'b'} \qquad (3)$$

γ_a and γ_b are the surface tensions of liquids "a" and "b," and $\gamma_{a'b'}$ is the interfacial tension of "a" and "b," the prime superscripts indicating that "a" is saturated with "b" and *vice versa*. When S_{ba} is positive, spreading will occur spontaneously; when S_{ba} is zero or negative, no spreading will occur, and the drop will remain unchanged.[24] Table IV presents measured values of γ_a, γ_b, and $\gamma_{a'b'}$ for a few selected systems. Interfacial tensions were measured by the ring method, and corrected by the method of Zuidema and Waters.[25] Excellent agreement was found with compounds against water for which literature values were available.[26] Although the ring method for interfacial tension had not previously been reported on systems comprising highly fluorinated compounds of low surface tension and high density against water or organic liquids, it was considered acceptable for this investigation, since the reproducibility of the measurements was never greater than ±0.3% (mostly ±0.1%). As expected from the low solubility of the oxyperfluoropropylenes in either water or organic liquids (<25 ppm), the $\gamma_{a'b'}$ values were relatively large and remained stable over observation times up to 68 hr.

For homologous series of spreading liquids on the same substrate liquid, S_{ba} became larger (more positive) the lower γ_b of each individual member of that series, *i.e.*, the greater $\gamma_a - \gamma_b$ (Table IV). Similarly, S_{ba} was larger for increasing γ_a of organic liquids with respect to γ_b. The γ_b values of all four OPFP liquids were sufficiently low to enable spreading on any substrate, and S_{ba} for all the systems was positive; the rapid spreading of OPFP-1, especially on water and on propylene carbonate, can now easily be explained by the large values of S_{ba} for these systems. In the Krytox series, spreading on propylene carbonate was observed for all compounds whose values of γ_b

TABLE IV: Interfacial Tensions, Spreading Coefficients, and Equilibrium Spreading Pressures of Various Systems at 25°[a]

Liquid "a"	Liquid "b"	γ_a	γ_b	$\gamma_a - \gamma_b$	$\gamma_{a'b'}$	S_{ba} (eq 3)	$\gamma_{a'}$	F_{ba} (eq 4)
Water	Krytox AX	72.0	17.5	54.5	53.1	1.4	72.4	−0.4
Water	Krytox AZ	72.0	16.5	55.5	54.8	0.7	72.4	−0.4
Water	OPFP-4	72.0	14.9	57.1	49.2	7.9	65.9	6.1
Water	OPFP-1	72.0	12.7	59.3	42.7	16.6	62.4	9.6
$PrCO_3$[b]	Krytox AX	41.1	17.5	23.6	18.6	5.0	36.3	4.8
$PrCO_3$[b]	Krytox AZ	41.1	16.5	24.6	18.3	6.6	35.4	5.7
$PrCO_3$[b]	OPFP-4	41.1	14.9	26.2	11.3	14.9	26.6	14.5
$PrCO_3$[b]	OPFP-1	41.1	12.7	28.4	6.9	21.5	31.1	10.0
n-C_{16}	Krytox AX	27.3	17.5	9.8	10.4	−0.6	27.1	0.2
n-C_{16}	Krytox AZ	27.3	16.5	10.8	9.8	1.0	25.9	1.4
n-C_{16}	OPFP-4	27.3	14.9	12.4	8.7	3.7	24.9	2.4
n-C_{16}	OPFP-1	27.3	12.7	14.6	7.0	7.6	24.0	3.3

[a] Values in dyn/cm. [b] Propylene carbonate.

and $\gamma_{a'b'}$ were sufficiently low to result in positive values of S_{ba}. On hexadecane, only the lower members would spread, and Table IV shows that S_{ba} on hexadecane was only 1.0 dyn/cm for Krytox AZ; S_{ba} of any polymer with greater γ_b or $\gamma_{a'b'}$ approached zero or became negative, as shown with Krytox AX. No spreading of the Krytox liquids occurred on a water surface, although γ_a is 72.0 dyn/cm, because the value of $\gamma_{a'b'}$ was so high as to make S_{ba} approach zero. For any given oxyperfluoropropylene liquid, whether the OPFP or Krytox series, S_{ba} on water is smaller than on an organic liquid which may be the result of an insufficient number of hydrophilic adsorbing groups in the spreading liquid.

As a result of very low solubility of any of the oxyperfluoropropylenes in the liquid substrate, $\gamma_{a'}$ measured after initial contact between liquids "a" and "b" and after several hours was almost identical for the nonvolatile liquids "b." When a volatile liquid "b," such as OPFP-1, was brought in contact with water, the initial $\gamma_{a'}$ of 62.4 dyn/cm increased to 63.7 dyn/cm after 2 min and to 71.0 dyn/cm after 10 min where it remained unchanged for the next 68 hr. The rapid increase in $\gamma_{a'}$ was clearly the result not only of volatilization of the OPFP-1 molecules from the water surface (rapid volatilization had also been observed when a drop of OPFP-1 was placed on a bulk water surface) but also of low solubility of OPFP-1 in water; although the water layer rested on the OPFP-1 layer throughout the 68-hr period, not enough OPFP-1 molecules traveled through the "ab" interface and subsequently through the water phase to significantly depress the surface tension of the water. The lower initial value of γ_a, then, must be due only to the OPFP-1 molecules originally adsorbed on first contact of the two phases and subsequently transported to the water/air interface. When OPFP-1 was in contact with n-hexadecane, $\gamma_{a'}$ changed from 25.8 dyn/cm initially to 24.9 dyn/cm after 2 hr to 24.0 dyn/cm after 4 hr, and thereafter remained unchanged for 68 hr. There the solubility was apparently high enough to overcome volatilization and to provide a sufficient number of molecules for adsorption on the surface. A similar surface activity effect could be observed in the system OPFP-1–propylene carbonate.

When a film has spread from a drop of liquid "b" placed on liquid "a," and some of the drop remains as a lens on the film-covered surface "a," the resulting surface tension decrease $\gamma_a - \gamma_{a'}$ is the equilibrium spreading pressure of "b" on "a"[27] and is denoted by

$$F_{ba} = \gamma_a - \gamma_{a'} \quad (4)$$

When solubility of "a" in "b" and *vice versa* is very low, then F_{ba} approaches $F_{b'a'}$ where "a" had been previously saturated with "b," and "b" with "a." Pomerantz, Clinton, and Zisman[28] proved that under these conditions

$$F_{ba} = S_{ba} \quad (5)$$

Values of F_{ba} as obtained by eq 4 are listed in Table IV and are shown to be very close to the S_{ba} values with the exception of systems comprising OPFP-1. Here equilibrium conditions at the surface are prevented by the high volatility and concomitant desorption of the OPFP-1 molecules.

We can conjecture that the spreading of the lower molecular weight oxyperfluoropropylenes on organic liquids and water is not the result of a propitious organophilic–organophobic balance, as demonstrated by surface-active molecules[1] nor of functional or hydrophilic molecular groups which facilitate adsorption at a liquid/air interface; rather, it is the result of a positive, and at times sizeable, initial spreading coefficient and spreading pressure. Similar conclusions have been drawn for the spreading on water of perfluoro n-alkanes[2] which are totally devoid of hydrophilic groups, yet had positive spreading pressures. Spreading characteristics thus are not altered by the inclusion of oxygen atoms in the surface constitution.

Surface-Chemical Displacement by Oxyperfluoropropylenes

For a liquid to be effective in surface-chemically displacing another liquid, several qualifications and interactions between the two compounds are necessary.[3] Although the OPFP liquids lack the two advantageous properties of good solubility in the organic liquids studied (<0.1%) and a characteristic molecular structure of a surface-active agent, they do display the necessary qualifications of having (a) very low surface tensions, and (b) the ability to depress the surface tension of hexadecane and propylene carbonate when added in small quantities (Table IV).

Experimental procedures were discussed earlier[3] and consist essentially of covering a horizontal glass or stainless steel panel to a depth of 0.2 mm with the organic liquid to be displaced (n-hexadecane, bp = 287°, and propylene carbonate, bp = 240°) and delivering a drop of the

TABLE V: Behavior of Oxyperfluoropropylenes as Displacing Agents at 25°

Agent	Hexadecane		Propylene carbonate	
	Σ_{max}, cm²	t_{max}, min	Σ_{max}, cm²	t_{max}, min
OPFP-1	12.6	1	44.2	1
OPFP-2	38.5	15	50.2	1
OPFP-3	72.4	30	50.2	3
OPFP-4	63.6	30	38.5	15
OPFP-1 in Freon 113[a]	0.8	1	0.8	1
OPFP-2 in Freon 113[a]	1.8	1	19.6	1
OPFP-3 in Freon 113[a]	4.9	3	33.2	3
OPFP-4 in Freon 113[a]	<0.8	1	33.2	10
Freon 113	0.8	1	1.8	1

[a] 1% vol of OPFP in Freon 113.

pure displacing agent (here the OPFP liquid) to the wet surface from a clean platinum wire tip. Table V shows Σ_{max}, the maximum area of oil displacement, and t_{max}, the time required to attain Σ_{max} for each of the OPFP liquids. The large values of Σ_{max} prove the OPFP liquids to be very effective liquid displacing agents. Since γ_a of propylene carbonate is higher than γ_a of hexadecane, we would expect Σ_{max} to be larger on propylene carbonate for each OPFP liquid, and the data in Table V confirm this for OPFP-1 and OPFP-2. However, in the case of OPFP-3 and OPFP-4, the reverse order was found. Bernett and Zisman[3] had also established that compounds free of functional specifically adsorbing groups (the OPFP liquids would have to be considered to fall into this category) can be effective displacing agents provided that, besides a considerable surface tension differential, there also exists a considerable volatility differential between agent and the liquid displaced. Thus as the bp of the OPFP liquids increases with increasing molecular weight, the order of Σ_{max} is larger with OPFP-3 and OPFP-4 on hexadecane than on propylene carbonate. This indicates that the difference in volatility of substrate liquid and displacing agent becomes of primary importance; the boiling points of the OPFP-3 and OPFP-4 approach that of the propylene carbonate sufficiently so that the surface tension difference alone becomes inadequate to effect superior displacement.

Many efficient liquid displacing agents remain effective even when they are present as minor concentrations in a solvent.[4] As can be seen in Table V, the OPFP liquids also remain effective, although to a much smaller degree, when dissolved in 1% volume concentrations in CCl_2FCClF_2 (Freon 113). In this solution system, however, Σ_{max} is always larger for propylene carbonate; because of the lower concentration, evaporation of the liquid in excess of the fraction adsorbed on the solid substrate is completed more rapidly, and thus equilibrium conditions are reached more rapidly.

Conclusions

Alteration of the fluorinated aliphatic chain by incorporation of ether oxygen atoms had only a moderate effect on some of the investigated properties characteristic of organic fluorochemicals. Surface tensions as well as critical surface tensions of wetting remained very low; moreover, the latter property proved to be governed by the same rules previously established for hydrocarbons, *i.e.*, γ_c increases on the introduction of oxygen atoms in the surface constitution. Atomic and group parachors for fluorine agreed with those from other compounds where the fluorine was attached to highly fluorinated carbon atoms, and were considerably lower than those in alkyl mono- or trifluorides.

There were, however, some notable differences. Introduction of the ether oxygen in the aliphatic fluorinated chain considerably extends the liquid range with molecular weight of the fluorinated compounds, greatly enlarging the usefulness of such compounds. The electronic configuration of the ether oxygen linked to highly fluorinated carbon atoms was altered to change the behavior of the atom from hydrophilic to nonhydrophilic. Despite the absence of an organophobic–organophilic balance in the fluorochemical molecule (because of the lack of such molecular groups), the oxyperfluoropropylenes were surface active in liquids, as shown by the ability to depress their surface tensions, as well as adsorptive on liquid substrates, as shown by their spreadability. These qualities may possibly be extended by modifying such polyether molecules through addition of judiciously selected molecular constituents.

Preparation and surface chemical investigation of homologous series of fluorochemicals, modified by other inclusions in the aliphatic chain, such as sulfur or amide groups, may yield further valuable information.

References and Notes

(1) N. L. Jarvis and W. A. Zisman, *Encycl. Chem. Technol.*, **9**, 707 (1966).
(2) L. A. Halper, C. O. Timmons, and W. A. Zisman, *J. Colloid Interface Sci.*, **38**, 511 (1972).
(3) M. K. Bernett and W. A. Zisman, *J. Phys. Chem.*, **70**, 1064 (1966).
(4) M. K. Bernett and W. A. Zisman, *Ind. Eng. Chem., Prod. Res. Develop.*, **11**, 83 (1972).
(5) *Chem. Eng. News*, Aug 7, 18, (1967); Du Pont Bulletin No. EL-8B (1967).
(6) Du Pont Bulletin No. L-5 (1968).
(7) H. W. Fox and C. H. Chrisman, Jr., *J. Phys. Chem.*, **56**, 284 (1952).
(8) O. R. Quayle, *Chem. Rev.*, 53, 439 (1953).
(9) A. I. Vogel, *J. Chem. Soc.*, 1833 (1948).
(10) P. D. Faurote, C. M. Henderson, C. M. Murphy, J. G. O'Rear, and H. Ravner, *Ind. Eng. Chem.*, **48**, 445 (1956).
(11) N. L. Jarvis and W. A. Zisman, *J. Phys. Chem.*, **63**, 727 (1959).
(12) A. I. Vogel, *J. Chem. Soc.*, 133 (1946).
(13) A. I. Vogel, W. T. Cresswell, G. H. Jeffery, and J. Leicester, *J. Chem. Soc.*, 514 (1952).
(14) G. H. Jeffery, V. C. Kyte, and A. I. Vogel, *J. Appl. Chem.*, **10**, 6 (1960).
(15) G. H. Jeffery, J. Leicester, W. A. T. Macey, and A. I. Vogel, *Chem. Ind. (London)*, 1045 (1954).
(16) T. W. Gibling, *J. Chem. Soc.*, 236 (1945).
(17) H. W. Fox and W. A. Zisman, *J. Colloid Sci.*, 5, 514 (1950).
(18) M. K. Bernett and W. A. Zisman, *J. Phys. Chem.*, **65**, 2266 (1961).
(19) M. K. Bernett and W. A. Zisman, *J. Phys. Chem.*, **64**, 1292 (1960).
(20) A. H. Ellison and W. A. Zisman, *J. Phys. Chem.*, **58**, 503 (1954).
(21) B. R. Ray, J. R. Anderson, and J. J. Scholtz, *J. Phys. Chem.*, **62**, 1220 (1958).
(22) L. H. Lee, *Advan. Chem. Ser.*, **No. 87**, 106 (1968).
(23) I. Langmuir and V. J. Schaefer, *J. Amer. Chem. Soc.*, **59**, 2400 (1937).
(24) W. D. Harkins and A. Feldman, *J. Amer. Chem. Soc.*, **44**, 2665 (1922).
(25) H. H. Zuidema and G. W. Waters, *Ind. Eng. Chem., Anal. Ed.*, **13**, 312 (1941).
(26) A. Weissberger, "Technique of Organic Chemistry," Vol. 1, 2d ed, Interscience, New York, N. Y., 1949, p 360.
(27) A. Cary and E. K. Rideal, *Proc. Roy. Soc., Ser. A*, **109**, 328 (1925).
(28) P. Pomerantz, W. C. Clinton, and W. A. Zisman, *J. Colloid Interface Sci.*, **24**, 16 (1967).

Ultrasonic Absorption in Aqueous Solutions of Nucleotides and Nucleosides. I. Effect of pH and Concentration

Jacques Lang, Jean Sturm, and Raoul Zana*

C.N.R.S., Centre de Recherches sur les Macromolécules. 67083 Strasbourg, Cedex, France *(Received March 5, 1973)*

Ultrasonic absorption measurements have been performed at 2.82 MHz and 25° on aqueous solutions of eleven nucleotides, seven nucleosides, thymine, and D-ribose 5-phosphate between pH 2 and 13. For all of these compounds except three nucleosides the ultrasonic absorption *vs.* pH curves show maxima in the acid and/or in the alkaline range. These maxima are attributed to two types of proton transfer equilibria: (a) proton transfer with the solvent and (b) direct proton exchange between different ionized forms of the nucleotide molecule. In the alkaline range the absorption maxima are due to equilibria of the (a) type except in the case of thymidine 5′-monophosphate (5′TMP) diammonium salt where it is due to a proton exchange between NH_4^+ and 5′TMP anion. In the acid range absorption maxima are observed only with nucleotides and D-ribose 5-phosphate and appear to involve the phosphate group. For nucleotides having a chemical group other than phosphate with a pK_a in the acid range the maxima are mainly due to equilibria of the (b) type whereas (a) type equilibria account for the maxima observed with nucleotides having no such chemical group. The implications of these findings for the excess ultrasonic absorption of nucleic acids are examined.

I. Introduction

In several instances[1-5] it has been observed that, at a given ultrasonic frequency f, the excess ultrasonic absorption $\Delta\alpha/f^2$ ($\Delta\alpha = \alpha - \alpha_0$ difference between the ultrasonic absorption coefficients for the solution and for the solvent) of aqueous solutions of nucleic acids shows a large variation when the pH is changed, at pH below 5 and above 9. For 0.005 g/ml DNA solutions in the alkaline range, $\Delta\alpha/f^2$ goes through a well-defined maximum at pH 11.7.[2,3] In the acid range $\Delta\alpha/f^2$ increases as the pH decreases.[2,4] Similar results have been found with RNA solutions.[5] Conformational equilibria have often been thought to be responsible for the above absorption changes.[1,3] However, in recent work[2] we have shown that these changes are in fact due to the perturbation by the ultrasonic waves of proton transfer equilibria on protonable groups of nucleic acid molecules. In the alkaline range the maximum was assumed to be due to proton transfer on the lactam groups of guanine and thymine. In the acid range the excess ultrasonic absorption was assumed to be due to proton transfer on the amino group of guanine, adenine, and cytosine. In order to check these assumptions we have undertaken an extensive ultrasonic absorption study of aqueous solutions of the various components of nucleic acids.

The experimental results obtained with eleven nucleotides, seven nucleosides, thymine, and D-ribose 5-phosphate are given in this paper. The results have permitted assignment of the chemical groups involved in proton transfer equilibria in nucleic acid solutions. Moreover, evidence for a new type of proton transfer occurring in solutions of nucleotides has been obtained. This process occurs between molecules of the same nucleotide in different states of ionization. It is observed only with nucleotides whose base moiety includes a nitrogen atom or an =NH–CO– group with a pK_a in the acid range.

II. Materials and Methods

The compounds studied in this work have been obtained from various sources: deoxyadenosine 5′-monophosphate $2Na^+$ (5′dAMP), adenosine 5′-monophosphate $2Na^+$ (5′AMP), xanthosine 5′-monophosphate $2Na^+$ (5′XMP), deoxycytidine 5′-monophosphoric acid (5′dCMP), cytidine 5′-monophosphate $2Na^+$ (5′CMP), inosine 5′-monophosphate $2Na^+$ (5′IMP), thymidine 5′-monophosphate $2Na^+$ (5′TMP), thymidine 5′-monophosphate diammonium salt ($5'TMPNH_4^+$), uridine 5′-monophosphate $2Na^+$ (5′UMP), guanosine 5′-monophosphoric acid (5′GMP), xanthosine, and D-ribose 5-phosphate from Sigma; adenosine 5′-phosphoramide Na^+ ($5'AMPNH_2$), deoxycytidine, inosine, and thymine from Calbiochem; deoxyadenosine and thymidine from Mann Research Laboratories; and uridine and deoxyguanosine from Biochemical Research. All compounds were of the best grade available and have been used without further purification.

All solutions were prepared with freshly deionized distilled water. The pH was adjusted by small additions of reagent grade HCl or NaOH. The pH measurements were performed in the range 2–13 using a Tacussel pH meter with a glass electrode for highly alkaline solutions and a standard calomel electrode. The pH meter was calibrated using Merck buffers. Potentiometric titrations have been performed on solutions of all of the above compounds.

The ultrasonic absorption coefficients were measured at 2.82 MHz using a two-crystal interferometer.[6]

III. Results and Discussion

The variation of α/f^2 (α = absorption coefficient of the solution) with pH has been found to greatly depend on the nature of the compound, as can be seen in Figures 1–3 which show some typical results. Other data (Figures 5–10) are given in the microfilm edition of this paper.[7] Table I summarizes all of the results obtained. pH_A and

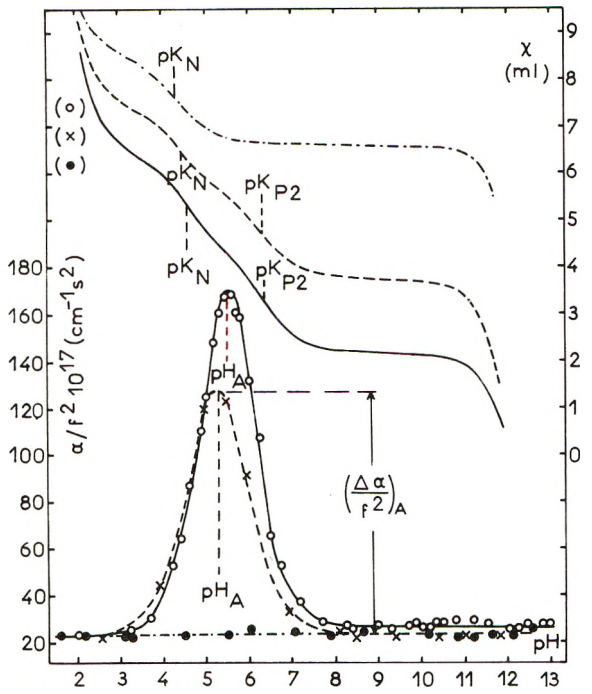

Figure 1. Potentiometric titration curves and variations of α/f^2 *vs.* pH at 2.82 MHz for 0.02 *M* aqueous solutions of 5′dCMP (——), 5′CMP (— —), and deoxycytidine (—•—) at 25°. × is the volume of added HCl solution for the titration experiments.

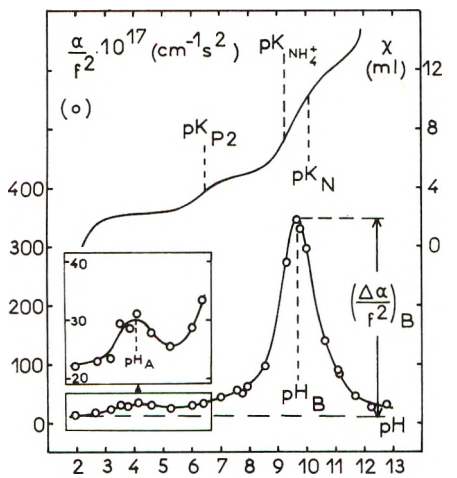

Figure 2. Potentiometric titration curve and variation of α/f^2 *vs.* pH (O) at 2.82 MHz for 0.02 *M* aqueous solution of 5′TMPNH$_4^+$ at 25°. × is the volume of added NaOH solution for the titration experiments.

pH_B refer to the pH where the maximum occurs in the acid and in the alkaline ranges, respectively. $(\Delta\alpha/f^2)_{A,B}$ is equal to $(\alpha/f^2)_{A,B} - (\alpha/f^2)_N$ where $(\alpha/f^2)_A$ and $(\alpha/f^2)_B$ are the values of α/f^2 at pH_A and pH_B, respectively, and $(\alpha/f^2)_N$ is the value of α/f^2 where no maximum occurs (see Figures 1 and 2). In all instances but deoxyadenosine, xanthosine, and deoxycytidine, the plots α/f^2 *vs.* pH go through a maximum either in the acid range and/or in the alkaline range.

The fact that α/f^2 is pH dependent indicates that the absorption maxima are associated with proton transfer equilibria or with processes which are coupled with proton transfers. For the sake of clarity we shall deal separately with the results relative to the alkaline range and to the acid range.

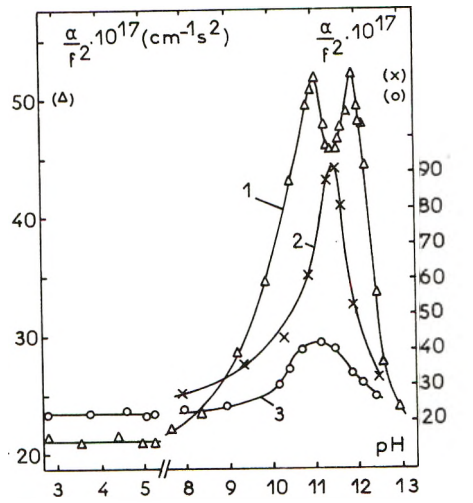

Figure 3. Variations of α/f^2 *vs.* pH at 2.82 MHz and 25° for aqueous solutions of thymidine, 0.02 *M* (O) and 0.19 *M* (×), and of thymine, 0.02 *M* (Δ).

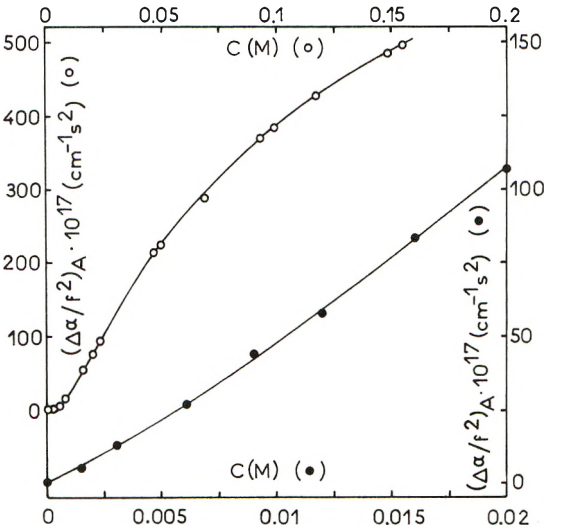

Figure 4. Variations of $(\Delta\alpha/f^2)_A$ *vs.* concentration at 2.82 MHz and 25° for aqueous solution of 5′AMP (O) at pH_A 5.05 and 5′XMP (●) at pH_A 5.9.

1. Alkaline Range. Table I indicates that, except for 5′TMPNH$_4^+$ and the second maximum observed at pH 11.9 for thymine, $(\Delta\alpha/f^2)_B$ varies only from 11 to 30 × 10^{-17} cm^{-1} sec^2 and pH_B varies in a narrow range between 10.3 and 11.1. Moreover both thymine, thymidine, and 5′TMP show an absorption maximum around 11. Table I also indicates that when a nucleoside presents no absorption maximum in the alkaline range the corresponding nucleotide shows the same behavior.

The effect of ionic strength μ was investigated in the case of 5′TMP, thymidine, and deoxyguanosine. No effect on pH_B and $(\Delta\alpha/f^2)_B$ was found when μ was increased from 0 to 0.15 *M* NaCl. This result seems to indicate that stacking of nucleotides or nucleosides is not at the origin of the observed ultrasonic absorption maxima. On the other hand, a comparison between the titration curves of the compounds listed in Table I and the corresponding curves α/f^2 *vs.* pH (see, for instance, Figure 1 and 2 and ref 7) permits identification of the process responsible of the absorption maxima. In each instance it is found that pH_B corresponds within the experimental error to the pH value at the equivalence point associated with the ionization of a lactam (or lactim)[8] group according to reaction 1.

TABLE I: Summary of the Results Obtained with 0.02 *M* Solutions at 2.82 MHz and 25°

	Acid range			Alkaline range		
	pH_A		$(\Delta\alpha/f^2)_A \times 10^{17}$ sec²/cm	pH_B		$(\Delta\alpha/f^2)_B \times 10^{17}$ sec²/cm
	Expt	Calcd[a]		Expt	Calcd[a]	
5′dAMP	5.05 ± 0.1	5.12 (b)	76 ± 4			0
5′AMP	5.05 ± 0.1	5.12 (b)	76 ± 4			0
5′AMPNH$_2$	3.15 ± 0.1	3.1 (a)	13.5 ± 2			
5′XMP	5.9 ± 0.1	5.88 (b)	102 ± 5			0
5′dCMP	5.5 ± 0.1	5.42 (b)	141 ± 7			0
5′CMP	5.35 ± 0.1	5.37 (b)	103 ± 5			0
5′IMP	4.1 ± 0.2	3.97 (c)	9 ± 2	10.55 ± 0.3	10.8 (e)	11 ± 2
5′TMP	4.2 ± 0.2	4.07 (c)	9 ± 2	11.1 ± 0.15	11.22 (e)	24 ± 3
5′TMPNH$_4^+$	4.1 ± 0.2	4.09 (c)	8.5 ± 2	9.7 ± 0.1	9.69 (d)	315 ± 10
5′UMP	4.3 ± 0.3	4.04 (c)	7.5 ± 2.5	10.8 ± 0.3	11.02 (e)	12 ± 3
5′GMP	4.2 ± 0.2	4.1 (c)	12.5 ± 2.5	10.9 ± 0.2	11.02 (e)	19 ± 3
		4.3 (b)				
Deoxyadenosine			0			0
Xanthosine	Precipitation occurs at pH <4.9					0
Deoxycytidine			0			0
Inosine			0	10.6 ± 0.2	10.6 (e)	11 ± 3
Thymidine			0	11.1 ± 0.2	11.05 (e)	20 ± 2
Uridine			0	10.45 ± 0.3	10.7 (e)	12.5 ± 2.5
Deoxyguanosine			0	10.7 ± 0.15	10.8 (e)	23 ± 2
Thymine			0	11 ± 0.1	11.1 (e)	30.5 ± 3
				11.9 ± 0.1		31.5 ± 3
D-Ribose 5-phosphate	4.15 ± 0.2	3.98 (c)	6 ± 2			

[a] The calculated values of $pH_{A,B}$ have been obtained using (a) $pH_A = \frac{1}{2}(pK_{P1} + pK_N)$; (b) $pH_A = \frac{1}{2}(pK_{P2} + pK_N)$; (c) $pH_A = \frac{1}{2}(pK_{P2} - \log c)$; (d) $pH_B = \frac{1}{2}(pK_N + pK_{NH_4^+})$ with $pK_{NH_4^+} = 9.26$; and (e) $pH_B = \frac{1}{2}(14 + pK_N + \log c)$.

$$-NH-CO- + OH^- \underset{k_{-1}}{\overset{k_1}{\rightleftharpoons}} H_2O + -N-CO-^- \quad (1)$$

The assignment of the absorption maxima in the alkaline range to the hydrolysis equilibrium 1 explains the results of Table I.

(a) Adenine and cytosine molecules do not contain lactam groups and no absorption maximum is observed in the alkaline range for the nucleotides and nucleosides corresponding to these two bases. The same explanation holds for D-ribose 5-phosphate.

(b) The presence of two lactam groups in thymine explains the two absorption maxima found for this compound (see Figure 3 and Table I). From the value of pH_B for the second maximum the corresponding pK_a may be estimated to be around 12. Thus our results appear to confirm those obtained in an ultraviolet study[9] of thymine. Two ionizations were detected: that of the 2-hydroxyl group characterized by a pK_a equal to 9.6 and that of the 4-hydroxyl group with a pK_a around 13.[9] It must be pointed out that the second ionization is not apparent on the potentiometric titration curve. In going from thymine to thymidine the second absorption maximum vanishes (see Figure 3) as the proton of the 4-hydroxyl group is replaced by the sugar.

(c) The absorption maximum associated with reaction 1 should occur at a pH given by[10]

$$pH_B = \tfrac{1}{2}(14 + pK_a + \log c) \quad (2)$$

where pK_a has its usual meaning and c is the concentration in equiv/l. of titrable groups. The pK_a values reported in the literature[9,11-13] or determined as part of this work have been used to calculate pH_B for the compounds presenting an absorption maximum in the alkaline range. As indicated by Table I the agreement between calculated and experimental values is quite good.

On the other hand, eq 2 predicts an increase of pH_B with c. Figure 3 relative to thymidine shows that indeed pH_B is increased by 0.3 to 0.4 pH units when c is increased from 0.02 to 0.19 *M*.

(d) The amplitude of the absorption maximum $(\Delta\alpha/f^2)_B$ at frequency f and at pH = pH_B can be calculated according to[10]

$$(\Delta\alpha/f^2) = 1.18 \times 10^{-7}\Delta V_0^2[OH^-]^2\frac{k_1\tau_B^2}{1 + 4\pi^2f^2\tau_B^2} \quad (3)$$

with

$$1/\tau_B = k_{-1} + 2k_1[OH^-];\ k_1/k_{-1} = 10^{14}K_a \quad (4)$$

where τ_B is the relaxation time, k_1 and k_{-1} are the rate constants for reaction 1, ΔV_0 is the volume change associated with this reaction. The calculations have been carried out for thymidine and inosine which are characterized by quite different values of pK_a: 9.75 and 8.9, respectively. k_1 was taken as 10^{10} M^{-1} sec^{-1} as can be expected from results reported on adenine[14] and purine.[15] The value of ΔV_0 is not known. However, for a reaction such as 1 values of the order of 10 cm³/mol or more are to be expected,[16] on the basis of the volume changes upon ionization of compounds such as phenol derivatives and for the neutralization reaction $H^+ + OH^- \rightarrow H_2O$. With ΔV_0 = 10 ± 2 cm³/mol the calculated values of $(\Delta\alpha/f^2)_B$ have been found to be (20 ± 7) × 10^{-17} and (8 ± 3) × 10^{-17} cm^{-1} sec² for thymidine and inosine, respectively, in good agreement with the experimental results.

The results of Figure 3 for thymidine permit a direct although approximate calculation of k_1 and ΔV_0 from the values of $(\Delta\alpha/f^2)_B$ at c = 0.02 and 0.19 *M*, by means of eq 3 and 4. The values $k_1 = 4.10^9$ M^{-1} sec^{-1} and ΔV_0 = 11.5 cm³/mol were obtained.

(e) Equations 3 and 4 also provide an explanation for the fact that xanthosine and 5′XMP do not show an ab-

sorption maximum in the alkaline range although they contain lactam groups. Indeed the pK_a of these groups is low (5.7 as compared with 9.8–11 for the lactam group of the other compounds of Table I). As a result $[OH^-]$ in eq 3 and 4 is at least 100 times smaller than for the other compounds, yielding an absorption maximum of negligible amplitude in the alkaline range, at 2.82 MHz, in agreement with the experimental results (see Table I and Figure 6 of ref 7).

(f) Implications for the ultrasonic absorption of nucleic acids. In nucleic acids base pairing through H bonds involves the lactam groups of thymidine, guanine, and uridine. Proton transfers on these groups remain, however, possible as shown by potentiometric studies,[17] but the pK_a's are higher than those of the corresponding nucleotides. For example, the pK_a's of the lactam group of 5′GMP and 5′TMP are 9.8 and 10.2, respectively, while in DNA they are 11.6 and 11.4, respectively.[17] As a result the absorption maximum is found at around pH 11 for nucleotides and 11.7 for DNA, in excellent agreement with the values calculated by means of eq 2. On the other hand, it is easy to show, using eq 3 and 4, that a pK_a increase should result in an increase of $\Delta\alpha/f^2$ in agreement with the experimental results. Indeed, a 0.005 g/cm³ solution of DNA has a content of about 0.01 *M* of thymidine and deoxyguanosine and its excess absorption has been found to be about 25×10^{-17} cm^{-1} sec^2 as compared with about 22×10^{-17} cm^{-1} sec^2 for a 0.02 *M* solution of deoxyguanosine or thymidine.

It must be pointed out that in a recent paper[4] on the ultrasonic absorption of DNA solutions it was incorrectly stated that proton transfer in the alkaline range involves the NH_2 group of the bases while in fact lactam groups are involved. Also the authors claimed that the absorption maximum should occur between pH 12.5 and 13 and for this reason concluded that "there was reasonable doubt that proton transfer can be involved to account for such maxima." However, in their calculations the authors used the equation $pH_B = (14 + pK_a)/2$ instead of eq 2. In doing so they neglected the concentration term which amounts to about −1 pH unit at the concentration used in their work (~0.004 g/cm³).

In conclusion, the ultrasonic absorption maximum occurring at pH 11.7 in DNA solutions appears to be due to proton transfer equilibria involving the lactam groups of guanine and thymine. For RNA solutions this process involves the lactam group of uracil and guanine.[5]

2. Acid Range. An inspection of Table I reveals the following two salient features.

(a) Absorption maxima are present only for those compounds which comprise the phosphate group, *i.e.*, nucleotides and D-ribose 5-phosphate, but not for nucleosides and bases.

(b) The nucleotides for which an absorption maximum has been observed in the alkaline range (5′IMP, 5′TMP, 5′TMPNH$_4^+$, 5′UMP, and 5′GMP) show in the acid range a maximum whose amplitude and position are practically independent of the nature of the nucleotide, and quite close to those found for D-ribose 5-phosphate. On the contrary, the nucleotides which present no absorption maximum in the alkaline range (5′dAMP, 5′AMP, 5′XMP, 5′dCMP, and 5′CMP) show in the acid range a maximum of large amplitude whose position and amplitude depend very much on the nature of the nucleotide. Again, for the sake of clarity, we shall deal separately with the two series of nucleotides. The results relative to 5′AMPNH$_2$ will be examined in part d. However, an explanation must be first given for the fact that deoxyadenosine, deoxycytidine, and deoxyguanosine, which comprise a nitrogen atom protonable in the acid range,[9,10-13] do not show an absorption maximum in this range.

a. Deoxyadenosine, Deoxycytidine, and Deoxyguanosine. The reaction of protolysis which could give rise to an absorption maximum in the acid range writes

$$-NH^+ \underset{k_1}{\overset{k_{-1}}{\rightleftharpoons}} -N + H^+ \qquad (5)$$

The position of the absorption maximum, pH_A, and the relaxation time τ_A and excess absorption $(\Delta\alpha/f^2)_A$ associated with reaction 5 at pH = pH_A are given by[10]

$$pH_A = \tfrac{1}{2}(pK_N - \log c) \qquad (6)$$

$$1/\tau_A = k_{-1} + 2[H^+]k_1 \qquad (7)$$

$$\left(\frac{\Delta\alpha}{f^2}\right)_A = 1.18 \times 10^{-7}[H^+]^2 k_1 \Delta V_0^2 \frac{\tau_A^2}{1 + 4\pi^2 f^2 \tau_A^2} \qquad (8)$$

where c is the concentration of protonable groups and pK_N the pK_a of the protonable nitrogen atoms. The calculations were carried out on deoxyadenosine, deoxycytidine, and deoxyguanosine whose pK_N's are respectively 3.7 (this work), 4.3 (this work and ref 9, p 369), and 2.[13] Throughout the calculations k_1 was taken as 2.4×10^{10} M^{-1} sec^{-1}, a value obtained by means of nmr[18] on purine. On the other hand, for reaction 5, ΔV_0 usually varies between 2.5 and 5 cm³/mol.[19] At f = 2.82 MHz and for a nucleoside concentration of 0.02 *M*, calculations yield values of $(\Delta\alpha/f^2)_A$ below 3×10^{-17} cm^{-1} sec^2 even with ΔV_0 = 5 cm³/mol. Absorption maxima with such small amplitudes would barely show on the plots of α/N^2 *vs.* pH, given the experimental error. Since the actual values of ΔV_0 are likely to be smaller than 5 cm³/mol the excess absorption due to reaction 5 will be negligible for the three nucleosides at 0.02 *M*.

b. 5′IMP, 5′TMP, 5′TMPNH$_4^+$, 5′UMP, and 5′GMP. The small absorption maximum found in the acid range has the same characteristics for the five nucleotides and D-ribose 5-phosphate. It therefore must be attributed to the phosphate group and not to the base. Although this maximum has not been observed for phosphoric acid,[7] it will be shown below that these two sets of results are not incompatible.

The comparison of the potentiometric neutralization curves of the above five nucleotides to the corresponding α/f^2 *vs.* pH curves show that in each instance pH_A corresponds to the pH at the equivalence point for the reaction of protolysis of the secondary phosphoric acid function

$$R\text{-}O\text{-}PO_3H^- \underset{k_1}{\overset{k_{-1}}{\rightleftharpoons}} R\text{-}O\text{-}PO_3^{2-} + H^+ \qquad (9)$$

where R refers to the rest of the nucleotide molecule (base plus sugar). It can be shown that for such a reaction the ultrasonic absorption maximum occurs at a pH given by[10]

$$pH_A = \tfrac{1}{2}(pK_{P2} - \log c) \qquad (10)$$

where pK_{P2} is the pK_a of the secondary phosphoric acid function and c the nucleotide concentration.

Equation 10 permits us to explain why the position of the absorption maximum observed for the above five nucleotides does not depend on the nature of the nucleotide. Indeed our potentiometric data, as well as results of other workers,[12] show that pK_{P2} depends very little on the na-

ture of the nucleotide. This in turn results in values of pH_A independent of the nucleotide.

Equation 8 gives the maximum excess absorption associated with reaction 9. This expression can be used to evaluate $(\Delta\alpha/f^2)_A$ for the five nucleotides since (a) pK_a is known to be 6.65 ± 0.05;[12] (b) ΔV_0 for reaction 9 can be taken as the volume change upon ionization of the secondary acid function in phosphoric acid, *i.e.*, 28 cm³/mol;[20a] and (c) k_1 can be taken as 5×10^{10} M^{-1} sec^{-1} as reaction 9 involves H^+.[14] The calculations then yield $(\Delta\alpha/f^2)_A = 6 \times 10^{-17}$ cm^{-1} sec^2 at 2.82 MHz and with $c = 0.02$ M, in agreement with the experimental results for 5′IMP, 5′TMP, 5′TMPNH$_4^+$, and 5′UMP, but too small compared with the results for 5′GMP. A possible explanation for this difference will be given in paragraph c.

The calculations were also carried out for phosphoric acid for which $pK_a = 7.2$,[20b] with the same assumptions as for nucleotides. $(\Delta\alpha/f^2)_A$ was found to be below 2×10^{-17} cm^{-1} sec^2, *i.e.*, too small to be detected, in agreement with our experimental results which do not show any absorption maximum on the curve α/f^2 *vs.* pH for phosphoric acid.[7]

As predicted by eq 10 a decrease of pH_A with c has been obtained in the case of 5′IMP.[7] Decreasing c from 0.25 to 0.02 M, however, resulted in a decrease of pH_A by only 0.3 pH units instead of a predicted 0.5 pH units on the basis of eq 10. A possible explanation for this result is that at pH around 4 protons may be exchanged directly according to reaction 11 in addition to the transfer involving H_2O (reaction 9). As will be shown now proton exchange similar to reaction 11, although involving other protonable groups, plays a very important role in the ultrasonic absorption of the nucleotides considered in the next paragraph.

$$R\text{-}PO_3H_2 + R\text{-}PO_3^{2-} \rightleftharpoons 2R\text{-}PO_3H^- \qquad (11)$$

c. 5′dAMP, 5′AMP, 5′XMP, 5′dCMP, and 5′CMP. Comparison of the results for these nucleotides with those for the corresponding nucleosides shows that the phosphate group is at least in part responsible for the absorption maxima found for nucleotides. On the other hand, the results of Table I indicate that both the amplitude and position of the absorption maxima depend on the value of the pK_a of the nitrogen atom of the base moiety involved in reaction 5. As stated above the pH dependence of α/f^2 indicates that the absorption maxima displayed by these five nucleotides must be due to proton transfer equilibria or to other processes such as conformational equilibria and/or stacking equilibria coupled with proton transfers.

Indeed, the ultrasonic absorption of aqueous solutions of nucleosides and 5′AMP at neutral pH has been recently reported.[21] From results obtained in the range 10–250 MHz, Rhodes and Schimmel[21] concluded that the observed excess absorption was due to the syn–anti transition about the glycosidic bond, *i.e.*, to an intramolecular process. These authors attributed to the same process the sharp increase of absorption which they observed at lower pH. Although our results at neutral pH agree with those of Rhodes and Schimmel[21] when concentration is taken into account, the absorption maxima found in our work cannot be assigned to the syn–anti equilibrium for the following reasons. (a) Such a process should be characterized by a linear variation of $(\Delta\alpha/f^2)_A$ with the nucleotide concentration c while the curves of Figure 4 relative to 5′AMP and 5′XMP show a nonlinear behavior. (b) The absorption associated with such a process should be comparable for the different nucleotides derived from purine (or pyrimidine). In fact, Table I shows that this is not so and that $(\Delta\alpha/f^2)_A$ depends greatly on the pK_a of the nitrogen atom of the base moiety which is involved in reaction 5 in the acid range: pH_A increases with pK_N. (c) The variation of α/f^2 with pH would be difficult to explain in terms of conformational equilibrium, at the present state of knowledge.

On the other hand, much evidence has been obtained[22] for the stacking of nucleotides at concentrations comparable with those used in this work. Nevertheless this process alone cannot explain the absorption maxima.

Indeed one would expect stacking equilibria to be very sensitive to the ionic strength μ and to the urea content of the solution but this prediction is not confirmed by the experimental results relative to 5′AMP. No effect of μ on $(\Delta\alpha/f^2)_A$ has been found when μ is increased from 0 to 0.15 M KCl while pH_A undergoes only a minor change (0.05 pH units). On the other hand, raising the urea content of the solution to 7 M urea results in a 50% decrease of $(\Delta\alpha/f^2)_A$ and in a shift of +0.3 pH unit of pH_A. On the basis of stacking equilibria one would have expected a much larger decrease or eventually a complete disappearance of the absorption maximum as stacking must be considerably reduced in the presence of 7 M urea, in view of known effect of urea on hydrophobic association.[23] The effect of ionic strength and of 7 M urea on pH_A and $(\Delta\alpha/f^2)_A$ can be better understood if absorption maxima are assumed to be due to proton transfers. Indeed pK_a's are usually increased in the presence of urea[11] resulting in an increase of pH_A. Also, the magnitude of ΔV_0 is decreased in going from H_2O to H_2O–7 M urea,[24] thus bringing about a decrease of $\Delta\alpha/f^2$. On the contrary an increase of ionic strength from 0 to 0.15 M KCl results in very small changes in ΔV_0[16,24] and in pK_a[20c] thus explaining the very small changes of $(\Delta\alpha/f^2)_A$ and pH_A upon increasing μ.

Proton transfers thus appear as the main contributors to the observed absorption maxima in the case of 5′dAMP, 5′AMP, 5′XMP, 5′dCMP, and 5′CMP. The comparison between the α/f^2 *vs.* pH curves and the potentiometric titration curves of these five nucleotides supports this conclusion and reveals that in each instance the maximum occurs at a value of the pH given by

$$pH_A = \tfrac{1}{2}(pK_{P2} + pK_N) \qquad (12)$$

where both pK_{P2} and pK_N have already been defined (see eq 6 and 10). This result suggests that protons are exchanged between secondary phosphoric acid functions $-PO_3H^-$ which act as donors and protonable nitrogen atoms N which act as acceptors according to[14]

$$-PO_3H^- + {=}N\text{-} \rightleftharpoons -PO_3^{2-} + {=}NH^+\text{-} \qquad (13)$$

Equation 12, predicts that pH_A should be independent of concentration, in agreement with the experimental results for 5′AMP in the range 0.155–0.02 M and 5′XMP in the range 0.02–0.006 M.

The proton exchange in reaction 13 may be intramolecular and/or bimolecular. The results of Figure 4 show, however, that this reaction is at least in part bimolecular.[25] Indeed a linear variation would be expected in the case of a monomolecular reaction.

Whether or not both intramolecular and bimolecular proton transfers contribute to $(\Delta\alpha/f^2)_A$ cannot be decided on the basis of the results relative to the effect of concentration on $(\Delta\alpha/f^2)_A$ or of pH on α/f^2. The effect of frequency on $(\Delta\alpha/f^2)_A$ has been investigated for this purpose and some preliminary results for 5′AMP have already been reported[26] which support a bimolecular process.

It is now possible to understand the ultrasonic absorption behavior of 5′TMPNH$_4^+$ for which an absorption maximum of extremely large amplitude can be seen in the alkaline range in Figure 2. In this case again we are dealing with a couple donor-acceptor respectively NH_4^+ and 5′TMP$^-$ whose pK_a's are 9.26 and 10.12. Indeed the absorption peak occurs at a pH value equal to (p$K_{NH_4^+}$ + p$K_{5'TMP^-}$)/2 as for reaction 13.

The results for 5′GMP demand an additional remark. This nucleotide comprises a nitrogen atom with a pK_a around 2[12] which yields, according to eq 12, a value of pH_A 4.3. On the other hand, for reaction 9, eq 10 predicts an absorption maximum at pH_A 4.1. The experimental error on pH_A (4.2 ± 0.2) does not permit us to decide whether the observed maximum is due to reaction 13 and/or to reaction 9. A study of the variation of pH_A with concentration might have rendered the choice possible. Unfortunately the 0.2 *M* 5′GMP solution became gel-like in the acid range preventing ultrasonic absorption measurements. We have shown, however, in paragraph III.2b that for 5′GMP the experimental value of $(\Delta\alpha/f^2)_A$ is twice the calculated value for reaction 9. This result may indicate that indeed reactions 9 and 13 contribute together to the absorption maximum of 5′GMP. The contribution of reaction 13 would then be quite small as compared with other nucleotides because of the large difference between the pK_a's of the protonable nitrogen atom and of the secondary phosphoric acid function.

d. Tentative Explanation for the Ultrasonic Absorption of Nucleic Acids. For all the above nucleotides the secondary phosphoric acid function has been involved in the explanation of the observed ultrasonic absorption maxima. However, it is clear that neither reaction 9 nor reactions 11 and 13 can explain the excess ultrasonic absorption of solutions of nucleic acids where the secondary phosphoric acid function is replaced by a phosphate–sugar linkage. The results obtained with 5′AMPNH$_2$ might provide a possible explanation since in this nucleotide the secondary phosphoric acid function is also eliminated. Table I indicates that in going from 5′AMP to 5′AMPNH$_2$ the maximum does not disappear; however, pH_A decreases from 5.05 to 3.15 and $(\Delta\alpha/f^2)_A$ from 76 × 10^{-17} to 13.5 × 10^{-17} cm^{-1} sec^2. The comparison of the ultrasonic absorption curve with the potentiometric titration curve shows that in this case pH_A appears at a pH given by

$$pH_A = \tfrac{1}{2}(pK_{P_1} + pK_N) \qquad (14)$$

where pK_{P1} is the pK_a of the phosphoric acid function and pK_N has been defined in relation 6. This result suggests that in the case of 5′AMPNH$_2$ the ultrasonic absorption maximum results from a transfer between a donor and an acceptor, namely, $-PO_3NH_2H$ and $=N-$. Additional experimental results, however, would be needed for a more precise description of this mechanism (direct proton transfer between donor and acceptor and/or proton transfer through the solvent). Therefore it is not yet possible to give an accurate picture of the process responsible for the excess ultrasonic absorption found in the acid range for DNA[2,4] and RNA,[5] although a mechanism similar to the one involved in 5′AMPNH$_2$ is likely to contribute to this absorption. Indeed an ultrasonic absorption maximum has been found for DNA[4] at 5.69 MHz and at pH 3, *i.e.*, close to that found for 5′AMPNH$_2$ at pH 3.15.

It must be pointed out that nucleic acids contain, in addition to adenine, guanine and cytidine which also have a nitrogen atom which can exchange a proton with the primary phosphoric acid function in the acid range. These exchanges are therefore likely to contribute to the absorption of nucleic acids.

The proton exchange reaction proposed above as the cause of the absorption of nucleic acids in the acid range is at variance with the mechanism suggested in an earlier publication.[2] At that time the ionization of the $=NH^+-$ groups of guanine, cytidine, and adenine was thought to be responsible of the absorption of DNA solutions at pH below 4. We have shown, however, in paragraph III.2a that this reaction (eq 5) contributes a negligible amount to the absorption of nucleotides and nucleosides. Similar calculations show that this is also true for nucleic acids. The above results, however, leave no doubt, in spite of the opinion expressed by other workers,[4] that in the acid range proton transfers cause the absorption changes observed in nucleic acids.

Supplementary Material Available. Additional figures will appear following these pages in the microfilm edition of this volume of the journal. Photocopies of the supplementary material from this paper only or microfiche (105 × 148 mm, 20× reduction, negatives) containing all of the supplementary material for the papers in this issue may be obtained from the Journals Department, American Chemical Society, 1155 16th St., N.W., Washington, D. C. 20036. Remit check or money order for $3.00 for photocopy or $2.00 for microfiche, referring to code number JPC-73-2329.

References and Notes

(1) J. Lang and R. Cerf, *J. Chim. Phys. Physicochim. Biol.*, **66**, 81 (1969).
(2) J. Sturm, J. Lang, and R. Zana, *Biopolymers*, **10**, 2639 (1971).
(3) I. Elpiner, F. Braginskaya, and O. Zorina, *Proc. Int. Congr. Acoust., 7th*, **2**, 153, (1971).
(4) W. D. O'Brien, C. Christman, and F. Dunn, *J. Acoust. Soc. Amer.*, **52**, 1251 (1972).
(5) J. Lang and R. Zana, manuscript in preparation.
(6) R. Musa, *J. Acoust. Soc. Amer.*, **30**, 215 (1958); S. Candau, *Ann. Phys.*, **9**, 271 (1964).
(7) See paragraph at end of paper regarding supplementary material.
(8) Whether the lactim form is present in nonnegligible amount in nucleotide solutions is still open to question. See, for instance, G. C. Y. Lee, J. H. Prestegard, and S. I. Chan, *J. Amer. Chem. Soc.*, **94**, 951 (1972); G. C. Y. Lee and S. I. Chan, *ibid.*, **94**, 3128 (1972); Y. P. Wong, K. L. Wong, and D. M. Kearns, *Biochem. Biophys. Res. Commun.*, **49**, 1580 (1972). This question, however, affects in no way the conclusions of this work.
(9) D. Shugar and F. Fox, *Biochem. Biophys. Acta*, **9**, 199, 369 (1952).
(10) R. C. Parker, L. J. Slutsky, and K. Applegate, *J. Phys. Chem.*, **72**, 3177 (1968); *J. Amer. Chem. Soc.*, **90**, 6906 (1968).
(11) J. Stockx and L. Vandendriessche, *Biochem. Biophys. Acta*, **72**, 137 (1963); J. Clauwaert and J. Stockx, *Z. Naturforsch. B*, **23**, 25 (1968).
(12) R. Philips, P. Eisenberg, P. George, and R. Rutman, *J. Biol. Chem.*, **240**, 4393 (1965).
(13) J. Christensen, J. Rytting, and R. Izatt, *Biochemistry*, **9**, 4907 (1970); R. Izatt, J. Christensen, and J. Rytting, *Chem. Rev.*, **71**, 439 (1971).
(14) M. Eigen, *Angew. Chem., Int. Ed. Engl.*, **3**, 1 (1964).
(15) M. Brennan and K. Kustin, *J. Phys. Chem.*, **76**, 2838 (1972).
(16) J. Rasper and W. Kauzmann, *J. Amer. Chem. Soc.*, **84**, 1771 (1962); W. Kauzmann, A. Bodansky, and J. Rasper, *ibid.*, **84**, 1777 (1962); C. L. Liotta, A. Abidaud, and H. P. Hopkins, Jr., *ibid.*, **94**, 8624 (1972).
(17) A. Peacocke, *Chem. Soc., Spec. Publ.*, **No. 8**, 139 (1957); L. Cavalieri and A. Stone, *J. Amer. Chem. Soc.*, **77**, 6499 (1955).

(18) T. Marshall and E. Grunwald, *J. Amer. Chem. Soc.*, **91**, 4541 (1969).
(19) S. Cabani, G. Conti, L. Lepori, and G. Leva, *J. Phys. Chem.*, **76**, 1343 (1972); L. M. Krausz, S. Fitzig, and E. Gabbay, *J. Amer. Chem. Soc.*, **94**, 9194 (1972).
(20) (a) H. Harned and B. Owen, "Physical Chemistry of Electrolytic Solutions," 3rd ed, Reinhold, New York, N. Y., 1958, p 405; (b) p 755; (c) p 676.
(21) L. M. Rhodes and R. P. Schimmel, *Biochemistry*, **10**, 4426 (1971).
(22) G. P. Rosseti and K. E. Van Holde, *Biochem. Biophys. Res. Commun.*, **26**, 717 (1967); M. Schweizer, A. Broom, P. Ts'o, and D. Hollis, *J. Amer. Chem. Soc.*, **90**, 1042 (1968); J. F. Chantot, M. T. Sarocchi, and W. Guschlbauer, *Biochimie*, **53**, 347 (1971).
(23) P. Mukerjee and A. K. Ghosh, *J. Phys. Chem.*, **67**, 193 (1963).
(24) S. Katz and J. E. Miller, *J. Phys. Chem.*, **75**, 1120 (1971); **76**, 2778 (1972).
(25) B. Michels and R. Zana, *J. Chim. Phys. Physicochim. Biol.*, **66**, 240 (1969).
(26) J. Lang, J. Sturm, and R. Zana, *C. R. Acad. Sci., Ser. C*, **275**, 597 (1972).

Thermodynamics and the Effect of Guanidine Hydrochloride and Potassium Chloride on the Hydrophobic Hydration of Tetra-*n*-butylammonium Bromide and Tetra-*n*-pentylammonium Bromide in Water

B. Chawla, S. Sunder, and J. C. Ahluwalia*

Department of Chemistry, Indian Institute of Technology, Kanpur, India *(Received March 21, 1973)*

The partial molar enthalpies of n-Bu_4NBr and n-Pe_4NBr in 2, 4, and 6 M aqueous guanidine hydrochloride and of n-Bu_4NBr in 2 and 4 M aqueous potassium chloride solutions have been determined calorimetrically at 25 and 35°. These data have been used to derive enthalpies (at 25 and 35°) and heat capacities of transfer (at 30°) of these salts from water to aqueous guanidine hydrochloride and potassium chloride solutions. The results show that transfer of n-Bu_4NBr and n-Pe_4NBr salts from water to both aqueous guanidine hydrochloride and potassium chloride solutions is accompanied by a decrease in their excess partial molar heat capacities indicating that GuHCl and KCl reduce the structure-making or hydrophobic hydration capacity of these salts. However, GuHCl is found to be more effective than KCl in reducing hydrophobic hydration of n-Bu_4NBr. The results are compared with the effects of urea and NaCl on the same salts. The decreasing order (GuHCl > urea > KCl > NaCl) of effectiveness of the various solutes in reducing hydrophobic hydration of n-Bu_4NBr and n-Pe_4NBr correlates well with their decreasing effectiveness in protein denaturation.

Introduction

In continuation of our studies[1-6] of the effect of protein denaturants as well as of nondenaturants on the hydrophobic hydration of model hydrophobic solutes such as R_4N^+ salts, we report in this paper the results on the thermodynamic transfer functions of n-Bu_4NBr and n-Pe_4NBr from water to aqueous guanidine hydrochloride and potassium chloride solutions. This study represents an attempt first to find correlation between the structure-breaking or -making ability of various kinds of solutes and their effectiveness in reducing the hydrophobic hydration of hydrophobic solutes; second, to find a correlation between the effectiveness of solutes in reducing hydrophobic hydration and their effectiveness in protein denaturation.

In some of our recent studies[1,3] it was shown that while urea (up to 7 M) reduces the structure-making or hydrophobic hydration capacity of n-Bu_4NBr and n-Pe_4NBr, NaCl (up to 3 M) enhances the hydrophobic hydration of these solutes. The interpretation of these results[1,3] and those of other studies[7] support the model of Frank and Franks[8] which proposes that urea displaces the water equilibrium from a bulky species involving long-range order to a dense species involving only short-range structure by resembling water in its capacity to form hydrogen bonds but by having the wrong geometry to take part in extended water structures. The conclusions drawn from an excellent discussion of urea-water interactions in a recent detailed study[9] of nuclear magnetic resonance of aqueous urea solutions also support the above model of Frank and Franks.[8] Since there exists a belief that denaturants cause denaturation of proteins by weakening hydrophobic interactions, it would be interesting to study how the effectiveness of the various solutes as denaturants can be correlated with their effectiveness in altering the hydrophobic hydration of model hydrophobic solutes. Recently Mastroianni, *et al.*,[10] have concluded from their heats of dilution studies that the effect of cosolvents DMSO, urea, and GuHCl is to reduce the ability of Bu_4N^+ to promote structure, while NaCl appears not to interfere with the structure promotion by Bu_4N^+. Their results correlate quite well with the effect of cosolvents on protein stability.[10] We thought it would be worthwhile to study the heat capacity of transfer functions to deduce the effect of GuHCl and that of KCl on the hydrophobic hydration of n-Bu_4NBr and n-Pe_4NBr (the most structure-promoting solutes known so far) and to compare their behavior with that of urea and NaCl.

Experimental Section

The submarine calorimeter and the operational procedure for measurements of the integral heats of solution have been described previously,[3,11,12] *n*-Pe_4NBr and *n*-Bu_4NBr were obtained from Eastman Organic Chemicals Distillation Products Industries and were recrystallized from acetone–ether mixture by the method reported in the literature.[13] The recrystallized salts were dried *in vacuo* for several hours at 60°. The samples bulbs were filled with salts, dried to constant mass at 80°, and then sealed *in vacuo*. Guanidine hydrochloride (Fluka, A.G.-Pract.) was recrystallized from water containing HCl at pH 4.6 and dried *in vacuo* at 60°. Analytical reagent grade potassium chloride (assay >99.8%) was obtained from BDH Ltd. and was used as received. Deionized distilled water was used for making aqueous guanidine hydrochloride and aqueous potassium chloride solutions. All calorimetric measurements were made with freshly prepared guanidine hydrochloride and potassium chloride solutions.

Results

The values of partial molar heats of solutions $\Delta\bar{H}_s$ of *n*-Bu_4NBr and *n*-Pe_4NBr in 2, 4, and 6 *M* aqueous GuHCl solutions as well those of *n*-Bu_4NBr in 2 and 4 *M* KCl at 25 and 35° are given as supplementary material.[14] Since the measurements of $\Delta\bar{H}_s$ of *n*-Bu_4NBr and *n*-Pe_4NBr in aqueous GuHCl and that of *n*-Bu_4NBr in aqueous KCl solutions were carried out in very dilute solutions of *n*-Bu_4NBr and *n*-Pe_4NBr (0.3×10^{-3}–3×10^{-3} *M*) wherein any concentration effect is masked by the experimental error, the value of the limiting partial molar enthalpy $\Delta\bar{H}_s°$ was taken as the average of $\Delta\bar{H}_s$ values. The uncertainties in the $\Delta\bar{H}_s°$ values are computed as 95% confidence limits. The values of $\Delta\bar{H}_s°$ of *n*-Bu_4NBr and *n*-Pe_4NBr in 2, 4, and 6 *M* GuHCl and of *n*-Bu_4NBr in 2 and 4 *M* KCl solutions are given in Tables I, II, and III, respectively, along with the $\Delta H_s°$ values of these salts in pure water at the same temperatures reported earlier from this laboratory.[15] The enthalpies of transfer ΔH_{tr} ($\Delta H_{tr} = \Delta\bar{H}_s° - \Delta H_s°$) of *n*-$Bu_4NBr$ and *n*-Pe_4NBr from water to 2, 4, and 6 *M* GuHCl solutions are listed in Tables I and II, respectively, and plotted against molarity of GuHCl in Figure 1. The enthalpies of transfer of *n*-Bu_4NBr from water to aqueous KCl solutions at 25 and 35° are listed in Table III and plotted against molarity of KCl in Figure 1. The excess partial molar heat capacities, $\Delta\bar{C}_p°$ of *n*-Bu_4NBr and *n*-Pe_4NBr in aqueous GuHCl solutions, and those of *n*-Bu_4NBr in aqueous KCl solutions at 30° derived from the $\Delta\bar{H}_s°$ values by the integral heat method, are also listed in Table I, II, and III, respectively. The partial molar heat capacities of transfer ΔC_{ptr} of *n*-

TABLE I: Partial Molar Thermodynamic Functions of Transfer of Tetra-*n*-butylammonium Bromide from Water to Aqueous Guanidine Hydrochloride Solutions

	25.0°		35.0°		30.0°	
[GuHCl], *M*	$\Delta\bar{H}_s°$,[a] cal mol^{-1}	ΔH_{tr}, cal mol^{-1}	$\Delta\bar{H}_s°$,[a] cal mol^{-1}	ΔH_{tr}, cal mol^{-1}	$\Delta\bar{C}_p°$, cal K^{-1} mol^{-1}	ΔC_{ptr}, cal K^{-1} mol^{-1}
0[b]	−2050 ± 15		−260 ± 15		179 ± 2	
2.0	−1962 ± 17	88 ± 23	−655 ± 23	−395 ± 27	131 ± 3	−48 ± 4
4.0	−1581 ± 22	469 ± 27	−503 ± 20	−243 ± 25	108 ± 3	−71 ± 4
6.0	−1049 ± 34	1001 ± 37	−403 ± 20	−143 ± 25	65 ± 4	−114 ± 4

[a] $\Delta\bar{H}_s°$ values are computed average values with 95% confidence limits. [b] The values of $\Delta H_s°$ in pure water are taken from ref 15.

TABLE II: Partial Molar Thermodynamic Functions of Transfer of Tetra-*n*-pentylammonium Bromide from Water to Aqueous Guanidine Hydrochloride Solutions

	25.0°		35.0°		30.0°	
[GuHCl], *M*	$\Delta\bar{H}_s°$,[a] cal mol^{-1}	ΔH_{tr}, cal mol^{-1}	$\Delta\bar{H}_s°$,[a] cal mol^{-1}	ΔH_{tr}, cal mol^{-1}	$\Delta\bar{C}_p°$, cal K^{-1} mol^{-1}	ΔC_{ptr}, cal K^{-1} mol^{-1}
0[b]	796 ± 29		3791 ± 39		299 ± 5	
2.0	1022 ± 12	226 ± 31	3140 ± 32	−651 ± 50	212 ± 3	−87 ± 6
4.0	1314 ± 27	518 ± 40	2767 ± 29	−1024 ± 41	145 ± 4	−154 ± 6
6.0	1623 ± 23	827 ± 37	2441 ± 32	−1350 ± 50	82 ± 4	−217 ± 6

[a,b] See corresponding footnotes to Table I.

TABLE III: Partial Molar Thermodynamic Functions of Transfer of Tetra-*n*-butylammonium Bromide from Water to Aqueous Potassium Chloride Solutions

	25.0°		35.0°		30.0°	
[KCl], *M*	$\Delta\bar{H}_s°$,[a] cal mol^{-1}	ΔH_{tr}, cal mol^{-1}	$\Delta\bar{H}_s°$,[a] cal mol^{-1}	ΔH_{tr}, cal mol^{-1}	$\Delta\bar{C}_p°$, cal K^{-1} mol^{-1}	ΔC_{ptr}, cal K^{-1} mol^{-1}
0[b]	−2050 ± 15		−260 ± 15		179 ± 2	
2.0	−1828 ± 25	222 ± 29	−220 ± 4	40 ± 16	161 ± 3	−18 ± 4
4.0	−1048 ± 32	1002 ± 35	465 ± 22	725 ± 27	151 ± 4	−28 ± 4

[a,b] See corresponding footnotes to Table I.

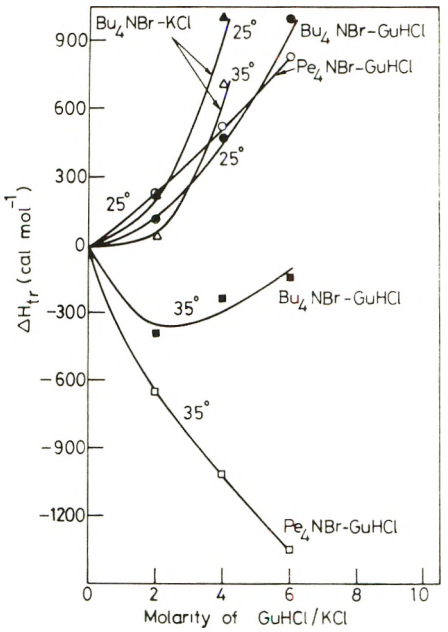

Figure 1. Enthalpy of transfer of n-Bu_4NBr and n-Pe_4NBr from water to aqueous guanidine hydrochloride and potassium chloride solutions as a function of molarity of guanidine hydrochloride and potassium chloride at 25 and 35°:(●) ΔH_{tr} for n-Bu_4NBr from water to aqueous GuHCl at 25°; (■) ΔH_{tr} for n-Bu_4NBr from water to aqueous GuHCl at 35°; (○) ΔH_{tr} for n-Pe_4NBr from water to aqueous GuHCl at 25°; (□) ΔH_{tr} for n-Pe_4NBr from water to aqueous GuHCl at 35°; (▲) ΔH_{tr} for n-Bu_4NBr from water to aqueous KCl at 25°; (△) ΔH_{tr} for n-Bu_4NBr from water to aqueous KCl at 35°.

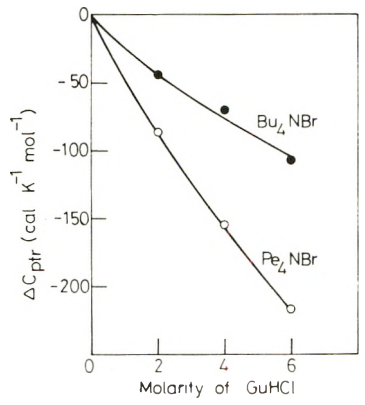

Figure 2. Excess partial molar heat capacity of transfer of n-Bu_4NBr and n-Pe_4NBr from water to aqueous guanidine hydrochloride solution as a function of molarity of guanidine hydrochloride at 30°.

Bu_4NBr and n-Pe_4NBr from water to aqueous GuHCl solutions are listed in Tables I and II and plotted against molarity of GuHCl in Figure 2. ΔC_{ptr} values of n-Bu_4NBr from water to aqueous KCl solutions are listed in Table III and plotted against molarity of KCl in Figure 3. For comparison, ΔC_{ptr} of n-Bu_4NBr and n-Pe_4NBr in aqueous urea, GuHCl, and NaCl and KCl (only for n-Bu_4NBr) are also plotted in Figure 3.

Discussion

The results given in Figure 1 show that the transfer of n-Bu_4NBr and n-Pe_4NBr from water to aqueous GuHCl solutions at 25° and n-Bu_4NBr from water to aqueous KCl solutions (at 25 and 35°) is accompanied by an increase in enthalpy which becomes appreciably larger with increasing concentration of GuHCl and KCl. These results are similar to those observed (for n-Bu_4NBr and n-Pe_4NBr) in aqueous urea and aqueous sodium chloride solutions[1-3] at 25 and 35°. However, at 35° while the ΔH_{tr} of n-Bu_4NBr from water to GuHCl decreases upto 2 M GuHCl increasing with further increasing concentration of GuHCl, the ΔH_{tr} of n-Pe_4NBr from water to GuHCl decreases appreciably with increasing concentration of GuHCl (up to 6 M).

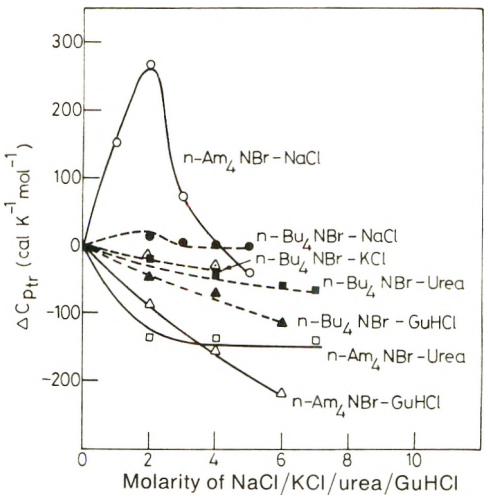

Figure 3. Excess partial molar heat capacity of transfer of n-Bu_4NBr and n-Pe_4NBr from water to aqueous sodium chloride, potassium chloride, urea, and guanidine hydrochloride solutions as a function of molarity of NaCl/KCl/urea/GuHCl at 30°.

Since the enthalpies of transfer represent the combined contribution of various effects it may not be correct to correlate them with the structural changes occurring in aqueous solutions. Therefore, we will limit our discussion to the excess partial molar heat capacities which reflect directly the structural changes occurring in aqueous solutions. The very large positive values of the excess partial molar heat capacities (at 30°) of n-Bu_4NBr[12] (ΔC_p° = 179 ± 2 cal deg^{-1} mol^{-1}) and n-Pe_4NBr[15] (ΔC_p° = 299 ± 5 cal deg^{-1} mol^{-1}) ascribe them to be great structure promotors. The results given in Tables I and II and Figure 2 show that the heat capacity of transfer of both these salts from water to aqueous GuHCl is negative and the negative value goes on increasing appreciably with increasing concentration of GuHCl. The values of ΔC_{ptr} (at 30°) are as much as −114 and −217 cal deg^{-1} mol^{-1} for n-Bu_4NBr and n-Pe_4NBr at 6 M GuHCl, respectively. This indicates a large decrease in the hydrophobic hydration capacity of both these salts brought about by the addition of GuHCl. The larger decrease in the case of n-Pe_4NBr as compared to that of n-Bu_4NBr is understandable because of the larger structure-making capacity of n-Pe_4NBr as compared to that of n-Bu_4NBr. In Figure 3 are shown the ΔC_{ptr} of n-Bu_4NBr and n-Pe_4NBr from water to aqueous solutions of GuHCl, urea, and NaCl. In addition the ΔC_{ptr} values for n-Bu_4NBr from water to aqueous solutions of KCl are also shown in Figure 3. The negative and positive values of ΔC_{ptr} imply the reduction and enhancement of hydrophobic hydration, respectively. It may be observed that the effect on the hydrophobic hydration capacity of both the solutes in the aqueous solutions of GuHCl, urea, and NaCl is more or less similar, the effect being larger in case of n-Pe_4NBr. The comparative effect of solutes GuHCl, urea, NaCl, and KCl on the effect of

hydrophobic hydration of n-Bu_4NBr and n-Pe_4NBr may also be seen in Figure 3. As discussed in our previous studies,[1,3] urea has almost no net effect on the structure of water (ΔC_p° in pure water being 3 ± 6 cal deg^{-1} mol^{-1}) yet it appreciably reduces the structure-making or hydrophobic hydration capacity of n-Bu_4NBr and n-Pe_4NBr. NaCl, a slight structure-breaker according to its negative ΔC_p° and $\bar{C}_{p_2}^\circ$ values[16] (though other evidence indicates it may be a structure maker[10]), shows an opposite effect, *i.e.*, enhancement of the hydrophobic hydration of n-Bu_4NBr and n-Pe_4NBr[1,2] up to 4 *M* NaCl concentration. Guanidine hydrochloride, which according to its negative ΔC_p° values in pure water could be classified as structure breaker, reduces tremendously the structure making capacity or the hydrophobic hydration capacity of n-Bu_4NBr and n-Pe_4NBr. In fact the effect of GuHCl is greater than that of urea for a similar concentration. It is interesting to note the correlation between the effectiveness of 4 *M* GuHCl and 7 *M* urea in protein denaturation and reduction in hydrophobic hydration of n-Bu_4NBr and n-Pe_4NBr. KCl is also known to act as structure breaker.[17] Our results on the excess partial molar heat capacities of KCl[18] and GuHCl[5] in water at infinite dilution at 30° indicate that KCl is more effective as a structure breaker than GuHCl, ΔC_p° values being −38 and −16.5 cal deg^{-1} mol^{-1} for KCl and GuHCl, respectively. However, it may be noted (see Figure 3) that KCl is much less effective in reducing hydrophobic hydration of n-Bu_4NBr than guanidine hydrochloride.

It may be concluded from the above discussion (i) that no correlation exists between the structure-making or -breaking capacity of a solute in pure water and its effect on hydrophobic hydration; (ii) even though urea and GuHCl, both effective denaturants, reduce the hydrophobic hydration, KCl, a nondenaturant (though in some cases KCl destabilizes native protein conformations but its efficacy is so small that it cannot be labeled as a denaturant in the sense urea and GuHCl are) also reduces considerably the hydrophobic hydration. This implies that reduction in hydrophobic hydration by a solute does not necessarily impart to it denaturation characteristics. (iii) However, the positive aspect is that the reduction in hydrophobic hydration caused by the effective denaturants is much more than that caused by corresponding structure-breaking non-denaturants or not so effective denaturants. The order (GuHCl > urea > KCl > NaCl) of decreasing effectiveness of the various solutes in reducing hydrophobic hydration of n-Bu_4NBr and n-Pe_4NBr correlates well with their decreasing effectiveness in protein denaturation. This conclusion finds support from the recent studies of Mastroianni, *et al.*,[10] of the effect of cosolvents NaCl, DMSO, urea, and GuHCl on the heat of dilution of solutions of n-Bu_4NBr. They also concluded that the order NaCl < DMSO < urea < GuHCl is both the order of increasing effectiveness as a denaturant and the order of increasing effectiveness in destroying the structure-making ability of Bu_4N^+.

Acknowledgment. We are thankful to the Council of Scientific and Industrial Research, India, for the award of Junior Research Fellowships to B. Chawla and S. Sunder.

Supplementary Material Available. A detailed listing of $\Delta \bar{H}_s$ values will appear following these pages in the microfilm edition of this volume of the journal. Photocopies of the supplementary material from this paper only or microfiche (105 × 148 mm, 20× reduction, negatives) containing all of the supplementary material for the papers in this issue may be obtained from the Journals Department, American Chemical Society, 1155 16th St., N.W., Washington, D. C. 20036. Remit check or money order for $3.00 for photocopy or $2.00 for microfiche, referring to code number JPC-73-2335.

References and Notes

(1) B. Chawla and J. C. Ahluwalia, *J. Chem. Soc., Faraday Trans. 1*, **69**, 434 (1973).
(2) B. Chawla and J. C. Ahluwalia, *J. Phys. Chem.*, **76**, 2582 (1972).
(3) T. S. Sarma and J. C. Ahluwalia, *J. Phys. Chem.*, **76**, 1366 (1972).
(4) B. Chawla, S. Subramanian, and J. C. Ahluwalia, *J. Chem. Thermodyn.*, **4**, 575 (1972).
(5) S. Subramanian, T. S. Sarma, D. Balasubramanian, and J. C. Ahluwalia, *J. Phys. Chem.*, **75**, 815 (1971).
(6) S. Subramanian, D. Balasubramanian, and J. C. Ahluwalia, *J. Phys. Chem.*, **73**, 266 (1969).
(7) R. B. Cassel and W. Y. Wen, *J. Phys. Chem.*, **76**, 1369 (1972).
(8) H. S. Frank and F. Franks, *J. Chem. Phys.*, **48**, 4746 (1968).
(9) E. G. Finer, F. Franks, and M. J. Tait, *J. Amer. Chem. Soc.*, **94**, 4424 (1972).
(10) M. J. Mastroianni, M. J. Pikal, and S. Lindenbaum, *J. Phys. Chem.*, **76**, 3050 (1972).
(11) S. Subramanian and J. C. Ahluwalia, *J. Phys. Chem.*, **72**, 2525 (1968).
(12) T. S. Sarma, R. K. Mohanty, and J. C. Ahluwalia, *Trans. Faraday Soc.*, **65**, 2333 (1969).
(13) A. K. Unni, L. Elias, and H. I. Schiff, *J. Phys. Chem.*, **67**, 1216 (1963).
(14) See paragraph at end of paper regarding supplementary material.
(15) R. K. Mohanty and J. C. Ahluwalia, *J. Chem. Thermodyn.*, **4**, 53 (1972).
(16) C. M. Criss and J. W. Cobble, *J. Amer. Chem. Soc.*, **83**, 3223 (1961).
(17) H. S. Frank and W. Y. Wen, *Discuss. Faraday Soc.*, **24**, 133 (1957).
(18) B. Chawla, S. Sunder, and J. C. Ahluwalia, unpublished results.

Equilibrium Studies by Electron Spin Resonance. IV. Enthalpies of Ion Pairing for Substituted Nitrobenzene Anion Radicals

Gerald R. Stevenson* and Luis Echegoyen

Chemistry Department, University of Puerto Rico, Rio Piedras, Puerto Rico 00931 *(Received April 11, 1973)*

Publication costs assisted by the University of Puerto Rico

The anion radicals of several substituted nitrobenzenes have been prepared by alkali metal reduction in hexamethylphosphoramide. For the systems in which the σ^+ value of the para substituent is less than 0.7, the esr spectra for the "free" ion and ion pair were observed simultaneously. $\Delta H°$ for the reaction between the ion pair and "free" ion was determined from temperature-dependent studies. $\Delta H°$ was found to correlate linearly with the σ^+ values of the para substituents. The negative value of ρ indicates that the enthalpy of the dissociation of the ion pair to form the "free" ion increases with the electron-withdrawing ability of the para substituent. This is due to the fact that there is more ordering of the solvent by weaker ion pairs.

To date there have been two reports of thermodynamic parameters controlling equilibria between a simultaneously observed anion radical ion pair and free ion.[1,2] Allendoerfer and Papez[1] have determined the enthalpy and other thermodynamic parameters for the equilibrium between the ion pair and free ion of alkali metal durosemiquinone solutions. More recently we have reported the simultaneous observation of the "free" ion and ion pair of nitrobenzene[2] ($PhNO_2$) and the enthalpies of ion pairing for the $PhNO_2$–hexamethylphosphoramide (HMPA)–metal systems.[3]

$PhNO_2$ reduced by lithium metal in HMPA yields a solution that not only contains the $PhNO_2$ "free" ion and ion pair, but it also contains the $PhNO_2$ dianion.[4] This fact makes it difficult to obtain the metal concentration for the metal that is not involved in ion pairing. This metal concentration is necessary in order to obtain the true thermodynamic equilibrium constant for the ion pair dissociation, eq 1. However, since the M^+ concentration is

$$\beta \rightleftarrows \alpha + M^+ \qquad \text{where } \beta = \text{ion pair} \qquad (1)$$

much larger than the concentration of the "free" ion (α), a plot of simply ln $(\alpha)/(\beta)$ *vs.* $1/RT$ yields a straight line with a slope of $-\Delta H°$ of dissociation of the ion pair.[3]

Esr has previously been used to determine the Hammett–Streitwieser correlation constants relating the coupling constants for substituted $PhNO_2$ anion radicals with σ values.[5] Krygowski, *et al.*,[6] have found that a linear correlation is obtained between the half-wave potential for the polarographic reduction of a series of nitroaromatic compounds and σ_r (the Streitwieser position constant).[7] However, there are no reports of a Hammett correlation with ion pairing equilibria. This correlation would be important to provide information as to the variation of the structure of ion pairs with changes in the charge density for the ion pair. Here we wish to report the enthalpies of ion pair dissociation for some para-substituted $PhNO_2$ anion radicals and a positive correlation of these enthalpies to Brown's σ^+ values.

Results

Para-substituted nitrobenzenes (I–XII) have been reduced to their respective anion radicals with lithium metal in HMPA. The coupling constants for the anion radicals observed are given in Table I.

Only for the compounds I–VIII, which have σ^+ values between 0.7 and −0.3, was it possible to observe the "free" ion and the ion pair simultaneously, Figure 1. For the para-substituted $PhNO_2$–HMPA–Li systems where the para substituent has a σ^+ value between 0.3 and −0.3 only the "free" ion could be observed at −10°, and only the ion pair could be observed at high temperatures, about 80°. The nitrogen hyperfine coupling constants, A_N, for the "free" anion radicals are insensitive to temperature changes and have the values given in Table I, while those for the ion pairs always increase with increasing temperature. At intermediate temperatures, relative esr line intensities are taken from the line height multiplied by the extrema to extrema line width squared.

Plots of ln $(\alpha)/(\beta)$ *vs.* $1/RT$ for all of these systems yield straight lines with slopes that are independent of the concentrations of anion radical, Figure 2. These simple modified van't Hoff plots yield slopes of $-\Delta H°$ for the ion pair dissociation reaction, eq 1. The enthalpy of equilibrium 1 varies greatly with the para substituent. Subjecting these data to a Hammett type correlation, we have obtained a reasonably linear relationship between σ^+ values for the para substituent and $\Delta H°$ of the dissociation reaction, Figure 3. The slope of the line resulting from a plot of $\Delta H°$ *vs.* σ^+ is taken to be $-RT\rho$. At 25° ρ has a value of -23 ± 4. The error represents the standard deviation taken from a computer analysis of the best slope. A more accurate determination of ρ would necessitate the use of more para-substituted nitrobenzenes. However, the choice of para substituents is severely limited in that the anion radical of the compound must be thermally stable, the anion radical must allow simultaneous observation of the ion pair and the "free" ion, and the two superimposed spectra must be simple enough for analysis.

Compounds IX–XI gave only the "free" ion upon reduction with Li in HMPA. For the case of *p*-dinitrobenzene the two nitrogen coupling constants are identical with those of the protons yielding an esr spectrum consisting of nine equally spaced lines. The intensities, 0.9:5.1:15:30:36:30:15.5:5.1:0.9, compared to the theoretical values, 1:6:17:30:36:30:17:6:1, give excellent agreement.

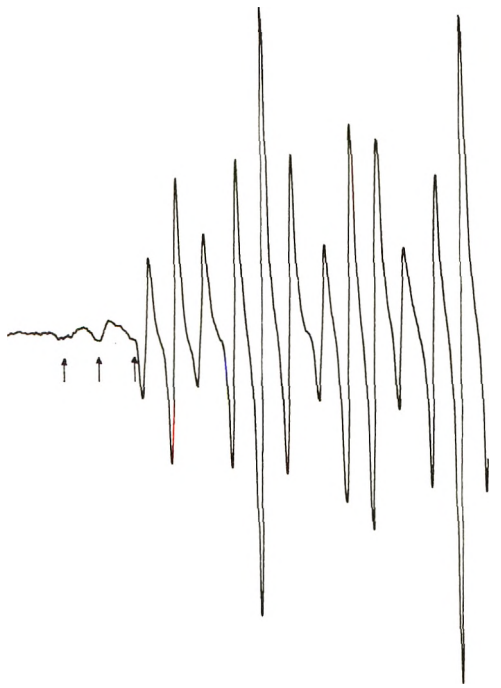

Figure 1. Low-field half of the esr spectrum for the system *p*-chloronitrobenzene–HMPA–Li at 25°. The arrows mark the first three lines of the ion pair. At lower temperatures only the "free" ion is observed, and at high temperatures only the ion pair is observed.

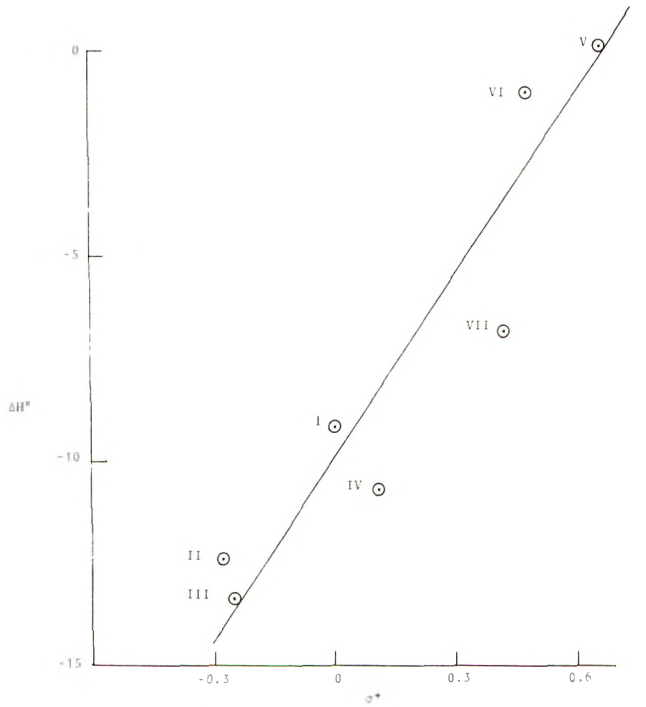

Figure 3. A plot of ΔH° of dissociation of the ion pair to form the "free" ion *vs.* the σ^+ value of the substituents I–VII. ρ taken from this plot is −23.

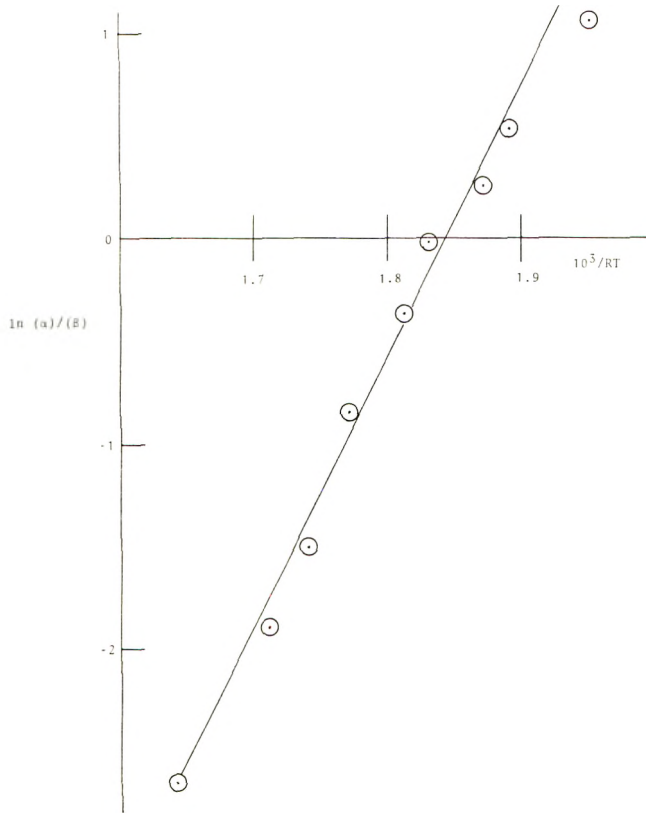

Figure 2. A plot of ln $(\alpha)/(\beta)$ *vs.* $1/RT$ for the system *p*-isopropylnitrobenzene–HMPA–Li.

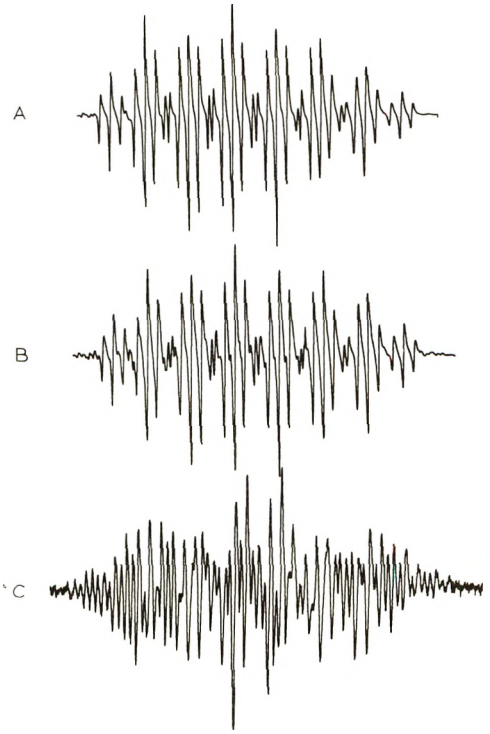

Figure 4. Esr spectra of the $PhNO_2$–HMPA–Na system as a function of temperature: (A) −10°, "free" ion; (B) 20°, "free" ion and ion pair simultaneously; (C) 70°, ion pair.

For the system XII–HMPA–Li only one anion radical could be observed between −10 and 80°. The coupling constant for the nitrogen is 10.82 G, Table I. This value is too large to be attributed to the "free" ion even for the electron-pushing methoxy group. Further, A_N increases with increasing temperature, and all of the "free" ions show A_N's that are independent of temperature. This conclusion is confirmed by the fact that sodium and lithium reductions exhibit pronounced g tensor anisotropy (this is characteristic of ion pairs).[8]

For the system $PhNO_2$–HMPA–Na, only the "free" anion radical is observed at −10°, while above 80° only the ion pair is apparent, Figure 4. Unlike the Li reductions,

TABLE I: Coupling Constants in Gauss, Enthalpies of Equilibrium 1, and σ^+ Values for the Para Substituents for the Systems Para-Substituted $PhNO_2$–HMPA–Li at 25°

		"Free" ion				Ion pair					
Compd	Substituent	A_N	A_o	A_m	A_{subst}	A_N	A_o	A_m	A_{subst}	σ^+ [b]	$-\Delta H°$, kcal/mol
I	H	8.48[a]	3.34	1.01	4.22 (H)	10.85	3.40	1.09	4.10	0	9.0 ± 0.8
II	*i*-Pro	8.93	3.44	1.00	1.89 (H)	11.39	3.43	1.11	1.92	−0.28	12.5 ± 1.2
III	*t*-Bu	8.85	3.43	1.23		11.25	3.44	1.18		−0.25	13.3 ± 0.8
IV	Cl	7.77	3.43	1.08		10.27	3.58	1.24		0.11	10.8 ± 0.4
V	CN	4.90	2.89	0.51	0.86 (1N)	9.81	2.9	0.5	0.9	0.66	0
VI	$COOCH_3$	5.18	2.76	0.40	0.40 (3H)	7.63	2.8	0.4	0.4	0.48	1.1 ± 0.2
VII	$CONR_2$	6.53	3.09	0.80		9.97	3.09	1.14		0.4[c]	7.0 ± 0.6
VIII	Et	8.71	3.36	1.02	3.09 (2H)	11.17	3.36	1.02	3.09	−0.30	
IX	CHO	3.54	0.12	0.12	2.61 (H)	No ion pair was observed					
			1.92	1.70							
X	NO_2	1.16	1.16	1.16	1.16 (1N)	No ion pair was observed				0.79	
XI	COPh	3.92	2.30			No ion pair was observed					
XII	OCH_3	No "free" ion was observed				10.82	3.46	1.13	0.26	−0.78	

[a] The uncertainty in the coupling constants is 0.05 G for all cases where three significant figures are given. [b] σ^+ values are taken from C. D. Ritchie and W. F. Sager, *Progr. Phys. Org. Chem.*, **2**, 334 (1964). [c] σ^+ for this group has not been reported. The value given is estimated from that for CONH.

metal splitting from the Na nuclei is observed at all temperatures for the ion pair. Owing to the large amount of overlap between the "free" ion and ion pair spectra, the ratio of (α) to (β) could only be determined accurately over a narrow temperature range. The plot of ln (α)/(β) *vs.* $1/RT$ yields an enthalpy of −7.2 kcal/mol for dissociation of the ion pair.

Addition of hexane to solutions containing the two ions always increases the concentration of the ion pair at the expense of the "free" ion.

Discussion

It has been established that the two ions simultaneously observed by esr are the "free" ion and ion pair.[2,4,9] Here we have observed that the enthalpy for the ion pair dissociation (eq 1) is a function of the para substituent, but all of the systems for which $\Delta H°$ could be determined yield a negative $\Delta H°$. The negative values of $\Delta H°$ indicate that there is more solvent ordering due to the "free" ion plus the cation than there is for the ion pair. This is in agreement with the work of Hirota.[10] For the para-substituted $PhNO_2$–HMPA–Li systems the large negative enthalpies of ion pair dissociation are a result of the strong solvation of the unassociated cation by the HMPA. Tighter ion pairs are generated by stronger electron-pushing groups in the para position, which increases the charge density in the NO_2 group, thus requiring less solvation of the cation by the HMPA. From this it is obvious that the ion pair dissociation involving tighter ion pairs will yield more negative enthalpies. The "free" ion plus the solvated lithium cation, however, have essentially the same solvation shield for all of the systems studied. This would require that the enthalpy for reaction 2 would grow more negative with the electron-releasing character of the para substituent. This is in accord with our observed negative ρ value. We should note here that $\Delta G°$ changes in the opposite direction with the para substituent. Of course, this is due to $\Delta S°$, which is negative for reaction 1.

For the cases of strong electron-withdrawing groups, *i.e.*, NO_2, CN, CHO, etc., very little if any ion pairing is observed. This is the expected result, since the charge density on the NO_2 group is relatively small, as evidenced by the lower A_N's for these systems. The *p*-methoxy group has just the opposite effect. The increased charge density on the NO_2 group due to the electron-pushing nature of this substituent ($\sigma^+ = -0.78$) favors the ion pair, accounting for the fact that only the ion pair is observed in solution.

Increasing the temperature always results is an increase in A_N for the ion pair due to the fact that the dielectric constant of the solvent decreases with increasing temperature allowing the formation of tighter ion pairs. This same effect was observed when hexane was added to the HMPA solutions. The fact that ion pairing increases at higher temperatures is confirmed by the observation that A_{Na} increases with increasing temperature for the $PhNO_2$–HMPA–Na system. Decreasing the dielectric constant of the solvent by the addition of hexane also has the same effect upon the ratio of (α) to (β) as does increasing the temperature.

The sign of ρ, the large negative values of $\Delta H°$, and the variation of A_N and A_{Na} for the ion pairs all indicate stronger solvent interactions with the unassociated cation and "free" ion than with the ion pair. The large negative value for ρ (−23) is explained in part by the fact that HMPA is the most powerful cation solvator known,[11] and small changes in the structure of the ion pair result in large changes in the heat of solution of the ion pair.

Experimental Section

The esr spectrometer system and the method of formation of the anion radicals were exactly the same as previously described.[3]

p-Ethyl- and *p*-isopropylnitrobenzene were prepared by nitration of the corresponding alkylbenzene. The products were purified by vacuum distillation and preparative gas–liquid chromatography. The *N*-methyl-*N*-*tert*-butyl-*p*-nitrobenzamide[12] and *p*-nitromethylbenzoate[13] were prepared as described in the literature. All of the remaining compounds were purchased from Aldrich Chemical Co. and recrystallized before use.

Acknowledgment. We are very grateful to Research Corporation for support of this work. We also wish to thank Dr. G. M. Rubottom for helpful discussion.

References and Notes

(1) R. D. Allendoerfer and R. J. Papez, *J. Phys. Chem.*, **76**, 1012 (1972).
(2) G. R. Stevenson, L. Echegoyen, and L. R. Lizardi, *J. Phys. Chem.*, **76**, 2058 (1972).
(3) G. R. Stevenson, L. Echegoyen, and L. R. Lizardi, *J. Phys. Chem.*, **76**, 1439 (1972).
(4) G. R. Stevenson and L. Echegoyen, *J. Phys. Chem.*, submitted for publication.
(5) W. C. Danen, C. T. West, T. T. Kensler, and T. J. Tipton, *J. Amer. Chem. Soc.*, **94**, 4830 (1972).
(6) T. M: Krygowski, M. Stencel, and Z. Galus, *J. Electroanal. Chem.*, **39**, (1972).
(7) A. Streitwieser, Jr., "Molecular Orbital Theory for Organic Chemists," Wiley, New York, N. Y., 1962, p 326.
(8) G. R. Stevenson and L. Echegoyen, unpublished results.
(9) G. R. Stevenson and H. Hidalgo, *J. Phys. Chem.*, **77**, 1027 (1973).
(10) N. Hirota, *J. Phys. Chem.*, **71**, 127 (1967).
(11) H. Normant, *Angew. Chem., Int. Ed. Engl.*, **6**(12), 1046 (1967).
(12) G. M. Rubottom, *Tetrahedron Lett.*, **44**, 3887 (1969).
(13) R. E. Ireland, D. A. Evans, D. Glover, G. M. Rubottom, and H. Young, *J. Org. Chem.*, **34**, 3717 (1969).

Transitions in Mesophase Forming Systems. V. Kinetics of Transformation and Properties of Cholesteryl Stearate[1]

Fraser P. Price* and Joachim H. Wendorff

Polymer Science and Engineering, University of Massachusetts, Amherst, Massachusetts 01002

(Received March 15, 1973)

Publication costs assisted by the National Institutes of Health

The equilibrium density-temperature behavior and the interphase transformation kinetics have been studied for carefully purified cholesteryl stearate employing the techniques of precision dilatometry. In the crystalline solid the density at a given temperature depends upon the thermal path followed in attaining that temperature. The effect is not large, amounting to at most 5% in the density. However, it is reproducible and does not seem to be due to voids in the sample. There is an approximately 5% volume change at the solid–isotropic transition temperature of 81.5°. The isotropic–cholesteric volume change is 0.17% and occurs at 77.5°. The transformation kinetics into the solid state indicate the homogeneous nucleation of spheres at temperatures below 74.7°. The isotropic–cholesteric transformation in the range 75.4–77.0° is characterized by the growth of homogeneously nucleated rods which develop from disk-like nucleii. This seems to be the general case for transformations in which the developing phase is a liquid crystal.

Introduction

In this laboratory we are engaged in studies of the transformation kinetics in mesophase forming systems and in the precise determination of the temperature behavior of the densities of these systems. Previously, we have studied cholesteryl acetate,[2] cholesteryl nonanoate,[3] cholesteryl myristate,[4] as well as *p*-azoxyanisole (PAA).[5] All three esters of cholesteryl exhibit a cholesteric phase. In the myristate and the nonanoate this mesophase is enantiotropic while in the acetate it is monotropic. The smectic state does not occur in the acetate, is enantiotropic in the myristate, and is monotropic in the nonanoate. In PAA the nematic mesophase is enantiotropic.[6] All these mesophase formers exhibit density–temperature behavior indicative of marked pretransition effects only on the low-temperature side of the transition. In the cholesteryl esters the rate of transformation from a given state to one stable at a lower temperature usually is sufficiently slow for the kinetics of the transformation to be observed. The transformations into the solid states are particularly slow and apparently are governed by the kinetics of the nucleation process.[7] In PAA, however, the isotropic–nematic transformation is too rapid to follow with our techniques and the transformation into the solid state is also nucleation controlled but it occurs at such high supercoolings that, when it takes place, it occurs essentially instantaneously. In cholesteryl stearate, as in cholesteryl acetate, all the mesophases are monotropic. The solid–isotropic transformation temperature of the stearate is variously given as 81.8–85.1°, the isotropic–cholesteric transition as 71.4–71.0°, and the cholesteric–smectic transition is 69.9°.[8] We are interested in delineating quantitatively the effects of chemical structure on mesophase behavior of the esters of cholesterol and this paper deals with the properties of the various transitions of cholesteryl stearate. We are concerned with the equilibrium values of the densities as well as with the kinetics of transformation.

Experimental Section

Material. The mercury used to fill the dilatometers was obtained from the Sargent Welch Co. (Reagent Grade ACS). Samples of cholesteryl stearate were obtained from the Eastman Kodak Co., Rochester, N. Y. The cholesteryl stearate was purified by recrystallization from 1-pentanol, washed several times with a water–ethanol mixture, and dried under vacuum at various temperatures, up to temperatures above the melting point. Sometimes this recrystallization and washing procedure, without the drying, was repeated several times.

As in previous studies high precision dilatometry was the technique of choice to investigate both the transformation kinetics and the densities of these substances. Details of the experimental techniques are given in previous papers.[2,4,5]

X-Ray Measurements. X-Ray diffraction patterns of a number of samples crystallized under different conditions were taken using a forward reflection camera with pinhole collimation. The radiation used was nickel filtered copper Kα (1.5418 Å). The distance between the sample and the film was 7.3 cm.

Results and Discussion

Previous experience with the cholesteryl esters has indicated that the crystallization behavior and to some extent the final equilibrium properties of the crystallized systems depend to a remarkable extent upon annealing the sample under the appropriate conditions. In the present case, the samples were first heated to 90° for 12 hr in the hopes of getting reproducible measurements. It was subsequently determined that this annealing time was unnecessarily long and that it was sufficient to anneal for 4 hr at 90°. Crystallizations were carried out by quenching from 90° to a series of temperatures in the range of 20–75°. The volumes which were finally attained at the end of such crystallizations fell on a good straight line as is indicated by the crosses in Figure 1. These experiments were reproducible. However, the expansion coefficients of samples crystallized at various temperatures were not the same. Thus, the volume of the sample crystallized at temperature T_1 and subsequently brought to temperature T_2 is not the same as the final volume of the sample crystallized at T_2. The range of this effect is shown in Figure 1 wherein are displayed the volume–temperature relationships for samples crystallized at 75 and at 20°. The values of the expansion coefficients for these particular samples are 3.6×10^{-4} and 3.0×10^{-4} for the samples crystallized at 20 and 75°, respectively. Samples crystallized between these temperatures had intermediate expansion coefficients. Attempts were made to bring the behavior of the various samples into concurrence by annealing at a series of temperatures below the melting point. These attempts were unsuccessful. These remarks along with the equilibrium volume–temperature behavior for the solid state of material crystallized at 20° shown in Figure 2 and for the isotropic–cholesteric transition region displayed in Figure 3 are summarized in Table I. In the solid, nearly linear volume temperature behavior persists up to temperatures very close to the solid–isotropic transition temperature. Further, deviations from this behavior are only weakly dependent upon the temperature of crystallization. The range of actual melting is quite small (*ca.* 2.5°) compared with the melting ranges of cholesteryl myristate (4.5°) and acetate (20°). For the sample crystallized at 20° and displayed in Figure 2, the melting point is 81.5°, as indicated by the end of the melting range. Above this temperature, the isotropic state shows an essentially linear increase of volume with temperature. On cooling down through the isotropic solid transformation temperature to 77.5° and somewhat below, the cholesteric state is obtained. The results displayed in Figure 3 show the volume–temperature behavior for a sample recrystallized three times. The results indicate that there is no hysteresis in the transition and there are no observable pretransition effects on the high-temperature side. As noted with other cholesteryl esters, the expansion coefficient of the cholesteric state exceeds that of the isotropic state. An unusual and somewhat disturbing aspect of this isotropic–cholesteric transition is that its temperature seems to depend upon the

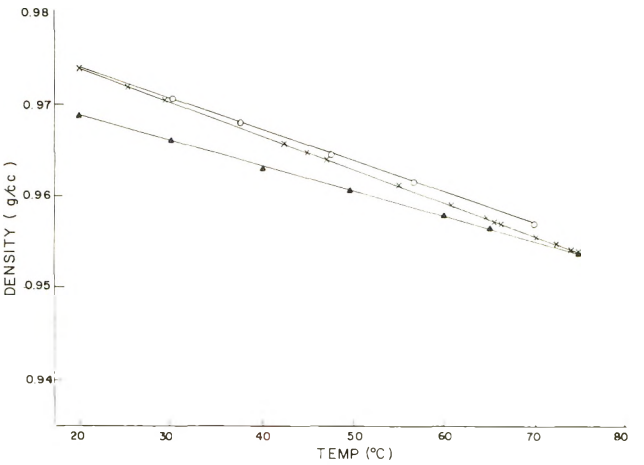

Figure 1. Plot of density of the solid state of cholesteryl stearate as a function of temperature for several different conditions: ×, density finally attained by crystallizing from the isotropic state at this temperature; O, density temperature behavior of material crystallized at 20° from the isotropic state and heated or cooled over the indicated temperature range; ▲, density of material crystallized at 75° and heated or cooled over the indicated temperature range.

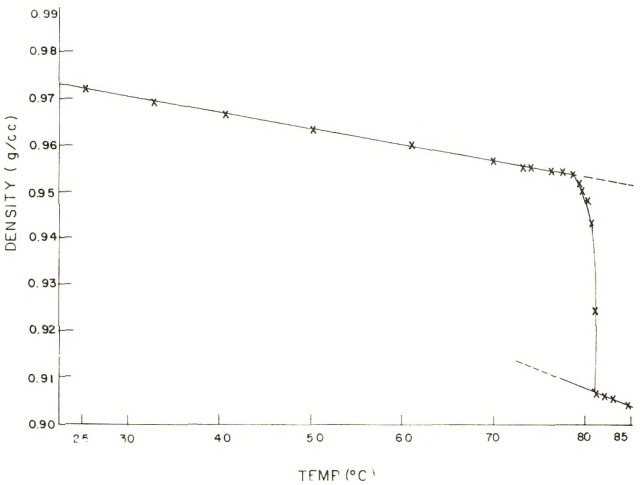

Figure 2. Plot of equilibrium density *vs.* temperature for cholesteryl stearate crystallized at 20°.

TABLE I: Summary of Equilibrium Density Temperature Relations and Transition Behavior of Cholesteryl Stearate

Temp, °C	State	Volume changes at transition, %	α(°C^{-1}) × 10^4
20–79	Solid (crystallized at 20°)		3.6
20–79	Solid (crystallized at 75°)		3.0
$79.0 \leq T \leq 81.5$		4.8[a]	
$81.5 \leq T$	Isotropic[b]		8.1
$T \leq 77.5$	Cholesteric		10.0
$77.0 \leq T \leq 77.5$		0.17	

[a] Crystallized at 20°. [b] Isotropic state studied up to 90°.

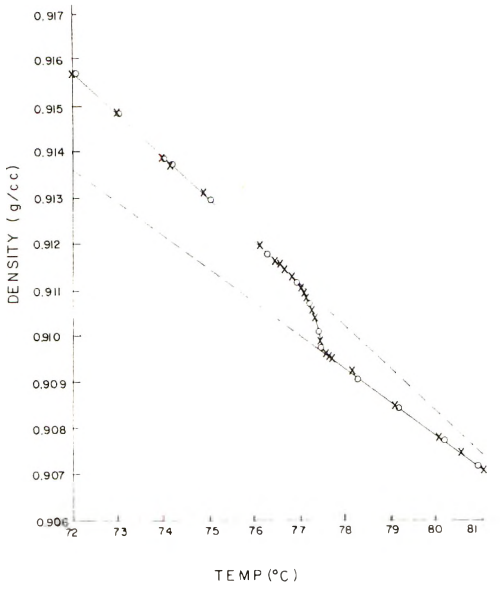

Figure 3. Plot of equilibrium density *vs.* temperature for the cholesteric and isotropic states of cholesteryl stearate: O, temperature decreasing; ×, temperature increasing.

number of recrystallizations which the sample has undergone and that increasing the number of recrystallizations decreases the transition temperature (78.7, 77.8, and 77.5°[6] after one, two, and three recrystallizations, respectively). Among these same samples, the melting points and melting regions of the solid–isotropic transition were identical within experimental error. The decrease of a transition temperature with (presumed) increased purity is unusual. It is possible that the supposed purification process actually introduces impurities. Alternatively, it is also possible that the effect could arise from segregation of impurities in the isotropic rather than in the cholesteric phase. In work with cholesteryl myristate,[4] we observed no such effect with increased number of crystallizations although as the number of recrystallizations was increased the kinetics of the phase transformation changed. The transformation became more rapid as the number of crystallizations was increased. In all the cholesteryl stearate samples studied, the cholesteric–isotropic transition showed a transition region rather than a sharp transition point. The width of this region was essentially constant for all the samples regardless of the number of times they had been crystallized. With the techniques used, we were not able to observe a smectic phase. In the temperature ranges where the smectic phase is supposed to be stable, the crystallization is very fast and the induction period is very short. Thus, no studies were made of the smectic phase.

Since the solid behaved in a somewhat irreproducible manner, in that it was impossible to get all of the volume–temperature relationships to coincide, room temperature X-ray diffraction measurements were carried out on samples crystallized in various temperature ranges in order to see whether there were any obvious structural differences among these samples. The results of these studies are summarized in Table II. In this Table, low-temperature crystallization implies crystallization in the temperature range between 0–40° and high-temperature crystallization between 70–76°. In the low-temperature range, one observes only rings on the photographic plate indicative of a random orientation of the crystals. In the high-temperature range, in many instances, the diagram consisted of sets of points arranged in particular types of patterns, *i.e.*,

TABLE II: Summary of Results of X-Ray Diffraction Study of Crystalline Cholesteryl Stearate Crystallized from the Isotropic State at Different Temperatures

		Crystallization range	
"d" spacing, Å	Strength[a]	Low temperature	High temperature[b]
27.9	S		
18.56	S		
13.85	VW	Rings	Rings
10.04	W	Rings	2P ↕
9.23	W		
7.49	VW	Rings	2P ↔
7.16	VW		
5.97	S	Rings	4P ✖
5.71	W		
5.18	VW		
5.01	W	Rings	2P ↕
4.90	W		
4.77	W		
4.09	S broad	Rings	4P ✖
3.76	S	Rings	2P ↔

[a] S = strong, W = weak, VW = very weak. [b] 2P = two-point diagrams, 4P = four-point diagrams: ↕, ↔, ✖ = direction of orientation.

two points or four points. These results are consistent with the concept that at low temperature many, many crystals are produced, as a result of homogeneous nucleation, and these crystals are all small and oriented at random, whereas, in the higher temperature range, most of the few crystals that are initiated appear as a result of heterogeneous nucleation and result in the diffraction pattern being a set of points. The low-temperature crystallizations undoubtedly take place from the smectic state but the high-temperature crystallization could occur from either the cholesteric or the isotropic phase. While it is possible that the nucleation rate is affected by the initial state (smectic, cholesteric, or isotropic), in the present case this seems improbable because the differences among these states are minimal compared to the differences between each of these and the crystalline state. A few experiments were done in the determination of the X-ray diffraction diagram of crystals grown from solution. These showed no new spacings but the three longest spacings were missing. In Table II, the first column displays the "d" spacings calculated from the usual Bragg relation[9] and the second column indicates qualitatively the strengths of the reflections. The third and fourth columns are concerned with the types of patterns produced at various temperatures. The "d" spacings given in the first column are not identical with the "d" spacings that we have presented in another paper concerned with the X-ray investigation of the structure of cholesteryl stearate.[10] However, in the present case, these samples were all crystallized in bulk. In the other paper, the data presented were from specimens crystallized by slow removal of solvent.

We now turn to a description of the kinetics of transformation from the isotropic state into the cholesteric and solid states. In these experiments, the sample is cooled down from a temperature of around 90° to a temperature below 76°. Crystallization takes place after an induction period which decreases rapidly with decreasing temperature. Depending upon the temperature, the crystallization takes place from either the cholesteric or smectic state.

We will consider first the isotropic–cholesteric transformation. Measurements were carried out on a sample

TABLE III: Avrami Constants for the Isotropic–Cholesteric Transformation in Cholesteryl Stearate with Similar Information for Cholesteryl Myristate Included for Comparison

Stearate				Myristate			
T, °C	$-\Delta T$, °C	n	K, min^{-2}	T, °C	ΔT, °C	n	K, min^{-2}
77.0	0.5	2.0	4.7×10^{-1}	83.25	0.55	2.0	5.8×10^{-1}
76.7	0.8	2.0	7.6×10^{-1}	82.90	0.90	1.9	9.5×10^{-1}
76.4	1.1	2.0	1.08	82.40	1.40	1.9	1.42
76.0	1.5	1.9	2.17	82.10	1.70	1.9	2.23
75.4	2.1	1.9	3.40				
	Av	2.0				Av 1.9	

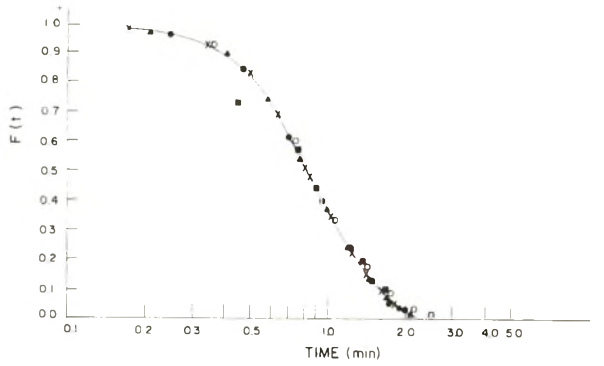

Figure 4. Plots of $F(t)$ *vs.* ln t for the cholesteric–isotropic transformation. Data shifted to 1.1° supercooling. Shift factor in brackets: ×, 77.0° {0.70}; ▲, 76.7° {0.83}; ●, 76.4° {1.0}; ○, 76.0° {1.51}; ■, 75.4° {1.85}.

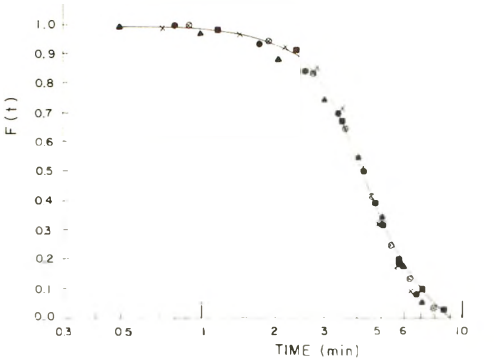

Figure 5. Plots of $F(t)$ *vs.* ln t for cholesteric–solid transformation. Data shifted to 10.4° supercooling. Shift factor in brackets; ×, 74.7° {0.71}; ●, 73.5° {0.85}; ▲, 71.0° {1.0}; ⊗, 63.9° {1.84}; ■, 60.25° {2.40}.

TABLE IV: Avrami Constants for the Isotropic Solid Transformation in Cholesteryl Stearate with Similar Information for Cholesteryl Myristate and Cholesteryl Acetate Included for Comparison

T, °C	ΔT, °C	n	K, min^{-4}
	Stearate		
74.7	7.0	3.8	6.8×10^{-4}
73.5	8.0	3.6	2.5×10^{-3}
71.1	10.4	3.6	6.7×10^{-3}
63.9	17.5	3.8	3.0×10^{-2}
	Myristate		
	33.2	3.9	5.8×10^{-6}
	36.2	4.0	4.5×10^{-5}
	38.3	4.1	3.9×10^{-4}
	43.5	3.9	1.7×10^{-2}
	Acetate		
	21.4	4.0	3.7×10^{-3}
	26.2	4.0	1.4×10^{-2}
	32.2	4.0	1.4×10^{-1}

which had been recrystallized three times. Even at very small supercoolings, the transformation is very rapid. The results are displayed in Table III and Figure 4. In the figure are plotted $F(t)$ (the fraction of the transformation that has not taken place at time t) *vs.* ln t.[4] For the temperature range from 75.4 to 77.0°, in this figure the set of data points for each temperature were shifted along the ln t axis until the best fit was obtained with the set taken at 76.4° (1.1° supercooling). It is seen that with the exception of the lowest temperature data point at the shortest time, all the data can be fitted to one master curve. This is indicative of only one mechanism of transformation taking place over this temperature range. The one point that is off the curve is the one to which one could attach the greatest imprecision. The data were reduced by use of the Avrami equation[4,11] which yields two constants n and K. The first, n, depends upon the modes of nucleation and growth of the transforming regions and the latter, K, reflects the magnitudes of the nucleation and growth processes as well as the mode of growth. Avrami plots of the data shown in Figure 4 yield straight lines and the K values and the n values of these plots are given in Table III along with the comparable data for cholesteryl myristate.[4] It is seen that the stearate has an n of essentially 2 which is indicative of the same type of disk-like nucleation process that was postulated for the myristate. The actual magnitudes of the K values are determined by both the nucleation and the growth rates. However, it has been shown previously that the temperature coefficient of K depends exclusively upon the temperature coefficient of the nucleation rate.[4] In the case of the stearate, it is seen that this material undergoing the isotropic–cholesteric transformation has a slightly more temperature-sensitive nucleation rate than does the myristate.

We turn now to a discussion of the crystallization into the solid state. This transformation also takes place after an induction period which decreases rapidly with decreasing temperature. Thus, at the lower temperatures measured, it is essentially impossible to get a constant volume from which the crystallization takes place. In this situation, the necessary corrections produce results of significantly less precision. In comparison with our previous investigations[2-5] we are less confident in the conclusions of the present work because we do not precisely know what the final volume of the solid state should be, as this volume is dependent upon the crystallization temperature as mentioned above. The differences among the final crystalline volumes in the crystallization range studied are less

than 5% of the total volume change occurring during the transition. Thus, it seems probable that the gross effects of temperature upon the transition can be elucidated. In the results discussed below the final volume used in the calculations obtained by interpolation of the curve with crosses in Figure 1 was that which would have been attained by crystallizing at the particular temperature. The results of the studies of the isotropic-crystalline transformation are displayed in Figure 5 and Table IV. Figure 5 shows plots of $F(t)$ *vs.* ln t for crystallizations taking place in the range 60.25–74.70°. These plots have all been normalized to a supercooling of 10.4° (71.1°), by shifting along the ln t axis. The fact that they are all superposable indicates that here also only one mechanism of transformation is taking place. In concordance with the previous results on the kinetics of crystallization of cholesteryl esters, it seems probable that this is the temperature range in which homogeneous nucleation is predominant. Avrami plots of these data yield straight lines from which it is possible to derive the values of the n and K constants of the Avrami equation. These results are displayed in Table IV along with comparable results for cholesteryl myristate and acetate. The value of the Avrami n of the stearate does not so closely approximate 4.0 as do those for the myristate and the acetate. However, it is close enough to 4.0 to make us believe here again that we have sporadic nucleation of spherically developing transforming regions. A very notable difference in the behavior of the stearate from the other two esters is the small degree of supercooling which is necessary to attain the homogeneous nucleation range. With the stearate, it is less than 10° whereas both the myristate and the acetate required several times that supercooling to attain the region in which homogeneous nucleation was dominant and in which heterogeneous nucleation played an inconsequential part. It has been shown for the myristate, nonanoate, and acetate that the spherulitic growth rates in the crystallization range of interest were essentially independent of temperature.[7] This means that the temperature coefficient of the K's reflects only the temperature coefficient of the nucleation rate. If it is assumed that the stearate behaves similarly then it is noteworthy that the temperature coefficient of the nucleation rate of spherulites of the stearate and the acetate are about the same, increasing about 40-fold in a 10° interval, whereas the myristate is much more temperature sensitive, increasing almost 3000-fold in a similar temperature range. We do not wish to speculate further upon these differences.

Acknowledgments. The authors wish to express their appreciation to Professors R. S. Porter and R. S. Stein for helpful discussion during the course of this investigation.

References and Notes

(1) This work supported by Grant No. HL13188 from the National Institutes of Health.
(2) F. P. Price and J. H. Wendorff, *J. Phys. Chem.*, **75**, 2849 (1971).
(3) F. P. Price and J. H. Wendorff, *J. Phys. Chem.*, **76**, 276 (1972).
(4) F. P. Price and J. H. Wendorff, *J. Phys. Chem.*, **75**, 2839 (1971).
(5) F. P. Price and J. H. Wendorff, *J. Phys. Chem.*, **76**, 2605 (1972).
(6) G. W. Gray, "Molecular Structure and Properties of Liquid Crystals," Academic Press, New York, N. Y., 1962.
(7) F. P. Price and A. K. Fritzsche, *J. Phys. Chem.*, **77**, 396 (1973).
(8) G. J. Davis, R. S. Porter, and E. M. Barrall, III, *Mol. Cryst. Liquid Cryst.*, **10**, 1 (1970).
(9) G. H. Stout, "X-Ray Structure Determination," Macmillan, New York, N. Y., 1968.
(10) J. H. Wendorff and F. P. Price, *Mol. Cryst. Liquid Cryst.*, in press.
(11) M. Avrami, *J. Chem. Phys.*, **7**, 1103 (1939); **8**, 212 (1940).

The Chromium–Iodine System

Chyi-Feng Shieh and N. W. Gregory*

Department of Chemistry, University of Washington, Seattle, Washington 98195 *(Received April 18, 1973)*

Publication costs assisted by the National Science Foundation

Torsion effusion, spectrophotometric, and transpiration experiments have been used to study the equilibria $CrI_3(s) = CrI_2(s) + \frac{1}{2}I_2(g)$, $CrI_3(s) = CrI_3(g)$, $CrI_3(s) + \frac{1}{2}I_2(g) = CrI_4(g)$ in the temperature range 300–600°. Thermodynamic properties and bond energies for the chromium iodides have been derived. Extrapolation of effusion data to zero orifice area gives predicted equilibrium pressures in good agreement with spectrophotometric results. The condensation coefficient of iodine on CrI_3-CrI_2 appears to be *ca.* 10^{-2} and to decrease with increasing temperature. Molar absorptivities of iodine vapor between 100 and 525° have been measured in the interval 370–500 mμ.

The thermal decomposition of chromium(III) iodide was

$$CrI_3(s) = CrI_2(s) + {}^1/_2I_2(g) \quad (1)$$

studied in this laboratory some time ago by measurement of the quantity of iodine vapor leaving effusion cells over relatively long periods of time.[1] Recent studies using the torsion effusion method, which gives steady-state pressures over short time intervals, have shown that vapor concentrations generated by solid-state reactions frequently show a significant fall-off with time as the reaction becomes diffusion controlled.[2] In such a case apparent equilibrium pressures based on collection of total effu-

sate over periods of many hours would reflect only an average of diminishing steady-state pressures and be unsuitable as a basis for derivation of equilibrium characteristics. Indeed in the earlier work[1] apparent equilibrium pressures of iodine based on effusion were found to be somewhat lower than those indicated by a diaphragm gauge experiment in which total pressure in a sealed system was measured at higher temperatures. In the latter, however, a question arises about possible contribution of volatile iodides.

To clarify these matters and to seek evidence concerning the molecular nature and properties of volatile compounds of chromium in iodine atmospheres we have undertaken a reexamination of the chromium–iodine system. Steady-state iodine pressures have been measured by the torsion effusion method, and predicted equilibrium behavior for reaction 1 verified by determination of the equilibrium iodine vapor concentration by a spectrophotometric absorption technique. The dependence of the concentration of volatile iodides of chromium on iodine pressure has also been determined by transpiration experiments in which argon–iodine mixtures were used as a carrier gas. When iodine partial pressures are significant evidence is found for the formation of $CrI_4(g)$. Thermodynamic constants for the various vaporization processes in the system and bond energies for $CrI_3(g)$ and $CrI_4(g)$ have been evaluated.

Experimental Section

The torsion effusion apparatus and the cells used have been described earlier.[3] CrI_3 was prepared by reaction of iodine with chromium powder (Fisher) in an evacuated and sealed Pyrex tube at 500°.[4] A black, shiny crystalline product of relatively small particle size was obtained. This material is not appreciably hygroscopic when pure and was quickly transferred to the various cells without the use of a drybox. The torsion effusion apparatus was flushed with dry nitrogen prior to and while mounting the cells.

About half the volume of the effusion cells was initially filled with CrI_3. Reproducible results at various temperatures over a total period of about 10 hr were obtained except for the largest orifice area cell (no. 2) for which a decrease in steady-state pressure was noticeable after about 3 hr (time dependent on temperature) of heating. Only those results which showed no measurable time dependence were used to derive thermodynamic constants.

The molar absorptivity of iodine vapor was studied between 370 and 500 mμ in the temperature interval 100–525°, using a Cary 14H recording spectrophotometer. The quartz absorption cells, furnace, and general technique have also been described previously.[3,5] Samples A, B, D, and E, obtained from resublimed iodine (Allied), were sublimed into absorption cells, previously pumped to 10^{-6} Torr and baked for 10 hr at 500°. Sample C was prepared by decomposition of CrI_3. A, B, and C, which ranged in concentration from 0.588 to 2.06 m*M* (as determined by subsequent titration with standard $Na_2S_2O_3$), were used to measure the molar absorptivity. D and E were used to verify these results by measurement of the apparent concentration of the saturated vapor of iodine and subsequent comparison with reported vapor pressure data.

The concentration of iodine vapor established by equilibrium 1, using five independent samples, was then determined from absorbance measurements and iodine molar absorptivities over the temperature range 482–539°. The samples studied were prepared in different ways to check for possible solid solution effects. Two samples (of the formation reaction product) were placed directly in absorbance cells, which were then evacuated at 10^{-6} Torr and heated at 200° for several hours before sealing off. The next two samples were heated at 350 and 400° for 0.5 and 1 hr, respectively, to partially decompose the CrI_3. After cooling the cells were sealed off from the vacuum system and small amounts of the solid were mechanically transferred from a side arm into the cell by tilting the apparatus. The remaining excess in the side arm was then sealed off. In the fifth sample a small excess of iodine was introduced along with CrI_3 by heating some excess CrI_3 left in the transfer side arm; the residual matter was then sealed off. Within experimental error all samples gave the same temperature dependent apparent iodine concentrations for equilibrium 1; hence solid solutions of appreciable concentration were assumed not to form.

The transpiration apparatus used to study the volatilization of chromium iodides in argon–iodine mixtures in the temperature range 500–600° was basically the same as that described by Zaugg.[6] An argon–iodine gas mixture was passed over heated samples of CrI_3 and/or CrI_2 formed by decomposition of CrI_3 at flow rates between 20 and 59 ml min^{-1}, calculated at the reaction temperature and pressure; the apparent equilibrium characteristics in the vapor phase were independent of flow rate in this range. As the gas mixture left the equilibrium vessel, the chromium iodide vapors condensed in the exit tube in the cooler regions adjacent to the main furnace; iodine vapor was collected in a following trap, cooled with liquid oxygen (most collected in the tubing just preceding the trap), and argon was collected in a second trap, cooled with liquid nitrogen.

Iodine was initially introduced into the argon carrier gas by permitting the latter to flow through a trap containing crystalline iodine immediately preceding the main furnace and heated to various temperatures to introduce the desired partial pressure of iodine. The quantities of material condensed from the effluent gas stream were determined by titration of iodine with $Na_2S_2O_3$, measurement of the pressure of the evaporated sample of argon in a standard volume, and oxidation of chromium to chromate followed by complexation with diphenylcarbazide and comparison of absorbance against standards with a Beckman DU spectrophotometer as described by Sandell.[7] Dalton's law was then used to relate the relative numbers of moles of the various species to the total pressure, measured manometrically, and the respective partial pressures.

Results and Discussion

Torsion Effusion. Total steady-state pressures in the effusion cells were evaluated from observed angles of rotation and apparatus constants determined by calibration, with the vapor pressure of zinc in the range 286–351° used as a reference standard.[3] The transpiration experiments to be discussed confirm that chromium iodide species do not contribute significantly in the temperature range of the effusion measurements, 300–350°. However the dissociation of I_2 into iodine atoms must be considered; the relative contributions of the two species were evaluated using equilibrium constants for the dissociation provided in the JANAF

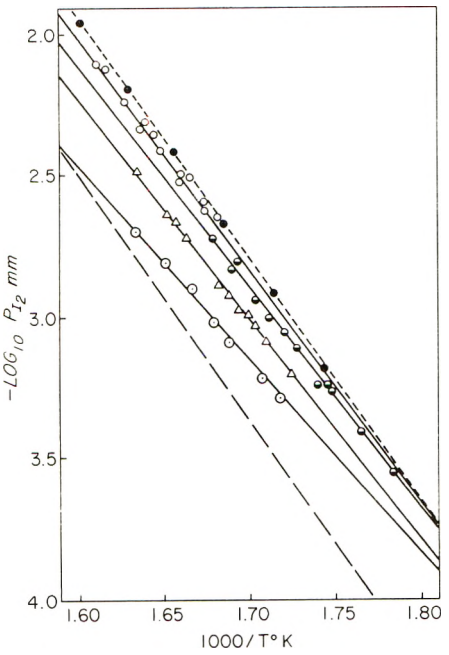

Figure 1. Steady-state effusion pressures of I_2 established by reaction 1: ◒, cell 1; ⊙ cell 2; O, cell 4; △, cell 5; ●, equilibrium pressure predicted by extrapolation; Knudsen effusion data[1] (— —).

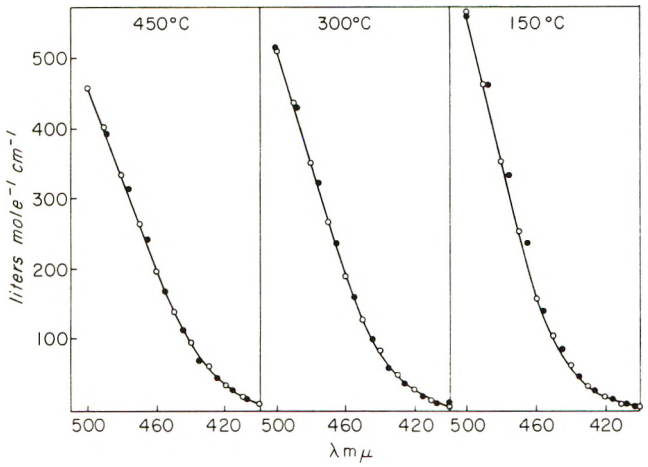

Figure 2. Molar absorptivities reported for I_2 vapor: ●, Sulzer and Wieland;[12] O, this work.

TABLE I: Torsion Effusion Data[a] for Reaction 1[b]

Cell	Orifice area × 10^3 cm^2	Tungsten fiber diameter, mil	A	B
2	90.9	2	8.761	7036
5	46.0	1	10.495	7960
1	7.18	1	9.948	7573
4	2.05	1	11.519	8455
P_e (extrapolation intercept)			11.906	8677
Knudsen data[c]			11.832	8936
Apparent condensation coefficient, $\alpha \times 10^3$, at various temperatures (°C): 12 (300°); 11 (310°); 10 (320°); 8 (330°); 6 (340°); 5 (350°)				

[a] Reference 3. [b] A and B (least-squares constants) for log P(Torr) = $A - BT^{-1}$. [c] Reference 1.

tables.[8] Partial pressures of I_2 were used to derive equilibrium constants for (1). Data from each cell were fitted to the form log P(torr) = $A - BT^{-1}$ by a least-squares treatment; the linear correlation and actual data points are displayed in Figure 1. It is clear that steady-state pressures depend markedly on cell orifice area. The dashed line indicates the apparent equilibrium pressures derived from a plot of the reciprocal of the steady-state pressures *vs.* the orifice area and extrapolation to zero orifice area. It was necessary in some cases to extrapolate the least-squares lines for the various cells to a common temperature range to facilitate the comparison. An apparent condensation coefficient was estimated using the equation $P_e = P_s(1 + a_0/\alpha A)$ where the surface area A was taken as the cross sectional area of the cell, a_0 represents the orifice area, and α is the apparent condensation coefficient for the reaction.[8a] The Freeman–Searcy orifice factors are included in the calibration constants. (Torsion effusion data for reaction 1 are listed in Table I.)

As illustrated on Figure 1, apparent pressures from the Knudsen studies are substantially lower than the torsion data and the derived equilibrium values; the slope for the latter is fortuitously close to that of the Knudsen data. The lower steady-state pressures apparently result from a combination of the effect of a low condensation coefficient and a time-dependent fall-off of the Knudsen data. The figure also shows that the deviation of the torsion steady-state pressures from the projected equilibrium value increases as the temperature is increased. This indicates an apparent enthalpy of activation (27 kcal mol^{-1} of I_2) smaller than the enthalpy of vaporization (40 kcal mol^{-1}),[9] a behavior similar to that observed for the sublimation of elementary iodine.[10] The condensation coefficient for (1) also appears to have a similar magnitude to that of crystalline iodine. Projected thermodynamic constants for (1) will be discussed after consideration of spectrophotometric data.

Absorbance Measurements. A number of investigators have used the absorbance in the region around 480 mμ, which is fairly insensitive to temperature variation between 60 and 120° and to the presence of foreign gases, as a measure of the concentration of iodine vapor.[11] There is some disagreement as to the correct value of the molar absorptivity; a value around 350 M^{-1} cm^{-1} at 100°, somewhat lower than the value (365) of Sulzer and Wieland,[12] has been used in recent work.[11] Molar absorptivities determined in the present study are shown graphically in Figure 2.[3] Data from the three samples were averaged. At 150 and 300° our values are also somewhat lower than those of Sulzer and Wieland,[12] especially between 450 and 490 mμ; at 500 mμ, however, our results correspond well with theirs. We confirm that the molar absorptivity in the region near 480 mμ is relatively insensitive to temperatures as high as 250° and find the value 350 ± 2 M^{-1} cm^{-1} at 480 mμ acceptable. A comparison of the vapor pressure of iodine derived from our absorbance data (samples D and E) with the early transpiration work of Baxter, *et al.*,[13] and Ramsay and Young[14] is shown in Figure 3. These workers are considered most reliable by the authors of the JANAF tables.[8]

The molar absorptivities of iodine at 5-mμ intervals between 460 and 500 mμ were then used to determine the iodine vapor concentration in equilibrium with CrI_3(s) and CrI_2(s). At a given temperature the apparent value of the concentration was evaluated at each wavelength and

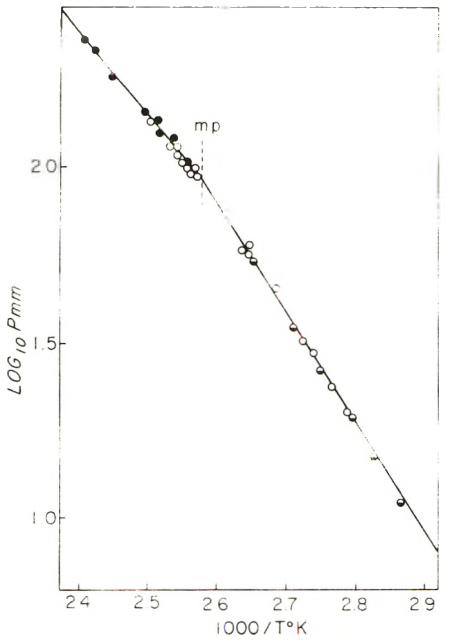

Figure 3. Iodine vapor pressure: ◒, Baxter, *et al.*;[13] ◒, Ramsay and Young;[14] O, this work.

the results averaged. The results from the various samples were in good agreement. The data, displayed in Figure 4, were least squared in the form $\log P(\text{torr}) = 11.893 - 8608T^{-1}$ for the interval 482–539°. To facilitate comparison with effusion data ΔC_p° for (1) was estimated as −0.4 cal deg^{-1} mol^{-1}. A final least-squares treatment led to the expression $\Delta G^\circ = 20{,}000 + 0.921T \log T - 23.7T$, ($\sigma = \pm 0.012$).

Thermodynamic constants derived for (1) are presented in Table II. It is seen that torsion effusion and optical absorption experiments give virtually the same mean values for ΔH° and ΔS°. Though the apparent dissociation pressures measured earlier by the Knudsen method were lower by a factor *ca.* 3 than the extrapolated equilibrium pressures derived from the torsion data, the heat of reaction and entropy changes predicted for (1) differ by only 0.6 kcal and 0.2 cal deg^{-1} mol^{-1}, respectively. The difference in entropy of CrI_3 and CrI_2 is in close agreement with that predicted by Latimer's rule.[15]

Transpiration Studies. Thermodynamic constants derived for (1) indicate that the iodine pressures developed by equilibrium between $CrI_3(s)$ and $CrI_2(s)$ are in the Torr range above 500°. Transpiration experiments between 500 and 600° show the appreciable transport of volatile species containing chromium. We have found it possible to explain the relationship of the quantity of chromium transported and the partial pressure of iodine on the basis that the following reactions are important along with the dissociation equilibrium $I_2(g) = 2I(g)$. When iodine pressures are sufficiently high to stabilize $CrI_3(s)$, case a, we have

$$CrI_3(s) + {}^1/_2I_2(g) = CrI_4(g) \qquad K_{34} \quad (2)$$

$$CrI_3(s) = CrI_3(g) \qquad K_3 \quad (3)$$

$$CrI_3(s) = CrI_2(g) + {}^1/_2I_2(g) \qquad K_{32} \quad (4)$$

When iodine pressures are below the value necessary to stabilize $CrI_3(s)$, but above that necessary to stabilize $CrI_2(s)$ relative to Cr, case b, we have

$$CrI_2(s) + {}^1/_2I_2(g) = CrI_3(g) \qquad K_{23} \quad (5)$$

$$CrI_2(s) + I_2(g) = CrI_4(g) \qquad K_{24} \quad (6)$$

$$CrI_2(s) = CrI_2(g) \qquad K_2 \quad (7)$$

The formation of CrI_4 was anticipated from earlier reports of evidence for corresponding species in the chloride and bromide systems.[16,17] Tumarev and Panyushin[18] have suggested formation of chromium IV iodide in the solid state, but evidence was not felt to be conclusive.

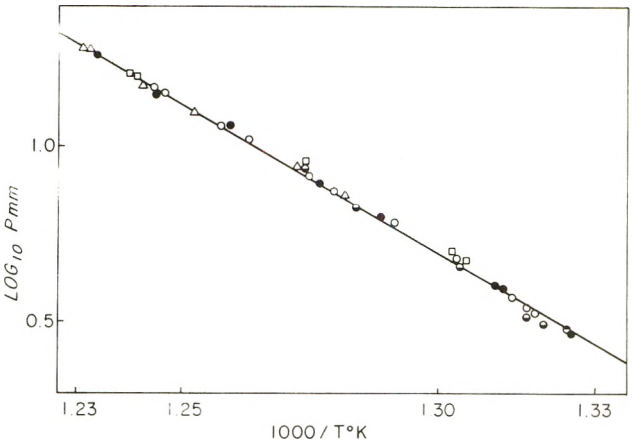

Figure 4. Dissociation pressures of I_2 for reaction 1 derived from absorbance measurements: O, A; ●, B; ◒, C; △, D; □, E.

TABLE II: Thermodynamic Constants for Reaction 1[a]

Method	Ref	ΔH°, kcal mol^{-1}	ΔS°, cal deg^{-1} mol^{-1}	Temp interval, °C
Knudsen	1	20.4	20.4	309–373
Diaphragm	1	19.6	20.9	490–666
Torsion	Present work	19.8	20.6	287–346
Absorbance	Present work	19.7	20.6	482–539

[a] Estimated overall uncertainty (present work) ±2%.

For case a, one expects a plot of $P(\Sigma CrI_x) - P(CrI_2)$ *vs.* $P(I_2^{1/2})$ to give a straight line, the slope of which is, K_{34} and an intercept (at zero iodine pressure) equal to K_3. $P(\Sigma CrI_x)$ represents the apparent total pressure of chromium iodide molecules, derived from the total number of moles of chromium transported in relation to the number of moles of argon carrier gas and the measured total pressure of argon. It was not found necessary to assume the existence of polymers or of higher oxidation states. However, the precision of our data was not sufficient to detect small amounts of such species. The relatively high partial pressure of iodine prevented us from seeking mass spectrometric evidence for the molecular forms. Similarly for case b a plot of $(P(\Sigma CrI_x) - P(CrI_2))/P(I_2^{1/2})$ *vs.* $P(I_2^{1/2})$ should give a slope equal to K_{24} and an intercept equal to K_{23}. It will be apparent that when the iodine pressure has the unique value fixed by reaction 1, both sets of equations apply and all partial pressures are fixed at a given temperature by the phase rule.

The data are shown in Figure 5.[3] Values of K_2 (*i.e.*, $P(CrI_2)$) were based on the results of Allen.[19] The plot for case b could only be constructed at 591°. Values of K_{24} and K_{23} were derived from the slope and intercept, respectively. K_{34} at this temperature may also be calculated from the value of K for reaction 1 and K_{24}. Since data for

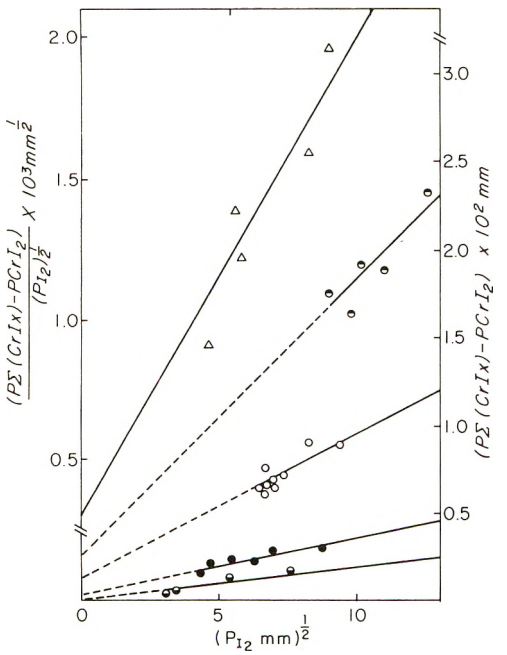

Figure 5. Transpiration data: left ordinate scale △, 591°; right ordinate scale ◓, 591°; ○, 566°; ●, 539°; ◒, 519°.

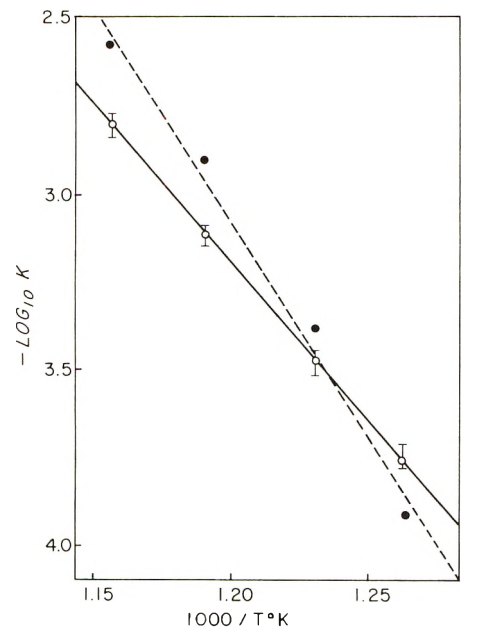

Figure 6. Equilibrium constants: ●, K_3; Φ, K_{34}.

case a at 591° were rather limited and inadequate to establish a meaningful slope, the value of K_{34} derived from case b was used to establish the slope and the line shown for case a at 591° has this slope. This line (Figure 5) was then placed in a reasonable position relative to the data points and extrapolated to derive the value of K_3 at this temperature. The latter can again be compared with that predicted by combining K_{23} and K. Results were consistent. Data at 566, 539, and 519° corresponded to case a and were used to derive values of K_{34} and K_3 at these temperatures. The relatively large scatter of the points reflects the difficulty of these experiments. As can be seen, iodine partial pressures range as high as 160 Torr and were difficult to control at constant values.

TABLE III: Comparison of Standard Enthalpies of Formation and Bond Energies (kcal mol^{-1}) and Standard Entropies (cal mol^{-1} deg^{-1}) Derived for the Chromium Iodides with Those for the Chlorides and Bromides Based on the Work of Others[a]

	$\Delta H°$	$S°$	$\Delta H°$	$S°$	Vapor-phase bond energy
X	$CrX_2(s)$		$CrX_2(g)$		Cr–X
Cl	−94.6[b]	27.8[b]	−30.8[g]	74.2[g]	91.4
Br[b]	−[74]	[30]	−[14.3][d]	[75.2][d]	[80.8]
[c]		[32]		[77.2][d]	
I	−37.8[e]	36.9[f]	33.6[f]	95.3[f]	55.7
	$CrX_3(s)$		$CrX_3(g)$		
Cl	−132.5[b]	30[b]	−70.7[a]	84.2[g]	83.9
Br[b]	−[91]	[44]	−[30.2][d]	[96.4][d]	[68.1]
[c]		[37]		[89.6][d]	
I	−47.8[e]	47.1	12.2	94.3	52.7
			$CrX_4(g)$		
Cl			−101.6[g]	87.5[g]	77.8
Br[d]			−[42.6]	[106.9]	[60.9]
				[100.1]	
I			4.1	112.3	48

[a] Brackets indicate estimate. (Corrected to 25°, using estimated $\Delta C_p°$ values cited in text). [b] Reference 20. [c] Reference 15. [d] Reference 17. [e] Reference 21. [f] Reference 19. [g] Reference 22.

Values of the equilibrium constants derived, displayed in Figure 6, follow: t, °C; $K_3 \times 10^3$, Torr; $K_{34} \times 10^3$, Torr$^{1/2}$; 591°, 2.6, 1.63; 566°, 1.2, 0.85; 539°, 0.4, 0.325; 519°, 0.13, 0.183. The other constants can be derived from these and values of K for (1). Considering the general scatter of the data, the correlation in Figure 6 is remarkably good.

To facilitate estimation of properties at 25° and bond energies at 25°, values of $\Delta C_P°$ of −5.0[16] and −6.0 cal mol^{-1} deg^{-1} were assumed[16] for reactions 2 and 3, respectively. A least-squares treatment gave the following expressions for the free energies of reaction: for (2) $\Delta G° = 45{,}860 + 5.0T \ln T - 67.54T$ cal mol^{-1}; for (3) $\Delta G° = 61{,}790 + 6.0T \ln T - 87.38T$ cal mol^{-1}.

The thermodynamic properties evaluated for the iodides may be compared with those of the chlorides and bromides in Table III.[20-22] References to related worked providing data used to complete the table are shown. We have used the more recent values[21] for the heats of formation of CrI_3 and $CrI_2(s)$ which seem more consistent with other data than the early value reported in Bichowsky and Rossini.[23] Data for $CrBr_2$ have only been estimated. The values derived for the bond energies, enthalpies, and entropies show reasonable trends.

Acknowledgment. This work was carried out with financial support from the National Science Foundation, Grants No. GP 6608X and GP 37033X, which is acknowledged with thanks.

References and Notes

(1) L. L. Handy and N. W. Gregory, *J. Amer. Chem. Soc.*, **72**, 5049 (1950); **74**, 2050 (1952).
(2) J. H. Rai and N. W. Gregory, *J. Phys. Chem.*, **74**, 529 (1970).
(3) C. F. Shieh and N. W. Gregory, *J. Chem. Eng. Data*, in press; for details see the doctoral dissertation of Chyi-Feng Shieh, University of Washington, Seattle, 1973.

(4) N. W. Gregory and L. L. Handy, "Inorganic Syntheses," Vol. 5, McGraw-Hill, New York, N. Y., 1957, Chapter VIB, Section 34, p 128–130.
(5) D. L. Hilden, Doctoral Dissertation, University of Washington, Seattle, 1971; D. L. Hilden and N. W. Gregory, *J. Phys. Chem.*, **76**, 1632 (1972).
(6) W. E. Zaugg, Doctoral Dissertation, University of Washington, Seattle, 1965; University Microfilms No. 66-588, Ann Arbor, Mich.; W. E. Zaugg and N. W. Gregory, *J. Phys. Chem.*, **70**, 486 (1966).
(7) E. B. Sandell, "Colorimetric Metal Analysis," 3rd ed, Interscience, New York, N. Y., 1959.
(8) "JANAF Tables," The Dow Chemical Co., Midland, Mich., Sept 30, Dec 31, 1961.
(8a) A. W. Searcy and R. D. Freeman, *J. Amer. Chem. Soc.*, **76**, 5229 (1954); C. I. Whitman, *J. Chem. Phys.*, **20**, 161 (1952); K. Motzfeldt, *J. Phys. Chem.*, **59**, 139 (1955).
(9) A. W. Searcy, "Chemical and Mechanical Behavior of Inorganic Materials," A. W. Searcy, D. V. Ragone, and U. Colombo, Ed., Wiley-Interscience, New York, N. Y., 1970, Chapter 6.
(10) J. H. Stern and N. W. Gregory, *J. Phys. Chem.*, **59**, 105 (1955).
(11) M. Tames and J. Grundness, *J. Amer. Chem. Soc.*, **93**, 801 (1971); M. Tames and S. N. Bhat, *J. Phys. Chem.*, **75**, 1057 (1971); F. T. Lang and R. L. Strong, *J. Amer. Chem. Soc.*, **87**, 2345 (1965).
(12) P. Sulzer and K. Wieland, *Helv. Phys. Acta*, **25**, 653 (1952).
(13) G. P. Baxter, C. H. Hickey, and W. C. Holmes, *J. Amer. Chem. Soc.*, **29**, 127 (1907); G. P. Baxter and M. R. Grose, *ibid.*, **37**, 1061 (1915).
(14) W. Ramsay and S. Young, *J. Chem. Soc.*, **49**, 453 (1886).
(15) W. M. Latimer, *J. Amer. Chem. Soc.*, **73**, 1480 (1951).
(16) H. A. Dorner, *U. S., Bur. Mines, Tech. Pap.* 577 (1973).
(17) R. J. Sime and N. W. Gregory, *J. Amer. Chem. Soc.*, **82**, 93 (1960).
(18) A. S. Tumarev and L. A. Panyushin, *J. Appl. Chem. USSR*, **35**, 968 (1962).
(19) T. L. Allen, *J. Amer. Chem. Soc.*, **78**, 5476 (1956).
(20) C. F. Wicks and F. E. Block, *U. S., Bur. Mines, Bull.*, 605 (1963).
(21) N. W. Gregory and T. R. Burton, *J. Amer. Chem. Soc.*, **75**, 6054 (1953).
(22) C. G. Maier, *U. S., Bur. Mines, Bull.*, 436 (1942).
(23) F. R. Bichowsky and F. D. Rossini, "The Thermochemistry of Chemical Substances," Reinhold, New York, N. Y., 1936; A. Mosnier, *Ann. Chim. Phys.*, **12**, *Ser. 7*, 374 (1897).

Equilibrium Distribution of Lithium and Bismuth between Liquid Lithium–Bismuth Alloys and Molten Lithium Chloride at 650–800°[1]

L. M. Ferris,* M. A. Bredig, and F. J. Smith

Oak Ridge National Laboratory, Oak Ridge, Tennessee 37830

(Received July 21, 1972; Revised Manuscript Received April 6, 1973)

Publication costs assisted by Oak Ridge National Laboratory

The distribution of lithium and bismuth between liquid Li–Bi alloys and molten LiCl was measured at several temperatures between 650 and 800°. The extent of their distribution to the LiCl increased dramatically at each temperature with a moderate increase in the lithium concentration of the alloy; for example, at 650°, the bismuth concentration in the LiCl increased from about 5 to 4800 ppm as the lithium concentration in the alloy increased from 10 to 50 at. %. The ratio of "excess" lithium to bismuth in the LiCl generally was about 3, suggesting that salt-like Li_3Bi was selectively dissolved from the alloys. The measured equilibrium bismuth concentrations in the LiCl in the temperature range 650–800° can be expressed as $\ln N_{Bi(d)} = 4 \ln N_{Li(m)} + 2.579 N_{Li(m)} + 2.211 - 9465/T(°K) + 0.0832 \exp[3090/T(°K)]$, with an estimated uncertainty in $\ln N_{Bi(d)}$ of ±0.2. In this expression, N, (d), and (m) denote mole fraction, dissolved in salt phase, and dissolved in alloy phase, respectively. Some data were obtained using molten LiBr as the salt phase at 650°. Bismuth concentrations (mole fractions) in the LiBr were about twice as high as those obtained with LiCl at the same alloy concentrations.

Introduction

A metal-transfer process for separating rare-earth fission products from thorium was considered as one step in the chemical processing of molten-salt breeder reactors (MSBRs). In this process,[2,3] some of the thorium and rare earths are extracted from the $LiF-BeF_2-ThF_4$ carrier salt into a Li–Th–Bi solution and, then, the rare earths are selectively extracted into molten LiCl. Finally, the rare earths are extracted from the LiCl by reduction into a Li–Bi solution in which the lithium concentration is 5 to 50 at. %. The net result is the transfer of a large fraction of the rare earths, but only a very small fraction of the thorium, from the fluoride salt to Li–Bi solutions of high lithium concentration. This separation is implicitly and significantly based on the reversal of the sequence of free energies of formation (per equivalent) of chlorides *vs.* fluorides of metal cations of varying polarizing power (di- and tripositive rare earths less than tetrapositive thorium) by virtue of the large difference in polarizabilities[4] of the two anions, $\alpha(Cl^-) = 3.55$ Å^3 and $\alpha(F^-) = 0.97$ Å^3.

Results from the initial tests of the metal-transfer process indicated that, when molten LiCl was contacted with liquid Li–Bi alloys at about 650°, the distribution of "excess" lithium[5] and of bismuth to the salt phase was significant.[6] This behavior was not entirely unexpected since Li_3Bi is quite soluble in LiCl–LiF (70–30 mol %), and the distribution of lithium and bismuth to this salt phase is significant when the salt is in contact with liquid Li–Bi (50–50 at. %) at 650–1000°.[7,8] We have investigated the equilibrium distribution of lithium and bismuth between

liquid Li–Bi alloys and molten LiCl in the temperature range 650–800°; similar measurements were made at 650° with LiBr as the salt phase. The results of these studies are summarized in this paper.

Experimental Section

Reagents. The reagent-grade LiCl and LiBr were oven dried at about 120° before use. Analyses of the salt after melting under high-purity argon showed that the Li_2O content was less than 0.05 mol %. The bismuth was Cominco American Co. 69 grade. Necessary amounts of lithium were cut under oil from reagent-grade stock and were washed with benzene just prior to use. High-purity argon was further treated by passage through a Molecular Sieve trap and a titanium sponge trap that was held at 600°.

Procedure. Equilibrations were conducted in an argon atmosphere, using the apparatus and general procedure described previously.[9] About 125 g of LiCl or LiBr and a total of 100 g of lithium and bismuth, in the desired proportions, were loaded into a molybdenum crucible. After the crucible had been sealed in the containment vessel, the system was heated to the desired temperature in an atmosphere of pure argon. After reaching this temperature, the system was allowed to equilibrate for at least 24 hr before samples of the respective phases were taken. Molybdenum pipettes were used to obtain 2–15-g samples of the salt phase, whereas samples of the alloy phase were taken with stainless steel filter sticks. The color of quenched samples of the salts changed from nearly snow-white to a deep red-brown as the lithium concentration in the alloy was increased from about 10 to 50 at. %.

One experiment was conducted to determine the solubility of Li_3Bi in LiCl over the temperature range 650–800°. In this experiment, the lithium concentration in the alloy was 70 at. %. According to the Bi–Li phase diagram,[10] this gives a two-phase equilibrium mixture of solid Li_3Bi and a liquid Li–Bi alloy in which the lithium concentration varies from about 52 to 62 at. % as the temperature increases from 650 to 800°. It is important to realize that with its solid phase as the standard state, the Li_3Bi in the mixture is at unit activity. The temperature of the system was randomly varied between 650 and 800°. At least 24 hr was allowed for attainment of equilibrium at each temperature before several samples of the salt phase were removed for analysis. The quenched salt samples had a very deep red-brown color.

Analyses. The salt samples were analyzed for "excess" lithium and for bismuth by, first, hydrolyzing the samples in water and collecting the evolved hydrogen on a Molecular Sieve column at liquid nitrogen temperature. After hydrolysis was complete, the hydrogen was eluted from the column with helium and the amount eluted was determined by gas chromatography. The amount of hydrogen evolved was assumed to be equivalent to the amount of "excess" lithium in the salt. The hydrolysis residue was then acidified to dissolve bismuth that had precipitated. Aliquots of the resultant solution were used for the determination of the bismuth concentration. When the bismuth concentration in solution was equivalent to a concentration of 100 ppm or greater in the salt, the analysis was made using the spectrophotometric iodide method for bismuth. When bismuth was present at lower concentrations, it was determined by an inverse-polarographic method. The bismuth concentrations in the salts could be determined more accurately than the lithium concentrations could. The lithium concentrations in the alloy samples were determined by flame photometry.

Results

The equilibrium concentrations of bismuth and lithium, expressed as mole fractions (N), measured in LiCl at several temperatures and alloy compositions are tabulated elsewhere.[11] At each temperature the concentrations of these elements in the LiCl increased dramatically as the lithium concentration in the alloy [$N_{Li(m)}$] was increased. The equilibrium bismuth concentrations measured in LiCl can be expressed as a function of $N_{Li(m)}$ and temperature as follows

$$\ln N_{Bi(d)} = \{4 \ln N_{Li(m)} + 2.579 N_{Li(m)} + 2.211 - 9465/T(^\circ K) + 0.0832 \exp[3090/T(^\circ K)]\} \pm 0.2 \quad (1)$$

The correlation of the data according to eq 1 is shown in Figures 1 and 2. In a large fraction of the cases, the mole ratio of "excess" lithium to bismuth dissolved in the salt phase, *i.e.*, $N_{Li(d)}/N_{Bi(d)}$, was about 3, although a significant number of the ratios were higher or lower than 3. The data[11] indicate that the ratio decreased somewhat with increasing temperature, but at a given temperature, no systematic trend of the ratio with alloy composition is evident.

The results of the few measurements made of the distribution of lithium and bismuth between Li–Bi alloys and molten LiBr at 650° are given in Table I. The bismuth concentrations in the LiBr can be represented by

$$\ln N_{Bi(d)} = 4 \ln N_{Li(m)} + 2.579 N_{Li(m)} - (5.048 \pm 0.4) \quad (2)$$

which is of the same form as eq 1. The correlation of the data according to eq 2 is shown in Figure 3. As seen in Table I, only two sets of samples were analyzed for both "excess" lithium and bismuth. The results of these analyses showed the ratio $N_{Li(d)}/N_{Bi(d)}$ to be about 3.

The values determined for the solubility of Li_3Bi in molten LiCl over the temperature range 650–800° are given in Table II. These data indicate that $N_{Li(d)}/N_{Bi(d)}$ was 3. In Figure 4, the data are compared with the values obtained by Foster, *et al.*[7] (the solid line), using LiCl–LiF (70–30 mol %) as the salt phase. Within the range of uncertainty (±0.08 in log S), the solubility of Li_3Bi was the same in both salt phases. Since the measurements of Foster, *et al.*,[7] covered a much larger temperature range (650–1000°) than ours, it is felt that the equation $\log S$ (mol %) = $[3.437 - 4110/T(^\circ K)] \pm 0.08$ derived from their data gives a more accurate representation of the solubility values than an equation derived solely from our data.

Discussion of Results

The equilibrium bismuth concentrations in LiCl determined in this investigation with either Li_3Bi or Li–Bi (about 50–50 at. %) as the metal phase are almost identical with those obtained at Argonne National Laboratory (ANL)[7,8] with LiCl–LiF (70–30 mol %) as the salt phase. In addition, the decrease in the ratio $N_{Li(d)}/N_{Bi(d)}$ with increasing temperature indicated by our data is similar to that obtained at ANL[8] with Li–Bi (50–50 at. %) alloys in equilibrium with molten LiCl–LiF.

The results obtained in the present study cannot be explained by the distribution between the two phases of lithium and bismuth *per se*. The solubility of bismuth in

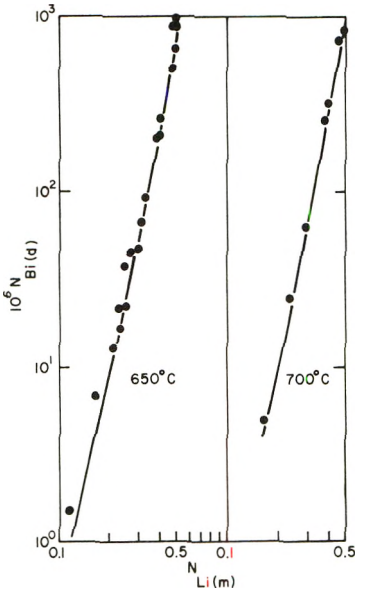

Figure 1. Correlation of equilibrium bismuth concentrations in LiCl at 650 and 700° according to eq 1.

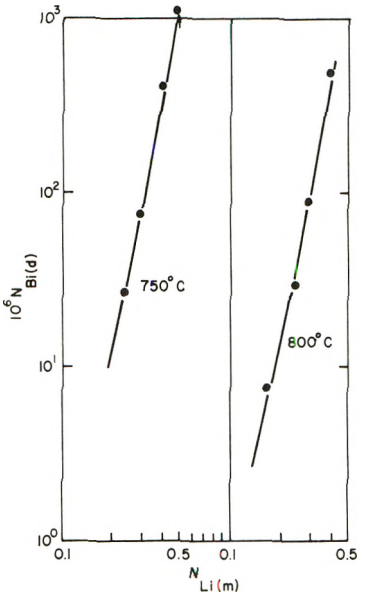

Figure 2. Correlation of equilibrium bismuth concentrations in LiCl at 750 and 800° according to eq 1.

TABLE I: Data Obtained by Equilibrating Liquid Li–Bi Alloys with Molten LiBr at 650°

Expt	$N_{Li(m)}$	$10^6 N_{Bi(d)}$	$10^6 N_{Li(d)}$	$N_{Li(d)}/N_{Bi(d)}$
37	0.167	4.7 ± 1.7		
38	0.273	111 ± 15		
39	0.273	85 ± 15		
40	0.354	232 ± 45	638 ± 40	2.8 ± 0.9
41	0.487	1220 ± 25	4060 ± 150	3.3 ± 0.3

molten LiCl is extremely low, only about 0.1 ppm at 650°.[12] Estimates based on the measured activities of lithium in liquid Li–Bi alloys[13] and the solubility of lithium in molten LiCl[14-16] show that the equilibrium lithium concentrations in LiCl would be insignificant in comparison with those determined experimentally. For example, if lithium *per se* distributed between the two phases, a possible equilibrium would be

$$Li_{(m)} = Li_{(d)} \qquad (3)$$

in which (m) and (d) denote the alloy and LiCl phases, respectively. By choosing pure liquid lithium as the standard state, it is easily shown that when the lithium concentration in the salt is low

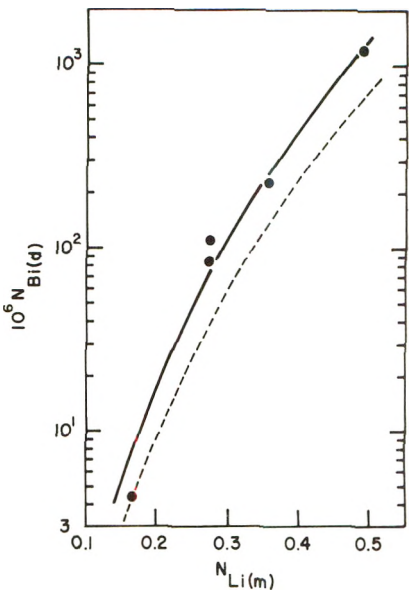

Figure 3. Equilibrium bismuth concentrations in LiBr and LiCl at 650°. Data points were obtained with LiBr as the salt phase. Solid curve calculated for LiBr from eq 2; dashed curve calculated for LiCl from eq 1.

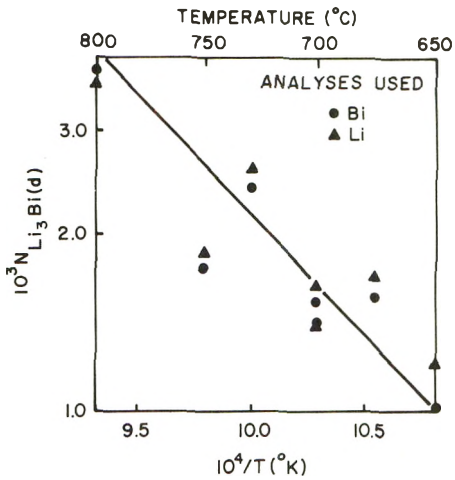

Figure 4. Solubility of Li_3Bi in molten LiCl. The line represents data obtained by Foster, *et al.*,[7] with molten LiCl–LiF (70–30 mol %).

TABLE II: Solubility of Li_3Bi in Molten LiCl in the Temperature Range 650–800°

Temp, °C	$10^3 N_{Bi(d)}$	$10^3 N_{Li(d)}$	$N_{Li(d)}/N_{Bi(d)}$
650	1.04 ± 0.1	3.72 ± 0.04	3.6 ± 0.4
675	1.57 ± 0.04	5.16 ± 0.4	3.3 ± 0.3
700	1.55 ± 0.01	4.94 ± 0.4	3.2 ± 0.3
700	1.41 ± 0.02	4.20 ± 0.2	3.0 ± 0.2
725	2.42 ± 0.06	7.80 ± 0.4	3.2 ± 0.2
750	1.76 ± 0.01	5.61 ± 0.9	3.2 ± 0.5
800	3.82 ± 0.4	10.8 ± 1.0	2.8 ± 0.7

$$N_{Li(d)} = N_{Li(m)}\gamma_{Li(m)}/\gamma_{Li(d)} \quad (4)$$

in which N is mole fraction and the γ's are activity coefficients. If we assume that the value of $\gamma_{Li(d)}$ estimated from the solubility of lithium in LiCl[14-16] is independent of $N_{Li(d)}$ and utilize the values of $\gamma_{Li(m)}$ given by Foster, *et al.*,[13] we estimate from eq 4 that, at 650°, $N_{Li(d)}$ is about 1×10^{-6} when $N_{Li(m)}$ is 0.5. This value is negligible when compared with the value obtained experimentally, and the result is typical of those obtained over the range of our experimental conditions.

Since the experimental results are inexplicable on the basis of the distribution of lithium and bismuth *per se* between the two phases and the ratio $N_{Li(d)}/N_{Bi(d)}$ was about 3 in a large fraction of the cases, we suggest that the results can best be interpreted in terms of the distribution of salt-like Li_3Bi between the two phases. This suggestion is not unprecedented. Okada, *et al.*,[17] who studied the distribution of sodium and bismuth between liquid Na–Bi alloys and molten NaCl–NaI (37–63 mol %), concluded that the presence of "excess" sodium and bismuth in the salt phase was due to "preferential solution of Na_3Bi from the alloys." They also suggested that the distribution process "involves the solution of substantially ionic sodium compounds in the melt." We will adopt their suggestion and assume that the "excess" lithium and bismuth found in the salt phases were present primarily as Li_3Bi ($3Li^+ + Bi^{3-}$). Based on this assumption, extrapolation of the distribution curves [Figures 1-3, or eq 1 and 2] to the liquidus values of $N_{Li(m)}$ at which precipitation of solid Li_3Bi occurs should give an estimate of the solubility of Li_3Bi in the respective salt phases. Estimates of the values of $N_{Li(m)}$ at the liquidus were made using two approaches. Foster, *et al.*,[13,18] obtained emf data with two types of cells: (1) Bi saturated with Li_3Bi(s)/LiCl-LiF/Li in Bi(l), and (2) Li(l)/LiCl-LiF/Bi saturated with Li_3Bi(s). The data of these two cells can be combined to give those for a theoretical third cell: (3) Li(l)/LiCl-LiF/Li in Bi(l). The excess chemical potential of lithium in the alloy is given by

$$\mu_{Li(m)}^{E} = -FE - RT \ln N_{Li(m)} \quad (5)$$

in which F is the value of the faraday, E is the emf of cell 3, and R is the gas constant. Foster, *et al.*,[13] correlated their data as follows

$$-\mu_{Li(m)}^{E}\ [\text{cal/mol}] = (9397 + 18.16T - 0.0109T^2) + (7103 - 19.44T + 0.0068T^2)N_{Li(m)} \quad (6)$$

The emf for cell 2, which is a special case for cell 3, was found[18] to be

$$E(\text{volts}) = 0.5264 + (7.3958 \times 10^{-4})T - (6.4317 \times 10^{-7})T^2 \quad (7)$$

Values of $N_{Li(m)}$ at the liquidus were calculated at several temperatures using eq 5–7; these values, along with those derived from the phase diagram reported by Hansen and Anderko,[10] and the corresponding estimated solubilities of Li_3Bi in LiCl and LiBr, are given in Table III. The solubilities in LiCl estimated using the values of $N_{Li(m)}$ from the phase diagram are in good agreement with those measured in this study (Table II), whereas the values estimated from the emf data are somewhat higher. The estimated solubility of Li_3Bi in LiBr at 650° is about twice that in LiCl. This result is consistent with the expectation that less work would be required to substitute large Bi^{3-} ions into the anion sublattice of molten LiBr since the Br^- ion is larger than the Cl^- ion.

TABLE III: Estimated Solubilities of Li_3Bi in LiCl and LiBr Using Values of $N_{Li(m)}$ at the Liquidus and Eq 1 or 2

Salt	Temp, °C	Lithium concn in Li–Bi alloy at the liquidus, atom fraction: From phase diagram[a]	Lithium concn in Li–Bi alloy at the liquidus, atom fraction: From emf data[b]	Estimated solubility of Li_3Bi in salt, mol %: Using $N_{Li(m)}$ from phase diagram	Estimated solubility of Li_3Bi in salt, mol %: Using $N_{Li(m)}$ from emf data
LiCl	650	0.524	0.544	0.10	0.12
LiBr	650	0.524	0.544	0.19	0.23
LiCl	700	0.558	0.579	0.16	0.20
LiCl	750	0.588	0.616	0.26	0.34
LiCl	800	0.616	0.654	0.42	0.58

[a] Reference 10. [b] References 13 and 18.

Continuing with the hypothesis that the data obtained in this study can be interpreted in terms of the distribution of Li_3Bi between the two phases, in principle it should be possible to calculate the distribution behavior if the activity of Li_3Bi in each phase is known. In this connection, we will define the activity of Li_3Bi in the salt phase by

$$a_{Li_3Bi(d)} = N_{Li_3Bi(d)}\ \gamma_{Li_3Bi(d)} \quad (8)$$

and assume that $\gamma_{Li_3Bi(d)}$ is constant at a given temperature. Thus, $\gamma_{Li_3Bi(d)}$ would simply be the reciprocal of the solubility of Li_3Bi in the salt at that temperature. The measurements of the solubility of Li_3Bi in LiCl and LiCl–LiF mentioned earlier yield

$$\ln \gamma_{Li_3Bi(d)} = [-3.309 + 9465/T(°K)] \pm 0.2 \quad (9)$$

When the Li_3Bi concentration in the LiCl is low, eq 8 can be written as

$$a_{Li_3Bi(d)} = N_{Bi(d)}\gamma_{Li_3Bi(d)} = [N_{Li(d)}/3]\gamma_{Li_3Bi(d)} \quad (10)$$

in which $N_{Bi(d)}$ and $N_{Li(d)}$ are the measured mole fractions of bismuth and "excess" lithium in the LiCl.

Activities of Li_3Bi in bismuth solution can be calculated from the emf data of Foster, *et al.*,[13,18] as follows. The net reaction for cell 3 is

$$Li(l) = Li(m) \quad (11)$$

If we assume that the reaction

$$Li(m) + {}^1/_3Bi(m) \longrightarrow {}^1/_3Li_3Bi(m) \quad (12)$$

occurs in the alloy, the cell reaction can be written as

$$Li(l) + {}^1/_3Bi(m) = {}^1/_3Li_3Bi(m) \quad (13)$$

By choosing the standard state for lithium as the pure liquid and considering the liquid alloy as an Li_3Bi–Bi binary, the emf of the cell can be expressed as

$$E = E^\circ - (RT/3F) \ln a_{Li_3Bi(m)} + (RT/3F) \ln a_{Bi(m)} \quad (14)$$

or, in differential form

$$dE = (-RT/3F)\ d \ln a_{Li_3Bi(m)} + (RT/3F)\ d \ln a_{Bi(m)} \quad (15)$$

We will assume that Li_3Bi in the alloy is completely dissociated according to

$$Li_3Bi \longrightarrow 3Li^+ + Bi^{3-} \quad (16)$$

and partially define its activity by

$$a_{Li_3Bi(m)} = (a_{Li^+}{}^3)(a_{Bi^{3-}}) \quad (17)$$

The assumption of complete ionization may not be too unreasonable. Solid Li_3Bi is a salt-like or ionic compound[19] formed from elements of vastly different electronegativities. Furthermore, the ions Li^+ and Bi^{3-} have the electronic configurations of the stable gases helium and radon, respectively. Other considerations which led to the assumption of complete ionization were (1) the fact that the activity coefficient for lithium in the alloy (relative to pure lithium) is very low and does not change drastically with alloy composition[13] not only reflects the strong interaction involved but also suggests that the lithium is in essentially the same environment over a wide range of alloy compositions; (2) the experimentally determined ratio $N_{Li(d)}/N_{Bi(d)}$ was about 3; and (3) the experimentally determined values of $N_{Li(d)}$ and $N_{Bi(d)}$ were strongly dependent on the lithium concentration in the alloy.

The definition of $a_{Li_3Bi(m)}$ is completed by defining

$$a_{Li^+(m)} = 3[n_{Li_3Bi(m)}/n_{Bi(m)}]\gamma_{Li^+(m)} = [n_{Li^+(m)}/n_{Bi(m)}]\gamma_{Li^+(m)} \quad (18)$$

$$a_{Bi^{3-}(m)} = [n_{Li_3Bi(m)}/n_{Bi(m)}]\gamma_{Bi^{3-}(m)} = (1/3)[n_{Li^+(m)}/n_{Bi(m)}]\gamma_{Bi^{3-}(m)} \quad (19)$$

in which $n_{Bi(m)}$ is the number of moles of bismuth not present as Bi^{3-} and $n_{Li^+(m)}$ is the number of moles of lithium ions. Since we have assumed that all the lithium present in the alloy exists as Li^+

$$n_{Li^+(m)} = n_{Li} \quad (20)$$

$$n_{Bi(m)} = n_{Bi} - 1/3 n_{Li} \quad (21)$$

in which n_{Li} and n_{Bi} represent the total moles of lithium and bismuth, respectively, in the Li-Bi alloy. By substituting eq 20 and 21 into eq 18 and 19 and dividing both the numerator and denominator by $(n_{Li} + n_{Bi})$, we obtain

$$a_{Li^+(m)} = \left[\frac{n_{Li}}{n_{Bi} - 1/3 n_{Li}}\right]\gamma_{Li^+(m)} = \left[\frac{N_{Li(m)}}{1 - (4/3)N_{Li(m)}}\right]\gamma_{Li^+(m)} \quad (22)$$

$$a_{Bi^{3-}(m)} = (1/3)\left[\frac{n_{Li}}{n_{Bi} - 1/3 n_{Li}}\right]\gamma_{Bi^{3-}(m)} = (1/3)\left[\frac{N_{Li(m)}}{1 - (4/3)N_{Li(m)}}\right]\gamma_{Bi^{3-}(m)} \quad (23)$$

in which $N_{Li(m)}$ is the atom fraction of lithium in the alloy. Substituting eq 22 and 23 into eq 17 yields

$$a_{Li_3Bi(m)} = (1/3)\left[\frac{N_{Li(m)}{}^4}{[1 - (4/3)N_{Li(m)}]^4}\right]\gamma_\pm{}^4 \quad (24)$$

in which $\gamma_\pm$ is a mean activity coefficient for Li_3Bi in the alloy. From the Gibbs-Duhem relationship, we obtain

$$d \ln a_{Bi(m)} = \left[\frac{(-1/3)N_{Li(m)}}{1 - (4/3)N_{Li(m)}}\right] d \ln a_{Li_3Bi(m)} \quad (25)$$

Substitution of eq 25 into eq 15 yields, on rearrangement

$$dE = (-RT/3F)\left[\frac{[1 - N_{Li(m)}]}{[1 - (4/3)N_{Li(m)}]} d \ln a_{Li_3Bi(m)}\right] \quad (26)$$

TABLE IV: Constants of Integration for Eq 31 Derived from the Emf Data of Foster, *et al.*[a]

Temp, °C	β	$N_{Li(m)}$ at liquidus, atom fraction	$\gamma_\pm$ at liquidus	Γ
650	−5047	0.544	0.666	−0.0283
700	−5374	0.579	0.519	−0.107
750	−5668	0.616	0.383	−0.172
800	−5927	0.654	0.259	−0.222

[a] References 13 and 18.

As indicated by eq 5 and 6, at a given temperature the emf data of Foster, *et al.*,[13] can be represented by an equation of the form

$$E = (\alpha/F) + (\beta/F)N_{Li(m)} - (RT/F) \ln N_{Li(m)} \quad (27)$$

or

$$dE = (\beta/F)\, dN_{Li(m)} - (RT/F)\, d \ln N_{Li(m)} \quad (28)$$

where α and β are constants. We also note from eq 24 that

$$d \ln a_{Li_3Bi(m)} = 4\, d \ln \gamma_\pm + 4\, d \ln N_{Li(m)} - 4\, d \ln [1 - (4/3)N_{Li(m)}] \quad (29)$$

Substitution of eq 28 and 29 into eq 26 yields, after rearrangement and simplification

$$d \ln \gamma_\pm = \frac{(-4/3)\, d N_{Li(m)}}{[1 - (4/3)N_{Li(m)}]} - (3\beta/4RT)\left[\frac{1 - (4/3)N_{Li(m)}}{1 - N_{Li(m)}}\right] d N_{Li(m)} - \frac{dN_{Li(m)}}{N_{Li(m)}} + \left[\frac{3[1 - (4/3)N_{Li(m)}]}{4[1 - N_{Li(m)}]N_{Li(m)}}\right] dN_{Li(m)} \quad (30)$$

Integration of eq 30 from the standard state (st.st.) of Li_3Bi to $N_{Li(m)}$, *i.e.*, between the limits of $\gamma_{\pm(st.st.)}$ to $\gamma_{\pm(N_{Li(m)})}$ and $N_{Li(m)(st.st.)}$ to $N_{Li(m)}$, gives

$$\ln \gamma_{\pm[N_{Li(m)}]} = \ln [1 - (4/3)N_{Li(m)}] - (1/4) \ln N_{Li(m)} - (\beta/RT)N_{Li(m)} - [(\beta/4RT) - (1/4)] \ln [1 - N_{Li(m)}] + \Gamma \quad (31)$$

in which Γ is the integration constant at a given temperature. By choosing the pure solid as the standard state for Li_3Bi, values of $\gamma_\pm$ can be calculated at the liquidus values of $N_{Li(m)}$, using eq 24 with $a_{Li_3Bi(m)} = 1$; then Γ can be evaluated from eq 31. The values of β and of $N_{Li(m)}$ at the liquidus derived at selected temperatures from the work of Foster, *et al.*,[13,18] are presented in Table IV, along with the calculated values of Γ and of $\gamma_\pm$ at the liquidus. At a given temperature, $\gamma_\pm$ does not change markedly over a wide range of values of $N_{Li(m)}$. For example, at 650°, $\gamma_\pm$ decreases from 1.79 to 0.796 as $N_{Li(m)}$ increases from 0.1 to 0.5.

The following expression for the distribution of bismuth between molten LiCl and liquid Li-Bi alloys

$$N_{Bi(d)} = N_{Li(m)}{}^4\, \gamma_\pm{}^4/3[1 - (4/3)N_{Li(m)}]^4\, \gamma_{Li_3Bi(d)} \quad (32)$$

is obtained by equating eq 10 and 24 since, at equilibrium, the activities of Li_3Bi in the two phases are the same. Values of $N_{Bi(d)}$ were calculated as a function of $N_{Li(m)}$ from eq 32, using the values of $\gamma_{Li_3Bi(d)}$ represented by eq 9 and the appropriate values of $\gamma_\pm$ derived from the emf data. The values of $N_{Bi(d)}$ calculated from eq 32 at

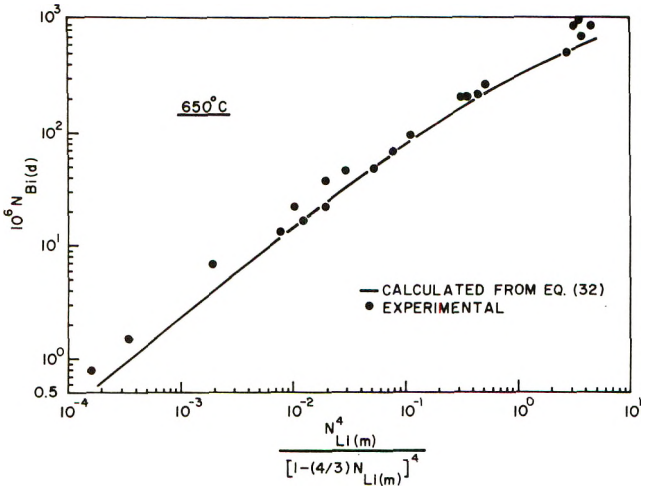

Figure 5. Comparison of calculated equilibrium bismuth concentrations in LiCl with those determined experimentally at 650°.

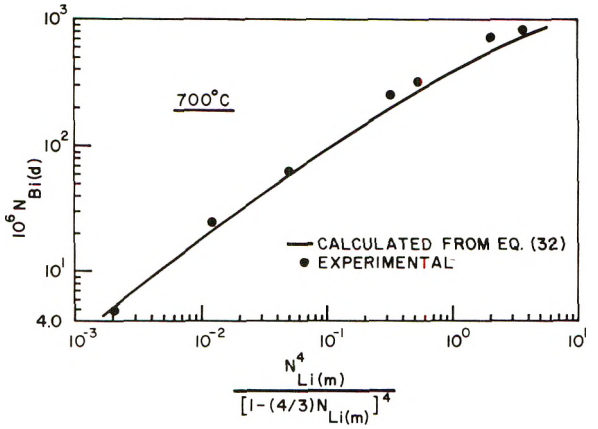

Figure 6. Comparison of calculated equilibrium bismuth concentrations in LiCl with those determined experimentally at 700°.

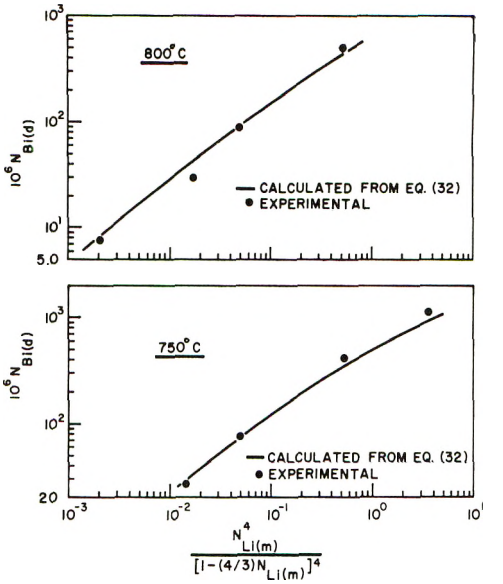

Figure 7. Comparison of calculated equilibrium bismuth concentrations in LiCl with those determined experimentally at 750 and 800°.

the various temperatures are compared with the experimental data in Figures 5–7. As seen, the agreement is quite good.

The results of the present study suggest that the observed distribution of lithium and bismuth between liquid Li–Bi alloys and molten LiCl or LiBr is due mainly to the distribution of Li_3Bi, and not the respective elements, between the two phases. It should be emphasized, however, that the success of the mathematical treatment used in describing the distribution does not constitute proof that the species assumed were actually those present. In fact, any mathematically tractable definition of the activity of Li_3Bi in the alloy phase, when used in conjunction with the emf data of Foster, *et al.*,[13,18] and the values of $\gamma_{Li_3Bi(d)}$ derived from the solubility measurements, results in the same good correlation between calculated and experimental values as was obtained by use of eq 32. We chose to represent the Li_3Bi in the alloy as a completely ionized species for the reasons stated earlier and the resultant fact that the activity coefficient derived on this basis was relatively insensitive to changes in alloy composition in the approximate range $N_{Li(m)} = 0$ to 0.6.

Finally, we discuss our results briefly in the general context of a solution of an "ionic" compound ("salt"), S = $A_x^{n+}B_y^{m-}$ ($m = nx/y$), in a liquid metal, M = A or B, and make some comparisons with a few known related systems. The molecular and electronic structures of such solutions are of considerable theoretical interest and are not well understood at this time.[16,20] In the present study, in which we assumed Li_3Bi to be present in Bi, we have been dealing with the second case above; *i.e.*, M = B. In this case, it is the *anion* ($B^{m-} = Bi^{3-}$) which in its elemental nature is identical with the metal solvent, B = Bi. For the opposite case, M = A, there are the numerous systems involving 1:1 electrolytes ($n = x = y = 1$), namely, the alkali halides with the corresponding alkali metals as the solvents,[16] in which the question of ion association cannot be attacked by thermodynamic considerations. However, a few data are also available for systems with $n > 1$ where this is indeed possible. These systems include some with $n = 2$, $x = 1$, $y = 2$ (AB_2–A), and one with $n = 3$, $x = 1$, $y = 3$ (AB_3–A), in which not the anion, but the *cation*, of the salt in its elemental nature matches the metal solvent and, in fact, is the "common ion" for salt and metal. Examples are solutions of alkaline earth dihalides in the corresponding liquid alkaline earth metals (CaF_2 in liquid calcium, and $BaCl_2$ in liquid barium[21]), and the bismuth trihalides BiX_3 (X = Cl, Br, or I) in bismuth metal,[22] which are especially interesting for comparison with the Li_3Bi–Bi system. In such cases, the change in the activity of the metal solvent on addition of small amounts of salt solute (halide) was determined by measuring the depression of either the freezing point[21,22] or the vapor pressure of the metal.[23] The magnitude of this depression was taken to reflect complete dissociation of the dissolved salt, at least as far as the separation of the halide ions from each other was concerned. Distinction between more detailed models involving either the loss of identity of the "common ion" of salt and metal among the cations of the metal solvent or, alternatively, the presence of complex species such as (BiCl), (CaF), and (BaF), each containing only one halide atom, is not possible in this way, at least not for dilute solutions.[22] It is recognized, however, that the extreme mobility of charge in a metal implies ready screening of the fields, and consequently causes the separation of ions of opposite charge or "solvation" of the ions of the salt by the oppositely charged species of the metal

solvent, *i.e.*, of A^{n+} by some e^- and by B^{m-} by some A^{n+}.

In the present case of Li_3Bi in Bi, with the assumed three separated lithium cations, the interesting new question arises as to whether the Bi^{3-} anion may not also lose its identity among the Bi^{3+} cores and "metallic" electrons, e^-, of the metal solvent, according to $Bi^{3-} = Bi^{3+} + 6e^-$. In such a model, the dependence of $a_{Li_3Bi(m)}$ or $\gamma_\pm$ on $N_{Li(m)}$ would be somewhat, but not greatly, different from that of eq 24, in which the Bi^{3-} species is distinguished from the Bi of the metal solvent. Further studies of quite a different nature would be required for establishing a more detailed model.

Although the bismuth data could be correlated by assuming distribution of Li_3Bi between the two phases, the experimental data indicated that the ratio $N_{Li(d)}/N_{Bi(d)}$ was not 3 in all cases, perhaps somewhat less than 3 at higher temperatures. This detail requires further examination.

Acknowledgments. The authors thank J. F. Land and C. T. Thompson for conducting the experimental work. Analyses were provided by W. R. Laing, J. L. Botts, N. Marion Ferguson, and G. Goldberg of the ORNL Analytical Chemistry Division. The authors extend special thanks to J. Braunstein, ORNL Reactor Chemistry Division, for many helpful discussions and his critical review of the manuscript.

Supplementary Material Available. A listing of equilibrium data will appear following these pages in the microfilm edition of this volume of the journal. Photocopies of the supplementary material from this paper only or microfiche (105 × 148 mm, 20× reduction, negatives) containing all of the supplementary material for the papers in this issue may be obtained from the Journals Department, American Chemical Society, 1155 16th St., N.W., Washington, D. C. 20036. Remit check or money order for $3.00 for photocopy or $2.00 for microfiche, referring to code number JPC-73-2351.

References and Notes

(1) This research was sponsored by the U. S. Atomic Energy Commission under contract with the Union Carbide Corporation.
(2) L. E. McNeese, MSR Program Semiannual Progress Report Feb 28, 1971, USAEC Report No. ORNL-4676, Oak Ridge National Laboratory, Oak Ridge, Tenn., p 234.
(3) D. E. Ferguson and Staff, Chemical Technology Division Annual Progress Report Mar 31, 1971, USAEC Report No. ORNL-4682, Oak Ridge National Laboratory, Oak Ridge, Tenn., p 2.
(4) M. A. Bredig, MSR Program Semiannual Progress Report Aug 31, 1970, USAEC Report No. ORNL-4622, Oak Ridge National Laboratory, Oak Ridge, Tenn., p 85.
(5) "Excess" lithium is defined as the total number of equivalents of lithium in the salt phase minus the number of equivalents of Cl^- or Br^-.
(6) E. L. Youngblood and L. E. McNeese, MSR Program Semiannual Progress Report Aug 31, 1971, USAEC Report No. ORNL-4728, Oak Ridge National Laboratory, Oak Ridge, Tenn., p 202.
(7) M. S. Foster, C. E. Crouthamel, D. M. Gruen, and R. L. McBeth, *J. Phys. Chem.*, **68**, 980 (1964).
(8) E. J. Cairns, C. E. Crouthamel, A. K. Fischer, M. S. Foster, J. C. Hesson, C. E. Johnson, H. Shimotake, and A. D. Tevebaugh, "Galvanic Cells with Fused-Salt Electrolytes," USAEC Report No. ANL-7316, Argonne National Laboratory, Argonne, Ill., 1967, p 119.
(9) L. M. Ferris, J. C. Mailen, J. J. Lawrance, F. J. Smith, and E. D. Nogueira, *J. Inorg. Nucl. Chem.*, **32**, 2019 (1970).
(10) M. Hansen and K. Anderko, "Constitution of Binary Alloys," McGraw-Hill, New York, N. Y., 1958, p 316.
(11) See paragraph at end of paper regarding supplementary material.
(12) L. M. Ferris and J. F. Land, MSR Program Semiannual Progress Report Aug 31, 1971, USAEC Report No. ORNL-4728, Oak Ridge National Laboratory, Oak Ridge, Tenn., p 192.
(13) M. S. Foster, S. E. Wood, and C. E. Crouthamel, *Inorg. Chem.*, **3**, 1428 (1964).
(14) A. S. Dworkin, H. R. Bronstein, and M. A. Bredig, *J. Phys. Chem.*, **66**, 572 (1962).
(15) N. Watanabe, K. Nakanishi, A. Komura, and T. Nakajima, *Kogyo Kagaku Zasshi*, **71**(10), 1599 (1968).
(16) M. A. Bredig in "Molten Salt Chemistry," M. Blander, Ed., Interscience, New York, N. Y., 1964, p 377.
(17) M. Okada, R. A. Guidotti, and J. D. Corbett, *Inorg. Chem.*, **7**, 2118 (1968).
(18) M. S. Foster and R. Eppley, Chemical Engineering Division Summary Report Jan–Mar 1963, USAEC Report No. ANL-6687, Argonne National Laboratory, Argonne, Ill., p 190.
(19) P. M. Robinson and M. B. Bever in "Intermetallic Compounds," J. H. Westbrook, Ed., Wiley, New York, N. Y., 1967, p 43.
(20) K. H. Pitzer, *J. Amer. Chem. Soc.*, **84**, 2025 (1962).
(21) A. S. Dworkin and M. A. Bredig, Chemistry Division Annual Progress Report May 1965, USAEC Report No. ORNL-3832, Oak Ridge National Laboratory, Oak Ridge, Tenn., p 113.
(22) S. W. Mayer, S. J. Yosim, and L. E. Topol, *J. Phys. Chem.*, **64**, 238 (1960).
(23) J. A. van Westenburg, Thesis, Iowa State University 1964, University Microfilms, Ann Arbor, Mich., No. 64-9291.

Electronic Interaction between the Vinyl Group and Its Substituents

A. Katrib and J. W. Rabalais*

Department of Chemistry, University of Pittsburgh, Pittsburgh, Pennsylvania 15260 *(Received April 13, 1973)*

Publication costs assisted by the Petroleum Research Fund

The He I photoelectron spectra of the substituted ethylenes CH_2=CHX, where X = $-CH_3$, $-CH_2NH_2$, $-CH_2SH$, $-CH_2OH$, -CHO, and -COOH, have been obtained. The observed ionization bands have been identified through vibrational structure analysis and by using the results of *ab initio*, INDO, and CNDO/2 calculations. Electronic interaction, in the form of resonance and inductive effects, has been observed between the C=C π MO and the n and/or π orbitals of the substituent. The relative magnitudes and directions of these effects are assessed for the various substituents from a correlation diagram of the energy levels. From the orbital shifts observed it is possible to arrange the substituents according to their increasing electron-withdrawing power as $-CH_3 < -CH_2NH_2 < -CH_2SH < -CH_2OH < -COOH < -CHO$.

Introduction

The technique of photoelectron spectroscopy has provided a direct method of evaluating inductive and resonance effects between ethylene and its substituents.[1-4] The types of interactions that have been observed in vinyl halides, CH=CHX, where X = F, Cl and Br, are as follows. (a) A resonance effect occurs as a result of interaction between the C=C π orbital and the halogen "nonbonding" orbital which is perpendicular to the molecular plane (both orbitals are a'' in the C_s molecule). This conjugation produces two π orbitals, an antibonding combination of predominantly C=C π character and a bonding combination of predominantly halogen n character. Acquization of antibonding character in the C=C π orbital is confirmed by its destabilization (*i.e.*, shift to lower binding energy) and by the increase in the C-X stretching frequency of the ion with respect to the neutral molecule. Evidence for acquization of bonding character in the halogen n orbital is its stabilization (*i.e.*, shift to higher binding energy) and the broadening of its sharp "nonbonding" photoelectron band.[5a] (b) The second type of interaction is due to the inductive effect of the electronegative halogen which serves to draw electron density from the vinyl group to the halogen. This effect tends to stabilize the C=C π orbital and destabilize the halogen n orbitals. The relative strengths of these two opposing effects have been studied as a function of varied halogen substituents.[5b]

This paper presents an investigation of the electronic structure of some substituted ethylenes CH_2=CHX, where X = $-CH_3$, $-CH_2NH_2$, $-CH_2OH$, $-CH_2SH$, -CHO, and -COOH, by means of photoelectron spectroscopy. The purpose of the work is to evaluate the interactions of the C=C π orbital with the methyl group orbitals and the substituent π and/or n orbitals. Resonance interactions between orbitals of the same symmetry and inductive interactions caused by electronegativity differences in these systems are not, in general, in the same direction as those of the vinyl halides. The difference is due to the linking alkyl group (CH_2, CH, or C) which can itself cause shifts in the inherent energies of the n and π orbitals. The ionization bands observed in the spectra are identified by correlation with those of ethylene and some simpler molecules, by using quantum chemical calculations, and by vibrational analysis of the existing fine structure. The electronic structures are discussed in terms of the information obtained from the experimental spectra and *ab initio*,[6] INDO, and CNDO/2 molecular orbital calculations.

Experimental Section

The photoelectron spectra were obtained with a Perkin-Elmer Model PS-16 photoelectron spectrometer using He I resonance radiation. All compounds studied were commercially available reagent grade chemicals. The spectra were calibrated with the $3p_{1/2}$ and $3p_{3/2}$ lines of Ar and the $4p_{1/2}$ and $4p_{3/2}$ lines of Kr in a mixed gas sample.

Results

Propylene. The photoelectron spectrum of propylene in Figure 1a has six bands below 21 eV with vibrational structure only in the low-energy band. The experimental IP's along with those obtained from MO calculations are reported in Table I. The adiabatic ionization energy of the first band at 9.72 eV is in good agreement with the 9.73 eV value reported by Watanabe, *et al.*,[7] using photoionization techniques. In accordance with the MO results this band is attributed to ionization of an electron from the C=C π orbital. This orbital contains some methyl group orbital character in an antibonding combination (Figure 1c).[8] The decrease in this IP by 0.79 eV with respect to the corresponding one of ethylene[9,10] is caused by (1) the inductive effect of the methyl group which serves as an electron donor and (2) the resonance interaction with the methyl group orbital of a'' symmetry which is inherently more stable than the C=C π orbital. Thus, unlike the vinyl halides, the large destabilization of the propylene C=C π orbital results from combined inductive and resonance effects which both tend to shift the orbital in the same direction.

Two vibrational progressions are observed in this band. The principal progression, with a mean spacing of 1340 cm^{-1}, is most likely due to the C=C stretching vibration, ν_6, which is 1647 cm^{-1} in the neutral molecule.[11] The short secondary progression of ~600 cm^{-1} is identified with ν_{14}, the C=C-C bending mode at 578 cm^{-1} in the neutral molecule. The large decrease in the C=C π stretching frequency and the constancy of the C=C-C bending frequency reflects the bonding character of this orbital in the C=C region and the antibonding character

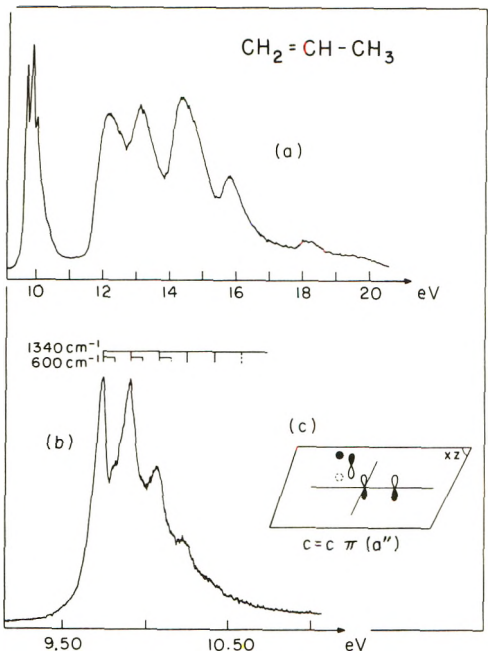

Figure 1. The He I photoelectron spectrum of propylene: (a) the complete spectrum, (b) the first band on an expanded scale, and (c) a qualitative orbital diagram of the outer π a'' orbital.

TABLE I: Measured and Calculated Ionization Potentials of Propylene

Measured IP, eV[b]	Calculated[a] IP's: Ab initio	CNDO/2	INDO	Electron density	MO type[c]
9.72 (A) 9.88 (V)	9.6	10.3	9.9	0.32 C_α 0.45 C_β 0.07 C_γ 0.16 H's	C=C(π)a''
12.4 (V)	13.1	11.5	11.3		a'
13.2 (V)	14.1	12.5	12.2		a'
14.5 (V)	15.5	16.5	16.2		a'
14.6 (V)	15.6	18.1	17.9		a''
15.8 (V)	17.3	19.9	19.7		a'
18.2 (V)	20.5	23.8	23.7		a'

[a] The propylene molecule is considered to have C_s symmetry (*i.e.*, a planar bent carbon chain) for these calculations. A standard value of 4 eV is subtracted from all of the INDO and CNDO/2 eigenvalues in order to compensate for deficiencies in Koopmans' approximation. [b] (A) = adiabatic ionization energy, (V) = vertical ionization energy. [c] The MO order listed is that obtained from the calculations. The exact assignment of the higher ionization bands is uncertain and, at this time, one can only assume the MO ordering indicated for these high-energy bands.

between the vinyl and the methyl group. The outer orbitals of propylene are correlated with those of ethylene in Figure 2.

Allylamine. The nine ionization bands observed in the spectrum of allylamine are shown in Figure 3 and the experimental IP's are listed in Table II. By comparison with the spectra of propylene and ammonia,[12] two ionization bands are expected, and indeed observed, below 11 eV corresponding to orbitals which are mainly C=C π and nitrogen nonbonding. The positions of these two bands can be understood from the following considerations. The nitrogen nonbonding orbital is directed out of the molecular plane and can thus interact with other orbitals of a'' symmetry, such as the methylene group orbital and the C=C π orbital of propylene. The C=C π orbital of propylene is more stable than the n orbital of methylamine. Therefore, as a consequence of the resonance effect, the C=C π orbital will be stabilized and the nitrogen nonbonding orbital will be destabilized when they interact in allylamine. Since the nitrogen atom is more electronegative than the carbons, it will exert an inductive effect which will draw electron density from the carbons. This inductive effect will also stabilize the C=C π orbital and destabilize the nonbonding orbital. Thus, the inductive and resonance effects in allylamine are of the same sign. The positions of the π and n orbitals of propylene, allylamine, and methylamine are plotted in Figure 3b. The stabilization energy of the C=C π orbital, ~0.16 eV, is equal to the destabilization energy of the nitrogen n orbital. The outer orbitals of allylamine are correlated with those of propylene in Figure 2.

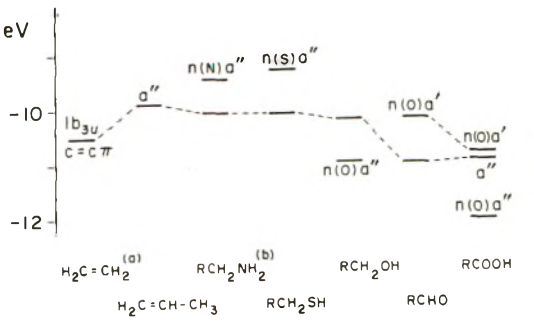

Figure 2. Energy level correlation diagram for the outer orbitals of some substituted ethylenes: (a) from ref 9 and 10, (b) R = H_2C=CH–.

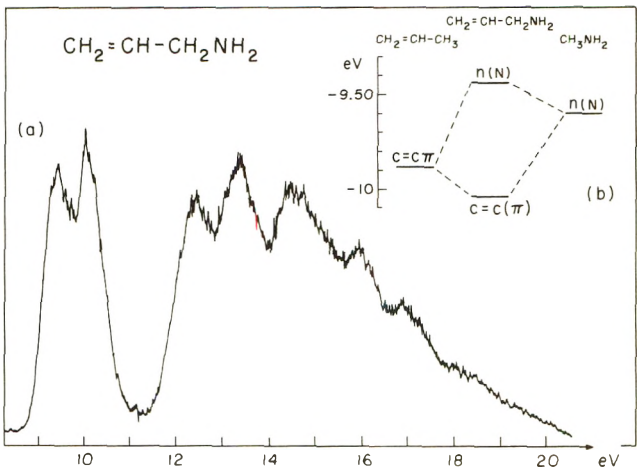

Figure 3. The He I photoelectron spectrum of allylamine: (a) the complete spectrum and (b) an energy level correlation diagram of the n(N) and C=C π orbitals as derived from their respective orbitals in methylamine and propylene.

Allyl Mercaptan. The spectrum of allyl mercaptan, Figure 4a, shows the presence of at least nine bands below 21 eV. The first band at 9.25 eV, Figure 4b, is relatively sharp and exhibits a short vibrational progression of ~780 cm^{-1}. This frequency is of the same order as that observed in methyl mercaptan[13] and is attributed to a C–S stretching mode. The band is assigned to the removal of a mainly sulfur 3p nonbonding electron. The second band at 10.05 eV, Figure 4b, contains a short vibrational progression of ~1410 cm^{-1} which corresponds to the C=C stretching frequency of the molecule. It is assigned to ionization of the C=C π electrons.

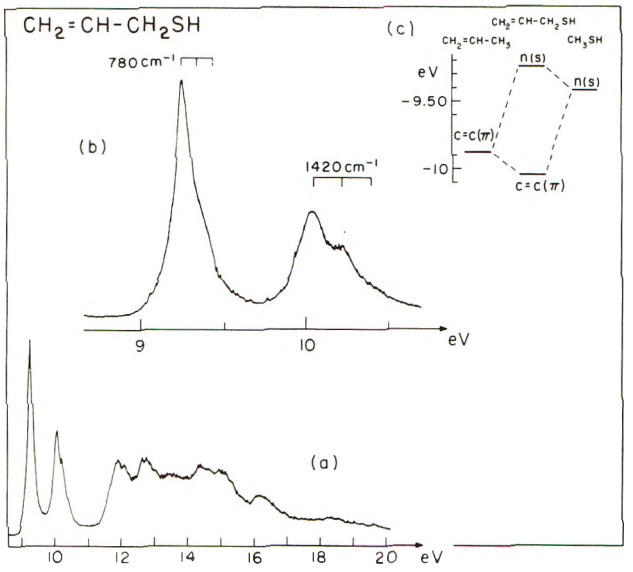

Figure 4. The He I photoelectron spectrum of allylmercaptan: (a) the complete spectrum, (b) the first and second bands on an expanded scale, and (c) an energy level correlation diagram of the n(S) and C=C π orbitals as derived from their respective orbitals in methylmercaptan and propylene.

TABLE II: Ionization Potentials of Substituted Propylenes

Molecule	IP's no.	Measured vert. IP, eV	MO type
	1	8.76 (0)[a]	
Allylamine	1	9.44 (V)	n(N)a''
	2	10.04	C=C(π)a''
	3	12.5	
	4	13.4	
	5	14.6	
	6	14.9	
	7	15.9	
	8	16.9	
	9	18.3	
Allyl mercaptan	1	9.25 (A = V)	n(S)a''
	2	10.05	C=C(π)a''
	3	11.9	
	4	12.7	
	5	13.6	
	6	14.6	
	7	15.1	
	8	16.2	
	9	18.4	
	1	9.63 (A)	
Allyl alcohol	1	10.16 (V)	C=C(π)a''
	2	10.93	n(O)a''
	3	12.2	
	4	13.3	
	5	14.2	
	6	15.2	
	7	16.4	
	8	17.3	
	9	18.7	

[a] (0) = onset of first band.

The positions of the n and π orbitals in allyl mercaptan can be explained in a manner similar to that of allylamine. In this molecule also, the resonance and inductive effects are of the same sign. A plot of the positions of the n and π orbitals of methyl mercaptan, propylene, and allyl mercaptan in Figure 4c shows that the stabilization energy of the C=C π orbital, 0.17 eV, is equal to the destabilization energy of the sulfur n orbital. The experimental IP's are listed in Table II and the outer orbitals are correlated with those of the other molecules in Figure 2.

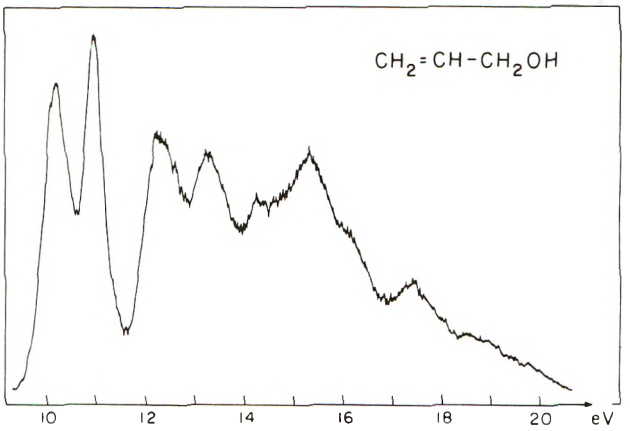

Figure 5. The He I photoelectron spectrum of allyl alcohol.

Allyl Alcohol. The spectrum of allyl alcohol, Figure 5, exhibits at least nine ionization bands below 21 eV. The first band at 10.16 eV is attributed to ionization of a C=C π electron while the relatively sharp band at 10.93 eV is attributed to ionization of an oxygen n electron. Two factors should be noted about this assignment. First, the ordering of the n and π orbitals is changed compared to that of allylamine and allyl mercaptan and second, the C=C π orbital is stabilized by ~0.28 eV while the oxygen n orbital is destabilized by only ~0.05 eV when compared to propylene and methyl alcohol, respectively. In order to understand these differences, the high electronegativity of the oxygen atom must be considered. The prevailing type of interaction in the outer orbitals is the inductive effect by which electron density is drawn toward the oxygen atom, thereby stabilizing the C=C π orbital.

The resonance effect appears to be of minor importance compared to the strong inductive effect of the oxygen atom. The experimental IP's are listed in Table II and the outer orbitals are correlated with those of the other molecules in Figure 2.

Acrolein. The spectrum of acrolein shows the presence of at least seven ionization bands below 21 eV, with resolved vibrational structure in the first two bands, Figure 6a.

The first band, Figure 6b, consists of a very intense adiabatic IP at 10.13 eV followed by two weak vibrational components with a spacing of 1220 cm^{-1}. This band is very similar to the first IP of formaldehyde[9] at 10.88 eV which corresponds to ionization of the oxygen nonbonding a' orbital. The INDO and CNDO/2 calculations also predict that the outermost orbital of acrolein is mainly of oxygen nonbonding type with some admixture of vinyl and formyl group orbitals. The decrease in binding energy of the oxygen nonbonding (a') orbital in acrolein as compared to formaldehyde is due to an inductive interaction with the allyl group. Evidence for this interaction is contained in the vibrational structure which accompanies the 0-0 band. As a result, the vibrational progression is assigned to either ν_8, the formyl CH rock at 1360 cm^{-1}, or ν_9, the vinyl CH rock at 1276 cm^{-1}, in the neutral molecule.[14] This assignment is expected since excitation of the

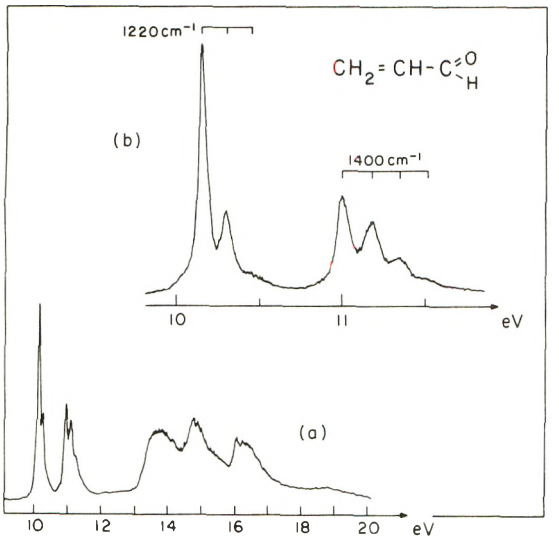

Figure 6. The He I photoelectron spectrum of *acrolein*: (a) the complete spectrum and (b) the first and second bands on an expanded scale.

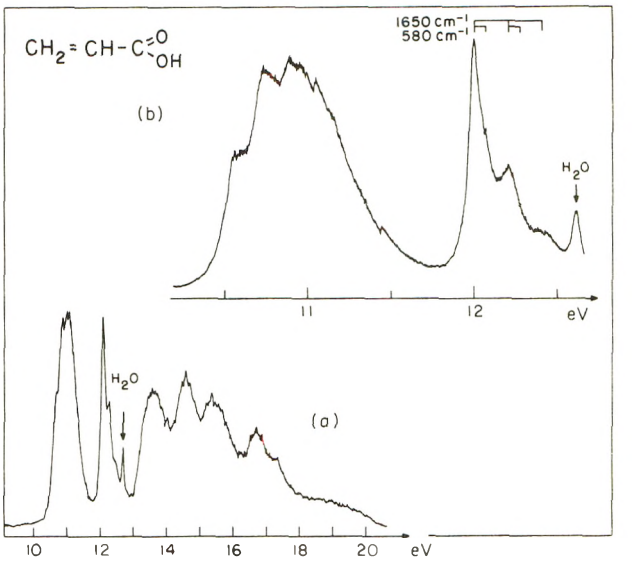

Figure 7. The He I photoelectron spectrum of acrylic acid: (a) the complete spectrum and (b) the first, second, and third bands on an expanded scale.

CH_2 deformation mode has been observed upon ionization of the b_2 in-plane oxygen non-bonding orbital in formaldehyde.[9] The small reduction in the vibrational frequency of the neutral molecule is expected when an electron is removed from a mainly nonbonding orbital. This n orbital differs from that of allyl alcohol by being in the plane of the molecule and therefore it cannot enter into resonance interaction with the C=C π orbital. It should be noted that the oxygen nonbonding orbital in acetyladehyde[15] is at 10.22 eV which is very similar to acrolein.

The second band at 10.95 eV, Figure 6b, consists of four vibrational peaks with a mean spacing of 1400 cm^{-1}. This band is very similar to the first IP of the isoelectronic molecule butadiene,[16] where it is assigned to ionization of electrons from a π MO. Unlike the case of butadiene where resonance interaction between the two final groups is very large, the calculations indicate that resonance interaction between the C=C and the C=O π electrons of acrolein is rather small. This weak resonance interaction can be attributed to the large energy difference between the C=C π and C=O π orbitals. Thus, the stabilization of the C=C π orbital of acrolein as compared to propylene is mainly due to the inductive effect of the carbonyl group which draws electron density from the vinyl group. The vibrational progression at 1400 cm^{-1} is assigned to the C=C π stretching mode at 1625 cm^{-1} in the neutral molecule. The experimental and calculated IP's are listed in Table III[17,18] and the outer orbitals are correlated with those of the other molecules in Figure 2.

Acrylic Acid. The spectrum of acrylic acid is shown in Figure 7a and the low binding energy bands are shown on an expanded scale in Figure 7b. The band centered at ~10.8 eV appears to be composed of two different photoelectron transitions for the following reasons. It contains a complicated vibrational structure which cannot be readily assigned to one transition. It is approximately twice as intense as the band at ~12.0 eV which contains a simple vibrational structure that must be due to a single transition. Thus, the 10.8-eV band is considered to be composed of two overlapping ionization bands.

In order to interpret the spectrum of acrylic acid it is necessary to consider which molecular orbitals are expected in the low binding energy region. The MO calculations predict three orbitals in this low-energy region; (1) a nonbonding orbital which is predominantly localized in the in-plane orbitals of the carbonyl oxygen and the hydroxyl oxygen, designated as n(0)a′; (2) a π orbital which is the prodigy of the C=C π mixing with the out-of-plane oxygen orbitals; (3) a nonbonding orbital with a″ symmetry situated mainly on the hydroxyl oxygen with some admixture of carbon a″ orbitals, designated as n(0)a″. The IP's obtained from the calculations match very well with those obtained experimentally if the bands at 10.77, 10.91, and 12.00 eV are assigned as n(0)a′, π, and n(0)a″, respectively. This assignment also agrees with a study of a series of carboxylic acids[19] in which the separation between n(0)a′ and n(0)a″ was found to be at least 1 eV.

A vibrational frequency of 1320 cm^{-1} is observed in the 10.77-eV band. Due to the nature of the band, this probably corresponds to the C=O stretching frequency at 1705 cm^{-1} or the COOH group frequency at 1727 cm^{-1} in the neutral molecule.[20,21] It is not possible to follow vibrational progressions in the second band. Two vibrational progressions are observed in the third band with intervals of 1650 and 580 cm^{-1}. The 580-cm^{-1} progression most likely corresponds to the COOH deformation at 628 cm^{-1} in the molecule. The 1650-cm^{-1} progression probably corresponds to the molecular modes at 1705 or 1727 cm^{-1} mentioned above.

As in the case of acrolein, the resonance interaction between the C=C π orbital and the C=O π orbital is very small in acrylic acid. The outer orbitals of acrylic acid are correlated with those of the other molecules in Figure 2.

General

The analysis of the photoelectron spectra of these substituted ethylene compounds has shown that the C=C π orbital of the vinyl group and the π or n electrons of the substituents do not remain localized on their respective groups. Instead, they generally become delocalized over a large portion of the molecule with the nonbonding orbitals acquiring more bonding character in the composite system than they possessed in their constituent molecules.

TABLE III: Measured and Calculated IP's of Acrolein and Acrylic Acid

Molecule	IP's no.	Measured vert. IP's, eV	Calculated IP's CNDO/2	Calculated IP's INDO	Electron density	MO type[b]
trans-Acrolein[a]	1	10.13 (A = V)	9.6	8.7	0.07 $C_\alpha(2p_x)$ 0.04 $C_\beta(2p_z)$ 0.07 $C_\gamma(2p_z)$ 0.09 $O(2p_x)$ 0.50 $O(2p_z)$ 0.17 H_1	n(a′)
	2	10.95	10.8	10.4	0.26 $C_\alpha(2p_y)$ 0.34 $C_\beta(2p_y)$ 0.08 $C_\gamma(2p_y)$ 0.32 $O(2p_y)$	π(C=C)(a″)
	3	13.8	12.5	12.0		a′
	4	14.9	15.4	14.6	0.25 $C_\alpha(2p_y)$ 0.14 $C_\beta(2p_y)$ 0.33 $C_\gamma(2p_y)$ 0.28 $O(2p_y)$	π(C=O)a″
	5	15.5	16.4	15.4		a′
	6	16.4	16.6	16.0		a′
	7	18.8	21.5	21.1		a′
	1	10.60 (A)				
Acrylic acid[a]	1	10.77 (V)	9.8	8.9	0.10 $C_\alpha(2p_z)$ 0.02 ($C_\beta(2p_z)$ 0.05 $C_\gamma(2p_z)$ 0.08 $O_1(2p_x)$ 0.52 $O_1(2p_z)$ 0.13 $O_2(2p_x)$ 0.04 H_1 0.02 H_2 0.03 H_3	n(a′)
	2	10.91	10.2	9.8	0.13 $C_\alpha(2p_y)$ 0.20 $C_\beta(2p_y)$ 0.06 $C_\gamma(2p_y)$ 0.45 $O_1(2p_y)$ 0.15 $O_2(2p_y)$	π(a″)
	3	12.00	12.8	11.6	0.19 $C_\alpha(2p_y)$ 0.15 $C_\beta(2p_y)$ 0.01 $C_\gamma(2p_y)$ 0.03 $O_1(2p_y)$ 0.62 $O_2(2p_y)$	n(a″)
	4	13.5	12.9	11.8		a′
	5	14.5	13.4	13.0		a′
	6	15.3	16.1	15.2	0.15 $C_\alpha(2p_y)$ 0.06 $C_\beta(2p_y)$ 0.33 $C_\gamma(2p_y)$ 0.18 $O_1(2p_y)$ 0.27 $O_2(2p_y)$	π(C=O)
	7	16.6	18.2	16.9		a′
	8	17.2	18.6	18.1		a′
	9	18.8	19.0	18.5		a′

[a] The bond lengths and angles employed in CNDO/2 and INDO calculations were obtained from ref 17 and 18. The structures of the molecules with the designation of the atoms are as follows (the molecular plane is *xz*):

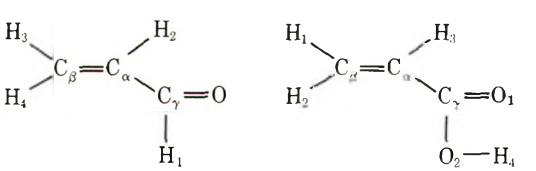

[b] The MO order listed is that obtained from the calculations. The exact assignment of the higher ionization bands is uncertain and, at this time, one can only assume the MO ordering indicated for these high-energy bands.

The low-energy IP's are strongly dependent on resonance and inductive effects that occur between the two constituents in the molecules. The signs of the resonance and inductive effects depend on the relative positions of the constituent molecules IP's and the electronegativities of these constituents. In propylene, resonance interaction

(sometimes called hyperconjugation) occurs between the methyl group orbital and the C=C π orbital (both a''). Since the methyl group orbital is inherently the more stable of the two, the C=C π orbital acquires antibonding character and is destabilized while the methyl group orbital acquires bonding character and is stabilized. The methyl group is also a good electron donor and supplies electron density through its inductive effect. Thus, resonance and inductive effects in propylene are of the same sign resulting in a low-energy C=C π orbital.

In allylamine and allyl mercaptan, the C=C π orbital is inherently more stable than the N or S nonbonding orbital. As a result, resonance interaction destabilizes the n orbital and stabilizes the π orbital. The nitrogen atom is more electronegative than the carbon atoms and its inductive effect withdraws electron density from the vinyl group. Thus, the resonance and inductive effects in allylamine are of the same sign resulting in a stabilization of the C=C π orbital. This shift is just the opposite of that occurring in propylene.

In allyl alcohol, acrolein, and acrylic acid the main effect is the inductive influence of the electronegative oxygen atoms resulting in a stabilization of the C=C π orbital. Resonance interactions in these three molecules are very small due to the large energy difference between the C=C π orbital and the C=O π or n orbitals of the substituent. It is possible to distinguish two nonbonding ionization bands in acrylic acid, the n(0)a' and n(0)a'' orbitals.

From the analysis of shifts in the C=C π orbital, the substituents can be arranged according to their increasing electron-withdrawing power as $-CH_3 < -CH_3NH_2 < -CH_2SH < -CH_2OH < -COOH < -CHO$.

Acknowledgment. Acknowledgment is made to the donors of the Petroleum Research Fund, administered by the American Chemical Society, for support of this research.

References and Notes

(1) D. Chadwick, D. C. Frost, A. Katrib, C. A. McDowell, and R. A. N. McLean, *Can. J. Chem.*, **50**, 2642 (1972).
(2) H. Bock and K. Wittel, *J. Chem. Soc., Chem. Commun.*, 602 (1972).
(3) R. F. Lake and H. Thompson, *Proc. Roy. Soc., Ser. A*, **315**, 323 (1970).
(4) N. Jonathan, K. Ross, and V. Tomlinson, *Int. J. Mass Spectrom. Ion Phys.*, **1**, 111 (1968).
(5) (a) It should be noted that there is an additional halogen n orbital parallel to the molecular plane (a' symmetry) which retains its nonbonding character and provides a sharp photoelectron band. (b) A. Katrib and J. W. Rabalais, to be submitted for publication.
(6) L. Radom, W. A. Lathan, W. J. Hehr, and J. A. Pople, *J. Amer. Chem. Soc.*, 93, 5339 (1971).
(7) K. Watanabe, T. Nakayama, and J. Motte, *J. Quant. Spectrosc. Radiat. Transfer*, **2**, 369 (1962).
(8) This type of interaction is sometimes called "hyperconjugation," see R. S. Mulliken, *Tetrahedron*, **5**, 253 (1959).
(9) D. W. Turner, C. Baker, A. D. Baker, and C. B. Brundle, "Molecular Photoelectron Spectroscopy," Wiley-Interscience, New York, N. Y., 1970.
(10) G. R. Branton, D. C. Frost, T. Makita, C. A. McDowell, and I. A. Stenhouse, *Phil. Trans. Roy. Soc. London, Ser. A*, **268**, 77 (1970).
(11) G. Herzberg, "Infrared and Raman Spectra of Polyatomic Molecules," Van Nostrand, New York, N. Y., 1945, p 354.
(12) J. W. Rabalais, L. Karlsson, L. O. Werme, T. Bergmark, and K. Siegbahn, *J. Chem. Phys.*, **58**, 3370 (1973).
(13) D. C. Frost, F. G. Herring, A. Katrib, C. A. McDowell, and R. A. N. McLean, *J. Phys. Chem.*, **76**, 1030 (1972).
(14) J. C. D. Brand and D. G. Williamson, *Discuss. Faraday Soc.*, **35**, 184 (1963).
(15) B. J. Cocksey, J. H. D. Eland, and C. J. Danby, *J. Chem. Soc. B*, 790 (1971).
(16) C. R. Brundle and M. B. Robin, *J. Amer. Chem. Soc.*, **92**, 5550 (1970).
(17) R. Wagner, J. Fine, J. W. Simmons, and J. H. Goldstein, *J. Chem. Phys.*, **26**, 634 (1957).
(18) T. Ukaji, *Bull. Chem. Soc. Jap.*, **32**, 1266 (1959).
(19) D. A. Sweigart and D. W. Turner, *J. Amer. Chem. Soc.*, **94**, 5592 (1972).
(20) L. J. Bellamy in "Advances in Infrared Group Frequencies," Methuen, London, 1968.
(21) W. R. Feairheller and J. E. Katon, *Spectrochim. Acta, Part A*, **23**, 2225 (1967).

COMMUNICATIONS TO THE EDITOR

Hydrocarbon Adsorption Effects on the Unit Cell Constant of NaY Zeolites

Publication costs assisted by Centre National de la Recherche Scientifique

Sir: The cubic unit cell constant (U.C.) of Faujasite-type zeolites mainly depends on the relative amount of Si and Al atoms present in the zeolite aluminosilicate framework.[1] However, the framework slightly distorts in response to the positions of the exchangeable cations and to the nature of sorbed molecules and these short-range perturbations generally induce some change in the zeolite U.C. For instance, it was shown in a previous paper[2] that the U.C. of partly dehydrated NiY zeolites is a linear function of both exchange level and nickel population of hexagonal prisms, but the X-ray investigation of a NiY zeolite containing acetylene[3] proved that the relationship no longer holds, namely the U.C. reduction occuring on acetylene adsorption is not correlated to a migration of Ni^{2+} ions. The purpose of the present note is to determine the reasons why the zeolite lattice undergoes such a contraction on adsorption of C_2H_2 or other unsaturated hydrocarbons. The NaY zeolite was chosen because the effect is far more pronounced than in NiY zeolite.

The NaY zeolite was a Linde SK40 sample. The preparation of the two hydrogen zeolites $H_{29}Na_{27}Y$ and $H_{54}Na_2Y$ was described previously.[4] Every sample was activated for 15 hr in oxygen and for 6 hr under vacuum. The heating temperature was 600° for the NaY sample and 350° for the HY samples. Then the zeolites were placed in contact for 15 hr with 100 Torr pressure of gases previously dried over activated molecular sieves. The treated powder was then transferred into capillaries for the X-ray investigation which was performed according to the procedure previously described.[5]

Table I gives the U.C. of the samples containing various hydrocarbons. It comes out that the magnitude of the U.C. decrease is dependent on the total sodium content of the zeolite (NaY > $H_{29}Y$ > $H_{52}Y$ = 0) and to the multiple bond character of the hydrocarbon molecule (ethyne > ethylene > ethane = 0). The unsaturated hydrocarbons may interact with the zeolite either by a direct association of the molecule with the framework oxygens or through a bonding with the Na^+ ions. The two eventualities have been considered by Tsitsishvili, *et al.*,[6] to interpret their infrared measurements on zeolites containing acetylene. A recent crystallographic study of the Na A zeolite[7] has shown that the C_2H_2 molecules are associated with the Na^+ ions while no significant interaction between the CH groups and the framework oxygens takes place. The same behavior is expected with the present samples in order to prove that the crystal structure of an NaY zeolite was determined before and after acetylene adsorption.

The structures were determined from powder data (all reflections with $h^2 + k^2 + l^2 \leq 396$) according to the refinement procedure previously described.[5] The final refinements give R indices of 0.07 and 0.1, respectively, for the reference sample and for the sample containing acetylene.

It turns out that the cation distribution on SI, SI′, and SII sites is not significantly changed. Moreover, no lengthening of any T–O bond which could have indicated an interaction of a framework oxygen with an acidic acetylene proton is observed. Moreover, a bonding across the sodalite cage such as O---HC≡CH---O is very unlikely to occur because the distances from the sodalite cage center to all the oxygen atoms of the cage wall are longer in the sample containing C_2H_2 whereas a shortening of some distances should have been observed. However, the decrease of the distance between the center of the 12-membered oxygens ring (supercage aperture) and the O(1) belonging to that ring provides possible evidence for a C_2H_2 bridging two O(1) across the aperture. On the other hand, the Na(I′)–O(3) and Na(II)–O(2) distances are longer—and the T–O(3) and T–O(2) shorter—in the sample contacted with C_2H_2 than in the reference sample. These results strongly suggest that the C_2H_2 molecules are associated with the Na^+ ions of SI′ and SII sites. This would produce a weakening of the Na(I′)–O(3), and Na(II)–O(2) bonds (which are thus elongated) and a shortening of the T–O(3) and T–O(2) bonds. The U.C. decrease occuring on C_2H_2 adsorption may subsequently be explained by the shortening of these bonds.

The decrease of the zeolite U.C. on adsorption of other hydrocarbons probably proceeds *via* the same mechanism. The results given in Table I support this assumption since the hydrocarbons effects appear to be clearly related to the multiple bond character of the molecules and to the Na^+ ions available as well. The unsaturated molecules are

TABLE I: Cubic Unit Cell Constant of Y Zeolites (in Å, ±0.01Å)

Sample	Before gas adsorption	Acetylene	Propyne	Ethylene	1-Butene	Ethane
NaY	24.81	24.72 (24.79)[a]	24.72	24.76 (24.81)[a]	24.76 (24.79)[a]	24.81
$H_{29}Y$	24.75	24.71 (24.75)[a]				
$H_{52}Y$	24.69	24.70				

[a] The values in parentheses correspond to the U.C. of sample outgassed at room temperature for 6 hr (after gas contact).

loosely attached to the Na^+ ions since they can be almost entirely removed by outgassing the zeolite at room temperature (the U.C. variations are nearly reversible). Therefore, the unsaturated molecules may well be associated with the Na^+ ions through ions to induced-dipole forces as previously suggested.[7] This also corroborates the findings of Yates.[8,9] However, in contrast with ethylene, the acetylene molecules cannot be entirely removed at room temperature. This again shows that the cation to sorbed molecule bond is stronger when more π electrons are present.

This study proves that the interaction between unsaturated molecules adsorbed on Y zeolites and Na^+ ions is the main cause for the observed U.C. decrease. The variation observed must be taken into consideration before applying relations such as that given in a previous paper.[2]

References and Notes

(1) J. V. Smith, *Advan. Chem. Ser.*, **No. 101**, 171 (1971).
(2) P. Gallezot and B. Imelik, *J. Phys. Chem.*, **77**, 652 (1973).
(3) P. Pichat, J. Vedrine, P. Gallezot, and B. Imelik, *J. Catal.*, in press.
(4) P. Gallezot and B. Imelik, *J. Chim. Phys.*, **68**, 34 (1971).
(5) P. Gallezot, Y. Ben Taarit, and B. Imelik, *J. Catal.*, **26**, 295 (1972).
(6) G. V. Tsitsishvili, G. D. Bagratishvili, and N. I. Onashvili, *Russ. J. Phys. Chem.*, **43**, 524 (1969).
(7) A. A. Amaro and K. Seff, *J. Chem. Soc.*, **22**, 1201 (1972).
(8) J. L. Carter, D. J. C. Yates, P. J. Lucchesi, J. J. Elliott, and V. Kevorkian, *J. Phys. Chem.*, **70**, 1126 (1966).
(9) D. J. C. Yates, *J. Phys. Chem.*, **70**, 3693 (1966).

Institut de Recherches sur la Catalyse, C.N.R.S.
69100 Villeurbanne, France

P. Gallezot
B. Imelik*

Received June 29, 1973

Selective Hydrogen Atom Abstraction by Hydrogen Atoms in Neopentane–Alkane Mixtures at 77 K

Publication costs assisted by Faculty of Engineering, Nagoya University

Sir: Recently quite interesting phenomena have been reported on the hydrogen atom abstraction reaction by radicals in the solid phase at 77 K.[1,2] Here we report that H atoms produced by the photolysis of hydrogen iodide in neopentane containing a small amount of alkane react selectively with the solute alkane at 77 K.

Experimental procedures were identical with those described in the previous studies.[2,3] When the photolysis of hydrogen iodide (0.05 mol %) is performed in neopentane with 2537-Å radiation at 77 K, an esr spectrum of the neopentyl radical is obtained. H atoms produced by the photolysis of hydrogen iodide abstract hydrogen atoms from neopentane to form the neopentyl radical. When the photolysis of hydrogen iodide is performed in neopentane containing a small amount of an alkane such as ethane, propane, or isobutane, a quite different esr spectrum of the solute radical, such as ethyl, propyl, or the *t*-butyl radical, is obtained. The H atoms produced by the photolysis react selectively with the solute alkane to form the solute radical, even if the solute concentration is very low. The yields of solute radicals in the photolysis of *neo*-C_5H_{12}-*i*-C_4H_{10}(1%)-HI(0.05%) are 35 times as high as those in the photolysis of *neo*-C_5H_{12} -HI(0.05%). Therefore, most of the H atoms produced by the photolysis cannot react with neopentane in the pure neopentane matrix, while they can react with the solute alkane in the neopentane–alkane mixture.

One possible explanation for the selective formation of solute radicals is that hydrogen iodide and the alkane form a complex and dissolve in juxtaposition in the neopentane matrix. Though the possibility cannot be neglected at present, it may be small for the following reasons. First, there is no evidence to support the idea that the hydrogen iodide forms a complex with the alkane except neopentane. Since the yields of solute radicals in the photolysis of *neo*-C_5H_{12}-*i*-C_4H_{10}(1%)-HI(0.1%) are about 6 times as high as those in the photolysis of *neo*-C_5H_{12}–C_3H_8(1%)-HI(0.1%), it is expected from the complex hypothesis that isobutane is more favorable for the formation of the complex than propane. Propyl radical, however, is selectively formed in the photolysis of *i*-C_4H_{10}–C_3H_8(1%)-HI(0.1%) at 77 K. Therefore, the results cannot be explained by the hypothesis of the complex formation. Secondly, it was found that solute radicals were selectively formed in the radiolysis of neopentane containing a small amount of alkanes.[3] The results show that the selective C–H bond scission does occur in the absence of hydrogen iodide and that it is a phenomenon characteristic of the neopentane–alkane mixtures at 77 K. Thirdly, it has been observed that a large fraction of 3-methylpentyl radicals produced by the photolysis of HI in 3-methylpentane glass at 77 K decays within a few minutes, apparently by combination with iodine atoms formed near the same locations in the matrix when the HI is dissociated.[4] The *t*-C_4H_9 radicals produced by the photolysis of HI in a neopentane–isobutane(1%) mixture, however, do not decay at all at 77 K, even if the sample is stored for 5 hr after the photolysis. Therefore, it seems that the H atoms produced by the photolysis of hydrogen iodide migrate through the neopentane matrix and react selectively with the solute alkane. The yield of *t*-C_4H_9 radicals in the photolysis of *neo*-C_5H_{12}–*i*-C_4H_{10}–HI(0.05%) at 77 K was studied as a function of concentration of isobutane. Since the yields become a plateau over 0.2 mol % of isobutane, most of the H atoms react selectively with isobutane at 0.2%. The selective hydrogen atom abstraction by H atoms was also observed in the isobutane–propane mixture.

The relative probabilities for hydrogen atom abstraction by H atoms in a variety of alkane mixtures at 77 K are summarized in Table I. It is surprising that the relative probabilities for hydrogen atom abstraction from the solute alkanes are much larger than that from neopentane. The relative probabilities for deuterium atom abstraction in the solid phase are shown in the third column of Table I.[5] The relative rate constants of hydrogen atom abstraction by hot D atoms in the gas phase are also given in the fourth column of Table I.[6] The reported relative probabilities for hydrogen atom abstraction from alkanes are of the same order of magnitude as that from neopentane even in the solid phase. The extremely large values for the alkanes in the present work may be caused by the specific physical property of the neopentane–alkane mixture in the solid phase. Classical activation energies of hydrogen atom abstraction by thermal H atoms are shown in the last column in Table I. It should be noted that the activation energy for neopentane is smaller than that for ethane.

The present results obtained for the solid alkane mixture are quite mysterious for us. It is conceivable, how-

TABLE I: Relative Probability for Hydrogen Atom Abstraction in Alkane Mixtures at 77 K

Alkane	Relative probability for H-atom abstraction in alkane mixtures[a]	Relative probability for D-atom abstraction[b]	Relative rate constant for H-atom abstraction[c]	Classical activation energy for H-atom abstraction by thermal H atom, kcal/mol	
		neo-C_5H_{12}–RH(1%)–HI(0.05%) System			
neo-C_5H_{12} (pure)	1		1.00	9.3[d]	
C_2H_6	200	0.73	0.73	9.5[d]	9.9[e]
C_3H_8	620	1.1		8.5[d]	8.4[e]
n-C_4H_{10}	500				8.4[e]
i-C_4H_{10}	3500	1.6			7.4[e]
i-C_4H_9D	1400				
c-C_5H_{10}	2400				
i-C_5H_{12}	1300				
c-C_6H_{12}	270	4.6			
c-$C_5H_9CH_3$	1300				
n-C_6H_{14}	1000				
$(CH_3)_2CHCH(CH_3)_2$	800				
		i-C_4H_{10}–C_3H_8(1%)–HI(0.1%) System			
i-C_4H_{10} (pure)	1	1.0			
C_3H_8	40	0.69		8.5[d]	8.4[e]

[a] The relative probability, measured at 77 K by uv illumination for 3 min, is equal to (yield of solute radical per 3 min) × (concentration of *neo*-C_5H_{12})/(concentration of RH). The yields of solute radical were measured by double integration of the first-derivative esr signals of the solute radical. Since the formation of the solute radical is quite selective, serious overlapping of the spectra of the solute radical and the neopentyl radical does not occur. The microwave power level used did not result in saturation of any of the signals. [b] The relative probability for D-atom abstraction by CH_3 radical was measured by the photolysis of perdeuterated alkane containing methyl iodide (2%) in the solid phase at 20 K.[5] It was reported that the relative probabilities for D-atom abstraction from alkanes in the solid phase are the same as those in the gas phase and that there is no isotope effect between deuterium and hydrogen atom abstraction. [c] The rate constant of H-atom abstraction by hot deuterium atom was measured by the photolysis of alkane containing deuterium iodide in the gas phase at 298 K.[6] [d] T. Kagiya, Y. Sumida, I. Inoue, and F. S. Dyachkovskii, *Bull. Chem. Soc. Jap.*, **42**, 1812 (1969). [e] B. A. Thrush, *Progr. React. Kinet.*, **3**, 89 (1965).

ever, that the physical condition of the matrix, such as the local crystalline structure near the additive and the crystalline structure of the matrix, would affect the selective hydrogen atom abstraction reaction.

References and Notes

(1) (a) E. D. Sprague and F. Williams, *J. Amer. Chem. Soc.*, **93**, 787 (1971); (b) J. T. Wang and F. Williams, *ibid.*, **94**, 2930 (1972); (c) A. Campion and F. Williams, *ibid.*, **94**, 7633 (1972).
(2) T. Wakayama, T. Miyazaki, K. Fueki, and Z. Kuri, *Bull. Chem. Soc. Jap.*, **44**, 2619 (1971).
(3) (a) T. Miyazaki, T. Wakayama, M. Fukaya, Y. Saitake, and Z. Kuri, *Bull. Chem. Soc. Jap.*, **46**, 1030 (1973); (b) M. Kato, Y. Saitake, T. Miyazaki, and Z. Kuri, *ibid.*, **46**, 2004 (1973).
(4) W. G. French and J. E. Willard, *J. Phys. Chem.*, **72**, 4604 (1968).
(5) R. E. Rebbert and P. Ausloos, *J. Chem. Phys.*, **48**, 306 (1968); *cf.* footnote *b* in Table I.
(6) R. J. Carter, W. H. Hamill, and R. R. Williams, *J. Amer. Chem. Soc.*, **77**, 6457 (1955); *cf.* footnote c in Table I.

Department of Synthetic Chemistry **Terunobu Wakayama**
Faculty of Engineering **Tetsuo Miyazaki***
Nagoya University **Kenji Fueki**
Chikusa-ku, Nagoya, Japan **Zen-ichiro Kuri**

Received March 14, 1973

MACROMOLECULAR PHYSICS

Volume 1: **Crystal Structure, Morphology, Defects**

by BERNHARD WUNDERLICH

Contents: List of Tables. Preface. THE STRUCTURE OF MACROMOLECULES. The Macromolecular Hypothesis. The Synthesis of Macromolecules. The Molecular Weight. The Molecular Conformation. Isomers and Copolymers. References. THE MICROSCOPIC STRUCTURE OF CRYSTALS. Discovery and Proof of the Lattice Theory. Motif and Repetition Scheme. Structures of Minimum Free Energy. Crystal Structures of Macromolecules. References. THE CRYSTAL MORPHOLOGY. Crystal Morphology. Macromolecular Crystals. Lamellar Crystals. Epitaxy. Twinned Crystals. Dendrites. Spherulites. Fibrous Crystals. Isometric Crystals. THE DEFECT CRYSTAL. Macroscopic Recognition of Defects. Defect Concepts. Microscopic Defects. Deformation of Polymer Crystals. References.

1973, 568 pp., $35.00

PHYSIO-CHEMICAL PROPERTIES OF NUCLEIC ACIDS

edited by JULES DUCHESNE

Comprising such aspects as the electrical, optical, magnetic, thermodynamic and hydrodynamic properties of biomolecules, this major three-volume publication successfully fulfils the need for a critical approach towards the understanding of the physical chemistry of nucleic acids and their constituents. The first of these volumes is mainly concerned with the intrinsic properties of nucleic acids, considered as macromolecules, and their components. In addition, this study is completed by the analysis of different types of bindings or interaction mechanisms, including photodynamic and radiation effects, as well as fluorescence. In the second volume, the emphasis is placed on structural studies and especially on conformational changes, using spectroscopic techniques as well as methods of thermodynamics and hydrodynamics. The stage of specific biological functions is attained in the last volume, with some considerations on repair mechanisms in relation to the general problem of evolution.

Volume 1/**Electrical, Optical and Magnetic Properties of Nucleic Acids and Components**

1973, 336 pp., $15.75

Volume 2/**Structural Studies on Nucleic Acids and Other Biopolymers**

1973, about 300 pp., $21.00

Volume 3/**Electron Microscopy, Intra- and Intermolecular Interactions, Radiation Effects in DNA Cells, and Repair Mechanisms**

1973, about 300 pp., in preparation

PHYSICAL METHODS IN HETEROCYCLIC CHEMISTRY

edited by ALAN R. KATRITZKY

Volume 5: **Handbook of Molecular Dimensions: X-Ray Bond Angles and Lengths**

by P. J. WHEATLEY

So much progress has been made in the determination of molecular parameters that Volume 5 is devoted entirely to the values of bond lengths and angles obtained by X-ray crystallography. This handbook is a compendium of X-ray structure determinations of molecules and ions containing heterocyclic rings. It consists of a series of entries that lists the values of the more important lengths and angles in the heterocyclic component of each molecular species. Each entry is accompanied by a reference so that the reader can consult the original paper to assess the accuracy of the figures, and also includes the name of the compound used by the authors and the structural formula.

1972, 612 pp., $39.00

CONFORMATIONAL PROPERTIES OF MACROMOLECULES

by A. J. HOPFINGER

A Volume in the MOLECULAR BIOLOGY Series

This book provides a comprehensive discussion of the theory of conformational energy calculations and the application of this theory to the prediction of macromolecular properties. Special emphasis is given to the justification of the use of empirical potential functions in molecular structure calculations. Major topics covered include the following: macromolecular geometry and classic problems in chain statistics; in-depth discussions of the forces that dictate molecular conformation and illustrations of new and novel approaches to treating polymer-solvent interactions; the accuracy of conformational energy calculations and comparisons of many experimental and theoretical findings; conformational transitions; and the combining of conformational energy calculations with ORD/CD and NMR spectroscopies to study macromolecular structure. *1973, 348 pp., $24.50*

THEORY OF UNIMOLECULAR REACTIONS

by W. FORST

A Volume in the PHYSICAL CHEMISTRY Series

This book provides an up-to-date review of the principles and applications of the transition state version of the statistical theory of unimolecular reactions, also known as the Rice-Ramsperger-Kassel-Marcus (RRKM) or the quasi-equilibrium (QET) theory. This theory has been successful in interpreting a wealth of experimental data in a variety of gas phase experimental systems. The author shows how—under carefully stipulated conditions—this theory can be applied to any unimolecular reaction, regardless of mode of reactant excitation. He also shows how theoretical parameters are related to experimental observables, and deals at some length with the techniques used to obtain numerical answers. The book is divided into two parts. Part I discusses the fundamental theory of unimolecular reactions, assuming a basic knowledge of quantum and statistical mechanics and rudiments of reaction rate theory. Part II describes the applications of the theory to specific experimental systems—including the unimolecular reactions of neutral reactants in thermal, photochemical, and chemical-activation systems as well as the reactions of ions prepared by electron impact, charge exchange, photoionization, and radiolysis. *1973, about 375 pp., $29.50*

CHEMICAL APPLICATION OF NMR IN PARAMAGNETIC MOLECULES

edited by G. N. La MAR, W. D. HORROCKS, Jr. and R. H. HOLM

Tentative Contents: J. P. JESSON: The Paramagnetic Shift. T. J. SWIFT: The Paramagnetic Linewidth. G. N. La MAR: Spin Delocalization and Electronic Structure. W. D. HORROCKS, Jr.: Analysis Isotropic Shifts. D. R. EATON: Spin Distribution in Organic Ligands. MICHAEL F. RETTIG: Spin Distribution in Organometallic Compounds. R. H. HOLM and C. J. HAWKINS: Stereochemistry and Structural and Electronic Equilibria. G. N. La MAR and LOUIS H. PIGNOLET: Dynamics of Intra-Molecular Rearrangements. COOPER H. LANGFORD and THOMAS R. STENGLE: Solvation and the Second Coordination Sphere. G. N. La MAR: Novel Structural Studies in Solution. W. D. PHILLIPS: Biological Applications. W. D. HORROCKS, Jr.: Lanthanide Shift Reagents and Other Analytical Applications. R. D. FISCHER: Lanthanide and Actinide Complexes (Revised Version). B. R. McGARVEY and R. J. KURLAND: Nuclei Other than Protons. ROBERT W. KREILICK: NMR Studies of Organic Radicals. *1973, about 600 pp., in preparation*

Prices subject to change without notice

Your Ft nmr system can provide results like these!

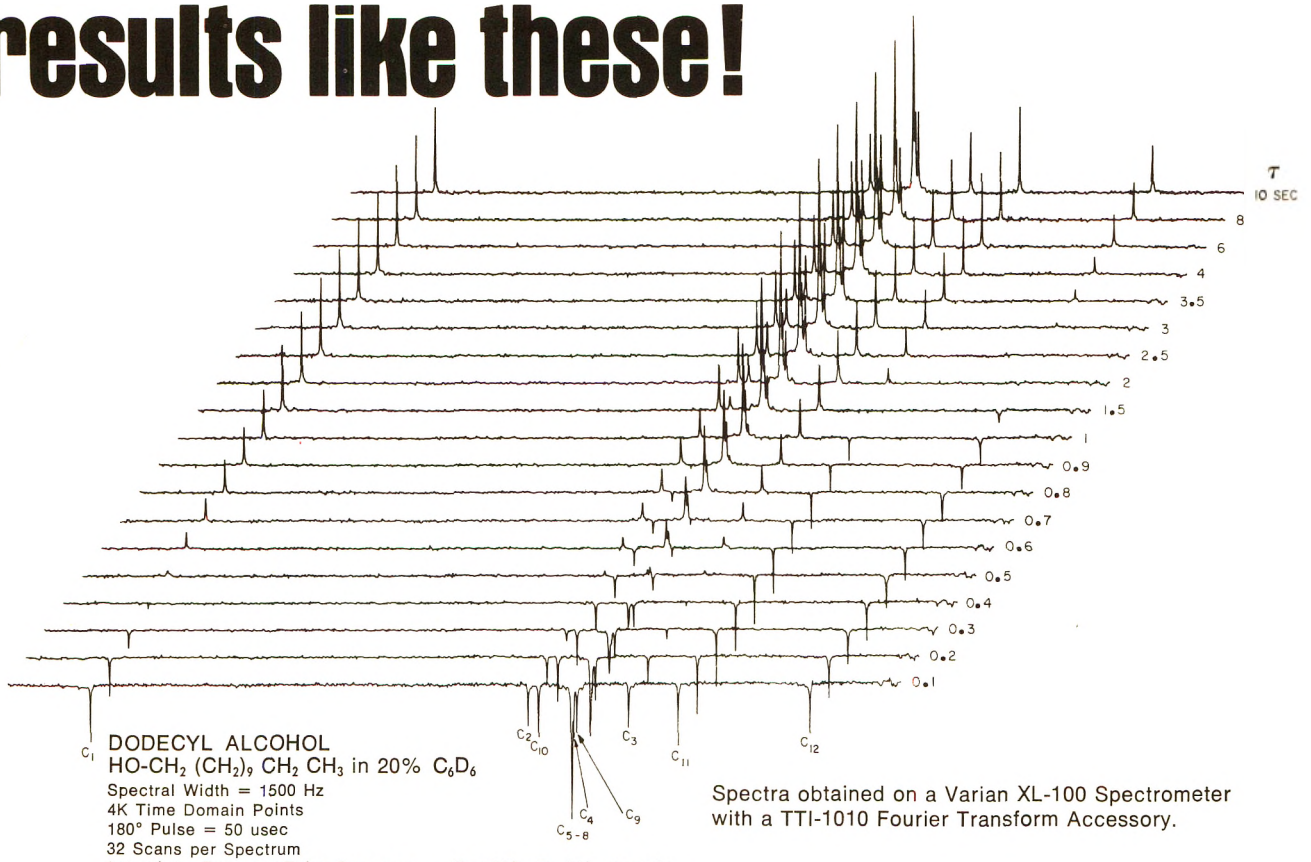

DODECYL ALCOHOL
$HO\text{-}CH_2\ (CH_2)_9\ CH_2\ CH_3$ in 20% C_6D_6
Spectral Width = 1500 Hz
4K Time Domain Points
180° Pulse = 50 usec
32 Scans per Spectrum
Inversion—Recovery Pulse Sequence . . . T - 180° - τ - 90° - Sample . .

Spectra obtained on a Varian XL-100 Spectrometer with a TTI-1010 Fourier Transform Accessory.

It's easy using the Nicolet 1080 Data System. The 1080 incorporates unique concepts designed specifically for the scientific laboratory. It has two processing units—a wired one for acquiring data and a programmable one for processing data. Thus each unit performs the functions it does best. Signals are digitized and added to memory by the wired processor while it is displaying the entire averaged signal in a continuous, flicker-free display. This unique signal averager approach to data acquisition allows the display to continue regardless of the data acquisition rate (up to 100 kHz) so that the user can examine the input signal or the averaged signal, at any vertical or horizontal expansion, **without interrupting the data acquisition process.** This allows instantaneous inspection of the signal to noise as well as examination of the data for pulse feedthrough, decoupling power, and frequency offset.

The unique 20-bit word 1080 data processor not only allows more single-precision dynamic range than any other, but it also has a much more powerful instruction set. This permits faster and more efficient data reduction and programming simplicity.

The above spectra of dodecyl alcohol were obtained using the Nicolet automatic T_1 program, which utilizes the $[180° - \tau - 90° - (\text{sample}) - T]_n$ inversion recovery[1] or PRFT[2] pulse sequence. In this experiment, the value of the inter-pulse interval τ is varied from a time much less than the shortest T_1 to a time about 5 times longer than the longest T_1 in the sample. Data are signal averaged at each value of τ and stored on the Nicolet 600,000 word cartridge disk memory.

For $\tau \ll T_1$, nuclear magnetization will still be inverted when the 90° pulse is applied, leading to inverted peaks in the transformed spectrum. For $\tau \approx T_1 \ln 2$, a null will be observed, since at this time the magnetization is just passing through zero when the 90° pulse is applied. Finally, when $\tau \gg T_1$, the nuclei will have returned to their usual precession about the $+z$ axis before the 90° pulse is applied, and the experiment reduces to the usual single pulse Ft nmr experiment.

After all spectra are obtained, they are processed all at once and displayed or plotted as shown. The spin-lattice relaxation times of each line can be estimated from the plots or calculated using a least squares treatment, from the equation $A = A_0\ [1 - 2 \exp(-\tau/T_1)]$. This calculation is performed directly by the program upon command.

This quality of data and ease of operation can be yours with the Nicolet 1080 Data System, including the 600,000, 20-bit word NIC-294 cartridge disk system and the NIC-293 Pulse Controller. This latter unit allows the production of up to eight computer-selectable times corresponding to rf pulses and pulse intervals. This unit is already in use measuring T_1's, T_2's, performing gated decoupling and homonuclear pulsed decoupling and providing the versatility for use in almost any definable experiment.

The Nicolet 1080 Data System has been successfully used with all major spectrometers and is also available with a complete Fourier pulse accessory package for the Varian XL-100 through Nicolet's affiliate, Transform Technology, Incorporated.

Why not investigate the features of the 1080 Data System and find out how it can make your nmr spectrometer perform more efficiently.

1. R. L. Vold, J. S. Waugh, M. P. Klein, and D. E. Phelps, **J. Chem. Phys. 48**, 3831 (1968).
2. A. Allerhand, D. Doddrell, V. Glushko, D. W. Cochran, E. Wenkert, P. J. Lawson and F. Gurd, **J. Am. Chem. Soc. 93**, 544 (1971).

NICOLET INSTRUMENT CORPORATION

5225 Verona Road, Madison, Wisconsin 53711
Phone 608/271-3333 TWX: 910-286-2713

In Europe: Nicolet Instrument GmbH, Goerdeler Strasse 48, D-605 Offenbach am Main, West Germany, 0611/852028, Telex: 841/4185411